

THIOETHER AND SULFOXIDE COMPLEXES OF RUTHENIUM; PRELIMINARY

IN VITRO STUDIES OF WATER-SOLUBLE SPECIES

By

ELIZABETH LAI SHUEN CHEU

B. Sc., University of British Columbia, 1991

A THESIS SUBMITTED IN PARTIAL FULFILLMENT OF

THE REQUIREMENTS FOR THE DEGREE OF

DOCTOR OF PHILOSOPHY

In

THE FACULTY OF GRADUATE STUDIES

(Department of Chemistry)

We accept this thesis as conforming

to the required standard

THE UNIVERSITY OF BRITISH COLUMBIA

January 2000

© Elizabeth Lai Shuen Cheu, 2000

In presenting this thesis in partial fulfilment of the requirements for an advanced degree at the University of British Columbia, I agree that the Library shall make it freely available for reference and study. I further agree that permission for extensive copying of this thesis for scholarly purposes may be granted by the head of my department or by his or her representatives. It is understood that copying or publication of this thesis for financial gain shall not be allowed without my written permission.

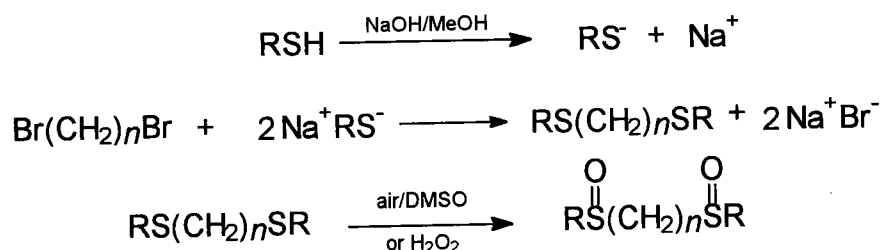
Department of Chemistry
The University of British Columbia
Vancouver, Canada

Date Jan 27, 2000

Abstract

Water-soluble ruthenium chemotherapeutic agents require further investigation. One approach is to study the coordination chemistry of a series of Ru-disulfoxide complexes, and preliminary *in vitro* surveys of the effects of these complexes in CHO (Chinese hamster ovary) cells are included. Other approaches, including the metallation of some free-base porphyrins, were investigated as well.

Dithioethers and disulfoxides were synthesized using the well established chemistry outlined below:[†]



The disulfoxide and dithioethers were reacted with Ru precursors to yield complexes characterized generally by a combination of elemental analyses, NMR, IR and UV-Visible spectroscopies, as well as conductivity, magnetic measurements and thermal

[†] Ten new disulfoxides (and the corresponding new dithioethers) have been made with: (a) $n = 2$: R = butyl, 1,2-bis(butylsulfinyl)ethane, BBSE; R = pentyl, 1,2-bis(pentylsulfinyl)ethane, BPeSE; R = hexyl, 1,2-bis(hexylsulfinyl)ethane, BHSE; R = cyclohexyl, 1,2-bis(cyclohexylsulfinyl)ethane, BCySE, and (b) $n = 3$: R = ethyl, 1,3-bis(ethylsulfinyl)propane, BESP; R = propyl, 1,3-bis(propylsulfinyl)propane, BPSP; R = ⁱpropyl, 1,3-bis(ⁱpropylsulfinyl)propane, BⁱPSP; R = butyl, 1,3-bis(butylsulfinyl)propane, BBSP; R = pentyl, 1,3-bis(pentylsulfinyl)propane, BPeSP and R = phenyl, 1,3-bis(phenylsulfinyl)propane, BPhSP. All alkyl groups are the normal isomer, unless otherwise indicated.

gravimetric analyses; fifteen Ru complexes were also characterized by X-ray crystallography. The Ru-sulfoxide complexes contained only S-bonded sulfoxides (except *mer*-RuCl₃(DPSO)₂(DPSO) where O and S represent O- and S-bonded diphenylsulfoxide, respectively). The following new, mononuclear, non-water-soluble, disulfoxide complexes were synthesized and characterized: *trans*-RuCl₂(BESE)₂ (BESE = 1,2-bis(ethylsulfinyl)ethane), *cis*-RuCl₂(BBSE)₂, *cis*-RuCl₂(BPSE)₂, *cis*-RuCl₂(BCySE)₂ and *cis*-RuCl₂(BESP)₂. RuCl₂(DMSO)(L) (where L = 3,6,9,14-tetrathiabicyclo[9.2.1]tetradeca-11,13-diene), and the water-soluble [Ru(12-S-4)(DMSO)(H₂O)][OTf]₂ (where 12-S-4 = 1,4,7,10-tetrathiacyclododecane and OTf = CF₃SO₃⁻), were synthesized to determine how the macrocyclic ligand might affect the *in vitro* properties of the Ru-sulfoxide moiety.

Novel, water-soluble, dinuclear[†] Ru(II)-disulfoxide complexes [RuCl(BESE)(H₂O)]₂(μ-Cl)₂, [RuCl(BPSE)(H₂O)]₂(μ-Cl)₂ (BPSE = 1,2-bis(propylsulfinyl)ethane) and [RuCl(BBSE)(H₂O)]₂(μ-Cl)₂ were characterized, and a new type of water-soluble, dinuclear, mixed-valence Ru(II)/Ru(III)-disulfoxide complex, [RuCl(BPSP)]₂(μ-Cl)₃, was characterized and its aqueous chemistry studied.

Two mononuclear, dithioether complexes (*trans*-RuCl₂(BPhTE)₂ and -RuCl₂(BCyTE)₂, where BPhTE = 1,2-bis(phenylthio)ethane and BCyTE = 1,2-bis(cyclohexylthio)ethane), and four dinuclear, Ru(III)/Ru(III) dithioether complexes ([RuCl₂(BETP)]₂(μ-Cl)₂, [RuCl₂(BPTP)]₂(μ-Cl)₂, [RuCl₂(BBTP)]₂(μ-Cl)₂ and [RuCl₂(BPETP)]₂(μ-Cl)₂, where BETP = 1,3-bis(ethylthio)propane, BPTP = 1,3-

[†] The loosely used "mononuclear," "dinuclear" and "trinuclear" terms refer to the number of metal atoms within a molecule.

bis(propylthio)propane, BBTP = 1,3-bis(butylthio)propane and BPeTP = 1,3-bis(pentylthio)propane) were also synthesized. The purpose of their synthesis was to determine whether the ligand set would retain its geometry at the Ru after oxidation of the coordinated S-atom to S=O, but such an oxidation was not affected.

A procedure involving the metallation of the water-soluble, free-base porphyrin TSPhP (the dianion of 5,10,15,20-tetrakis(4-sulfonato)phenylporphyrin), using $[\text{Ru}(\text{DMF})_6][\text{OTf}]_3$ as the precursor, to give $\text{Na}_4[\text{Ru}(\text{TSPhP})(\text{CO})] \cdot 4\text{H}_2\text{O}$ was also shown to be effective for metallation of several non-water-soluble, free-base porphyrins with formation of $\text{Ru}(\text{CO})(\text{Porp})$ species, where Porp = TPhP (the dianion of 5,10,15,20-tetraphenylporphyrin), BPhP (dianion of 5,15-bis(phenyl)porphyrin), TrPhPyNO (dianion of 5,10,15-triphenyl-20-(4-pyridyl-N-oxide)porphyrin), and OEP (dianion of 2,3,7,8,12,13,17,18-octaethylporphyrin).

The water-soluble $[\text{RuCl}(\text{S-S})(\text{H}_2\text{O})]_2(\mu\text{-Cl})_2$ (S-S = BESE, BPSE or BBSE), $[\text{RuCl}(\text{BPSP})]_2(\mu\text{-Cl})_3$ and $[\text{Ru}(12\text{-S-4})(\text{DMSO})(\text{H}_2\text{O})][\text{OTf}]_2$ complexes were examined *in vitro* using Chinese hamster ovary (CHO) cells. Toxicity, cell accumulation and DNA-binding assays were used to examine the ability of these complexes to traverse the cell membrane and bind to DNA. The biological data indicate that all five complexes are non-toxic but accumulate in CHO cells, with no difference in hypoxia. Of major interest $[\text{RuCl}(\text{BPSP})]_2(\mu\text{-Cl})_3$ and $[\text{RuCl}(\text{BESE})(\text{H}_2\text{O})]_2(\mu\text{-Cl})_2$ bind to DNA to a greater degree than *cis*- or *trans*- $\text{RuCl}_2(\text{DMSO})_4$, both of which are known to exhibit anti-cancer activity. The preliminary biological data strongly encourage further investigations into the use of water-soluble, dinuclear Ru-disulfoxide complexes as DNA-binding agents.

Table of Contents

Abstract.....	ii
Table of Contents.....	v.
List of Tables.....	xiii.
List of Figures.....	xviii.
List of Abbreviations.....	xxv.
Acknowledgements.....	xxviii.
 Chapter 1 Introduction	
1.1 Preamble.....	1.
1.2 Development of Platinum Chemotherapeutic Agents	2.
1.3 Ruthenium Chemotherapeutic Agents.....	5.
1.3.1 Dinuclear Ru(II)/Ru(III) Complexes.....	8.
1.3.2 Metallated Porphyrins.....	9.
1.4 Development of Ruthenium Dimethylsulfoxide Complexes.....	10.
1.4.1 Ru(II)-Dimethylsulfoxide Complexes: <i>Cis</i> -RuCl ₂ (DMSO) ₃ (DMSO) and <i>Trans</i> -RuCl ₂ (DMSO) ₄	10.
1.4.1.1 Chemical Behaviour of <i>Cis</i> -RuCl ₂ (DMSO) ₃ (DMSO) and <i>Trans</i> - RuCl ₂ (DMSO) ₄ in Aqueous Solutions.....	11.
1.4.1.2 Binding of <i>Cis</i> -RuCl ₂ (DMSO) ₃ (DMSO) and <i>Trans</i> -RuCl ₂ (DMSO) ₄ to DNA..	13.
1.4.2 Ru(III)-Dimethylsulfoxide Complexes: <i>trans</i> - [(DMSO) ₂ H] ⁺ [RuCl ₄ (DMSO) ₂] ⁻ and <i>Mer</i> -RuCl ₃ (DMSO) ₂ (DMSO).....	14.
1.4.3 Nitroimidazole Derivatives of RuCl ₂ (DMSO) ₄	17.
1.4.4 Ru Bis-chelating Sulfoxide Complexes.....	19.
1.5 Goals of This Thesis.....	21.
1.5.1 Synthesis of the Geometrical Isomers of the Known Bis-chelating Disulfoxide Complexes of Ru.....	21.

1.5.2	Synthesis of Water-soluble Sulfoxide Complexes of Ru.....	21.
1.5.3	Synthesis and Characterization of Novel Chelating Disulfoxide Complexes of Ru.....	22.
1.5.4	Synthesis of Chelating Dithioether Complexes of Ru.....	22.
1.5.5	Preliminary Biological Studies <i>In Vitro</i> of Sulfoxide Complexes of Ru.....	22.
1.5.6	Metallation of Water-Soluble Porphyrins.....	23.
1.6	References for Chapter 1.....	24.

Chapter 2 General Experimental and Synthesis of Ligands (Dithioethers and Disulfoxides) and Ruthenium Precursors and Sulfoxide Complexes

2.1	Chemicals and Reagents.....	32.
2.2	Physical Techniques and Instrumentation.....	32.
2.2.1	FT-NMR Instruments.....	32.
2.2.2	Infrared and UV-Vis Spectrophotometry, Thermal Gravimetric Analysis, Photochemistry and Conductivity and Melting Point Measurements.....	33.
2.2.3	Magnetic Susceptibility.....	34.
2.2.3.1	Calculation of χ_B , Magnetic Susceptibility of the Dissolved Paramagnetic Species and Magnetic Susceptibility per Gram of Sample.....	34.
2.2.3.2	Calculation of χ_M , the Molar Magnetic Susceptibility.....	35.
2.2.3.3	Calculation of μ_{eff} , the Effective Magnetic Moment.....	35.
2.2.3.4	Calculation of n, the Number of Unpaired Electrons.....	35.
2.2.4	Elemental Analyses, Mass Spectral Analyses and X-ray Crystallography...	36.
2.3	Synthesis of Dithioethers.....	36.
2.3.1	3,7-Dithianonane.....	36.
2.3.2	4,8-Dithiaundecane.....	37.
2.3.3	2,8-Dimethyl-3,7-dithianonane.....	37.
2.3.4	5,9-Dithiatridecane.....	38.
2.3.5	6,10-Dithiapentadecane.....	38.
2.3.6	1,3-Bis(phenylthio)propane.....	38.
2.3.7	5,8-Dithiadodecane.....	39.
2.3.8	6,9-Dithiatetradecane.....	39.

2.3.9	7,10-Dithiahexadecane.....	40.
2.3.10	1,2-Bis(phenylthio)ethane.....	40.
2.3.11	1,2-Bis(cyclohexylthio)ethane.....	40.
2.4	Oxidation of Dithioethers to Disulfoxides.....	41.
2.4.1	1,3-Bis(ethylsulfinyl)propane (BESP).....	41.
2.4.2	1,3-Bis(propylsulfinyl)propane (BPSP).....	42.
2.4.3	1,3-Bis(<i>i</i> -propylsulfinyl)propane (B'PSP).....	42.
2.4.4	1,3-Bis(butylsulfinyl)propane (BBSP).....	42.
2.4.5	1,3-Bis(pentylsulfinyl)propane (BP _e SP).....	43.
2.4.6	1,3-Bis(phenylsulfinyl)propane (BPhSP).....	43.
2.4.7	1,2-Bis(ethylsulfinyl)ethane (BESE).....	44.
2.4.8	1,2-Bis(propylsulfinyl)ethane (BPSE).....	44.
2.4.9	1,2-Bis(butylsulfinyl)ethane (BBSE).....	45.
2.4.10	1,2-Bis(pentylsulfinyl)ethane (BP _e SE).....	45.
2.4.11	1,2-Bis(hexylsulfinyl)ethane (BHSE).....	45.
2.4.12	1,2-Bis(cyclohexylsulfinyl)ethane (BCySE).....	46.
2.4.13	1,2-Bis(phenylsulfinyl)ethane (BPhSE).....	46.
2.5	Synthesis of Ru(III) Precursor Complexes.....	47.
2.5.1	[Ru(DMF) ₆][OTf] ₃	47.
2.5.2	K ₃ [RuCl ₆].....	48.
2.6	Synthesis of Monodentate Sulfoxide Complexes of Ruthenium.....	48.
2.6.1	<i>Cis</i> -RuCl ₂ (DMSO) ₄	48.
2.6.2	<i>Trans</i> -RuCl ₂ (DMSO) ₄	49.
2.6.3	<i>Mer-cis</i> -[RuCl ₃ (DPSO) ₂ (DPSO)].....	49.
2.6.4	<i>Cis</i> [Ru(12 S-4)(DMSO)(H ₂ O)][OTf] ₂ ·CH ₃ OH.....	50.
2.6.5	RuCl ₂ (DMSO)(L).....	50.
2.7	Synthesis of Mononuclear Ru(II) Disulfoxide Complexes.....	51.
2.7.1	<i>Cis</i> -RuCl ₂ (BESE) ₂	51.
2.7.2	<i>Trans</i> -RuCl ₂ (BESE) ₂ ·H ₂ O.....	51.
2.7.3	<i>Trans</i> -RuCl ₂ (BPSE) ₂ ·H ₂ O.....	52.

2.7.4	<i>Cis</i> -RuCl ₂ (BBSE) ₂	52.
2.7.5	<i>Cis</i> -RuCl ₂ (BPeSE) ₂	53.
2.7.6	<i>Cis</i> -RuCl ₂ (BCySE) ₂	53.
2.7.7	<i>Cis</i> -RuCl ₂ (BESP) ₂	54.
2.8	Synthesis of Dinuclear Ru(II)/Ru(II) Disulfoxide Complexes.....	55.
2.8.1	[RuCl(BESE)(H ₂ O)] ₂ (μ-Cl) ₂	55.
2.8.2	[RuCl(BPSE)(H ₂ O)] ₂ (μ-Cl) ₂	55.
2.8.3	[RuCl(BBSE)(H ₂ O)] ₂ (μ-Cl) ₂	56.
2.9	Synthesis of a Dinuclear Ru(II)/Ru(III) Disulfoxide Complex.....	56.
2.9.1	[RuCl(BPSP)] ₂ (μ-Cl) ₃	56.
2.10	Synthesis of Mononuclear Ru(II) Dithioether Complexes.....	57.
2.10.1	<i>Trans</i> -RuCl ₂ (BCyTE) ₂ ·2H ₂ O.....	57.
2.10.2	<i>Trans</i> -RuCl ₂ (BPhTE) ₂	58.
2.11	Synthesis of Dinuclear Ru(III)/Ru(III) Dithioether Complexes.....	59.
2.11.1	[RuCl ₂ (BETP)] ₂ (μ-Cl) ₂	59.
2.11.2	[RuCl ₂ (BPTP)] ₂ (μ-Cl) ₂	59.
2.11.3	[RuCl ₂ (BBTP)] ₂ (μ-Cl) ₂	59.
2.11.4	[RuCl ₂ (BPeTP)] ₂ (μ-Cl) ₂	60.
2.12	References for Chapter 2.....	61.

Chapter 3 Structural Properties of Sulfoxide and Thioether Complexes of Ruthenium

3.1	General Introduction.....	63.
3.2	Structural Properties of the S-O Moiety in Sulfoxides.....	64.
3.3	Metal-Sulfoxide Bonding.....	65.
3.3.1	Sulfur-Bonded Metal-Sulfoxide Complexes.....	67.
3.3.2	Oxygen-Bonded Metal-Sulfoxide Complexes.....	69.
3.3.3	Bridging Metal-DMSO Complexes.....	70.
3.4	NMR and IR Spectroscopic Methods for the Determination of Sulfur- or	

Oxygen-Bonding in Metal Complexes.....	71.
3.4.1 ¹ H NMR Spectroscopy.....	71.
3.4.2 IR Spectroscopy.....	72.
3.5 Disulfoxides and Their Metal Complexes.....	73.
3.5.1 Disulfoxide Complexes.....	76.
3.6 Mononuclear, Bidentate Disulfoxide Complexes of Ruthenium(II).....	80.
3.6.1 <i>Cis</i> -RuCl ₂ (BESE) ₂ and <i>Trans</i> -RuCl ₂ (BESE) ₂ ·H ₂ O.....	84.
3.6.2 <i>Trans</i> -RuCl ₂ (BPSE) ₂ ·H ₂ O.....	88.
3.6.3 <i>Cis</i> -RuCl ₂ (BBSE) ₂	89.
3.6.4 <i>Cis</i> -RuCl ₂ (BPSeSE) ₂	92.
3.6.5 <i>Cis</i> -RuCl ₂ (BCySE) ₂	92.
3.6.6 <i>Cis</i> -RuCl ₂ (BESP) ₂	95.
3.7 Dinuclear Ru(II)/Ru(II) Chelating Disulfoxide Complexes.....	99.
3.7.1 Characterization of [RuCl(BESE)(H ₂ O)] ₂ (μ-Cl) ₂ , [RuCl(BPSE)- (H ₂ O)] ₂ (μ-Cl) ₂ and [RuCl(BBSE)(H ₂ O)] ₂ (μ-Cl) ₂	100.
3.8 A Mixed-Valence Ru(II)/Ru(III) Chelating Disulfoxide Complex.....	105.
3.8.1 Introduction.....	105.
3.8.2 [RuCl(BPSP)] ₂ (μ-Cl) ₃	109.
3.8.3 Chemical Behaviour of [RuCl(BPSP)] ₂ (μ-Cl) ₃ in Aqueous Solutions.....	116.
3.9 Dithioether Complexes of Ru.....	126.
3.9.1 Literature Data.....	127.
3.9.2 The Mononuclear Ru(II) Dithioether Complexes: <i>Trans</i> - RuCl ₂ (BCyTE) ₂ ·2H ₂ O and <i>Trans</i> -RuCl ₂ (BPhTE) ₂	129.
3.9.3 Dinuclear Ru(III)/Ru(III) Dithioether Complexes: [RuCl ₂ (BETP)] ₂ (μ-Cl) ₂ , [RuCl ₂ (BPTP)] ₂ (μ-Cl) ₂ , [RuCl ₂ (BBTP)] ₂ (μ-Cl) ₂ and [RuCl ₂ (BPETP)] ₂ (μ-Cl) ₂	136.
3.10 <i>Mer</i> -RuCl ₃ (DPSO) ₂ (DPSO).....	140.
3.10.1 Characterization of <i>Mer-Cis</i> -RuCl ₃ (DPSO) ₂ (DPSO).....	141.
3.11 Macrocyclic Thioether, DMSO Complexes of Ruthenium.....	145.
3.11.1 3,6,9,14-Tetrathiabicyclo[9.2.1]tetradeca-11,13-diene [L].....	145.

3.11.2	$\text{RuCl}_2(\text{DMSO})(\text{L})$	146.
3.11.3	1,4,7,10-Tetrathiacyclododecane (12-S-4).....	151.
3.11.4	$[\text{Ru}(12\text{-S-4})(\text{DMSO})(\text{H}_2\text{O})][\text{OTf}]_2$	151.
3.12	References for Chapter 3.....	155.

Chapter 4 Preliminary *In Vitro* Examination of Water-soluble Ru Sulfoxide Complexes

4.1	Introduction.....	163.
4.2	Tumour Hypoxia, Radiotherapy and Progression.....	164.
4.3	Experimental.....	166.
4.3.1	Media.....	166.
4.3.2	Phosphate Buffer Saline Solution.....	167.
4.3.3	Methylene Blue Solution.....	167.
4.3.4	Tris-EDTA (TE) Solutions.....	168.
4.3.5	TNE Solutions.....	168.
4.3.6	TNE-Equilibrated Phenol.....	168.
4.3.7	Cell Preparation.....	168.
4.3.8	Atomic Absorption Spectroscopy.....	169.
4.3.9	Cell Incubation Procedures.....	170.
4.3.10	Cell Toxicity Assays Under Oxidic and Hypoxic Conditions.....	171.
4.3.11	Cell Accumulation Assays.....	172.
4.3.12	DNA-Binding Assays.....	173.
4.4	<i>In Vitro</i> Studies of Five Ru Sulfoxides: Preliminary Results in CHO Cells... ..	174.
4.4.1	Toxicity of Ru Sulfoxides in CHO Cells under Oxidic and Hypoxic Conditions..	174.
4.4.2	Ruthenium Accumulation Under Oxidic and Hypoxic Conditions.....	175.
4.4.3	DNA-binding Under Oxidic and Hypoxic Conditions.....	178.
4.5	Conclusions.....	181.
4.6	References for Chapter 4.....	182.

Chapter 5 Metallation of Free-base Porphyrins

5.1	Introduction.....	184.
5.1.1	Metalloporphyrins as Hypoxic Radiosensitizers.....	184.
5.2	Ruthenium Porphyrins.....	185.
5.3	A New Route for the Insertion of Ruthenium into Selected Free-base Porphyrins.....	186.
5.4	Experimental.....	188.
5.4.1	Physical Techniques.....	188.
5.4.2	Synthesis of Precursors.....	188.
5.4.2.1	$\text{Na}_4[\text{H}_2\text{TSPHP}]\cdot 15\text{H}_2\text{O}$	188.
5.4.2.2	$[\text{Ru}(\text{DMF})_6][\text{OTf}]_3$	189.
5.5	Synthesis of $\text{Ru}(\text{Porp})(\text{CO})$ Complexes.....	189.
5.5.1	$\text{Na}_4[\text{Ru}(\text{TSPHP})(\text{CO})]\cdot 4\text{H}_2\text{O}$	189.
5.5.2	$\text{Ru}(\text{OEP})(\text{CO})(\text{THF})$	190.
5.5.3	$\text{Ru}(\text{TPhP})(\text{CO})(\text{H}_2\text{O})$	190.
5.5.4	$\text{Ru}(\text{BPhP})(\text{CO})$	191.
5.5.5	$\text{Ru}(\text{TrPhPyNO})(\text{CO})$	191.
5.6	Results and Discussion.....	192.
5.6.1	$\text{Na}_4[\text{Ru}(\text{TSPHP})(\text{CO})]\cdot 4\text{H}_2\text{O}$	193.
5.6.2	$\text{Ru}(\text{OEP})(\text{CO})(\text{THF})$	195.
5.6.3	$\text{Ru}(\text{TPhP})(\text{CO})(\text{py})$	199.
5.6.4	$\text{Ru}(\text{BPhP})(\text{CO})$	201.
5.6.5	$\text{Ru}(\text{TrPhPyNO})(\text{CO})$	201.
5.7	Fluorescent Properties of Porphyrins.....	201.
5.7.1	Fluorescence Spectra of Selected Ru Porphyrins.....	202.
5.8	Attempted Metallations.....	203.
5.9	Conclusions.....	206.
5.10	References for Chapter 5.....	207.

Chapter 6 Conclusions and Recommendations for Future Work

6.1	General Remarks.....	211.
6.2	Sulfoxide and Thioether Complexes of Ruthenium	211.
6.3	Metallation of Selected Free-base Porphyrins	216.
6.4	Preliminary <i>In Vitro</i> Examination Of Water-soluble Ru Sulfoxide Complexes ..	217.
6.5	References for Chapter 6.....	219.

Appendices

Appendix 1.	Crystallographic Data.....	A.221.
Appendix 1.1	Crystallographic Data for <i>trans</i> -RuCl ₂ (BESE) ₂	A.221.
Appendix 1.2	Crystallographic Data for <i>cis</i> -RuCl ₂ (BBSE) ₂ ·EtOH.....	A.223.
Appendix 1.3	Crystallographic Data for <i>cis</i> -RuCl ₂ (BCySE) ₂ ·EtOH·1/3MeOH.....	A.227.
Appendix 1.4	Crystallographic Data for <i>cis</i> -RuCl ₂ (BESP) ₂ ·EtOH·H ₂ O.....	A.231.
Appendix 1.5	Crystallographic Data for [RuCl(BESE)(H ₂ O)] ₂ (μ-Cl) ₂ ·H ₂ O.....	A.233.
Appendix 1.6	Crystallographic Data for [RuCl(BPSP)] ₂ (μ-Cl) ₃ ·2H ₂ O·2.5CH ₂ Cl ₂ ..	A.238.
Appendix 1.7	Crystallographic Data for <i>trans</i> -RuCl ₂ (BCyTE) ₂ ·2CH ₂ Cl ₂	A.245.
Appendix 1.8	Crystallographic Data for <i>trans</i> -RuCl ₂ (BPhTE) ₂	A.249.
Appendix 1.9	Crystallographic Data for [RuCl ₂ (BETP)] ₂ (μ-Cl) ₂	A.253.
Appendix 1.10	Crystallographic Data for [RuCl ₂ (BPTP)] ₂ (μ-Cl) ₂	A.255.
Appendix 1.11	Crystallographic Data for <i>Mer-Cis</i> -RuCl ₃ (DPSO) ₂ (DPSO).....	A.257.
Appendix 1.12	Crystallographic Data for RuCl ₂ (DMSO)(L).....	A.260.
Appendix 1.13	Crystallographic Data for [Ru(12-S-4)(DMSO)(H ₂ O)][OTf] ₂	A.263.
Appendix 1.14	Crystallographic Data for Ru(OEP)(CO)(THF).....	A.266.
Appendix 1.15	Crystallographic Data for Ru(TPhP)(CO)(py).....	A.272.
Appendix 2.	Experimental for the Kinetic Studies of [RuCl(BPSP)] ₂ (μ-Cl) ₃	A.276.
Appendix 3.	Thermal Gravimetric Analyses Plots.....	A.277.
Appendix 4.	Accumulation Data of Ru in CHO Cells.....	A.280.
Appendix 5.	DNA-binding Data of Ru in CHO Cells.....	A.281.

List of Tables

Table 3.1. Selected Bond Lengths and Bond Angles for DMSO in the Gaseous and Solid States.....	65.
Table 3.2. Selected Structural Data for Selected Transition Metal-DMSO Complexes..	68.
Table 3.3. The Sulfur-oxygen Stretching Frequencies of S-bonded, O-bonded and Bridging DMSO Ru Complexes.....	73.
Table 3.4. The Melting Points and ν_{SO} (cm^{-1}) for Disulfoxides.....	75.
Table 3.5. IR Data (KBr) for ν_{SO} (cm^{-1}) Free and ν_{SO} (cm^{-1}) Bound, in Chelating Disulfoxide Complexes of Ru.....	83.
Table 3.6. Selected Bond Lengths (\AA) and Bond Angles ($^{\circ}$) for Some <i>trans</i> - $\text{RuCl}_2(\text{S-S})_2$ Complexes.....	85.
Table 3.7. Selected Bond Lengths (\AA) and Bond Angles ($^{\circ}$) for $[\text{RuCl}(\text{BESE})(\text{H}_2\text{O})]_2(\mu\text{-Cl})_2\cdot\text{H}_2\text{O}$, <i>trans</i> - $\text{RuCl}_2(\text{BESE})_2$ and <i>cis</i> - $\text{RuCl}_2(\text{BESE})_2$	86.
Table 3.8. The Relative Configurations of the S-atoms in Chelating Disulfoxide Complexes of Ru.	88.
Table 3.9. Selected Bond Lengths (\AA) and Bond Angles ($^{\circ}$) of <i>cis</i> - $\text{RuCl}_2(\text{BBSE})_2\cdot\text{EtOH}$ and <i>cis</i> - $\text{RuCl}_2(\text{BCySE})_2\cdot\text{EtOH}\cdot 1/3 \text{ MeOH}$	90.
Table 3.10. Selected Bond Lengths (\AA) and Bond Angles ($^{\circ}$) of <i>cis</i> - $\text{RuCl}_2(\text{BESP})_2\cdot\text{EtOH}\cdot\text{H}_2\text{O}$ and <i>cis</i> - $\text{RuCl}_2(\text{BMSP})_2$	98.
Table 3.11. Titration data for $[\text{RuCl}(\text{BESE})(\text{H}_2\text{O})]_2(\mu\text{-Cl})_2$ using NaOH.....	101.
Table 3.12. Classes of Mixed-valence Complexes.....	106.
Table 3.13. Selected Bond Lengths for the Two Asymmetric Units of $[\text{RuCl}(\text{BPSP})]_2(\mu\text{-Cl})_3$	115.
Table 3.14. Selected Bond Angles for the Two Asymmetric Units of $[\text{RuCl}(\text{BPSP})]_2(\mu\text{-Cl})_3$	115.
Table 3.15. Titration data for $[\text{RuCl}(\text{BPSP})]_2(\mu\text{-Cl})_3$ using NaOH.....	118.
Table 3.16. Kinetic Data for the Hydration Reaction of $[\text{RuCl}(\text{BPSP})]_2(\mu\text{-Cl})_3$ in H_2O	125.

Table 3.17. Selected Bond Lengths (Å) and Angles (°) for <i>trans</i> -RuCl ₂ (BCyTE) ₂ ·2CH ₂ Cl ₂ and <i>trans</i> -RuCl ₂ (BPhTE) ₂	133.
Table 3.18. Selected Bond Lengths (Å) and Bond Angles (°) for [RuCl ₂ (BETP)] ₂ (μ-Cl) ₂ and [RuCl ₂ (BPTP)] ₂ (μ-Cl) ₂	137.
Table 3.19. Selected Bond Lengths (Å) and Bond Angles (°) for <i>mer-cis</i> -[RuCl ₃ (DPSO) ₂ (DPSO)] and <i>mer</i> -[RuCl ₃ (DPSO)(DPSO)(MeOH)].....	144.
Table 3.20. Comparison of Selected Bond Angles (°) of L and RuCl ₂ (DMSO)(L).	149.
Table 3.21. Comparison of Selected Bond Lengths (Å) of L and RuCl ₂ (DMSO)(L).....	150.
Table 3.22. Comparison of Selected Bond Angles (°) of 12-S-4 and [Ru(12-S-4)(DMSO)(H ₂ O)][OTf] ₂	152.
Table 3.23. Comparison of Selected Bond Lengths (Å) of 12-S-4 and [Ru(12-S-4)(DMSO)(H ₂ O)][OTf] ₂	154.
Table 4.1. Water-soluble Ru sulfoxide complexes studied <i>in vitro</i>	164.
Table 4.2. Furnace parameters used in AAS for Ru, at λ 265.9 nm.....	170.
Table 5.1. Ru(Porp)(CO) species.....	187.
Table 5.2. Selected Bond Angles and Lengths for Ru(OEP)(CO)(THF).....	197.
Table 5.3. Comparison of Selected Bond Lengths for Ru(TPhP)(CO)(py).....	199.
Table 5.4. Fluorescence wavelengths for selected Ru porphyrins.....	203.
Table 5.5. Free-Base Porphyrins. 5,10,15,20-tetrapyridylporphyrin (TPyP), 5,10-bis(phenyl)-15,20-bis(4-pyridyl-N-oxide)porphyrin (BPhBPyNOP), 5,10,15,20-tetramesitylporphyrin (TMP), 5,10,15,20-tetra(pentafluorophenyl)-porphyrin (TPFPhP), 5,15-dibromo-10,20-bisphenylporphyrin (DBrBPhP), and protoporphyrin(IX)dimethylester (PPIXDME).....	205.
Table A.1.1. Experimental Details for X-ray Crystal Structure of <i>trans</i> -RuCl ₂ (BESE) ₂	A.221.
Table A.1.2. Bond Angles (°) for <i>trans</i> -RuCl ₂ (BESE) ₂	A.222.
Table A.1 3. Bond Lengths (Å) for <i>trans</i> -RuCl ₂ (BESE) ₂	A.222.
Table A.1 4. Atomic Coordinates for <i>trans</i> -RuCl ₂ (BESE) ₂	A.222.

Table A.1 5. Experimental Details for X-ray Crystal Structure of <i>cis</i> - RuCl ₂ (BBSE) ₂ ·EtOH.....	A.223.
Table A.1 6. Bond Angles (°) for <i>cis</i> -RuCl ₂ (BBSE) ₂ ·EtOH.....	A.224.
Table A.1 7. Bond Lengths (Å) for <i>cis</i> -RuCl ₂ (BBSE) ₂ ·EtOH.....	A.224.
Table A.1 8. Atomic Coordinates for <i>cis</i> -RuCl ₂ (BBSE) ₂ ·EtOH.....	A.225.
Table A.1 9. Hydrogen bond parameters for A-H...B interactions.....	A.225.
Table A.1 10. Experimental Details for X-ray Crystal Structure of <i>cis</i> - RuCl ₂ (BCySE) ₂ ·EtOH·1/3MeOH.....	A.227.
Table A.1 11. Bond Angles (°) for <i>cis</i> -RuCl ₂ (BCySE) ₂ ·EtOH·1/3MeOH.....	A.228.
Table A.1 12. Bond Lengths (Å) for <i>cis</i> -RuCl ₂ (BCySE) ₂ ·EtOH·1/3MeOH.....	A.228.
Table A.1 13. Atomic Coordinates for <i>cis</i> -RuCl ₂ (BCySE) ₂ ·EtOH·1/3MeOH.....	A.229.
Table A.1 14. Hydrogen bond structural parameters for A-H...B interactions	A.229.
Table A.1 15. Experimental Details for X-ray Crystal Structure of <i>cis</i> - RuCl ₂ (BESP) ₂ ·EtOH·H ₂ O.....	A.231.
Table A.1 16. Bond Angles (°) for <i>cis</i> -RuCl ₂ (BESP) ₂ ·EtOH·H ₂ O.....	A.232.
Table A.1 17. Bond Lengths (Å) for <i>cis</i> -RuCl ₂ (BESP) ₂ ·EtOH·H ₂ O.....	A.232.
Table A.1 18. Atomic Coordinates for <i>cis</i> -RuCl ₂ (BESP) ₂ ·EtOH·H ₂ O.....	A.233.
Table A.1 19. Hydrogen bond structural parameters for A-H...B interactions	A.233.
Table A.1 20. Experimental Details for X-ray Crystal Structure of [RuCl(BESE)(H ₂ O)] ₂ (μ-Cl) ₂ ·H ₂ O.....	A.233.
Table A.1 21. Bond Angles (°) for [RuCl(BESE)(H ₂ O)] ₂ (μ-Cl) ₂ ·H ₂ O.....	A.234.
Table A.1 22. Bond Lengths (Å) for [RuCl(BESE)(H ₂ O)] ₂ (μ-Cl) ₂ ·H ₂ O.....	A.235.
Table A.1 23. Atomic Coordinates for [RuCl(BESE)(H ₂ O)] ₂ (μ-Cl) ₂ ·H ₂ O.....	A.236.
Table A.1 24. Hydrogen bond parameters for A-H...B interactions.....	A.236.
Table A.1 25. Experimental Details for X-ray Crystal Structure of [Ru(BPSP)Cl] ₂ (μ-Cl) ₃ ·2H ₂ O·2.5CH ₂ Cl ₂	A.238.
Table A.1 26. Bond Angles (°) for [RuCl(BPSP)] ₂ (μ-Cl) ₃ ·2H ₂ O·2.5CH ₂ Cl ₂	A.239.
Table A.1 27. Bond Lengths (Å) for [RuCl(BPSP)] ₂ (μ-Cl) ₃ ·2H ₂ O·2.5CH ₂ Cl ₂	A.240.
Table A.1 28. Atomic Coordinates for [RuCl(BPSP)] ₂ (μ-Cl) ₃ ·2H ₂ O·2.5CH ₂ Cl ₂ ...	A.241.

Table A.1 29. Hydrogen bonds and C-H...Cl/O interactions.....	A.242.
Table A.1 30. Experimental Details for X-ray Crystal Structure of <i>trans</i> - RuCl ₂ (BCyTE) ₂ ·2CH ₂ Cl ₂	A.245.
Table A.1 31. Bond Angles (°) for <i>trans</i> -RuCl ₂ (BCyTE) ₂ ·2CH ₂ Cl ₂	A.246.
Table A.1 32. Bond Lengths (Å) for <i>trans</i> -RuCl ₂ (BCyTE) ₂ ·2CH ₂ Cl ₂	A.246.
Table A.1 33. Atomic Coordinates for <i>trans</i> -RuCl ₂ (BCyTE) ₂ ·2CH ₂ Cl ₂	A.246.
Table A.1 34. Hydrogen bond parameters for A-H...B interactions	A.247.
Table A.1 35. Experimental Details for X-ray Crystal Structure of <i>trans</i> - RuCl ₂ (BPhTE) ₂	A.249.
Table A.1 36. Bond Angles (°) for <i>trans</i> -RuCl ₂ (BPhTE) ₂	A.250.
Table A.1 37. Bond Lengths (Å) for <i>trans</i> -RuCl ₂ (BPhTE) ₂	A.250.
Table A.1 38. Atomic Coordinates for <i>trans</i> -RuCl ₂ (BPhTE) ₂	A.251.
Table A.1 39. Experimental Details for X-ray Crystal Structure of [RuCl ₂ (BETP)] ₂ (μ-Cl) ₂	A.253.
Table A.1 40. Bond Angles (°) for [RuCl ₂ (BETP)] ₂ (μ-Cl) ₂	A.254.
Table A.1 41. Bond Lengths (Å) for [RuCl ₂ (BETP)] ₂ (μ-Cl) ₂	A.254.
Table A.1 42. Atomic Coordinates for [RuCl ₂ (BETP)] ₂ (μ-Cl) ₂	A.254.
Table A.1 43. Experimental Details for X-ray Crystal Structure of [RuCl ₂ (BPTP)] ₂ (μ-Cl) ₂	A.255.
Table A.1 44. Bond Angles (°) for [RuCl ₂ (BPTP)] ₂ (μ-Cl) ₂	A.256.
Table A.1 45. Bond Lengths (Å) for [RuCl ₂ (BPTP)] ₂ (μ-Cl) ₂	A.256.
Table A.1 46. Atomic Coordinates for [RuCl ₂ (BPTP)] ₂ (μ-Cl) ₂	A.256.
Table A.1 47. Experimental Details for X-ray Crystal Structure of <i>Mer-Cis</i> - RuCl ₃ (DPSO) ₂ (DPSO).....	A.257.
Table A.1 48. Bond Angles (°) for <i>Mer-Cis</i> -RuCl ₃ (DPSO) ₂ (DPSO).....	A.258.
Table A.1 49. Bond Lengths (Å) for <i>Mer-Cis</i> -RuCl ₃ (DPSO) ₂ (DPSO).....	A.259.
Table A.1 50. Atomic Coordinates for <i>Mer-Cis</i> -RuCl ₃ (DPSO) ₂ (DPSO).....	A.260.
Table A.1 51. Experimental Details for X-ray Crystal Structure of RuCl ₂ (DMSO)(L).....	A.260.

Table A.1 52. Bond Angles (°) for RuCl ₂ (DMSO)(L).....	A.261.
Table A.1 53. Bond Lengths (Å) for RuCl ₂ (DMSO)(L).....	A.262.
Table A.1 54. Atomic Coordinates for RuCl ₂ (DMSO)(L).....	A.262.
Table A.1 55. Experimental Details for X-ray Crystal Structure of [Ru(12-S-4)(DMSO)(H ₂ O)][OTf] ₂	A.263.
Table A.1 56. Bond Angles (°) for [Ru(12-S-4)(DMSO)(H ₂ O)][OTf] ₂	A.264.
Table A.1 57. Bond Lengths (Å) for [Ru(12-S-4)(DMSO)(H ₂ O)][OTf] ₂	A.264.
Table A.1 58. Atomic Coordinates for [Ru(12-S-4)(DMSO)(H ₂ O)][OTf] ₂	A.265.
Table A.1 59. Hydrogen bonds and C-H...O/F interactions.....	A.266.
Table A.1 60. Experimental Details for X-ray Crystal Structure of Ru(OEP)(CO)(THF).....	A.266.
Table A.1 61. Bond Angles (°) for Ru(OEP)(CO)(THF).....	A.267.
Table A.1 62. Bond Lengths (Å) for Ru(OEP)(CO)(THF).....	A.269.
Table A.1 63. Atomic Coordinates for Ru(OEP)(CO)(THF).....	A.270.
Table A.1 64. Experimental Details for X-ray Crystal Structure of Ru(TPhP)(CO)(py).....	A.272.
Table A.1 65. Bond Angles (°) for Ru(TPhP)(CO)(py).....	A.272.
Table A.1 66. Bond Lengths (Å) for Ru(TPhP)(CO)(py).....	A.274.
Table A.1 67. Atomic Coordinates for Ru(TPhP)(CO)(py).....	A.275.

List of Figures

Figure 1.1. 1 = <i>Cis</i> -diamminedichloroPt(II) (Cisplatin), 2 = Diammine(cyclobutane-1-1-dicarboxylato)Pt(II) (Carboplatin), 3 = Bis(acetato)amminedichloro-(cyclohexylamine)Pt(IV) (JM 216), 4 = Amminedichloro(2-methylpyridine)Pt(II) (AMD 473).....	4.
Figure 1.2. Structures of deoxyguanosine (1) and deoxyadenosine (2).....	7.
Figure 1.3. Central structure of a Ru porphyrin.....	9.
Figure 1.4. Abbreviated structures of <i>cis</i> -RuCl ₂ (DMSO) ₃ (DMSO) and <i>trans</i> -RuCl ₂ (DMSO) ₄ , respectively. (S = S-bound DMSO and O = O-bound DMSO).....	10.
Figure 1.5. Dissolution behaviour of (1) <i>cis</i> -RuCl ₂ (DMSO) ₄ and (2) <i>trans</i> -RuCl ₂ (DMSO) ₄ in aqueous solutions. (S = S-bound DMSO; O = O-bound DMSO).....	12.
Figure 1.6. Structures of reaction products of <i>cis</i> - and <i>trans</i> -RuCl ₂ (DMSO) ₄ with 2'-deoxyguanosine. (S = S-bound DMSO and 2'-dG = deoxyguanosine)....	14.
Figure 1.7. Dissolution behaviour of (1) <i>mer</i> -RuCl ₃ (DMSO) ₂ (DMSO) and (2) <i>trans</i> -[(DMSO) ₂ H] ⁺ [RuCl ₄ (DMSO) ₂] ⁻ in aqueous solutions. (S = S-bound DMSO and O = O-bound DMSO).....	15.
Figure 1.8. Abbreviated structures of <i>mer</i> -RuCl ₃ (DMSO) ₂ Im and Na[<i>trans</i> -RuCl ₄ (DMSO)(Im)]. (S = S-bound DMSO, O = O-bound DMSO and Im = imidazole).....	16.
Figure 1.9. Structures of 2-nitroimidazole (R = CH ₂ CHOHCH ₂ OCH ₃ = misonidazole, R = CH ₂ C(O)NHCH ₂ CH ₂ OH = etanidazole), 4-nitroimidazole (R = H) and 5-nitroimidazole (R = CH ₂ CH ₂ OH = metronidazole).....	18.
Figure 1.10. Structure of disulfoxides. ((<i>n</i> = 2) BMSE, R = Me; BESE, R = Et; BPSE, R = Pr; BBSE, R = Bu; BPeSe, R = Pe; BHSE, R = He; BCySE, R = Cy; BPhSE, R = Ph and (<i>n</i> = 3) BMSP, R = Me; BESP, R = Pr; BPSP, R = Pr; B ⁱ PSP, R = ⁱ Pr; BBSP, R = Bu; BPeSP, R = Pe; BPhSP, R = Ph).....	20.

Figure 2.1. Diagram showing the labelling of the H-atoms of 1,2-bis(cyclohexylthio)ethane.....	41.
Figure 3.1. Structure (1) and resonance forms (2) of a sulfoxide.....	64.
Figure 3.2. Structures of <i>catena</i> -poly[<i>cis</i> -Cl ₂ - <i>trans</i> -CH ₃ Sn(IV)](<i>μ</i> -O, O'- <i>meso</i> -BPSE) (1) and [SnCl- <i>cis</i> -Ph ₃] ₂ (<i>μ</i> -O, O'- <i>rac</i> -1,2-bis(<i>n</i> -propylsulfinyl)ethylene) (2).....	77.
Figure 3.3. Structures containing <i>μ</i> -BPhSE.....	78.
Figure 3.4. (1) R = H, (<i>SS</i>)-bis(<i>p</i> -tolylsulfinyl)methane; and R = CH ₃ , (<i>SS</i>)-2,2-bis- <i>p</i> -tolylsulfinylpropane. (2) (<i>SS</i>)-1,2-bis(<i>p</i> -tolylsulfinyl)benzene.....	79.
Figure 3.5. Structures of dios ((2 <i>R</i> 3 <i>R</i>)-2,3- <i>O</i> -isopropylidene-2,3-dihydroxy-1,4-bis(methylsulfinyl) butane monohydrate) (1), bdios ((2 <i>R</i> 3 <i>R</i>)-2,3- <i>O</i> -isopropylidene-2,3-dihydroxy-1,4-bis(benzylsulfinyl) butane monohydrate) (2), and ddios ((2 <i>R</i> 3 <i>R</i>)-2,3-dihydroxy-1,4-bis(methylsulfinyl) butane (3)...	80.
Figure 3.6 General structure for (1) <i>cis</i> -RuCl ₂ (BMSP) ₂ and <i>cis</i> -RuCl ₂ (BESE) ₂ and (2) <i>trans</i> -RuCl ₂ (BMSE) ₂ and <i>trans</i> -RuCl ₂ (BPSE) ₂ ; S [^] S = chelating disulfoxide.....	82.
Figure 3.7. An ORTEP drawing of <i>trans</i> -RuCl ₂ (BESE) ₂ with 50 % probability thermal ellipsoids shown (crystal data given in Appendix 1.1). For the data of Table 3.8, S(4) and S(3) are taken as <i>trans</i> to S(2) and S(1), respectively.	87.
Figure 3.8. An ORTEP drawing of the Δ configuration of <i>cis</i> -RuCl ₂ (BBSE) ₂ ·EtOH with 50 % probability thermal ellipsoids shown; H-atoms (except for that of EtOH) are omitted for clarity	91.
Figure 3.9. An ORTEP drawing of the Λ configuration of <i>cis</i> -RuCl ₂ (BCySE) ₂ ·EtOH·1/3MeOH with 50 % probability thermal ellipsoids shown; H-atoms are omitted for clarity (crystal data given in Appendix 1.3)	94.
Figure 3.10. An ORTEP drawing of the Δ configuration of <i>cis</i> -RuCl ₂ (BESP) ₂ ·EtOH·H ₂ O with 50 % probability thermal ellipsoids shown; H-atoms are omitted for clarity (crystal data given in Appendix 1.4).....	96.
Figure 3.11. The unit cell of <i>cis</i> -RuCl ₂ (BESP) ₂ ·EtOH·H ₂ O showing the EtOH and H ₂ O solvate molecules (crystal data given in Appendix 1.4).....	97.

Figure 3.12. An ORTEP drawing of $[\text{RuCl}(\text{BESE})(\text{H}_2\text{O})]_2(\mu\text{-Cl})_2$ with 50 % probability thermal ellipsoids (crystal data given in Appendix 1.5).....	103.
Figure 3.13. Diagram of $[\text{RuCl}(\text{BESE})(\text{H}_2\text{O})]_2(\mu\text{-Cl})_2$ showing the H_2O solvate (crystal data given in Appendix 1.5).....	104.
Figure 3.14. Structures of <i>SS</i> -chiraphos and <i>RR</i> -diop.....	107.
Figure 3.15. Structures of α -pyridone (1), 1-methylthymine (2) and creatinine (3)..	109.
Figure 3.16. Structures of $[(\text{NH}_3)_4\text{Pt}_2(\text{C}_5\text{H}_4\text{NO})_2]_2(\text{NO}_3)_5 \cdot \text{H}_2\text{O}$ (1), $[(\text{NH}_3)_2\text{Pt}(\text{C}_6\text{H}_7\text{N}_2\text{O}_2)_2\text{Pt}(\text{NH}_3)_2](\text{NO}_3)_2 \cdot \text{H}_2\text{O}$ (2), $[\text{Pt}_2(\text{NH}_3)_4(\text{C}_4\text{H}_7\text{N}_3\text{O})_2](\text{NO}_3)_2$ (3), and $[(\text{NH}_3)_2\text{Pt}(\text{CH}_3\text{CONH})_2\text{Pt}(\text{NH}_3)_2]_4\text{-(NO}_3\text{)}_{10} \cdot 4\text{H}_2\text{O}$ (4).....	109.
Figure 3.17. The ^1H NMR (200 MHz, CDCl_3) spectrum showing the paramagnetic shift caused by $[\text{RuCl}(\text{BPSP})]_2(\mu\text{-Cl})_3$ (8.8×10^{-2} M) of the residual CHCl_3 relative to that of the reference CHCl_3 . (A = residual CHCl_3 in CDCl_3 , and B = residual CHCl_3 peak shifted by $[\text{RuCl}(\text{BPSP})]_2(\mu\text{-Cl})_3$).....	111.
Figure 3.18. An ORTEP drawing of one of the $[\text{RuCl}(\text{BPSP})]_2(\mu\text{-Cl})_3$ units with 50 % probability thermal ellipsoids shown; H-atoms are omitted for clarity (crystal data given in Appendix 1.6).....	113.
Figure 3.19. A diagram of $[\text{RuCl}(\text{BPSP})]_2(\mu\text{-Cl})_3$ showing short H-bonds connecting two asymmetric units via four H_2O molecules (the CH_2Cl_2 atoms are not shown) (crystal data given in Appendix 1.6).....	114.
Figure 3.20. Proposed mechanism for the behaviour of $[\text{RuCl}(\text{BPSP})]_2(\mu\text{-Cl})_3$ in aqueous solution; the two Ru(II)/Ru(III) centres are not distinguished crystallographically, and loss of the chlorides is assumed to be from the terminal positions (the propyl groups of BPSP are omitted for clarity).....	117.
Figure 3.21. ^1H NMR spectra of equilibrated $[\text{RuCl}(\text{BPSP})]_2(\mu\text{-Cl})_3$ in D_2O (after 2 h) (A) and immediate spectrum of $[\text{RuCl}(\text{BPSP})]_2(\mu\text{-Cl})_3$ (2.02×10^{-3} M) after addition of two or three equivalents of AgNO_3 in D_2O (B).....	118.

Figure 3.22. A representative spectrum of the UV-Vis spectral changes (200-600 nm region, 1 cm cell) of $[\text{RuCl}(\text{BPSP})]_2(\mu\text{-Cl})_3$ (2.96×10^{-4} M) in an aqueous solution at 27 °C as a function of time (half life $t_{1/2} = 120$ s, for the pseudo-first order process); isosbestic points are observed at the noted wavelengths.....	120.
Figure 3.23. Absorption spectral changes at $\lambda = 362$ nm as a function of time for the reaction of $[\text{RuCl}(\text{BPSP})]_2(\mu\text{-Cl})_3$ in H_2O (55.6 M) at 27 °C.....	121.
Figure 3.24. A representative rate-plot analyzed for a first-order dependence on $[\text{RuCl}(\text{BPSP})]_2(\mu\text{-Cl})_3$; A_t and A_∞ represent the absorption at 362 nm at times t and ∞ , respectively, at 27 °C.....	121.
Figure 3.25. The dependence of the pseudo-first-order rate constant, k_{obs} , on $[\text{H}_2\text{O}]$ at 27 °C; including the k_{obs} values obtained from reactions run in 0.25 M aqueous NaCl and 0.1 M aqueous toluene-4-sulfonic acid (in $\text{H}_2\text{O}/\text{CH}_3\text{CN}$ solutions).....	122.
Figure 3.26. The dependence of the second-order rate constant k_1 on $[\text{RuCl}(\text{BPSP})]_2[(\mu\text{-Cl})_3]$ in H_2O (22.2 M) at 27 °C. ($\text{Ru} = [\text{RuCl}(\text{BPSP})]_2(\mu\text{-Cl})_3$).....	123.
Figure 3.27. Eyring plot for the temperature dependence of the rate constant k_1 for the reaction of $[\text{RuCl}(\text{BPSP})]_2(\mu\text{-Cl})_3$ (2.96×10^{-4} M) with H_2O (22.2 M).....	123.
Figure 3.28. An ORTEP drawing of <i>trans</i> - $\text{RuCl}_2(\text{BCyTE})_2 \cdot 2\text{CH}_2\text{Cl}_2$ with 50 % probability shown; H-atoms are omitted for clarity (the CH_2Cl_2 molecules are not shown) (crystal data are given in Appendix 1.7).....	131.
Figure 3.29. The unit cell of <i>trans</i> - $\text{RuCl}_2(\text{BCyTE})_2 \cdot 2\text{CH}_2\text{Cl}_2$ showing the 2 CH_2Cl_2 solvate molecules (crystal data given in Appendix 1.7).....	132.
Figure 3.30. Resonance structures of a phenyl ring with a thioether.....	134.
Figure 3.31. An ORTEP drawing of <i>trans</i> - $\text{RuCl}_2(\text{BPhTE})_2$ with 50 % probability thermal ellipsoids shown; H-atoms are omitted for clarity (crystal data are given in Appendix 1.8).....	135.

Figure 3.32. An ORTEP drawing of $[\text{RuCl}_2(\text{BETP})]_2(\mu\text{-Cl})_2$ with 50 % probability thermal ellipsoids shown; H-atoms are omitted for clarity (crystal data are given in Appendix 1.9).....	138.
Figure 3.33. An ORTEP drawing of $[\text{RuCl}_2(\text{BPTP})]_2(\mu\text{-Cl})_2$ with 50 % probability thermal ellipsoids shown. The H-atoms are omitted for clarity (crystal data are given in Appendix 1.10).....	139.
Figure 3.34. Structure of <i>mer</i> - $[\text{RuCl}_3(\text{DPSO})(\text{DPSO})(\text{MeOH})]$; O and S are O- and S-bonded DPSO, respectively.....	140.
Figure 3.35. An ORTEP diagram of <i>mer-cis</i> - $[\text{RuCl}_3(\text{DPSO})_2(\text{DPSO})]$ showing 50 % thermal ellipsoids; the H-atoms are omitted for clarity (crystal data are given in Appendix 1.11).....	143.
Figure 3.36. 3,6,9,14-Tetrathiabicyclo[9.2.1]tetradeca-11,13-diene (L), and 1,4,7,10-tetrathiacyclododecane (12-S-4); H-atoms omitted.	146.
Figure 3.37. An ORTEP diagram of $\text{RuCl}_2(\text{DMSO})(\text{L})$ showing 50 % thermal ellipsoids; the H-atoms are omitted for clarity (crystal data are given in Appendix 1.12).....	148.
Figure 3.38. An ORTEP diagram of $[\text{Ru}(12\text{-S-4})(\text{DMSO})(\text{H}_2\text{O})][\text{OTf}]_2$ showing 50 % thermal ellipsoids; the H-atoms are omitted for clarity (crystal data are give in Appendix 1.13).....	153.
Figure 4.1. The absence of toxicity of $[\text{RuCl}(\text{BPSP})]_2(\mu\text{-Cl})_3$ in CHO cells.....	174.
Figure 4.2. Accumulation of Ru (A) and Ru-DNA-binding (B) in CHO cells after 2 h incubation with $[\text{Ru}(12\text{-S-4})(\text{DMSO})(\text{H}_2\text{O})][\text{OTf}]_2$ (1), $[\text{RuCl}(\text{BPSP})]_2(\mu\text{-Cl})_3$ (2), $[\text{RuCl}(\text{BESE})(\text{H}_2\text{O})]_2(\mu\text{-Cl})_2$ (3), $[\text{RuCl}(\text{BPSE})(\text{H}_2\text{O})]_2(\mu\text{-Cl})_2$ (4), $[\text{RuCl}(\text{BBSE})(\text{H}_2\text{O})]_2(\mu\text{-Cl})_2$ (5).....	176.

Figure 4.3. Accumulation (A) and DNA-binding (B) with 0.5 mM Ru. 1 = <i>cis</i> -RuCl ₂ (DMSO) ₄ , 2 = <i>trans</i> -RuCl ₂ (DMSO) ₄ , 3 = <i>cis</i> -RuCl ₂ (TMSO) ₄ , 4 = <i>trans</i> -RuCl ₂ (BMSE) ₂ , 5 = <i>cis</i> -RuCl ₂ (BESE) ₂ , 6 = <i>trans</i> -RuCl ₂ (BPSE) ₂ , 7 = <i>cis</i> -RuCl ₂ (BMSP) ₂ , 8 = [Ru(12-S-4)(DMSO)(H ₂ O)][OTf] ₂ , 9 = [RuCl(BPSP)] ₂ (μ-Cl) ₃ , 10 = [RuCl(BESE)(H ₂ O)] ₂ (μ-Cl) ₂ , 11 = [RuCl(BPSE)(H ₂ O)] ₂ (μ-Cl) ₂ , 12 = [RuCl(BBSE)(H ₂ O)] ₂ (μ-Cl) ₂	179.
Figure 5.1. Ru(II)(Porp)(CO) species, showing the numbering system.....	187.
Figure 5.2. An ORTEP diagram of Ru(OEP)(CO)(THF) showing 50 % thermal ellipsoids; the H-atoms are omitted for clarity (crystal data are given in Appendix 1.14).....	196.
Figure 5.3. Structures of (1) = TEMPO = 2,2,6,6-tetramethylpiperidine-1-oxyl, (2) = DAPO = <i>trans</i> 3,4,-diamino-2,2,6,6-tetramethyl piperidine-1-oxyl, (3) = TEMPICOL-2 = 4-hydroxy-4-(2-picolyl)-2,2,6,6-tetramethylpiperidine-1-oxyl.....	198.
Figure 5.4. An ORTEP diagram of Ru(TPhP)(CO)(py) showing 50 % thermal ellipsoids; the H-atoms have been omitted for clarity (crystal data are given in Appendix 1.15).....	200.
Figure 5.5. Fluorescence spectrum of Na ₄ [Ru(TSPHP)(CO)]·4H ₂ O. The excitation wavelength was 414 nm and emission was measured at 641 and 704 nm.....	202.
Figure 6.1. Structural diagram of <i>cis</i> -RuCl ₂ (BPhSP)(1-(phenylthio)-3-(phenylsulfinyl)propane).....	214.
Figure 6.2. A potentially water-soluble disulfoxide.....	215.
Figure A.1.1. Stereoview of <i>cis</i> -RuCl ₂ (BBSE) ₂ ·EtOH.....	A.226.
Figure A.1.2. Stereoview of <i>cis</i> -RuCl ₂ (BCySE) ₂ ·EtOH·1/3MeOH.....	A.230.
Figure A.1.3. Stereoview of [RuCl(BESE)(H ₂ O)] ₂ (μ-Cl) ₂ ·H ₂ O.....	A.237.
Figure A.1.4. Stereoview of [RuCl(BPSP)] ₂ (μ-Cl) ₃ ·2H ₂ O·2.5CH ₂ Cl ₂	A.244.
Figure A.1.5. Stereoview of <i>trans</i> -RuCl ₂ (BCyTE) ₂ ·2CH ₂ Cl ₂	A.248.
Figure A.1.6. Stereoview of <i>trans</i> -RuCl ₂ (BPhTE) ₂	A.252.
Figure A.1.7. Stereoview of Ru(OEP)(CO)(THF).....	A.271.

Figure A.3.1. TGA of $[\text{RuCl}(\text{BESE})(\text{H}_2\text{O})]_2(\mu\text{-Cl})_2$	A.277.
Figure A.3.2. TGA of $[\text{RuCl}(\text{BPSP})]_2(\mu\text{-Cl})_3$	A.278.
Figure A.3.3. TGA of $\text{Na}_4(\text{H}_2\text{TSPHP}) \cdot 15\text{H}_2\text{O}$	A.279.
Figure A.3.4. TGA of $\text{Na}_4[\text{Ru}(\text{TSPHP})(\text{CO})] \cdot 4\text{H}_2\text{O}$	A.279.
Figure A.4.1. Accumulation of Ru in CHO cells after a 2 h incubation with $[\text{Ru}(12\text{-S-4})(\text{DMSO})(\text{H}_2\text{O})][\text{OTf}]_2$ (1), $[\text{RuCl}(\text{BPSP})]_2(\mu\text{-Cl})_3$ (2), $[\text{RuCl}(\text{BESE})(\text{H}_2\text{O})]_2(\mu\text{-Cl})_2$ (3), $[\text{RuCl}(\text{BPSE})(\text{H}_2\text{O})]_2(\mu\text{-Cl})_2$ (4), $[\text{RuCl}(\text{BBSE})(\text{H}_2\text{O})]_2(\mu\text{-Cl})_2$ (5).....	A.280.
Figure A.5.1. Ru-DNA-binding after incubation with $[\text{Ru}(12\text{-S-4})(\text{DMSO})(\text{H}_2\text{O})][\text{OTf}]_2$ (1), $[\text{RuCl}(\text{BPSP})]_2(\mu\text{-Cl})_3$ (2), $[\text{RuCl}(\text{BESE})(\text{H}_2\text{O})]_2(\mu\text{-Cl})_2$ (3), $[\text{RuCl}(\text{BPSE})(\text{H}_2\text{O})]_2(\mu\text{-Cl})_2$ (4), $[\text{RuCl}(\text{BBSE})(\text{H}_2\text{O})]_2(\mu\text{-Cl})_2$ (5).....	A.281.

List of Abbreviations

Abbreviation	Meaning
AAS	atomic absorption spectroscopy
AMP	adenine monophosphate
APT	attached proton test
aq.	aqueous
BMSB	1,4-bis(methylsulfinyl)butane
BMSP	1,3-bis(methylsulfinyl)propane
BESP	1,3-bis(ethylsulfinyl)propane
BPSP	1,3-bis(propylsulfinyl)propane (all alkyl groups are <i>n</i> unless otherwise indicated)
B ⁱ PSP	1,3-bis(<i>i</i> -propylsulfinyl)propane
BBSP	1,3-bis(butylsulfinyl)propane
BPeSP	1,3-bis(pentylsulfinyl)propane
BPhSP	1,3-bis(phenylsulfinyl)propane
BMSE	1,2-bis(methylsulfinyl)ethane
BESE	1,2-bis(ethylsulfinyl)ethane
BPSE	1,2-bis(propylsulfinyl)ethane
BBSE	1,2-bis(butylsulfinyl)ethane
BPeSE	1,2-bis(pentylsulfinyl)ethane
BHSE	1,2-bis(hexylsulfinyl)ethane
BCySE	1,2-bis(cyclohexylsulfinyl)ethane
BPhSE	1,2-bis(phenylsulfinyl)ethane
BPhTE	1,2-bis(phenylthio)ethane
BCyTE	1,2-bis(cyclohexylthio)ethane
BETP	1,3-bis(ethylthio)propane
BPTP	1,3-bis(propylthio)propane
BBTP	1,3-bis(butylthio)propane
BPeTP	1,3-bis(pentylthio)propane
br	broad (NMR and IR)

B. M.	Bohr magneton
b. p.	boiling point
BPP	dianion of 5,15-bis(phenyl)porphyrin
CHO	Chinese hamster ovary (a cell line)
COSY	correlated spectroscopy
GMP	guanine monophosphate
2D	2-dimensional (NMR)
DMS <u>O</u>	dimethylsulfoxide coordinated via the S-atom
DMS <u>O</u>	dimethylsulfoxide coordinated via the O-atom
DPSO	diphenylsulfoxide
EI	electron impact ionization
e.s.d.	estimated standard deviation
FAB	fast atom bombardment
HEPES	N-2-hydroxyethylpiperazine-N'-2-ethane sulfonic acid
HETCOR	heteroatom correlation spectroscopy
m. p.	melting point
MALDI	matrix assisted laser desorption ionization
<u>O</u>	O-bonded
OD	optical density
OEP	dianion of 2,3,7,8,12,13,17,18-octaethylporphyrin
ORTEP	Oakridge Thermal Ellipsoid Program
OTf	triflate (CF_3SO_3^-)
PBS	phosphate buffered saline
PE	plating efficiency
Porp	porphyrin dianion
r. t.	room temperature
r. p. m.	revolutions per minute
<u>S</u>	S-bonded
SDS	sodium dodecylsulfate

TE	tris(hydroxymethyl)aminomethane+ethylenediaminetetraacetic acid
TGA	thermal gravimetric analysis
TMSO	tetramethylene sulfoxide
TNE	TE + 150 mM NaCl
TPhP	dianion of 5,10,15,20-tetraphenylporphyrin
TSPhP	dianion of 5,10,15,20-tetrakis(4-sulfonato)phenylporphyrin
TrPhPyNO	dianion of 5,10,15-triphenyl-20-(4-pyridyl- <i>N</i> -oxide)porphyrin
Λ_M	molar conductivity
μ_{eff}	magnetic moment

Acknowledgements

I would very much like to thank my supervisors Brian James and Kirsten Skov for their encouragement, guidance, patience and support over the years and for providing myself the opportunity to work with them.

Many thanks to the departmental services, especially Marietta Austria, Peter Borda, Lianne Diarge, Steve Rak and the late Steve Rettig and from the BC Cancer Research Centre Hans Adomat, Jennifer Dekker, Manuel Gierth and Haibo Zhou. I would also like to thank Joanne Crocker, Lionel Harrison, Peter Wassell and Dana Zendrowski.

I thank all past and present members of the James Gang.

Special thanks go to Bianca Kuipers, Heather Dobson, Annie Schnyder, Krystyna Skupinska and Gay and Ipi Yuyitung for the hiking, kayaking and skiing trips and of course, the coffee breaks. I would also like to thank Janet Gamelin, Hoa Ly, Matt Netherton, Dave Voadlo, Alex Wong, James Yee, Eliza Jang, Asa Sophia Timms Maglio, Trish Mah, Debbie Sangra and Lesia Zorniak.

Most importantly I must thank my father, mother, Lillian and Rod for all their love and support over the years.

Thanks for the many "Hello, how are you today?" –Larry Weiler.

I dedicate this thesis to the memory of Steve Rettig.

Chapter 1

Introduction

1.1 Preamble

Prior studies in this laboratory on sulfoxides, particularly chiral sulfoxides, were mainly focussed on the potential of complexes of ruthenium(II) as catalysts for homogeneous hydrogenations.¹ Recently, the Trieste group reported that *cis*- and *trans*-RuCl₂(DMSO)₄ possess mutagenic properties, exhibit anti-cancer activity and interact with nucleobases of DNA (see Section 1.4). Previous studies from our laboratories had utilized such complexes as precursors for the synthesis of Ru(II)-sulfoxide-nitroimidazole complexes as potential radiosensitizers (see Section 1.4.3).

Cancer is a progressive disease in which malignant tissue can be distinguished from normal tissue by its property of abnormal, uncontrolled and invasive growth.² Early stages of cancer may be treated by a combination of surgery and radiotherapy, but more advanced stages require chemotherapy.² Cancer occurs in many forms depending on the part of the body and the type of cells involved. For example, most tumours occur as a localized grouping of cancerous cells, while in others such as leukemia, the malignant cells are widely dispersed in the blood stream.³ Chemotherapy involves directing toxic agents towards the malignant cells. Chemotherapy for lung, breast and colorectal cancers, which account for approximately 50 % of all cancer deaths in the industrialized Western world, usually results only in prolonged survival.² One of the major problems of chemotherapy is that chemotherapeutic agents do not exhibit selective toxicity for cancer cells over normal cells. Understanding the mechanisms of tumour biology, cellular processes involving tumour cells, and the interaction of

chemotherapeutic agents with cancer cells will greatly improve treatment modalities of this disease.

Chemotherapeutic agents are primarily organic compounds or natural products including alkylating agents, antibiotics and alkaloids.⁴ Inorganic compounds were not extensively studied as anti-cancer agents until the discovery of cisplatin (Figure 1.1).⁵ Since this discovery, there has been substantial interest in the development of inorganic complexes as potential anti-tumour agents but progress has been slow.

1.2 Development of Platinum Chemotherapeutic Agents

Cisplatin has a proven efficacy against a wide variety of malignancies and is used in the treatment of solid tumours such as ovarian and testicular cancer, as well as head and neck, lung and cervical carcinomas.⁶ Breast cancer is also recognized as a potential target for cisplatin therapy.⁶ Furthermore, it is also used in combination chemotherapy for a variety of other malignancies.⁶ Extraordinarily good results were attained in the treatment of testicular cancer.⁶ Moreover, in ovarian cancer, remission rates of up to 50 % have been documented.⁶ However, because of the compound's toxicity (*e.g.* nausea, ear damage, vomiting, loss of sensation in hands and kidney toxicity),⁷ research has been on-going to develop analogues which are less toxic.

Sherman and Lippard have reported evidence that DNA is the cellular target of Pt drugs from studies of their incubation with DNA and interaction with lysogenic strains of *E. coli*,⁸ while Bloemink and Reedijk have presented reviews of the mechanism of cisplatin action and DNA-binding.^{7,9} The key elements of the mechanism appear to be: (1) controlled hydrolysis, transport and binding of cisplatin to DNA; (2) a specific binding at neighbouring

guanine bases, specifically at the N7 atoms; and (3) a specific distortion of DNA, altering interactions with proteins. Whitehead and Lippard have reported on the role of structure-specific proteins that mediate cisplatin cytotoxicity.¹⁰ Oldenberg and Los reviewed studies showing that cellular damage produced by cisplatin provokes a programmed response that results in the activation of some genes, the inactivation of others, major shifts in cellular metabolism, and cell cycle progression, eventually triggering apoptosis.⁶ They also summarize studies which show that proliferating cells are much more sensitive to the toxicity of the drug, indicating that cell-cycle associated events are involved in cisplatin cytotoxicity.⁶

A second generation analogue of cisplatin, carboplatin¹¹ (Figure 1.1), offers reduced toxicity together with therapeutic activity similar to that of cisplatin.

The complex bis(acetato)amminedichloro(cyclohexylamine)Pt(IV) (JM 216)¹² is the first orally bioavailable Pt complex and is currently in Phase II clinical trials (Figure 1.1). This novel Pt(IV) complex has demonstrated promising oral activity against a variety of murine and human tumour models, and *in vitro* cytotoxic effects against a tumour line that exhibits intrinsic resistance to cisplatin.¹² This complex was designed primarily to improve quality of life during Pt-based chemotherapy.

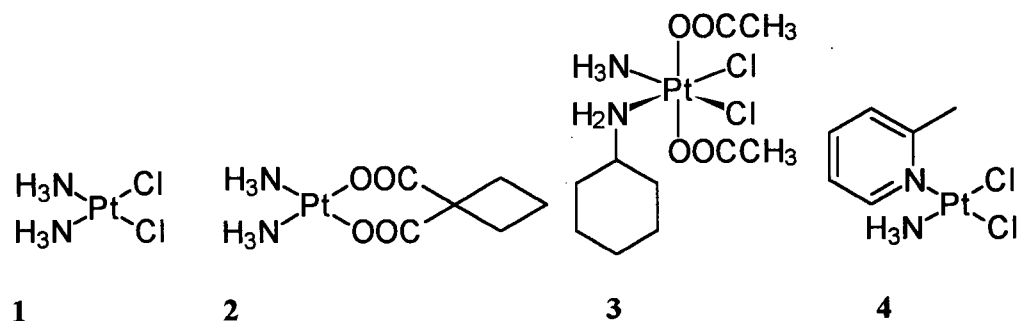


Figure 1.1. 1 = *Cis*-diamminedichloroPt(II) (Cisplatin), 2 = Diammine(cyclobutane-1-1-dicarboxylato)Pt(II) (Carboplatin), 3 = Bis(acetato)amminedichloro-(cyclohexylamine)Pt(IV) (JM 216),¹² 4 = Amminedichloro(2-methylpyridine)Pt(II) (AMD 473).¹³

Recently, the complex amminedichloro(2-methylpyridine)Pt(II) (AMD 473)¹³ (Figure 1.1) has been developed as a third generation Pt complex designed to circumvent cellular resistance *in vitro* and enhance *in vivo* activity. In recognition of an increasing awareness of the mechanisms by which tumours might become resistant to cisplatin (*e.g.* cytoplasmic detoxification by cellular thiols or increased DNA repair/tolerance of Pt-DNA adducts) in the clinic, AMD 473 was designed primarily to prevent thiol-mediated drug resistance by sterically hindering its reaction with glutathione by introduction of steric bulk (2-methylpyridine) at the Pt centre.¹³ This complex reached Phase I clinical trials.

Day and Sadler *et al.* have reported that iodo complexes of Pt(IV) show promise in the design of oxygen-independent photoactivated metallodrugs.¹⁴ Photoactive analogues of cisplatin, particularly *trans,cis*-[Pt(OCOCH₃)₂I₂(¹⁵N-en)] was shown to react with guanosine 5'-monophosphate upon exposure to visible light to give [Pt(5'-GMP-N7)₂(en)]²⁺.^{14b}

Development of new generation Pt complexes has taken into consideration these characteristics: charge, lipophilicity, stability in the gastric environment, oral bioavailability, a

cis arrangement of labile ligands (this permits binding and intrastrand cross-linking of DNA) and a limited toxicity to the host organism.¹⁵ An exception, work by Farrell *et al.*, has shown that certain *trans* and di- and tri-nuclear Pt complexes show anti-tumour activity with a mechanism of action that is different from that of cisplatin. One of these, a tri-nuclear Pt complex is in Phase I trials.¹⁶

1.3 Ruthenium Chemotherapeutic Agents

The potential of ruthenium complexes as anti-cancer agents has been extensively explored along with fundamental studies on their interactions with molecules of biological interest (*e.g.* nucleic acids).^{17,18} One difference between Pt-based and Ru-based anti-tumour agents is that Ru complexes are usually octahedral, six-coordinate as opposed to the square-planar, four-coordinate geometry of Pt(II) complexes. The two additional coordination sites for Ru complexes may allow new modes of binding to nucleic acids and, with some ligands, provide for chirality in the complexes and so in their interactions with the DNA helix.¹⁹ Of note, Milkevitch *et al.* have reported on mixed-metal Ru(II)/Pt(II) complexes as DNA-binding agents.²⁰

The sequence of events that Ru complexes undergo following injection into a living body have been elucidated.²¹

1. Ru binds to transferrin and is selectively distributed to transferrin-rich receptor tissues (of note, high amounts of transferrin receptors are found on tumour cells²²).
2. Ru exhibits a low capacity of exchange reactions but binds to molecules of biological interest (*e.g.* nucleic acids).
3. Ru exhibits a high DNA binding affinity.

Ru complexes have been studied in comparison to cisplatin in order to improve the efficacy of these metal-containing drugs by reducing toxicity and increasing potency.¹⁸ Several studies show that a number of Ru complexes serve as bacterial mutagens, and so indicate that some Ru complexes are capable of damaging genetic material.¹⁸ As well, studies have shown that ammine complexes of both Ru(II) and Ru(III) bind to DNA in a fashion analogous to that of cisplatin.²³ Keppler *et al.* have studied the anti-tumour activities of a series of imidazole complexes of Ru including $[\text{ImH}]_2[\text{RuImCl}_5]$,²⁴ $[\text{ImH}][\text{RuIm}_2\text{Cl}_4]$ ^{22,25} and other $[\text{HL}][\text{RuL}_2\text{Cl}_4]$ species ($\text{L} = e.g.$ imidazole derivatives such as 1-butyl, pyrazole and derivatives such as 3,5-diethyl, and indazole and derivatives such as 1-methyl), with clinical trials planned for $[\text{IndH}][\text{RuInd}_2\text{Cl}_4]$.²⁶ This compound is active against transplantable tumours and tumours induced by intrarectal application of a carcinogen and shows higher anti-tumour activity than that of $[\text{ImH}][\text{RuIm}_2\text{Cl}_4]$.²⁷ Of note, Mestroni *et al.* have synthesized and characterized the Rh analogue $[\text{ImH}][\text{RhIm}_2\text{Cl}_4]$, but there was no relevant anti-tumour activity.²⁸

The dominant mode of pentaammineruthenium coordination to purine nucleosides with a keto group at the 6-position is at the N7 position on the imidazole ring (Figure 1.2(1)).¹⁸ Attachment at the N(7) of deoxyguanosine, which is thought to be the initial point of attack of the Pt pharmaceuticals on DNA, has been shown to occur for ammineruthenium(II and III) ions.²⁹ Clarke and Stubbs have reviewed the interactions of “metallopharmaceuticals”, including Ru species, with DNA.³⁰

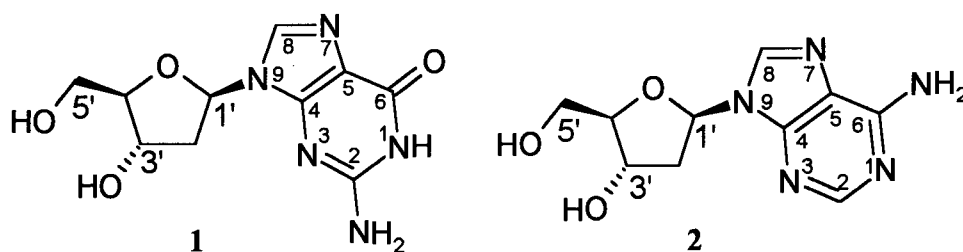


Figure 1.2. Structures of deoxyguanosine (1) and deoxyadenosine (2).

Advantage can be taken of the ready availability of both the Ru(II) and Ru(III) oxidation states under physiological conditions and the general inertness of these ions toward substitution, when coordinated to N-ligands.¹⁸ The chemical properties of Ru(II) vs. Ru(III) suggest that ammine Ru(III) ions should be far less active toward binding nitrogen ligands (*e.g.* nucleic acids) than analogous Ru(II) complexes.¹⁸ Thus, a relatively inactive and ideally non-toxic Ru(III) complex might be activated toward binding to nitrogen heterocycles by *in vivo* reduction.²¹ For example, a complex such as *cis*-Ru(H₂O)₂(NH₃)₄²⁺ readily substitutes its water molecules to bind nitrogen ligands in solution whereas analogous Ru(III) complexes are more substitution inert.¹⁸ Thus a complex such as *cis*-RuCl₂(NH₃)₄⁺, when introduced into an organism, might remain largely intact and so fairly innocuous until reduced to yield the “active” Ru(II) form, *cis*-Ru(H₂O)₂(NH₃)₄²⁺ which could then bind to critical cellular components and induce toxicity.¹⁸ This leads to the important proposal that some Ru(III) complexes could be administered as prodrugs which should be relatively non-toxic until activated by reduction,²¹ and indeed higher cytotoxicity and DNA-binding of [ImH][RuIm₂Cl₄] and *cis*-[Ru(NH₃)₄Cl₂]Cl were observed in human cervical cancer cells (HeLa) at low oxygen levels.³¹ This observation is consistent with the “activation-by-reduction” hypothesis where the Ru(II) should be more prevalent inside hypoxic tumours.³¹

1.3.1 Dinuclear Ru(II)/Ru(III) Complexes

The discovery of cisplatin as an effective anti-tumour agent was made after the observation that cisplatin induced filamentous growth in *E. coli*.⁵ The mechanism of cisplatin anti-tumour activity is based on cisplatin binding to DNA, modification of the DNA template and selective inhibition of DNA replication.⁶⁻¹⁰ One indication of DNA damage or error-prone repair in bacteria is filamentous growth. Thus the testing of filamentation in bacteria provides a useful indication of possible mutagenicity or toxicity of the complex.

Durig *et al.* extended the studies of filamentous growth of *E. coli* by Pt complexes to include Ru and Pd complexes.³² These studies showed that *fac*-Ru(NH₃)₃Cl₃ induced an amount of filamentous growth at concentrations comparable to that of cisplatin (6 µg/mL), while significantly higher concentrations of K₂[RuCl₅(H₂O)] were needed to induce the same amount of growth. The Pd complexes, however, induced only minimum filamentous growth compared to that of the Ru complexes and cisplatin, and as well were toxic at relatively high concentrations.

Gibson *et al.* studied a series of dinuclear, mixed-valence complexes of Ru of the general formula Ru₂(NH₃)₆X₅·H₂O (where X = Cl, Br, or I) for their ability to induce filamentation in *E. coli*,³³ again for comparison with cisplatin data. The chloro (10⁻⁴ to 10⁻⁵ M) and bromo (10⁻⁵ M) complexes were at least as effective as cisplatin in inducing filamentation in *E. coli*. The bromo analogue was more effective than the chloro analogue and cisplatin, while the iodo analogue (10⁻³ to 10⁻⁴ M) was the least effective in inducing filamentous growth. This effect of filamentation is reversible on prolonged incubation and the presence of 0.43 M DMSO was effective in inhibiting filamentous

growth.³³ Ion-exchange studies suggested that the chloro complex is doubly charged with three bridging chlorides, $[\text{Ru}_2(\text{NH}_3)_6\text{Cl}_3]\text{Cl}_2\cdot\text{H}_2\text{O}$.³⁴ Hughes *et al.* have structurally characterized $[\text{Ru}_2(\text{NH}_3)_6\text{Cl}_3][\text{BPh}_4]_2$ which has electronic spectra and magnetic properties identical to those of the chloride.³⁵

1.3.2 Metallated Porphyrins

Porphyrins have been reported to accumulate in tumours.³⁶ O'Hara *et al.* found certain metalloporphyrins to be effective hypoxic radiosensitizers³⁷ and previous work in this laboratory has involved the synthesis of water-soluble metalloporphyrins, including Ru(II) and Pt(II) species, as potential hypoxia selective agents.³⁸ Ru complexes have been shown to bind to DNA and have potential as anti-tumour agents (Section 1.3), and thus ideally, water-soluble Ru porphyrins (Figure 1.3) could result in a complex that is both a hypoxic radiosensitizer as well as an anti-tumour agent. Of note, Hartmann *et al.* have reported on the synthesis of water-soluble Ru porphyrins as potential "DNA cleavers and potential cytotoxic agents".³⁹

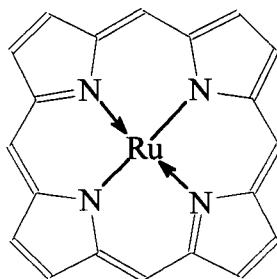


Figure 1.3. Central structure of a Ru porphyrin.

1.4 Development of Ruthenium Dimethylsulfoxide Complexes

DMSO increases the water-solubility of its complexes (thus facilitating membrane transport and penetration) and the good lability of an O-bonded DMSO, is linked to the nature of interactions with purine and pyrimidine bases.²¹ The characteristics of the DMSO ligand combined with those of Ru complexes have provided a new class of possible chemotherapeutic agents.

1.4.1 Ru(II)-Dimethylsulfoxide Complexes: Cis-RuCl₂(DMSO)₃(DMSO) and Trans-RuCl₂(DMSO)₄ (see Figure 1.4).

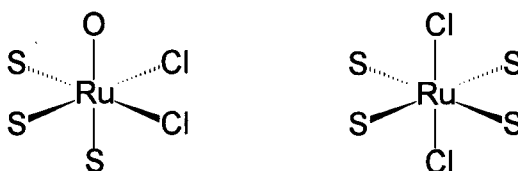


Figure 1.4. Abbreviated structures of *cis*-RuCl₂(DMSO)₃(DMSO) and *trans*-RuCl₂(DMSO)₄, respectively. (S = S-bound DMSO and O = O-bound DMSO).

In preliminary studies, *cis*-RuCl₂(DMSO)₄ exhibited interesting biological properties, in comparison to those of cisplatin, in Ehrlich ascites carcinoma and in L1210 lymphoid leukemia.⁴⁰ *Cis*-RuCl₂(DMSO)₄ at relatively high doses (100-800 mg/kg/day) exhibits marginal anti-tumour activity, but inhibits nucleic acid synthesis, and exerts a pattern of cell damage and mutagenicity similar to that of cisplatin at only (0.5-4 mg/kg/day).⁴⁰ The anti-neoplastic activity of *cis*-RuCl₂(DMSO)₄ was studied using three mouse tumour models: Lewis lung carcinoma, B16 melanoma and MCa mammary carcinoma.⁴¹ The complex (610 mg/kg) reduced primary tumour growth in all the tumours tested and, as well, these effects

were obtained with reduced host toxicity compared to equally effective dosages of cisplatin (0.52 mg/kg).⁴¹

The anti-tumour effects of *cis*- and *trans*-RuCl₂(DMSO)₄ tested on mice bearing the solid tumour, Lewis lung carcinoma, were then compared to those of cisplatin.⁴² The *trans* complex (76 µmol/kg/day) exhibited a greater antimetastatic effect compared to that of an equimolar concentration of the *cis* complex, particularly in the inhibition of primary tumour growth compared to metastatic growth.^{21,42} The toxicity of *trans*-RuCl₂(DMSO)₄ was 10-fold higher than that of the *cis* isomer.^{21,42} Sava *et al.* reported that the anti-tumour activities of these two complexes were qualitatively comparable, with the *trans* isomer being more effective, by preferentially inhibiting the weight rather than the number of artificial metastases.⁴² As well, both *cis*- and *trans*-RuCl₂(DMSO)₄ significantly prolonged the survival time of leukaemic mice, again with the effect of *trans*-RuCl₂(DMSO)₄ (48 mg/kg) being more pronounced than that of the *cis* isomer (800 mg/kg).⁴³ This prolongation of survival time of the mice suggests that these complexes can control the dissemination of tumour cells to the brain by a non-cytotoxic mechanism.⁴³

1.4.1.1 Chemical Behaviour of *Cis*-RuCl₂(DMSO)₃(DMSO) and *Trans*-RuCl₂(DMSO)₄ in Aqueous Solutions

The difference in activities between *cis*- and *trans*-RuCl₂(DMSO)₄ has been attributed to the different chemical behaviours of the species in aqueous solutions.⁴⁴ On dissolution, the *cis* isomer releases the single O-bonded DMSO immediately and then slow dissociation of Cl⁻ gives the mono-cationic species (Figure 1.5).^{44,45} The *trans* isomer, once

dissolved in water, releases two DMSO ligands, this step being followed by the slow release of the Cl^- ion (Figure 1.5).⁴⁴

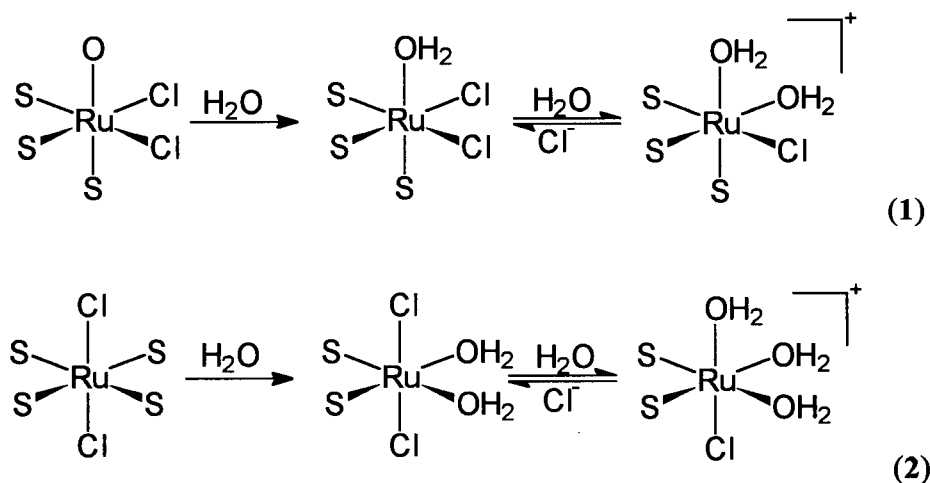


Figure 1.5. Dissolution behaviour of (1) *cis*- $\text{RuCl}_2(\text{DMSO})_4$ and (2) *trans*- $\text{RuCl}_2(\text{DMSO})_4$ in aqueous solutions. (S = S-bound DMSO; O = O-bound DMSO). Adapted from Ref. 44.

With the assumption that the coordinated water molecules are labile, the *cis* isomer under physiological conditions immediately generates a species with a single potential coordination site, while the *trans* isomer generates a species with two potential sites *cis* to one another. The neutral species should be able to cross the cell membrane. Once inside the cell, due to the low Cl^- concentration, both species should slowly lose a Cl^- and generate an additional coordination site. Accordingly, a higher reactivity in aqueous solution is expected for the *trans* isomer, under both extra- and intracellular conditions.⁴⁴ The relevant equilibria are affected by the presence of free Cl^- , and two Cl^- concentrations were tested, namely 3 mM and 150 mM, which represent conditions inside and outside the cell, respectively. In 3 mM aqueous NaCl solution the loss of Cl^- is observed, whereas in a 150 mM solution this process is inhibited (see Figure 1.5).⁴⁴

1.4.1.2 Binding of *Cis*-RuCl₂(DMSO)₃(DMSO) and *Trans*-RuCl₂(DMSO)₄ to DNA

Khan and Mehmood report that reactions between *cis*-RuCl₂(DMSO)₄ and adenine or cytosine lead to the isolation of Ru₂(adenine)₃(DMSO)₃Cl₄ or Ru₂(cytosine)₄(DMSO)₂Cl₄(CH₃OH)₄, respectively.⁴⁶ Cauci *et al.* reported that *cis*-RuCl₂(DMSO)₄ reacts in aqueous solution with double-stranded DNA to form Ru(II)-DNA complexes,⁴⁷ while a study of the interaction between *trans*-RuCl₂(DMSO)₄ and guanine by Alessio *et al.* indicated that the N7 and the α -phosphate group of guanine form a chelate with the composition [Ru(II)Cl(H₂O)(DMSO)₂(5'-d(GMP))]⁻.⁴⁸

NMR structural characterization and molecular modeling studies by Esposito *et al.* show that the reaction between *trans*-RuCl₂(DMSO)₄ and d(GpG) results in formation of a 1,2-intrastrand crosslink,⁴⁹ the final reaction product exhibiting structural features which are similar to those of the corresponding cisplatin complex with d(GpG).⁸ Studies by Tian *et al.* have provided further evidence for the binding modes of *cis*-RuCl₂(DMSO)₄ with 5'-GMP and 5'-AMP in aqueous solution under physiological conditions.⁵⁰ 5'-GMP can coordinate to the achiral *cis*-RuCl₂(DMSO)₄ to form two isomers which have opposite chirality at the Ru centre, with coordination of the nucleotide being via the N7 and a phosphate oxygen. This report also demonstrated that 5'-AMP can coordinate to *cis*-RuCl₂(DMSO)₄ through the phosphate group, but binding through N7 was not observed.

A recent study by Davey *et al.* using electrospray ionization mass spectrometry and ¹H NMR spectroscopy examined the reactions of *cis*- and *trans*-RuCl₂(DMSO)₄ with deoxynucleosides.⁵¹ Both complexes react with 2'-deoxyguanosine to give identical products, two diastereomers containing a single nucleoside coordinated to Ru, and a bis(nucleoside)

adduct (Figure 1.6). Coordination of the nucleoside is via the N7 atom of guanine in each complex (Figure 1.2(1)). *Trans*-RuCl₂(DMSO)₄ reacts with 2'-deoxyadenosine (Figure 1.2(2), p. 6) to give a pair of diastereomers in which the nucleosides are coordinated via the N1 atom. *Cis*-RuCl₂(DMSO)₄ reacts with 2'-deoxyadenosine to a lesser extent than *trans*-RuCl₂(DMSO)₄ resulting in a complex mixture of products, but did include the product containing a single 2'-deoxyadenosine ligand coordinated via the N1 atom. *Trans*-RuCl₂(DMSO)₄ reacts only to a small extent with 2'-deoxycytidine under conditions similar to those used for the other nucleosides, and does not react with thymidine. This suggests that Ru(II) complexes may react with adjacent guanine bases in DNA to form intrastrand crosslinks in a fashion analogous to that of cisplatin.⁵¹

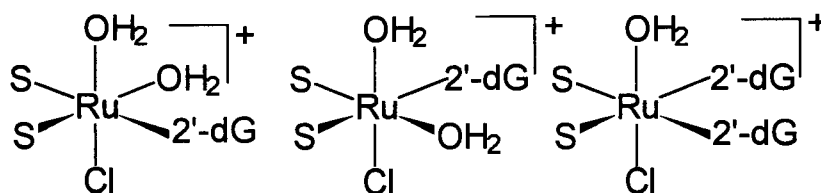


Figure 1.6. Structures of reaction products of *cis*- and *trans*-RuCl₂(DMSO)₄ with 2'-deoxyguanosine. (S = S-bound DMSO and 2'-dG = deoxyguanosine). Adapted from Ref. 51.

1.4.2 Ru(III)-Dimethylsulfoxide Complexes: *trans*-[(DMSO)₂H]⁺[RuCl₄(DMSO)₂]⁻ and *Mer*-RuCl₃(DMSO)₂(DMSO)

Two Ru(III)-dimethylsulfoxide complexes, *trans*-[(DMSO)₂H]⁺[RuCl₄(DMSO)₂]⁻⁵² and *mer*-RuCl₃(DMSO)₂(DMSO)⁵², have been synthesized and characterized, and their anti-tumour activity assessed.⁵³ The main feature of both complexes is the facile dissociation in aqueous solution of one of the two *trans*-S-bonded DMSO ligands (Figure 1.7).⁵³ Preliminary

results suggest that *mer*-RuCl₃(DMSO)₃ is as effective as cisplatin at inhibiting subcutaneous primary tumour growth and more potent than cisplatin for the prolongation of host survival time at the concentrations tested (4 mg/kg/day and 100 mg/kg/day, respectively).⁵⁴ The authors reported that these Ru(III) complexes preferentially concentrate in intestinal mucosa, lung epithelia and tumour tissues.⁵⁴

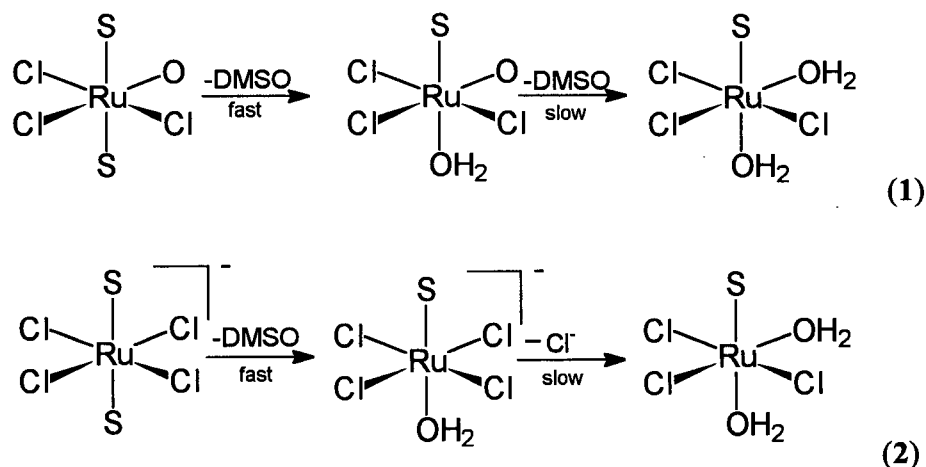


Figure 1.7. Dissolution behaviour of (1) *mer*-RuCl₃(DMSO)₂(DMSO) and (2) *trans*-[(DMSO)₂H]⁺[RuCl₄(DMSO)₂]⁻ in aqueous solutions. (S = S-bound DMSO and O = O-bound DMSO). Adapted from Ref. 53.

The complex Na[*trans*-RuCl₄(DMSO)₂] is a useful precursor for synthesis of a class of mixed DMSO-nitrogen ligand derivatives,⁵⁵ and the effects of two such complexes, *mer*-RuCl₃(DMSO)(DMSO)Im and Na[*trans*-RuCl₄(DMSO)(Im)] (Figure 1.8), were investigated. Endpoints were primary tumour growth and survival time using three solid, mouse tumours: Lewis lung carcinoma, B16 melanoma and MCa mammary carcinoma.⁵⁶

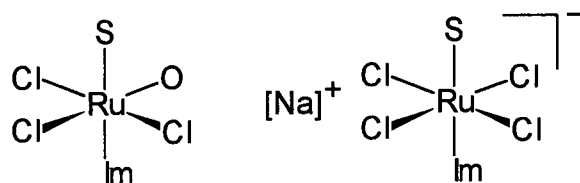


Figure 1.8. Abbreviated structures of *mer*-RuCl₃(DMSO)₂Im and Na[*trans*-RuCl₄(DMSO)(Im)]. (S = S-bound DMSO, O = O-bound DMSO and Im = imidazole). Adapted from Ref. 56.

Na[*trans*-RuCl₄(DMSO)(Im)] exhibited a higher activity against the tumour lines tested, this being attributed to the water-solubility of the complex. The presence of small amounts of DMSO (used as a vehicle of administration) reduced the activity of both complexes.⁵⁶ Sava *et al.* demonstrated that Na[*trans*-RuCl₄(DMSO)(Im)], in combination with surgical removal of the primary tumour, prevented new metastasis formation and inhibited the growth of existing lung metastases in mice bearing a mammary carcinoma.⁵⁷ This anti-metastatic action is comparable to that of [ImH]⁺[RuCl₄Im₂]⁻,^{25b} but the species exhibited lower activity than that of cisplatin on several Pt-sensitive lines.⁵⁸ Na[*trans*-RuCl₄(DMSO)(Im)] also prolonged the survival time of mice bearing MCa mammary carcinoma,⁵⁹ while showing minimal toxicity for normal tissues such as lung and kidney epithelia, muscle and liver cells, splenocytes and bone marrow.⁶⁰ Although the complex exhibits no cytotoxicity in tumour cells, it does interact with nucleic acids and results in a reduction of nucleic acid activity (a reduction in polyploidy DNA).⁶¹ A recent study of the effects of Na[*trans*-RuCl₄(DMSO)(Im)] on cell cycle modifications, tested in TLX5 lymphoma cells, strongly suggests the lack of direct cytotoxic effects in the anti-metastatic action of this complex.⁶² Bergamo *et al.*⁶³ suggest that this lack of direct cytotoxicity⁶⁰⁻⁶² may be explained by three observations. Firstly, lung metastasis

formation can be reduced when no contact occurs between tumour cells and Na[*trans*-RuCl₄(DMSO)(Im)]; secondly, a low amount of Ru (10 % of the administered dose) reaches tumour cells after treatment; and thirdly, the complex exhibits rapid clearance from the blood stream.⁶³

Several Ru(III) complexes of the type Na[*trans*-RuCl₄(DMSO)(L)] (L = imidazole, N-methylimidazole, isonicotinic acid, indazole, isoquinoline, oxazole, pyridine, methylpyridine and ethylpyridine) were tested in TLX5 lymphoma and MCa carcinoma to determine the degree of cytotoxicity and antimetastatic activity.⁶⁴ Na[*trans*-RuCl₄(DMSO)(Im)] was the most selective anti-metastatic compound, and *in vitro* cytotoxicity was present only at concentrations > 10⁻⁴ M, this being dependent upon lipophilicity. The comparison of the effects on *in vitro* cytotoxicity with *in vivo* anti-tumour and anti-metastatic action indicates that these compounds reduce metastasis formation by a mechanism independent of that for direct tumour cell cytotoxicity.⁶⁴ ImH[*trans*-RuCl₄(DMSO)(Im)], in which the cation is now ImH⁺ was tested for anti-metastatic effects in models of solid metastasizing tumours of the mouse, and was found to behave similarly to Na[*trans*-RuCl₄(DMSO)(Im)], implying that the anion was responsible for all the biological actions.⁶⁵

1.4.3 Nitroimidazole Derivatives of RuCl₂(DMSO)₄

Cis-RuCl₂(DMSO)₄ has been used as a precursor for the synthesis of Ru(II)-nitroimidazole complexes as hypoxic radiosensitizers.⁶⁶ Many tumours contain cells which are low in oxygen content and consequently relatively resistant to radiation treatment (see Section 4.2).⁶⁷ To compensate the relative radioresistance of hypoxic cells, compounds which mimic the effect of oxygen, *i.e.* hypoxic radiosensitizers, have been studied.⁶⁸ RuCl₂(DMSO)₂(4-

$\text{NO}_2\text{Im})_2$ was shown to be a more effective radiosensitizer and exhibited lower toxicity in Chinese hamster ovary cells (CHO) than the free 4-nitroimidazole.⁶⁶ This complex was also studied for clastogenic activity (chromosome damaging) and exhibited activity greater than that of *cis*- $\text{RuCl}_2(\text{DMSO})_4$ and 4- NO_2Im (Figure 1.9), but less than that of cisplatin.⁶⁹ $\text{RuCl}_2(\text{DMSO})_2\text{L}_n$ (L = 2-, 4- or 5-nitroimidazole and n = 1 or 2)^{70,71} (Figure 1.9) and several Ru -(substituted-4-nitroimidazole)⁷² complexes were synthesized, characterized and their radiosensitizing abilities, toxicity toward CHO cells, and DNA-binding properties examined. The Ru -(substituted-4-nitroimidazole) species were less effective sensitizers than $\text{RuCl}_2(\text{DMSO})_2(4\text{-NO}_2\text{Im})_2$ and did not bind to plasmid DNA.⁷² The complex with misonidazole (a 2-nitroimidazole) (Figure 1.9) was unstable in aqueous solution and was no better a radiosensitizer than the free nitroimidazole.⁷⁰ The complex with metronidazole (a 5-nitroimidazole) (Figure 1.9) was also found to dissociate in aqueous solution.⁷⁰ $\text{RuCl}_2(\text{DMSO})_2(\text{NMe-4-NO}_2\text{Im})$ exhibited increased sensitization and lower toxicity in CHO cells *in vitro* compared to those of the free imidazole.⁷¹

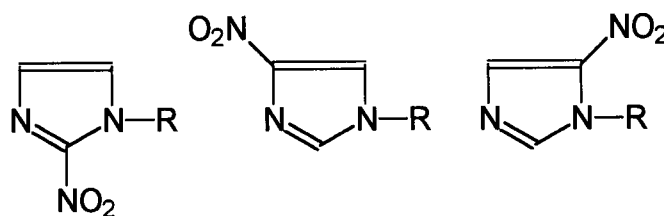


Figure 1.9. Structures of 2-nitroimidazole ($\text{R} = \text{CH}_2\text{CHOHCH}_2\text{OCH}_3$ = misonidazole, $\text{R} = \text{CH}_2\text{C}(\text{O})\text{NHCH}_2\text{CH}_2\text{OH}$ = etanidazole), 4-nitroimidazole ($\text{R} = \text{H}$) and 5-nitroimidazole ($\text{R} = \text{CH}_2\text{CH}_2\text{OH}$ = metronidazole).

The effects (*e.g.* toward sensitization, toxicity toward CHO cells and DNA-binding) of substitution of chloride by bromide, and DMSO by TMSO

(TMSO = tetramethylenesulfoxide), as well as varying the nitroimidazole, were studied for comparison with data for $\text{RuCl}_2(\text{DMSO})_2(4\text{-NO}_2\text{Im})_2$.⁷³ Replacement of chloride by bromide reduced the radiosensitizing ability of the 4- NO_2Im complexes, whereas replacement of DMSO by TMSO did not.⁷³ The TMSO complexes did not bind to DNA and TMSO/2-nitroimidazole complexes were stable in aqueous media (unlike the DMSO analogues).⁷³ $\text{RuCl}_2(\text{TMSO})_2(4\text{-NO}_2\text{Im})_2$ and $\text{RuCl}_2(\text{TMSO})_2(\text{etanidazole})$ (Figure 1.9) both exhibit promising sensitizing enhancement ratios compared to those of $\text{RuCl}_2(\text{DMSO})_2(4\text{-NO}_2\text{Im})_2$.⁷³ These Ru-nitroimidazole complexes did not show much toxicity compared to those of analogous Pt complexes.⁷⁴

1.4.4 Ru Bis-chelating Sulfoxide Complexes

There is potential for using Ru sulfoxide complexes as chemotherapeutic agents as can be seen from the studies on *cis*- and *trans*- $\text{RuCl}_2(\text{DMSO})_4$ (Section 1.3). Our group has extended the series of sulfoxide complexes of Ru to include disulfoxides of the type $\text{RS}(\text{O})(\text{CH}_2)_n\text{S}(\text{O})\text{R}$ ($n = 2$ with $\text{R} = \text{Me}$, Et and Pr ; and $n = 3$ with $\text{R} = \text{Me}$).⁷⁵ The precursor dithioethers were synthesized in air following the procedure of Morgan and Ledbury,⁷⁶ and were then oxidized in air by acid-catalyzed, DMSO oxidation following the procedure reported by Hull and Bargar.⁷⁷ The disulfoxides were prepared as mixtures of diastereomers (the *RR/SS* pair and the *meso RS/SR*) and repeat recrystallizations were used to isolate the diastereomers.^{75,77} The goals of the chelating disulfoxide studies were to reduce the number of possible isomers in the preparation of nitroimidazole complexes^{66,69-73} and to extend the database for the *in vitro* activity of Ru-sulfoxide complexes.⁷⁸

Four complexes, *trans*-RuCl₂(BMSE)₂, *trans*-RuCl₂(BPSE)₂, *cis*-RuCl₂(BESE)₂ and *cis*-RuCl₂(BMSP)₂ were synthesized, characterized (including crystallographic data) and studied [BMSE = 1,2-bis(methylsulfinyl)ethane, BESE = 1,2-bis(ethylsulfinyl)ethane, BPSE = 1,2-bis(propylsulfinyl)ethane, and BMSP = 1,3-bis(methylsulfinyl)propane; Figure 1.10].^{75,78}

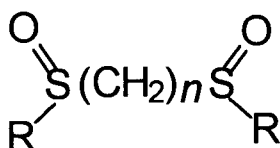


Figure 1.10. Structure of disulfoxides. (($n = 2$) BMSE, R = Me; BESE, R = Et; BPSE, R = Pr; BBSE, R = Bu; BPeSe, R = Pe; BHSE, R = He; BCySE, R = Cy; BPhSE, R = Ph and ($n = 3$) BMSP, R = Me; BESP, R = Pr; BPSP, R = Pr; B'PSP, R = ⁱPr; BBSP, R = Bu; BPeSP, R = Pe; BPhSP, R = Ph).

The chelating ligands in all four structures have opposite chiralities at the two chiral S-atoms. The *trans* complexes are centrosymmetric with mutually *trans* S-atoms having opposite configurations and are non-chiral. The two *cis* complexes have C_2 symmetry with the pair of mutually *trans* S-atoms having the same chirality. The *cis* complexes are chiral, but in both cases the crystal structures showed that the samples contain an equal number of the two enantiomers.^{75,78} Some preliminary *in vitro* experiments implied that the *trans* complexes accumulate in cells and bind to DNA to a greater degree than the *cis* complexes.^{75,78}

1.5 Goals of This Thesis

1.5.1 Synthesis of the Geometrical Isomers of the Known Bis-chelating Disulfoxide Complexes of Ru

As discussed in Section 1.4.1 the complexes *cis*-RuCl₂(DMSO)₄ and *trans*-RuCl₂(DMSO)₄ exhibit different efficacies in their anti-tumour properties. Previous work (Section 1.4.4) in this laboratory involved the synthesis, characterization and *in vitro* studies of a series of bis-chelating disulfoxide complexes of Ru. Only one geometrical isomer (of 2 possible) was isolated, dependent upon the disulfoxide used.^{75,78} The initial goal of this project was to use the precursors *cis*-RuCl₂(DMSO)₄ and *trans*-RuCl₂(DMSO)₄ as starting materials to synthesize the other corresponding geometrical isomer of the various bis-chelating disulfoxide Ru complexes (Section 1.4.4), and then to investigate the effect of the geometrical and optical isomerism and chirality on biological properties.

1.5.2 Synthesis of Water-soluble Sulfoxide Complexes of Ru

The complexes *cis*-RuCl₂(DMSO)₄ and *trans*-RuCl₂(DMSO)₄ are water-soluble, which facilitates *in vitro* examination. Of the previously synthesized bis-chelating disulfoxides complexes of Ru (Section 1.4.4), the only complex appreciably soluble in aqueous solutions was *cis*-RuCl₂(BESE)₂. One further aim was to synthesize sulfoxide complexes that readily dissolved in aqueous solutions.

1.5.3 Synthesis and Characterization of Novel Chelating Disulfoxide Complexes of Ru

For the bis-chelating disulfoxide complexes of Ru that were synthesized (Section 1.4.4) the disulfoxides used were $\text{RS(O)(CH}_2)_n\text{S(O)R}$ ($n = 2$ or 3 and $\text{R} = \text{Me, Et or Pr}$; Figure 1.10). One goal was to extend the number of disulfoxides (e.g. $\text{R} = \text{'Pr, Bu, Pent, Hexyl, Ph and Cy}$, Figure 1.10), to react these disulfoxides with various Ru precursor species and to characterize the resultant products, particularly the geometry of the ligand set at the Ru centre.

1.5.4 Synthesis of Chelating Dithioether Complexes of Ru

A further goal was to synthesize bis-chelating dithioether complexes of Ru in order to determine the geometry of the ligands at Ru, and then to oxidize the coordinated dithioethers to the corresponding disulfoxides. This was to determine whether the ligand set would retain its geometry at the Ru centre after oxidation of the coordinated S-atoms to S=O .

1.5.5 Preliminary Biological Studies in Vitro of Sulfoxide Complexes of Ru

Following reports on the anti-tumour and DNA-binding properties of *cis*- $\text{RuCl}_2(\text{DMSO})_4$ and *trans*- $\text{RuCl}_2(\text{DMSO})_4$ (see Sections 1.4.1 and 1.4.1.2, respectively), studies had been undertaken previously in this group to increase the number of sulfoxide complexes of Ru (Section 1.4.4) and study the cytotoxicity and the DNA-binding properties of these complexes.^{75,78} A present goal was to extend such studies (cytotoxicity, accumulation and DNA-binding in Chinese hamster ovary (CHO) cells) to include Ru complexes of novel disulfoxides.

1.5.6 Metallation of Water-soluble Porphyrins

Previous work in this group, initiated by Ware,⁷⁹ involved the insertion of Ru into water-soluble porphyrins using Ru precursors other than the traditional $\text{Ru}_3(\text{CO})_{12}$.⁸⁰ $[\text{Ru}(\text{DMF})_6][\text{OTf}]_3$ ⁸¹ (DMF = dimethylformamide and $\text{OTf} = \text{CF}_3\text{SO}_3^-$) was found to be a useful precursor which enabled the metallation of several free-base porphyrins including the water-soluble $\text{Na}_4[\text{H}_2\text{TSPHP}] \cdot 15\text{H}_2\text{O}$ (TSPHP = 5,10,15,20-tetrakis(4-sulfonatophenyl)porphyrin) which yielded $\text{Na}_4[\text{Ru}(\text{TSPHP})(\text{CO})(\text{DMF})] \cdot \text{solvate}$ (solvate = $2\text{DMF} \cdot 2\text{H}_2\text{O}$ or $6\text{H}_2\text{O}$).⁷⁹ The goal was to assess the general applicability of such metallation.

1.6 References for Chapter 1

- 1 (a) Davies, A. R.; Einstein, F. W. B.; Farrell, N. P.; James, B. R.; McMillan, R. S. *Inorg. Chem.* 1978, 17, 1965;
(b) James, B. R.; McMillan, R. S. *Can. J. Chem.* 1977, 55, 3927;
(c) James, B. R.; McMillan, R. S.; Reimer, K. J. *J. Mol. Catal.* 1976, 1, 439.
- 2 Fricker, S. P. Ruthenium Compounds in Cancer Therapy, in *Metal Compounds in Cancer Therapy* (ed. S. Fricker), Chapman and Hall, London, 1994, p. 1.
- 3 Roberts, L. Cancer Today. Origins, Prevention and Treatment, National Academy Press, Washington, 1984.
- 4 Haiduc, I.; Silvestru, C. *Coord. Chem. Rev.* 1990, 99, 253.
- 5 Rosenberg, B.; Van Camp, L.; Krigas, T. *Nature* 1969, 205, 698.
- 6 Oldenberg, J.; Los, G. Cellular Mechanisms of Cisplatin Resistance, in *Drug Resistance in Oncology* (ed. S. D. Bernal), Marcel Dekker, New York, 1997, p. 331.
- 7 Reédijk, J. *J. Chem. Soc., Chem. Commun.* 1996, 801.
- 8 Sherman, S. E.; Lippard, S. J. *Chem. Rev.* 1987, 87, 1153.
- 9 Bloemink, M. J.; Reédijk, J. Cisplatin and Derived Anti-cancer Drugs: Mechanism and Current Status of DNA Binding, in *Metal Ions in Biological Systems* (eds. A. Sigel and H. Sigel), Marcel Dekker Inc., New York, 1996, 32, p. 641.
- 10 Whitehead, J. P.; Lippard, S. J. Proteins that Bind to and Mediate the Biological Activity of Platinum Anti-cancer Drug-DNA Adducts, in *Metal Ions in Biological Systems* (eds. A. Sigel and H. Sigel), Marcel Dekker Inc., New York, 1996, 32, p. 687.
- 11 Heim, M. E. Platinum and Non-Platinum Complexes in Clinical Trials. Current Status and New Developments, in *Metal Complexes in Cancer Chemotherapy* (ed. B. K. Keppler), VCH, Weinheim, 1993, p. 9.
- 12 Giandomenico, C. M.; Abrams, M. J.; Murrer, B. A.; Vollano, J. F.; Rheinheimer, M. I.; Wyer, S. B.; Bossard, G. E.; Higgins III, J. D. *Inorg. Chem.* 1995, 34, 1015.

- 13 Holford, J.; Sharp, S. Y.; Murrer, B. A.; Abrams, M.; Kelland L. R. *Br. J. Cancer* 1998, 77, 366.
- 14 (a) Day, M. *New Scientist* 1999, 162, 11;
 (b) Kratochwil, N. A.; Parkinson, J. A.; Bednarski, P. J.; Sadler, P. J. *Angew. Chem. Int. Ed.* 1999, 38, 1460;
 (c) Guo, Z.; Sadler, P. J. *Angew. Chem. Int. Ed.* 1999, 38, 1512.
- 15 Kelland, L. R. Platinum Anti-cancer Drugs, in *Metal Compounds in Cancer Therapy* (ed. S Fricker), Chapman and Hall, London, 1994, p. 41.
- 16 (a) Farrell, N.; Qu, Y.; Bierbach, U.; Valsecci, M.; Menta, E. Structure-Activity Relationships within Di- and Trinuclear Platinum Phase-I Clinical Anti-cancer Agents, in *Cisplatin Chemistry and Biochemistry of a Leading Anti-cancer Drug* (ed. B. Lippert), Wiley-VCH, Weinheim, 1999, p. 479;
 (b) Kašpárková, J.; Nováková, O.; Vrána, O.; Farrell, N.; Brabec, V. *Biochemistry* 1999, 38, 10997;
 (c) Perego, P.; Caserini, C.; Gatti, L.; Carenini, N.; Romanelli, S.; Supino, R.; Colangelo, D.; Viano, I.; Leone, R.; Spinelli, S.; Pezzoni, G.; Manzotti, C.; Farrell, N.; Zunino, F. *Molecular Pharmacology* 1999, 55, 528;
 (d) Brabec, V.; Kašpárková, J.; Vrána, O.; Nováková, O.; Cox, J. W.; Qu, Y.; Farrell, N. *Biochemistry* 1999, 38, 6781;
 (e) Skov, K. A.; Adomat, H.; Farrell, N.; Matthews, J. B. *Anti-cancer Drug Des.* 1998, 13, 207;
 (f) Kharatishvili, M.; Mathieson, M.; Farrell, N. *Inorg. Chim. Acta* 1997, 255, 1;
 (g) Žaludová, R.; Žákovská, A.; Kašpárková, J.; Balcarová, Z.; Kleinwächter, V.; Vrána, Farrell, N.; Brabec, V. *Eur. J. Biochem.* 1997, 246, 508;
 (h) Mellish, K. J.; Qu, Y.; Scarsdale, N.; Farrell, N. *Nucleic Acids Res.* 1997, 25, 1265;
 (i) Farrell, N. Current Status of Structure-Activity Relationships of Platinum Anti-cancer Drugs: Activation of the *Trans* Geometry, in *Metal Ions in Biological Systems* (eds. A. Sigel and H. Sigel), Marcel Dekker Inc., New York, 1996, 32, p. 603;

- (j) Qu, Y.; Farrell, N. *Inorg. Chim. Acta* 1996, 245, 265;
- (k) Kašpárková, J.; Mellish, K. J.; Qu, Y.; Brabec, V.; Farrell, N. *Biochemistry* 1996, 35, 16705;
- (l) Farrell, N.; Appleton, T. G.; Qu, Y.; Roberts, J. D.; Soares Fontes, A. P.; Skov, K. A.; Wu, P.; Zou, Y. *Biochemistry* 1995, 34, 15480;
- (m) Wu, P. K.; Qu, Y.; Van Houten, B.; Farrell, N. *J. Inorg. Biochem.* 1994, 54, 207;
- (n) Van Houten, B.; Illenye, S.; Qu, Y.; Farrell, N. *Biochemistry* 1993, 32, 11794;
- (o) Zou, Y.; Van Houten, B.; Farrell, N. *Biochemistry* 1993, 32, 9632;
- (p) Landi, J.; Hacker, M. P.; Farrell, N. *Inorg. Chim. Acta* 1992, 202, 79;
- (q) Kraker, A. J.; Hoeschele, J. D.; Elliot, W. L.; Hollis Showalter, H. D.; Sercel, A. D.; Farrell, N. P. *J. Med. Chem.* 1992, 35, 4526;
- (r) Qu, Y.; de Almeida, S. G.; Farrell, N. *Inorg. Chim. Acta* 1992, 201, 123;
- (s) de Almeida, S. G.; Hubbard, J. L.; Farrell, N. *Inorg. Chim. Acta* 1992, 193, 149;
- (t) Johnson, A.; Qu, Y.; Van Houten, B.; Farrell, N. *Nucleic Acids Res.* 1992, 20, 1697;
- (u) Farrell, N.; Roberts, J. D.; Hacker, M. P. *J. Inorg. Biochem.* 1991, 42, 237;
- (v) Qu, Y.; Farrell, N. *J. Inorg. Biochem.* 1990, 40, 255;
- (w) Hoeschele, J. D.; Farrell, N.; Turner, W. R.; Rithner, C. D. *Inorg. Chem.* 1988, 27, 4106.
- 17 Farrell, N. *Transition Metal Complexes as Drugs and Chemotherapeutic Agents* (eds. R. Ugo and B. R. James), Kluwer Academic Publishers, Dordrecht, 1989, p. 147.
- 18 Clarke, M. J. *Oncological Implications of the Chemistry of Ruthenium*, in *Metal Ions in Biological Systems* (ed. H. Sigel), Marcel Dekker, New York, 1980, 11, p. 231.
- 19 Clarke, M. J. *Ruthenium Complexes: Potential Roles in Anti-cancer Pharmaceuticals*, in *Metal Complexes in Cancer Chemotherapy* (ed. B. K. Keppler), VCH, Weinheim, 1993, p. 129.

- 20 Milkevitch, M.; Storrie, H.; Brauns, E.; Brewer, K. J.; Shirley, B. W. *Inorg. Chem.* 1997, 36, 4534.
- 21 Sava G. Ruthenium Compounds in Cancer Therapy, in *Metal Compounds in Cancer Therapy* (ed. S. Fricker), Chapman and Hall, London, 1994, p. 65.
- 22 Kratz, F.; Keppler, B. K.; Messori, L.; Smith, L.; Baker, E. N. *Metal-Based Drugs* 1994, 1, 169 and references therein.
- 23 (a) Clarke, M. J. *Inorg. Chem.* 1980, 19, 1103.
(b) Clarke, M. J.; Bitler, S.; Rennert, D.; Buchbinder, M.; Kelman, A. D. *J. Inorg. Biochem.* 1980, 2, 79.
- 24 Keppler, B. K.; Wehe, D.; Endres, H.; Rupp, W. *Inorg. Chem.* 1987, 26, 844.
- 25 (a) Garzon, F. T.; Berger, M. R.; Keppler, B. K.; Schmähl, D. *Cancer Chemother. Pharmacol.* 1987, 19, 347;
(b) Keppler, B. K.; Rupp, W.; Juhl, U. M.; Endres, H.; Niebl, R.; Balzer, W. *Inorg. Chem.* 1987, 26, 4366;
(c) Ni Dhubhghaill, O. M.; Hagen, W. R.; Keppler, B. K.; Lipponer, K-G.; Sadler, P. J. *J. Chem. Soc. Dalton Trans.* 1994, 3305;
(d) Chatlas, J.; van Eldik, R.; Keppler, B. K. *Inorg. Chim. Acta* 1995, 233, 59;
(e) Pieper, T.; Keppler, B. K. *Analysis Magazine* 1998, 26, 84;
(f) Keppler, B. K. *New J. Chem.* 1990, 14, 389;
(g) Kersten, L.; Bräunlich, H.; Keppler, B. K.; Gliesing, C.; Wendelin, M.; Westphal, J. *J. Appl. Toxicol.* 1998, 18, 93.
- 26 (a) Keppler, B. K.; Lipponer, K-G.; Stenzel, B.; Kratz, F. New Tumour-Inhibiting Ruthenium Complexes, in *Metal Complexes in Cancer Chemotherapy* (ed. B. K. Keppler), VCH, Weinheim, 1993, p. 187.
(b) Keppler, B. K.; Henn, M.; Juhl, U. M.; Berger, M. R.; Niebel, R.; Wagner, F. E. New Ruthenium Complexes for the Treatment of Cancer, in *Progress in Clinical Biochemistry and Medicine* (eds. E. Baulieu; D. T. Forman; M. Ingelman-Sundberg; L. Jaenicke; J. A. Kellen; Y. Nagai; G. F. Springer; L. Träger; L. Will-Shahab; J. L. Wittliff), Springer-Verlag, Berlin, 1989, 10, p. 41.
- 27 Lipponer, K-G.; Vogel, E.; Keppler, B. K. *Metal-Based Drugs* 1996, 3, 243.

- 28 Mestroni, G.; Alessio, E.; o Santi, A. S.; Geremia, S.; Bergamo, A.; Sava, G.; Boccarelli, A.; Schettino, A.; Coluccia, M. *Inorg. Chim. Acta* 1998, 273, 62.
- 29 Clarke, M. J. The Potential of Ruthenium in Anti-cancer Pharmaceuticals, in *ACS Symposium Series* (ed. A. E. Martell), American Chemical Society, Washington, 1980, 140, p. 157.
- 30 Clarke, M. J.; Stubbs, M. Interactions of Metallopharmaceuticals with DNA, in *Metal Ions in Biological Systems* (eds. A. Sigel and H. Sigel), Marcel Dekker Inc., New York, 1996, 32, p. 727.
- 31 Frasca, D.; Ciampa, J.; Emerson, J.; Umans, R. S.; Clarke, M. J. *Metal-Based Drugs* 1996, 3, 197.
- 32 Durig, J. R.; Danneman, J.; Behnke, W. D.; Mercer, E. E. *Chem. Biol. Interact.* 1976, 13, 287.
- 33 Gibson, J. F.; Poole, R. K.; Hughes, M. N.; Rees, J. F. *Arch. Microbiol.* 1984, 139, 265.
- 34 Mercer, E. E.; Gray, L. W. *J. Am. Chem. Soc.* 1972, 94, 6426.
- 35 Hughes, M. N.; O'Reardon, D.; Poole, R. K.; Hursthouse, M. B.; Thornton-Pett, M. *Polyhedron* 1987, 6, 1711.
- 36 (a) Kessel, D.; Thompson, P.; Saatio, K.; Nantwi, K. D. *Photochem. Photobiol.* 1987, 45, 787;
(b) Fiel, R. J.; Mark, E.; Button, T.; Gilani, S.; Musser, D. *Cancer Lett.* 1988, 40, 23;
(c) Dougherty, T. J. *Photochem. Photobiol.* 1987, 45, 879;
(d) Miura, M.; Micca, P. L.; Heinrichs, J. C.; Gabel, D.; Fairchild, R. G.; Slatkin, D. N. *Biochem. Pharmacol.* 1992, 43, 467.
- 37 O'Hara, J. A.; Douple, E. B.; Abrams, M. J.; Picker, D. J.; Giandomenico, C. M.; Vollano, J. F. *Int. J. Radiat. Oncol. Biol. Phys.* 1989, 16, 1049.
- 38 James, B. R.; Meng, G. G.; Posakony, J. J.; Ravensbergen, J. A.; Ware, C. J.; Skov, K. A. *Metal-Based Drugs* 1996, 3, 85.
- 39 Hartmann, M.; Robert, A.; Duarte, V.; Keppler, B. K.; Meunier, B. *J. Biol. Inorg. Chem.* 1997, 2, 427.

- 40 Giraldi, T.; Sava, G.; Bertoli, G.; Mestroni, G.; Zassinovich, G. *Cancer Res.* 1977, 37, 2662.
- 41 Sava, G.; Zoret, S.; Giraldi, T.; Mestroni, G.; Zassinovich, G. *Eur. J. Cancer Clin. Oncol.* 1984, 20, 841.
- 42 Sava, G.; Pacor, S.; Zorzet, S.; Alessio, E.; Mestroni, G. *Pharmacol. Res.* 1989, 21, 617.
- 43 Coluccia, M.; Sava, G.; Loseto, F.; Nassi, A.; Boccarelli, A.; Giordano, D.; Alessio, E.; Mestroni, G. *Eur. J. Cancer* 1993, 29, 1873.
- 44 Alessio, E.; Mestroni, G.; Nardin, G.; Attia, W. M.; Calligaris, M.; Sava, G.; Zorzet, S. *Inorg. Chem.* 1988, 27, 4099.
- 45 (a) Evans, I. P.; Spencer, A.; Wilkinson, G. *J. Chem. Soc. Dalton Trans.* 1973, 204;
(b) McMillan, R. S.; Mercer, A.; James, B. R.; Trotter, J. *J. Chem. Soc. Dalton Trans.* 1975, 1006.
- 46 Khan, B. T.; Mehmood, A. *J. Inorg. Nucl. Chem.* 1978, 40, 1938.
- 47 Cauci, S.; Alessio, E.; Mestroni, G.; Quadrifoglio, F. *Inorg. Chim. Acta* 1987, 137, 19.
- 48 Alessio, E.; Xu, Y.; Cauci, S.; Mestroni, G.; Quadrifoglio, F.; Viglino, P.; Marzilli, L. G. *J. Am. Chem. Soc.* 1989, 111, 7068.
- 49 Esposito, G.; Cauci, S.; Fogolari, F.; Alessio, E.; Scocchi, M.; Quadrifoglio, F.; Viglino, P. *Biochem.* 1992, 31, 7094.
- 50 Tian, Y-N.; Yang, P.; Li, Q-S.; Guo, M-L.; Zhao, M-G. *Polyhedron* 1997, 16, 1993.
- 51 Davey, J. M.; Moerman, K. L.; Ralph, S. F.; Kanitz, R.; Sheil, M. M. *Inorg. Chim. Acta* 1998, 281, 10.
- 52 Jaswal, J. S.; Rettig, S. J.; James, B. R. *Can. J. Chem.* 1990, 68, 1808.
- 53 Alessio, E.; Balducci, G.; Calligaris, M.; Costa, G.; Attia, W. H.; Mestroni, G. *Inorg. Chem.* 1991, 30, 609.
- 54 Pacor, S.; Sava, G.; Ceschia, V.; Bregant, F.; Mestroni, G.; Alessio, E. *Chem. Biol. Interact.* 1991, 78, 223.

- 55 Alessio, E.; Balducci, G.; Lutman, A.; Mestroni, G.; Calligaris, M.; Attia, W. M. *Inorg. Chim. Acta* 1993, 203, 205.
- 56 Sava, G.; Pacor, S.; Mestroni, G.; Alessio, E. *Anti-Cancer Drugs* 1992, 3, 25.
- 57 Sava, G.; Pacor, S.; Coluccia, M.; Mariggio, M.; Cocchietto, M.; Alessio, E.; Mestroni, G. *Drug Invest.* 1994, 8, 150.
- 58 Mestroni, G. The Development of Tumour-Inhibiting Ruthenium Dimethylsulfoxide Complexes, in *Metal Complexes in Cancer Chemotherapy* (ed. B. K. Keppler), VCH, Weinheim, 1993, p. 157.
- 59 Sava, G.; Pacor, S.; Mestroni, G.; Alessio, E. *Clin. Exp. Metastasis* 1992, 10, 273.
- 60 Gagliardi, R.; Sava, G.; Pacor, S.; Mestroni, G.; Alessio, E. *Clin. Exp. Metastasis* 1994, 12, 93.
- 61 Sava, G.; Capozzi, I.; Bergamo, A.; Gagliardi, R.; Cocchietto, M.; Masiero, L.; Onisto, M.; Alessio, E.; Mestroni, G.; Garbisa, S. *Int. J. Cancer* 1996, 68, 60.
- 62 Capozzi, I.; Clerici, K.; Cocchietto, M.; Salerno, G.; Bergamo, A.; Sava, G. *Chem. Biol. Interact.* 1998, 113, 51.
- 63 Bergamo, A.; Cocchietto, M.; Capozzi, I.; Mestroni, G.; Alessio, E.; Sava, G. *Anti-Cancer Drugs* 1996, 7, 697.
- 64 Sava, G.; Pacor, S.; Bergamo, A.; Cocchietto, M.; Mestroni, G.; Alessio, E. *Chem. Biol. Interact.* 1995, 95, 109.
- 65 Sava, G.; Capozzi, I.; Clerici, K.; Gagliardi, G.; Alessio, E.; Mestroni, G. *Clin. Exp. Metastasis* 1998, 16, 371.
- 66 Chan, P. K.; Skov, K. A.; James, B. R.; Farrell, N. P. *Int. J. Radiat. Oncol. Biol. Phys.* 1986, 12, 1059.
- 67 Thomlinson, R. H.; Gray, L. H. *Br. J. Cancer* 1955, 9, 539.
- 68 Adams, G. E. *Radiat. Res.* 1992, 132, 129.
- 69 Chan, P. K. L.; Skov, K. A.; James, B. R.; Farrell, N. P. *Chem. Biol. Interact.* 1986, 59, 247.
- 70 Chan, P. K. L.; Skov, K. A.; James, B. R.; Farrell, N. P. Studies on Ruthenium Nitroimidazole Complexes as Radiosensitizers, in *Platinum and Other Metal*

- Coordination Compounds in Cancer Chemotherapy* (ed. M. Nicolini), Martinus Nijhoff Publishing, Boston, 1987, p. 638.
- 71 Chan, P. K. L.; Chan, P. K. H.; Frost, D. C.; James, B. R.; Skov, K. A. *Can. J. Chem.* 1988, 66, 117.
 - 72 Chan, P. K. L.; Skov, K. A.; James, B. R. *Int. J. Radiat. Biol.* 1987, 52, 49.
 - 73 Chan, P. K. L.; James, B. R.; Frost, D. C.; Chan, P. K. H.; Hu, H-L; Skov, K. A. *Can. J. Chem.* 1989, 67, 508.
 - 74 Farrell, N. Metal Complexes as Radiosensitizers, in *Progress in Clinical Biochemistry and Medicine* (eds. E. Baulieu; D. T. Forman; M. Ingelman-Sundberg; L. Jaenicke; J. A. Kellen; Y. Nagai; G. F. Springer; L. Träger; L. Will-Shahab; J. L. Wittliff), Springer-Verlag, Berlin, 1989, 10, p. 89 and references therein.
 - 75 Yapp, D. T. T.; Rettig, S. J.; James, B. R.; Skov, K. A. *Inorg. Chem.* 1997, 36, 5635.
 - 76 Morgan, S. T.; Ledbury, W. *J. Chem. Soc.* 1922, 121, 2882.
 - 77 Hull, M.; Bargar, T. W. *J. Org. Chem.* 1975, 40, 3152.
 - 78 Yapp, D. T. T. Ph. D. Dissertation, University of British Columbia, Vancouver, 1993.
 - 79 Ware, C. J. M. Sc. Dissertation, University of British Columbia, Vancouver, 1994.
 - 80 (a) Fleischer, E. B.; Thorp, R.; Venerable, D. *J. Chem. Soc., Chem. Commun.* 1969, 475;
 (b) Chow, B.; Cohen, I. *Bioinorg. Chem.* 1971, 1, 57;
 (c) Eaton, G. R.; Eaton, S. S. *J. Am. Chem. Soc.*, 1975, 97, 235.
 - 81 Judd, R. J.; Cao, R.; Biner, M.; Armbruster, T.; Bürgi, H-B.; Merbach, A. E.; Ludi, A. *Inorg. Chem.* 1995, 34, 5080.

Chapter 2

General Experimental and Synthesis of Ligands (Dithioethers and Disulfoxides) and Ruthenium Precursors and Sulfoxide Complexes

2.1 Chemicals and Reagents

3,6-Dithiaoctane and 4,7-dithiadecane were purchased from K & K Laboratories. Dimethylsulfoxide (DMSO) and 1,2-dibromoethane, were purchased from Fisher Scientific. 1,3-Dibromopropane was purchased from MCB, while ethane-, propane-, butane-, pentane-, hexane- and cyclohexyl-thiols, and 1,4,7,10-tetrathiacyclododecane and 3,6,9,14-tetrathiabicyclo[9.2.1]tetradeca-11,13-diene were obtained from Aldrich. Benzenethiol and phenylsulfoxide were Eastman products. The chemicals were used as provided. $\text{RuCl}_3 \cdot 3\text{H}_2\text{O}$ was obtained on loan from Johnson-Matthey Ltd. and Colonial Metals Inc. All common solvents used were at least of reagent grade. Deuterated solvents used for NMR studies (C_6D_6 , D_2O , CDCl_3 , $\text{DMSO}-d_6$ and MeOD) were purchased from MSD ISOTOPES or ISOTEC Inc. Alumina (neutral, Brockman activity I) was purchased from Fisher chemicals. All samples (products and solvents) were stored in air, and all syntheses and measurements were done in air unless otherwise stated.

2.2 Physical Techniques and Instrumentation

2.2.1 FT-NMR Instruments

Solution NMR spectra were obtained using a Bruker AC-200E (200 MHz), a Varian XL-300 (300 MHz) or Bruker WH-400 (400 MHz) instrument operating in the

Fourier Transform mode. Proton chemical shifts are given as δ in ppm with reference to the residual solvent peak as the internal standard, relative to TMS [C_6H_6 in C_6D_6 δ 7.15, CHCl_3 in CDCl_3 δ 7.24, HDO in D_2O δ 4.63, DMSO in d_6 -DMSO δ 2.49 and MeOH in CD_3OD δ 3.30, 4.78]. The ^1H -NMR chemical shifts are reported as indicated by s = singlet; d = doublet; t = triplet; q = quartet; m = multiplet.

2.2.2 Infrared and UV-Vis Spectrophotometry, Thermal Gravimetric Analysis, Photochemistry and Conductivity and Melting Point Measurements

Infrared spectra were obtained using an ATI Mattson Genesis Series FTIR instrument. The samples were prepared by evenly mixing a solid compound with KBr and then compressing the resulting mixture into a pellet. Bands are reported in cm^{-1} .

UV-visible spectroscopic data were obtained using a Hewlett-Packard HP 8452A Diode-Array Spectrophotometer. Wavelength maxima, λ_{max} , are given in nm, and extinction coefficients are given as $\log \epsilon$ following the reported wavelengths.

Thermal gravimetric measurements were obtained using a TA Instruments TGA 51 Thermogravimetric Analyzer fitted with a quartz furnace tube with a temperature range from ambient to 1200 $^{\circ}\text{C}$.

Photochemical experiments were carried out at r.t. using an Ace-Hanovia 450 Watt high pressure Hg vapour lamp (cat. #7825-34, Ace Glass Inc.).

Conductivity measurements were obtained at r.t. at $\sim 10^{-3}$ M concentrations using a Thomas Serfass conductivity bridge, and a cell from Yellow Springs Instrument Company.

Values are given in $\text{ohm}^{-1}\text{mol}^{-1}\text{cm}^2$. The value of the cell constant was determined to be 1.016.

Melting point measurements were obtained using a Fisher-Johns melting point apparatus and were uncorrected.

2.2.3 Magnetic Susceptibility

Solution magnetic moments were measured at r.t. using the Evans method.^{1,2} A solution of the complex dissolved in MeOD/ CDCl_3 was placed in a sealed capillary tube. This was placed inside an NMR tube, with CDCl_3 as the reference, and held in place with a Teflon spacer.² The paramagnetic shift of the residual CHCl_3 in CDCl_3 in the capillary sample was measured and compared to that of the corresponding peak in the CDCl_3 reference.

Solid-state magnetic measurements were obtained using a Johnson-Matthey magnetic susceptibility balance.

2.2.3.1 Calculation of χ_g , Magnetic Susceptibility of the Dissolved Paramagnetic Species and Magnetic Susceptibility per Gram of Sample

$\chi_g (10^{-6} \text{ cm}^3 \text{ g}^{-1})$ can be calculated according to $\chi_g = \chi_o + 3\Delta\nu/4\pi\nu_o c$

where χ_o = magnetic susceptibility of the pure solvent ($10^{-6} \text{ cm}^3 \text{ g}^{-1}$),

$\Delta\nu$ = paramagnetic shift (Hz), ν_o = operating frequency of the spectrometer (Hz),

and c = concentration (g/mL).²

For the solid state measurement, $\chi_g (10^{-6} \text{ cm}^3 \text{ g}^{-1})$ can be calculated according to the equation

$$\chi_g = C_{\text{bal}} (l)(R-R_o)/10^9 m$$

where l = sample length (cm), m = sample mass (g), R = reading for tube and sample, R_o = reading for the empty tube, and C_{bal} = balance calibration constant, 1.158.

2.2.3.2 Calculation of χ_M , the Molar Magnetic Susceptibility

χ_M ($10^{-6} \text{ cm}^3 \text{ mol}^{-1}$) can be calculated according to the equation $\chi_M = \chi_g M$

where M = molecular weight of the paramagnetic species (g/mole).

χ_M of a complex consists of the summation of χ_M' values for the central ion(s), the coordinated ligands, other species present, and the metal.

$$\text{Thus } \chi_{M \text{ complex}} = \chi_{M(\text{metal ion})}' + \chi_{M(\text{ligands})}' + \chi_{M(\text{other species})}' + \chi_{M(\text{metal})}'$$

where χ_M' for the ligands, solvent and metal can be determined from Pascal's constants.³

2.2.3.3 Calculation of μ_{eff} , the Effective Magnetic Moment

$\chi_{M(\text{metal ion})}'$ is related to μ_{eff} (B. M.) according to the equation

$$\mu_{\text{eff}} = 2.828(\chi_{M(\text{metal ion})}' \cdot T)^{1/2}$$

where T = absolute temperature (K)

2.2.3.4 Calculation of n , the Number of Unpaired Electrons

For the spin-only value, μ_{eff} is related to n and can be calculated according to the following equation

$$\mu_{\text{eff}} = (n(n+2))^{1/2}$$

2.2.4 Elemental Analyses, Mass Spectral Analyses and X-ray Crystallography

Elemental analyses were obtained by Mr. P. Borda. Mass spectral analyses were obtained in a facility headed by Dr. G. Eigendorf. Both EI and LSIMS (on thioglycerol and 3-nitrobenzylalcohol matrices) methods of ionization were used. X-ray crystallographic structures were obtained by the late Dr. S. J. Rettig with a Siemens SMART CCD diffractometer or a Rigaku AFC6S diffractometer (both with graphite monochromated Mo-K α radiation), or a Rigaku/ADSC CCD area detector with graphite monochromated Mo-K α or Cu-K α radiation; and by Dr. Victor G. Young, Jr. at the University of Minnesota on a Siemens SMART Platform CCD area detector (graphite monochromator, Mo-K α radiation).

2.3 Synthesis of Dithioethers

The dithioethers, 3,6-dithiaoctane and 4,7-dithiadecane were commercially available. The other dithioethers were synthesized in air following the procedure of Morgan and Ledbury.⁴ The dithioethers synthesized are new compounds unless otherwise indicated (by a superscript in the heading). The materials (except in the case of 1,2-bis(phenyl)dithiaethane) are oils and are hygroscopic in nature, and the determined elemental analyses values were not always satisfactory.

2.3.1 3,7-Dithianonane (*MW* = 164.32 g/mol)

Ethanethiol (30 mL, 400 mmol) was added dropwise to a saturated solution (50 mL) of NaOH in MeOH cooled in a dry-ice/acetone bath. The solution was allowed to warm

to r.t. and then stirred at 70 °C for 1 h. The solution was then cooled again with a dry-ice/acetone bath, and 1,3-dibromopropane (20.6 mL, 200 mmol) was added dropwise with constant stirring. The resulting mixture was then warmed to 70 °C and left for 1 h. This solution was then poured into H₂O (100 mL), when the oily, immiscible dithioether layer was collected. The aqueous layer was extracted three times with Et₂O (40 mL) portions; the organic residues were combined, the Et₂O was removed by rotary evaporation, and the oily product was dried over MgSO₄. Yield 21 g (64 %). Anal. Calcd for C₇H₁₆S₂: C, 51.17; H, 9.81. Found: C, 50.97; H, 9.77 %. ¹H-NMR (CDCl₃, 200 MHz) δ 2.60 (m, 8H, CH₂SCH₂), 1.85 (q, 2H, CH₂CH₂CH₂), 1.25 (t, 6H, CH₃). Mass spectrum [LSIMS, m/z] 164 [M]⁺, 135 [M-C₂H₅]⁺.

2.3.2 4,8-Dithiaunadecane (MW = 192.37 g/mol)

4,8-Dithiaunadecane was prepared according to the procedure described in Section 2.3.1, but using propanethiol (30 mL, 330 mmol) and 1,3-dibromopropane (16.8 mL, 165 mmol). Yield 28 g (88 %). Anal. Calcd for C₉H₂₀S₂: C, 56.19; H, 10.48. Found: C, 57.69; H, 10.77 %. ¹H-NMR (CDCl₃, 200 MHz) δ 2.60 (t, 4H, CH₂CH₂CH₂), 2.50 (t, 4H, CH₂CH₂CH₃), 1.85 (q, 2H, CH₂CH₂CH₂), 1.60 (s, 4H, CH₂CH₂CH₃), 1.02 (t, 6H, CH₃). Mass spectrum [LSIMS, m/z] 192 [M]⁺, 149 [M-C₃H₇]⁺.

2.3.3 2,8-Dimethyl-3,7-dithianonane (MW = 192.37 g/mol)

The title dithioether was prepared according to the procedure given in Section 2.3.1, but using 2-propanethiol (40 mL, 430 mmol) and 1,3-dibromopropane (21.9 mL, 210 mmol). Yield 32 g (80 %). Anal. Calcd for C₉H₂₀S₂: C, 56.19; H, 10.48. Found: C, 55.32;

H, 10.39 %. $^1\text{H-NMR}$ (CDCl_3 , 200 MHz) δ 2.90 (m, 2H, $(\text{CH}_3)_2\text{CHS}$), 2.60 (t, 4H, $\text{CH}_2\text{CH}_2\text{CH}_2$), 1.85 (qt, 2H, $\text{CH}_2\text{CH}_2\text{CH}_2$), 1.30 (d, 12H, $\text{SCH}(\text{CH}_3)_2$). Mass spectrum [LSIMS, m/z] 193 $[\text{M}]^+$.

2.3.4 5,9-Dithiatridecane ($MW = 220.42 \text{ g/mol}$)

5,9-Dithiatridecane was prepared according to the procedure given in Section 2.3.1, but using butanethiol (40 mL, 370 mmol) and 1,3-dibromopropane (18.9 mL, 187 mmol). Yield 36 g (87 %). Anal. Calcd for $\text{C}_{11}\text{H}_{24}\text{S}_2$: C, 59.94; H, 10.97. Found: C, 59.57; H, 11.10 %. $^1\text{H-NMR}$ (CDCl_3 , 200 MHz) δ 2.60 (m, 8H, CH_2SCH_2), 1.85 (q, 2H, $\text{CH}_2\text{CH}_2\text{CH}_2$), 1.56 (q, 4H, $\text{CH}_2\text{CH}_2\text{CH}_3$), 1.42 (s, 4H, CH_2CH_3), 0.92 (t, 6H, CH_3). Mass spectrum [LSIMS, m/z] 220 $[\text{M}]^+$, 163 $[\text{M}-\text{C}_4\text{H}_9]^+$.

2.3.5 6,10-Dithiapentadecane ($MW = 248.47 \text{ g/mol}$)

6,10-Dithiapentadecane was prepared according to the procedure described in Section 2.3.1, but using pentanethiol (23.8 mL, 192 mmol) and 1,3-dibromopropane (9.7 mL, 96 mmol). Yield 21 g (88 %). Anal. Calcd for $\text{C}_{13}\text{H}_{28}\text{S}_2$: C, 62.84; H, 11.36. Found: C, 60.58; H, 11.08 %. $^1\text{H-NMR}$ (CDCl_3 , 200 MHz) δ 2.56 (m, 8H, CH_2SCH_2), 1.85 (q, 2H, $\text{CH}_2\text{CH}_2\text{CH}_2$), 1.56 (q, 4H, $\text{CH}_2\text{CH}_2\text{CH}_2\text{CH}_3$), 1.35 (m, 8H, $\text{CH}_2\text{CH}_2\text{CH}_3$), 0.92 (t, 6H, CH_3). Mass spectrum [LSIMS, m/z] 248 $[\text{M}]^+$, 177 $[\text{M}-\text{C}_5\text{H}_{11}]^+$.

2.3.6 1,3-Bis(phenylthio)propane ($MW = 260.41 \text{ g/mol}$)⁵

The dithioether was prepared according to the procedure given in Section 2.3.1, but using benzenethiol (50 mL, 487 mmol) and 1,3-dibromopropane (24.7 mL, 244 mmol).

Yield 47 g (74 %). Anal. Calcd for $C_{15}H_{16}S_2$: C, 69.18; H, 6.19. Found: C, 68.28; H, 6.27 %. 1H -NMR ($CDCl_3$, 200 MHz) δ 7.55 (m, 10H, C_6H_5), 2.93 (m, 4H, $CH_2CH_2CH_2$), 2.10 (m, 2H, $CH_2CH_2CH_2$). Mass spectrum [LSIMS, m/z] 260 $[M]^+$. The 1H NMR data compare well with literature values.⁵

2.3.7 5,8-Dithiadodecane ($MW = 206.39$ g/mol)

5,8-Dithiadodecane was prepared according to the procedure given in Section 2.3.1, but using butanethiol (13 mL, 120 mmol) and 1,2-dibromoethane (5.3 mL, 61 mmol). Yield 14.5 g (58 %). Anal. Calcd for $C_{10}H_{22}S_2$: C, 58.19; H, 10.74. Found: C, 58.38; H, 10.76 %. 1H -NMR ($CDCl_3$, 200 MHz) δ 2.73 (s, 4H, SCH_2CH_2S), 2.55 (t, 4H, CH_2S), 1.45 (m, 8H, $CH_2CH_2CH_3$), 0.90 (t, 6H, CH_3). Mass spectrum [LSIMS, m/z] 206 $[M]^+$, 149 $[M-C_4H_9]^+$.

2.3.8 6,9-Dithiatetradecane ($MW = 234.44$ g/mol)

The dithioether was prepared according to the procedure given in Section 2.3.1, but using pentanethiol (9.8 mL, 80 mmol) and 1,2-dibromoethane (3.4 mL, 40 mmol). Yield 6.1 g (65 %). Anal. Calcd for $C_{12}H_{26}S_2$: C, 61.48; H, 11.18. Found: C, 61.09; H, 10.99 %. 1H -NMR ($CDCl_3$, 200 MHz) δ 2.75 (s, 4H, SCH_2CH_2S), 2.55 (t, 4H, CH_2S), 1.60 (q, 4H, $CH_2CH_2CH_2CH_3$), 1.35 (m, 8H, $CH_2CH_2CH_3$), 0.92 (t, 6H, CH_3). Mass spectrum [LSIMS, m/z] 234 $[M]^+$.

2.3.9 7,10-Dithiahexadecane ($MW = 262.49 \text{ g/mol}$)

7,10-Dithiahexadecane was prepared according to the procedure given in Section 2.3.1, but using hexanethiol (40 mL, 280 mmol) and 1,2-dibromoethane (12.2 mL, 142 mmol). Yield 25 g (67 %). Anal. Calcd for $C_{14}H_{30}S_2$: C, 64.06; H, 11.52. Found: C, 63.88; H, 11.39 %. $^1\text{H-NMR}$ (CDCl_3 , 200 MHz) δ 2.75 (s, 4H, $\text{SCH}_2\text{CH}_2\text{S}$), 2.55 (t, 4H, CH_2S), 1.55 (q, 4H, $\text{CH}_2\text{CH}_2\text{CH}_2\text{CH}_2\text{CH}_3$), 1.30 (m, 12H, $\text{CH}_2\text{CH}_2\text{CH}_2\text{CH}_3$), 0.95 (t, 6H, CH_3). Mass spectrum [LSIMS, m/z] 262 $[\text{M}]^+$.

2.3.10 1,2-Bis(phenylthio)ethane ($MW = 246.38 \text{ g/mol}$)^{5,6}

1,2-Bis(phenylthio)ethane was prepared generally according to the procedure given in Section 2.3.1, but using benzenethiol (50 mL, 480 mmol) and 1,2-dibromoethane (21 mL, 240 mmol), while the aqueous layer was extracted three times with CHCl_3 (40 mL) portions; the organic residues were combined and the CHCl_3 was removed by rotary evaporation. The white solid obtained after removal of CHCl_3 was recrystallized using CH_2Cl_2 (7 mL) and Et_2O (100 mL). Yield 39 g (65 %). Anal. Calcd for $C_{14}H_{14}S_2$: C, 68.25; H, 5.73. Found: C, 68.18; H, 5.71 %. $^1\text{H-NMR}$ (CDCl_3 , 200 MHz) δ 7.15 (m, 10H, C_6H_5), 3.10 (s, 4H, CH_2CH_2). The ^1H NMR data compare well with literature values.⁵

2.3.11 1,2-Bis(cyclohexylthio)ethane ($MW = 258.47 \text{ g/mol}$)

The dithioether was prepared according to the procedure given in Section 2.3.1, but using cyclohexylthiol (50 mL, 400 mmol) and 1,2-dibromoethane (17.6 mL, 204 mmol). Yield 23.7 g (45 %). Anal. Calcd for $C_{14}H_{26}S_2$: C, 65.06; H, 10.14. Found: C, 64.91; H, 10.03 %. $^1\text{H-NMR}$ (CDCl_3 , 400 MHz) δ 2.70 (s, 4H, CH_2CH_2), 1.95, 1.75 (m 4H each, H_2),

1.58 (m, 2H, H₁), 1.29 (m, 12H, H_{3,4}). Mass spectrum [LSIMS, m/z] 258 [M]⁺. The labelled H-atoms are associated with the corresponding C-atoms as shown in Figure 2.1.

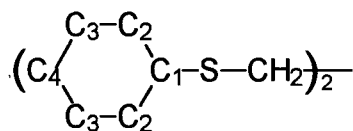


Figure 2.1. Diagram showing the labelling of the H-atoms of 1,2-bis(cyclohexylthio)ethane.

2.4 Oxidation of Dithioethers to Disulfoxides

The dialkylsulfoxides were synthesized by acid-catalyzed, DMSO oxidation of the corresponding dithioethers following the procedure reported by Hull and Bargar.⁷ The diarylsulfoxides were synthesized by H₂O₂ oxidation of the corresponding diarylsulfide following the procedure reported by Bennett *et al.*⁸ The disulfoxides synthesized are new unless otherwise indicated (by a superscript in the heading).

2.4.1 1,3-Bis(ethylsulfinyl)propane (BESP) (MW = 196.32 g/mol)

A solution consisting of 3,7-dithianonane (10 mL, 60 mmol), DMSO (9.5 mL, 120 mmol) and conc. HCl (200 μ L) was heated for 8 h at 85 °C with constant stirring. The sulfoxide precipitated as thin, white crystals when the reaction mixture was cooled to 0 °C. The crude product was collected and washed with acetone to remove excess DMSO and DMS. The filtrate was heated again for a further 4 h, and more product was obtained. The crude sulfoxide was recrystallized from EtOH (50 mL) three times. Yield 7.8 g (65 %). Anal. Calcd for C₇H₁₆O₂S₂: C, 42.83; H, 8.21. Found: C, 43.14; H, 8.19 %. ¹H-NMR (CDCl₃, 200

MHz) δ 2.90 (m, 8H, $\text{CH}_2\text{S}(\text{O})\text{CH}_2$), 2.45 (m, 2H, $\text{CH}_2\text{CH}_2\text{CH}_2$), 1.35 (t, 6H, CH_3). IR ν_{SO} : 1016, 1047. M. p. $^{\circ}\text{C}$: 127-130.

2.4.2 1,3-Bis(propylsulfinyl)propane (BPSP) ($MW = 224.37 \text{ g/mol}$)

BPSP was prepared according to the procedure given in Section 2.4.1, but using 4,8-dithiaunadecane (10 mL, 52 mmol), DMSO (8 mL, 100 mmol) and conc. HCl (200 μL). Yield 8.9 g (77 %). Anal. Calcd for $\text{C}_9\text{H}_{20}\text{O}_2\text{S}_2$: C, 48.18; H, 8.98. Found: C, 48.09; H, 9.09 %. $^1\text{H-NMR}$ (CDCl_3 , 200 MHz) δ 3.00 (m, 4H, $\text{CH}_2\text{CH}_2\text{CH}_2$), 2.90 (m, 4H, $\text{CH}_2\text{S}(\text{O})$), 2.20 (m, 2H, $\text{CH}_2\text{CH}_2\text{CH}_2$), 1.80 (m, 4H, $\text{CH}_2\text{CH}_2\text{CH}_3$), 1.07 (t, 6H, CH_3). IR ν_{SO} : 1021, 1075. M. p. $^{\circ}\text{C}$: 140-143.

2.4.3 1,3-Bis(*i*-propylsulfinyl)propane (BⁱPSP) ($MW = 224.37 \text{ g/mol}$)

BⁱPSP was prepared generally according to the procedure given in Section 2.4.1, but using 2,8-dimethyl-3,7-dithianonane (10 mL, 52 mmol), DMSO (8 mL, 100 mmol) and conc. HCl (200 μL). The sulfoxide precipitated as small white crystals when the reaction mixture was cooled to 0°C , after the sides of the flask were scratched and Et_2O (30 mL) was added. Yield 2.3 g (20 %). Anal. Calcd for $\text{C}_9\text{H}_{20}\text{O}_2\text{S}_2$: C, 48.18; H, 8.98. Found: C, 48.32; H, 9.06 %. $^1\text{H-NMR}$ (CDCl_3 , 200 MHz) δ 2.75 (m, 6H, $\text{CHS}(\text{O})\text{CH}_2\text{CH}_2\text{CH}_2\text{S}(\text{O})\text{CH}$), 2.35 (m, 2H, $\text{CH}_2\text{CH}_2\text{CH}_2$), 1.35 (d, 12H, $(\text{CH}_3)_2$). IR ν_{SO} : 1016.

2.4.4 1,3-Bis(butylsulfinyl)propane (BBSP) ($MW = 252.42 \text{ g/mol}$)

BBSP was prepared according to the procedure given in Section 2.4.1, but using 5,9-dithiatridecane (10 mL, 45 mmol), DMSO (7 mL, 90 mmol) and conc. HCl (200 μL).

Yield 9.9 g (87 %). Anal. Calcd for $C_{11}H_{24}O_2S_2$: C, 52.34; H, 9.58. Found: C, 52.36; H, 9.56 %. 1H -NMR ($CDCl_3$, 200 MHz) δ 2.80 (m, 8H, $CH_2S(O)CH_2$), 2.40 (m, 2H, $CH_2CH_2CH_2$), 1.75 (q, 4H, $CH_3CH_2CH_2$), 1.50 (s, 4H, CH_3CH_2), 0.95 (t, 6H, CH_3). IR ν_{SO} : 1021. M. p. $^{\circ}C$: 146-148.

2.4.5 1,3-Bis(pentylsulfinyl)propane (BPeSP) ($MW = 280.47$ g/mol)

BPeSP was prepared according to the procedure described in Section 2.4.1, but using 6,10-dithiapentadecane (10 mL, 40 mmol), DMSO (6 mL, 80 mmol) and conc. HCl (200 μ L). Yield 3.3 g (29 %). Anal. Calcd for $C_{13}H_{28}O_2S_2$: C, 55.67; H, 10.06. Found: C, 55.48; H, 10.12 %. 1H -NMR ($CDCl_3$, 200 MHz) δ 2.70 (m, 8H, $CH_2S(O)CH_2$), 2.25 (m, 2H, $CH_2CH_2CH_2$), 1.68 (q, 4H, $CH_3CH_2CH_2CH_2$), 1.28 (m, 8H, $CH_3CH_2CH_2$), 0.85 (t, 6H, CH_3). IR ν_{SO} : 1026. M. p. $^{\circ}C$: 125-129.

2.4.6 1,3-Bis(phenylsulfinyl)propane (BPhSP) ($MW = 292.41$ g/mol)

1,3-Bis(phenylthio)propane (10 g, 38 mmol) was added to 200 mL of glacial acetic acid, and the solution was cooled to 0 $^{\circ}C$. 9 mL of 30 % H_2O_2 (76 mmol) was added dropwise at 0 $^{\circ}C$. The resulting solution, after being stirred for 24 h at r.t., was then extracted three times with $CHCl_3$ (50 mL portions). The $CHCl_3$ was neutralized with a saturated $NaHCO_3$ solution. This $CHCl_3$ layer was then washed with H_2O and then dried over $MgSO_4$. The $MgSO_4$ was removed and the $CHCl_3$ was removed by rotary evaporation before the product was collected as a white solid. The crude product was recrystallized with a minimal of CH_2Cl_2 (7 mL) and Et_2O (50 mL). Yield 2.1 g (19 %). Anal. Calcd for $C_{15}H_{16}O_2S_2$: C, 61.61; H, 5.51. Found: C, 61.42; H, 5.42 %. 1H -NMR ($CDCl_3$, 200 MHz) δ 7.50 (m, 10H,

C_6H_5), 2.90 (m, 2H, $CH_2CH_2CH_2$), 2.15 (m, 4H, $CH_2CH_2CH_2$). IR ν_{SO} : 1021, 1040, 1084. M. p. °C: 137-140. Of note, an attempt to oxidize 1,3-bis(phenylthio)propane using air/DMSO oxidation led to an oily product, which by TLC, 1H NMR spectroscopy and ν_{SO} data appeared to be the disulfoxide. However, reaction of this oil with $RuCl_3 \cdot 3H_2O$, using the procedure described in Section 2.7.4, led to the isolation of red crystals which were submitted for X-ray analysis. The structural diagram (see Chapter 6) shows one coordinated disulfoxide and one 'half-oxidized' dithioether.

2.4.7 1,2-Bis(ethylsulfinyl)ethane (BESE) ($MW = 182.29 \text{ g/mol}$)^{9,10}

BESE was prepared according to the procedure given in Section 2.4.1, but using 3,6-dithiaoctane (10 mL, 66 mmol) in DMSO (11 mL, 150 mmol) and conc. HCl (200 μ L). Yield 7.8 g (65 %). 1H -NMR (D_2O , 200 MHz) δ 3.30 (m, 4H, CH_2CH_2), 2.92 (m, 4H, CH_3CH_2), 1.23 (t, 6H, CH_3). M. p. °C: 148-149. The 1H NMR data compare well with reported values.^{9,10}

2.4.8 1,2-Bis(propylsulfinyl)ethane (BPSE) ($MW = 210.34 \text{ g/mol}$)^{9,10}

BPSE was prepared according to the procedure given in Section 2.4.1, but using 4,7-dithiadecane (10 mL, 56 mmol) in DMSO (8.7 mL, 110 mmol) and conc. HCl (200 μ L). Yield 8.2 g (70 %). 1H -NMR ($CDCl_3$, 200 MHz) δ 3.20, 3.00 (m, 2H each, $S(O)CH_2CH_2S(O)$), 2.77 (m, 4H, $CH_2S(O)$), 1.92 (m, 4H, CH_3CH_2), 1.10 (t, 6H, CH_3). M. p. °C: 162-164. The 1H NMR data compare well with reported values.^{9,10}

2.4.9 1,2-Bis(butylsulfinyl)ethane (BBSE) ($MW = 238.34 \text{ g/mol}$)

BBSE was prepared according to the procedure described in Section 2.4.1, but using 5,8-dithiadodecane (10 mL, 48 mmol) in DMSO (8 mL, 97 mmol) and conc. HCl (200 μL). Yield 2.3 g (20 %). Anal. Calcd for $\text{C}_{10}\text{H}_{22}\text{O}_2\text{S}_2$: C, 50.37; H, 9.30. Found: C, 50.29; H, 9.43 %. $^1\text{H-NMR}$ (CDCl_3 , 200 MHz) δ 3.20, 3.00 (m, 2H each, $\text{S(O)CH}_2\text{CH}_2\text{S(O)}$), 2.75 (m, 4H, $\text{CH}_2\text{S(O)}$), 1.72 (m, 4H, $\text{CH}_3\text{CH}_2\text{CH}_2$), 1.45 (m, 4H, CH_3CH_2), 0.95 (t, 6H, CH_3). IR ν_{SO} : 1014. M. p. $^\circ\text{C}$: 172-173.

2.4.10 1,2-Bis(pentylsulfinyl)ethane (BPeSE) ($MW = 266.39 \text{ g/mol}$)

BPeSE was prepared according to the procedure given in Section 2.4.1, but using 6,9-dithiatetradecane (10 mL, 40 mmol) in DMSO (7 mL, 80 mmol) and conc. HCl (200 μL). Yield 3.9 g (34 %). Anal. Calcd for $\text{C}_{12}\text{H}_{26}\text{O}_2\text{S}_2$: C, 54.09; H, 9.83. Found: C, 54.11; H, 10.10 %. $^1\text{H-NMR}$ (CDCl_3 , 200 MHz) δ 3.20, 3.10 (m, 2H each, $\text{S(O)CH}_2\text{CH}_2\text{S(O)}$), 2.80 (m, 4H, $\text{CH}_2\text{S(O)}$), 1.80 (m, 4H, $\text{CH}_3\text{CH}_2\text{CH}_2\text{CH}_2$), 1.40 (m, 8H, $\text{CH}_3\text{CH}_2\text{CH}_2$), 0.93 (t, 6H, CH_3). IR ν_{SO} : 1014, 1073, 1100. M. p. $^\circ\text{C}$: 134-135.

2.4.11 1,2-Bis(hexylsulfinyl)ethane (BHSE) ($MW = 294.44 \text{ g/mol}$)

BHSE was prepared according to the procedure given in Section 2.4.1, but using 7,10-dithiahexadecane (10 mL, 38 mmol) in DMSO (6 mL, 76 mmol) and conc. HCl (200 μL). Yield 6.2 g (55 %). Anal. Calcd for $\text{C}_{14}\text{H}_{30}\text{O}_2\text{S}_2$: C, 57.09; H, 10.27. Found: C, 57.00; H, 10.19 %. $^1\text{H-NMR}$ (CDCl_3 , 200 MHz) δ 3.20, 3.10 (m, 2H each, $\text{S(O)CH}_2\text{CH}_2\text{S(O)}$),

2.80 (m, 4H, $\text{CH}_2\text{S}(\text{O})$), 1.80 (m, 8H, $\text{CH}_3\text{CH}_2\text{CH}_2\text{CH}_2\text{CH}_2$), 1.40 (m, 8H, $\text{CH}_3\text{CH}_2\text{CH}_2$), 0.93 (t, 6H, CH_3). IR ν_{SO} : 1016, 1114. M. p. °C: 176.5-177.5.

2.4.12 *1,2-Bis(cyclohexylsulfinyl)ethane (BCySE) (MW = 290.47 g/mol)*

BCySE was prepared according to the procedure given in Section 2.4.1, but using 1,2-bis(cyclohexylthio)ethane (10 mL, 40 mmol) in DMSO (6 mL, 77 mmol) and conc. HCl (200 μL). Yield 9.1 g (80 %). Anal. Calcd for $\text{C}_{14}\text{H}_{26}\text{O}_2\text{S}_2$: C, 57.89; H, 9.02. Found: C, 58.13; H, 9.13 %. ^1H -NMR (CDCl_3 , 400 MHz) δ 3.60 (m, 4H, CH_2CH_2), 2.56, 2.15 (m, 2H each, H_2), 1.69 (m, 2H, H_1), 1.35 (m, 12H, $\text{H}_{3,4}$). IR ν_{SO} : 1018. M. p. °C: 172-174. (See Section 2.3.11 for the labelling of the H-atoms).

2.4.13 *1,2-Bis(phenylsulfinyl)ethane (BPhSE) (MW = 278.38 g/mol)*⁶

BPhSE was prepared according to the procedure given in Section 2.4.6, but using 1,2-bis(phenylthio)ethane (10 g, 40 mmol) and 9 mL of 30 % H_2O_2 (80 mmol). Yield 7.4 g (65 %). Anal. Calcd for $\text{C}_{14}\text{H}_{14}\text{O}_2\text{S}_2$: C, 60.40; H, 5.07. Found: C, 60.52; H, 5.06 %. ^1H -NMR (CDCl_3 , 200 MHz) δ 7.45 (m, 10H, C_6H_5), 3.35, 2.70 (m, 2H each, CH_2CH_2). IR ν_{SO} : 1035, 1089. M. p. °C: 165-170. The spectroscopic data compare well with the literature data.⁶

2.5 Synthesis of Ru(III) Precursor Complexes

The precursors listed below were synthesized according to literature reports.

2.5.1 $[Ru(DMF)_6][OTf]_3$ ($MW = 986.85 \text{ g/mol}$)¹¹

The $[Ru(DMF)_6][OTf]_3$ was synthesized by a modified literature procedure by Judd *et al.*¹¹ A solution of $RuCl_3 \cdot 3H_2O$ (2.00 g, 10 mmol) in DMF (120 mL) with Sn granules (7.0 g, 59 mmol) was vigorously stirred at r.t. under N_2 . The suspension turned from dark-brown, through red-brown, green, to blue. $Pb(OTf)_2$ (6.50 g, 13 mmol) was then added. The mixture was stirred at 50 °C for 2 h, during which time the colour changed to deep brown-red. The mixture was then filtered to remove unreacted Sn and was concentrated on a rotary evaporator to 20 mL. CH_2Cl_2 (300 mL) was added, and the resulting suspension was then stirred in air at r.t. overnight. The mixture was filtered through Celite and the $PbCl_2$ was collected and discarded. CH_2Cl_2 was then removed. To the residue at r.t. was added 1,2- $C_2H_4Cl_2$ (40 mL), after which the solution was cooled to 4 °C to give a yellow precipitate. This was collected, redissolved in CH_2Cl_2 , and the solution filtered. The filtrate was evaporated to dryness, 5 mL of *n*-pentanol were added and the resulting yellow precipitate was collected, washed with Et_2O (50 mL), and dried *in vacuo*. The product was stored in the absence of light. Yield 2.3 g (31 %). Anal. Calcd for $C_{21}H_{42}N_6O_{15}S_3F_9Ru$: C, 25.56; H, 4.29; N, 8.52. Found: C, 25.43; H, 4.30; N, 8.54 %.

2.5.2 $K_3[RuCl_6]$ ($MW = 431.08 \text{ g/mol}$)¹²

$RuCl_3 \cdot 3H_2O$ (1.00 g, 4 mmol) was dissolved in 50 mL of MeOH. The solution was refluxed under H_2 , when the yellow-brown solution began to turn green after about 5 h. At this stage, KCl (0.90 g, 12 mmol) was added and the mixture refluxed in air. The KCl slowly dissolved with concomitant formation of a brown precipitate; this was filtered off from the colourless supernatant and washed with MeOH. The crude product was recrystallized from 12M HCl, washed with MeOH and vacuum-dried. Yield 1.1 g (67 %). UV-Vis (12 M HCl) 348 (3.45), 312 (3.33), 228 (4.38). The UV-Vis data compare well with the literature data.¹²

2.6 Synthesis of Monodentate Sulfoxide Complexes of Ruthenium

2.6.1 $Cis-RuCl_2(DMSO)_4$ ($MW = 484.50 \text{ g/mol}$)¹³

$RuCl_3 \cdot 3H_2O$ (2.00 g, 7.6 mmol) was dissolved in DMSO (8 mL, 110 mmol), and the reaction mixture was refluxed for 20 min. The complex precipitated as a fine, yellow, crystalline powder when the reaction mixture was cooled to r.t. Acetone (30 mL) was added and more complex precipitated. The yellow precipitate was collected in air and dried *in vacuo* at 70 °C. Yield 3.1 g (85 %). 1H -NMR ($CDCl_3$, 200 MHz) δ 3.55, 3.52, 3.46, 3.45 (DMSO), 2.75 (DMSO), 2.62 (free DMSO). The 1H NMR data and yield compare well with the literature data.¹³

2.6.2 *Trans*-RuCl₂(DMSO)₄ (MW = 484.50 g/mol)¹⁴

Cis-RuCl₂(DMSO)₄ (2.5 g, 5.2 mmol) was dissolved in DMSO (40 mL, 560 mmol), and this resulting solution was transferred to a glass photolysis tube (450 W Hg lamp, see Appendix 2, Figure A.2.1) outfitted with a water-cooled condenser and a septum that allowed for a constant flow of Ar through the solution. The solution was photolysed for 4 h after which a yellow/orange microcrystalline solid formed from the solution. The solid was collected in air and dried at 70 °C *in vacuo*. Yield 1.8 g (72 %). ¹H-NMR (D₂O, 200 MHz) δ 3.30 (s, DMSO), 2.63 (free DMSO). The spectroscopic data agree well with those previously reported.¹⁵

2.6.3 *Mer-cis*-[RuCl₃(DPSO)₂(DPSO)] (MW = 814.24 g/mol)

Conc. HCl (250 µL) was added to a solution of RuCl₃·3H₂O (250 mg, 1 mmol) in EtOH (15 mL), and the mixture was heated at 85 °C for 5 h until the solution turned green. DPSO (1.4 g, 7 mmol) was added and the mixture was refluxed for a further 6 h. The volume of the resulting dark-orange solution was then reduced until the reaction solution became oily. Ether was added and the resulting orange solution was set aside for 5-7 days at r.t. Crystals suitable for X-ray analysis formed on the side of the flask and were collected by filtration. Yield 360 mg (46 %). ¹H-NMR (CDCl₃, 200 MHz) δ 8.80 (broad peak), 7.70 and 7.45 (free DPSO). Anal. Calcd for C₃₆H₃₀Cl₃O₃RuS₃: C, 53.10; H, 3.71; S, 11.81. Found: C, 53.02; H, 3.72; S, 11.77 %. UV-Vis (CH₂Cl₂) 448 (3.14), 388 (3.39), 240 (4.46). IR ν_{SO}: 922, 1063, 1129. μ_{eff} (Evans) = 2.3 ± 0.1 B. M. During this thesis work, the Trieste group reported on the synthesis and structural characterization of this same DPSO complex.¹⁶

2.6.4 *Cis*-[Ru(12-S-4)(DMSO)(H₂O)][OTf]₂·CH₃OH (MW = 767.84 g/mol)

Cis-RuCl₂(DMSO)₄ (100 mg, 0.2 mmol) was added to 1,4,7,10-tetrathiacyclododecane (50 mg, 0.2 mmol) dissolved in CHCl₃ (25 mL) to give a yellow solution that was then refluxed for 3 h. The reaction solution was then cooled to r.t. when AgOTf (104 mg, 0.4 mmol) dissolved in acetone (10 mL) was added dropwise. The AgCl was filtered off through Celite, and to the filtrate was added CHCl₃ (5 mL). Yellow crystals suitable for X-ray analysis formed upon slow evaporation of the CHCl₃. Yield 66 mg (45 %). Anal. Calcd for C₁₂H₂₄F₆O₈RuS₇·CH₃OH: C, 20.33; H, 3.67. Found: C, 20.55; H, 3.49 %. ¹H-NMR (MeOD, 400 MHz) shows a multiplet centred at δ 3.1. IR ν_{SO}: 1027, 1082, 1158. UV-Vis (H₂O) 398 (3.19), 350 (3.05), 264 (4.01), 236 (3.99). Λ_M (H₂O) 139.

2.6.5 RuCl₂(DMSO)(L) (MW = 512.44 g/mol)

Cis-RuCl₂(DMSO)₄ (50 mg, 0.1 mmol) was added to a solution of 3,6,9,14-tetrathiabicyclo[9.2.1]tetradeca-11,13-diene (27 mg, 0.1 mmol) dissolved in CHCl₃ (20 mL) to give a yellow solution that was then refluxed for 3 h. The resulting red solution was cooled to r.t. and then evaporated to dryness. Hexanes (20 mL) was added to give an orange/red precipitate that was then dissolved in DMSO (1 mL). Crystals suitable for X-ray analysis were formed by vapour diffusion of Et₂O into the DMSO solution. Yield 22 mg (42 %). Anal. Calcd for C₁₂H₂₀Cl₂ORuS₅: C, 28.12; H, 3.93. Found: C, 28.46; H, 4.22 %. ¹H-NMR (DMSO *d*₆, 400 MHz) δ 7.1 (m, 2H, CH=CH) and a complex pattern between 2.7-4.5 (CH₂ protons of the macrocycle and methyls of DMSO). IR ν_{SO}: 1015, 1083, 1105. UV-Vis (DMSO) 416 (2.47), 272 (3.91).

2.7 Synthesis of Mononuclear Ru(II) Disulfoxide Complexes

2.7.1 *Cis-RuCl₂(BESE)₂* (*MW* = 536.57 g/mol)

To a solution of $K_3[RuCl_6]$ (250 mg, 0.6 mmol) in H_2O (15 mL) was added a solution of BESE (210 mg, 1.2 mmol) in MeOH (5 mL), and the mixture was heated to 50 °C for 5 h. The colour changed from light brown to yellow, and a yellow precipitate formed. Yield 112 mg (36 %). Anal Calcd for $C_{12}H_{28}Cl_2O_4RuS_4$: C, 26.86; H, 5.26. Found: C, 26.72; H, 5.22 %. 1H -NMR (D_2O , 200 MHz) δ 3.95-2.95 (m, 16H, $CH_2S(O)CH_2$), 1.45, 1.30 (t, 6H each, CH_3). IR ν_{SO} : 1092, 1122. The spectroscopic data agree well with those previously reported.^{9,10}

Other methods using $RuCl_3 \cdot 3H_2O$ and *trans*- $RuCl_2(DMSO)_4$ as precursors for the attempted synthesis of *trans*- $RuCl_2(BESE)_2$ led to the isolation of *cis*- $RuCl_2(BESE)_2$. Unsuccessful attempts were made to utilize photolysis (see Section 2.6.2) to effect the isomerization of *cis*- $RuCl_2(BESE)_2$ to *trans*- $RuCl_2(BESE)_2$, following a report by Alessio *et al.* in which the *cis* to *trans* isomerization of *cis*- $RuCl_2(DMSO)_4$ to *trans*- $RuCl_2(DMSO)_4$ was achieved using photolysis.¹⁴

2.7.2 *Trans-RuCl₂(BESE)₂·H₂O* (*MW* = 554.56 g/mol)

To a solution of $[RuCl(BESE)(H_2O)]_2(\mu-Cl)_2$ (25 mg, 0.035 mmol; see Section 2.8.1) in H_2O (10 mL) was added BESE (12.2 mg, 0.07 mmol), and the resulting yellow solution was refluxed for 4 h before being reduced in volume; the product formed as a crystalline powder. Crystals suitable for X-ray analysis were formed by slow evaporation of an aqueous solution of the complex. Yield 12 mg (33 %). Anal. Calcd for

$C_{12}H_{28}Cl_2O_4RuS_4 \cdot H_2O$: C, 25.98; H, 5.45. Found: C, 26.10; H, 5.18 %. 1H -NMR (D_2O , 200 MHz) δ 3.70 (m, 16H, $CH_2S(O)CH_2$), 1.45 (m, 12H, CH_3). IR ν_{SO} : 1093, 1119. UV-Vis (H_2O) 374 (2.78), 310 (3.19).

2.7.3 *Trans*- $RuCl_2(BPSE)_2 \cdot H_2O$ ($MW = 610.48$ g/mol)

To a solution of *cis*- $RuCl_2(DMSO)_4$ (172 mg, 0.36 mmol) in MeOH (10 mL) was added a solution of BPSE (150 mg, 0.70 mmol) in MeOH (5 mL). This yellow solution was refluxed for 3 h when a yellow precipitate formed. Yield 99 mg (47 %). Anal. Calcd for $C_{16}H_{36}Cl_2O_4RuS_4 \cdot H_2O$: C, 31.47; H, 6.27. Found: C, 31.62; H, 5.92 %. 1H -NMR ($CDCl_3$, 200 MHz) δ 3.75, 3.35 (m, 8H each, $CH_2S(O)CH_2$), 2.30, 2.85 (m, 4H each, CH_3CH_2), 1.10 (t, 12H, CH_3). IR ν_{SO} : 1094. The spectroscopic data agree well with those previously reported.^{9,10}

Other methods using $RuCl_3 \cdot 3H_2O$ and $K_3[RuCl_6]$ as precursors for the attempted synthesis of *cis*- $RuCl_2(BPSE)_2$ led to the isolation of *trans*- $RuCl_2(BPSE)_2$. Again, attempts were made to utilize photolysis to effect the isomerization of *trans*- $RuCl_2(BPSE)_2$ to *cis*- $RuCl_2(BPSE)_2$ (see Section 2.6.2), but these were unsuccessful.

2.7.4 *Cis*- $RuCl_2(BBSE)_2$ ($MW = 648.78$ g/mol)

Conc. HCl (100 μ L) was added to a solution of $RuCl_3 \cdot 3H_2O$ (100 mg, 0.4 mmol) in EtOH (30 mL), and the mixture was refluxed for 5 h. BBSE (182 mg, 0.8 mmol) was added and the mixture was refluxed for a further 6 h. The resulting yellow solution was then reduced in volume until a fine yellow precipitate formed, and this was collected. Yield 52 mg (21 %). Anal. Calcd for $C_{20}H_{44}Cl_2O_4RuS_4$: C, 37.03; H, 6.83. Found: C, 36.95; H, 6.80 %.

Crystals of an EtOH solvate suitable for X-ray analysis were formed by slow evaporation of an EtOH/CH₂Cl₂ solution of the complex. ¹H-NMR (CDCl₃, 200 MHz) δ 3.60 (m, 16H, CH₂S(O)CH₂), 1.55 (m, 16H, CH₃CH₂CH₂), 0.98 (m, 12H, CH₃). IR ν_{SO}: 1081, 1126. UV-Vis (CH₂Cl₂) 236 (4.38).

2.7.5 *Cis-RuCl₂(BPeSE)₂* (MW = 704.87 g/mol)

The procedure used was as given in Section 2.7.4, but using BPeSE (204 mg, 0.8 mmol). The yellow product was purified by column chromatography using neutral alumina with 5 % EtOH/CH₂Cl₂. Crystals, obtained by slow evaporation of an EtOH/CH₂Cl₂ solution of the complex, were subjected to X-ray analysis but excessive thermal motion due to the long pentyl groups prevented an accurate determination of the structure; however, *cis*-geometry was established. Yield 24 mg (9 %). Anal. Calcd for C₂₄H₅₂Cl₂O₄RuS₄: C, 40.89; H, 7.43. Found: C, 41.01; H, 7.58 %. ¹H-NMR (CDCl₃, 200 MHz) δ 3.70 (m, 16H, CH₂S(O)CH₂), 2.30, 1.85 (m, 4H each, CH₂CH₂S(O)), 1.45 (m, 16H, CH₃CH₂CH₂), 0.90 (m, 12H, CH₃). IR ν_{SO}: 1081, 1128. UV-Vis (CH₂Cl₂) 240 (4.17).

2.7.6 *Cis-RuCl₂(BCySE)₂* (MW = 752.92 g/mol)

The procedure used was given in Section 2.7.4, but BCySE (222 mg, 0.8 mmol) was used. An orange-yellow precipitate formed and was collected. Yield 86 mg (30 %). Anal. Calcd for C₂₈H₅₂Cl₂O₄RuS₄: C, 44.67; H, 6.96. Found: C, 44.34; H, 7.04 %. Crystals suitable for X-ray analysis were formed by slow evaporation of the reaction solution, and were found to contain one EtOH and 1/3 MeOH solvates per molecule. The ¹H-NMR spectrum of the title complex is a complicated pattern of overlapping multiplets in the δ 1.0-4.4 region.

Attempts to assign the spectrum using ^{13}C , HETCOR, ATP and ^1H decoupling experiments were unsuccessful. IR ν_{SO} : 1046, 1100. UV-Vis (CH_2Cl_2) 428 (2.81), 338 (3.01).

2.7.7 *Cis-RuCl₂(BESP)₂* ($MW = 564.60 \text{ g/mol}$)

The procedure used was described in Section 2.7.4, but BESP (150 mg, 0.8 mmol) was used, and the resulting yellow solution was evaporated to near dryness. The complex was purified by column chromatography as described in Section 2.7.5. Yield 77 mg (36 %). Anal. Calcd for $\text{C}_{14}\text{H}_{32}\text{Cl}_2\text{O}_4\text{RuS}_4$: C, 29.78; H, 5.71. Found: C, 29.57; H, 5.80 %. Crystals (containing one EtOH and one H_2O solvate molecules) suitable for X-ray analysis were formed by vapour diffusion of EtOH into a CH_2Cl_2 solution of the complex. ^1H -NMR (CDCl_3 , 200 MHz) δ 3.45 (m, 16H, $\text{CH}_2\text{S}(\text{O})\text{CH}_2$), 2.75, 2.10 (m, 2H each, $\text{CH}_2\text{CH}_2\text{CH}_2$), 1.45 (m, 12H, CH_3). IR ν_{SO} : 1042, 1088. UV-Vis (CH_2Cl_2) 348 (2.62), 262 (4.04), 246 (4.01).

Reactions of BPhSE, BHSE, BⁱPSP, BBSP, BPeSP, BPhSP and BMSB with $\text{RuCl}_3 \cdot 3\text{H}_2\text{O}$, utilizing the procedure in Section 2.7.4, led to yellow, uncharacterized products which by column chromatography yielded several bands or, in the case of BMSB, the isolated product was insoluble in common solvents. Elemental analyses for the products obtained from the major chromatography bands and the insoluble products were variable from repeat reactions.

2.8 Synthesis of Dinuclear Ru(II)/Ru(II) Disulfoxide Complexes

2.8.1 $[RuCl(BESE)(H_2O)]_2(\mu-Cl)_2$ ($MW = 744.59$ g/mol)

The procedure used was as given in Section 2.7.4, but using BESE (70 mg, 0.4 mmol). A yellow precipitate was formed, and was collected. Yield 87 mg (60 %). Anal. Calcd for $C_6H_{16}Cl_2O_3RuS_2$: C, 19.35; H, 4.33; S, 17.22. Found: C, 19.63; H, 4.38; S, 17.44 %. 1H -NMR (D_2O , 200 MHz) δ 3.60 (m, 16H, $CH_2S(O)CH_2$), 1.50 (m, 12H, CH_3). UV-Vis (H_2O) 424 (2.63), 326 (3.16), 278 (3.42), 238 (3.47). IR ν_{SO} : 1042, 1071, 1118. Crystals suitable for X-ray analysis were formed by slow evaporation of H_2O solution of the complex and were found to contain one H_2O solvate per molecule. TGA (crystals): Calcd loss of $3H_2O$: 7.1 % and 2BESE: 51.5 %. Found: 6.8 % (from $\sim 20^\circ C$ to $\sim 220^\circ C$) and 46.0 % (from $\sim 220^\circ C$ to $\sim 370^\circ C$), respectively (Appendix 4, Figure A.4.1). Λ_M (H_2O , increasing to a maximum, steady value at ≥ 20 min) 358.

Initial attempts to synthesize imidazole complexes using $[RuCl(BESE)(H_2O)]_2(\mu-Cl)_2$ as a precursor, with 2-nitroimidazole, 2-methyl-5-nitroimidazole and imidazole led to the isolation of water-soluble, red complexes that could not be purified by column chromatography and did not analyze well for C or H content. These reactions will be discussed in more detail in Chapter 6.

2.8.2 $[RuCl(BPSE)(H_2O)]_2(\mu-Cl)_2$ ($MW = 800.61$ g/mol)

The procedure used was as given in Section 2.7.4, but using BPSE (84 mg, 0.4 mmol). The yellow precipitate was collected. Yield 70 mg (46 %). Anal. Calcd for

$\text{C}_8\text{H}_{20}\text{Cl}_2\text{O}_3\text{RuS}_2$: C, 24.00; H, 5.03. Found: C, 23.64; H, 4.82 %. ^1H -NMR (D_2O , 400 MHz) δ 3.70 (m, 16H, $\text{CH}_2\text{S}(\text{O})\text{CH}_2$), 2.00 (m, 8H, CH_2CH_3), 1.05 (m, 12H, CH_3). IR ν_{SO} : 1048, 1083 and 1119. UV-Vis (H_2O) 268 (4.60). Λ_{M} (H_2O , increasing to a maximum, steady value at ≥ 30 min) 282.

2.8.3 $[\text{RuCl}(\text{BBSE})(\text{H}_2\text{O})]_2(\mu\text{-Cl})_2$ ($MW = 856.75$ g/mol)

The procedure used was as given in Section 2.7.4, but using BBSE (95 mg, 0.4 mmol). The yield of the yellow precipitate was 100 mg (61 %). Anal. Calcd for $\text{C}_{10}\text{H}_{24}\text{Cl}_2\text{O}_3\text{RuS}_2$: C, 28.04; H, 5.43. Found: C, 28.51; H, 5.43 %. ^1H -NMR (D_2O , 400 MHz) δ 3.65 (m, 16H, $\text{CH}_2\text{S}(\text{O})\text{CH}_2$), 2.00 (m, 8H, $\text{CH}_2\text{CH}_2\text{CH}_3$), 1.49 (m, 8H, CH_2CH_3), 0.95 (m, 12H, CH_3). IR ν_{SO} : 1046, 1098 and 1116. UV-Vis (H_2O) 424 (2.92), 268 (4.39). Λ_{M} (H_2O , increasing to a maximum, steady value at ≥ 30 min) 497.

2.9 Synthesis of a Dinuclear Ru(II)/Ru(III) Disulfoxide Complex

2.9.1 $[\text{RuCl}(\text{BPSP})]_2(\mu\text{-Cl})_3$ ($MW = 828.16$ g/mol)

The procedure used was as described in Section 2.7.4, but with use of BPSP (172 mg, 0.8 mmol). The final orange solution was evaporated to near dryness, CH_2Cl_2 (5 mL) was added, and crystals suitable for X-ray analysis were formed by slow evaporation of the solution. Elemental analysis was performed on a crystal sample that was crushed and dried *in vacuo* at 70 °C overnight. Yield 24 mg (15 %). Anal. Calcd for $\text{C}_{18}\text{H}_{40}\text{Cl}_5\text{O}_4\text{Ru}_2\text{S}_4$: C, 26.11; H, 4.87. Found: C, 26.05; H, 5.09 %. ^1H -NMR (CDCl_3 , 200 MHz) δ 2.18 (broad peak), 1.10 (broad peak). ^1H -NMR (D_2O , 200 MHz) δ 3.95 (m, 4H, $\text{S}(\text{O})\text{CH}_2\text{CH}_2\text{CH}_2\text{S}(\text{O})$), 3.40

(m, 4H, $\text{CH}_2\text{S}(\text{O})$), 2.62 (m, 2H, $\text{CH}_2\text{CH}_2\text{CH}_2$), 1.90 (m, 4H, $\text{CH}_2\text{CH}_2\text{CH}_3$), 1.10 (m, 6H, CH_3). IR ν_{SO} : 1053, 1084. UV-Vis (immediately upon dissolution in CH_3CN) 424 (2.52), 324 (2.94), 286 (3.32). UV-Vis (after 20 min in H_2O) 450 (3.78), 318 (4.42), 282 (4.78). No conductivity was observed in CH_3CN . Λ_{M} (CHCl_3 , time independent) 2. Λ_{M} (H_2O , increasing to a maximum, steady value at ≥ 20 min) 234. The colour of the solutions used for UV-Vis and conductivity did not change over the period of the experiments. The crystal structure revealed the presence of 2 H_2O and 2.5 CH_2Cl_2 . TGA (crystals; complex formulated as $2 \text{H}_2\text{O}$ or $2 \text{H}_2\text{O} \cdot 2.5 \text{CH}_2\text{Cl}_2$; the two formulations are used as the CH_2Cl_2 solvates are readily lost at ambient conditions): Calcd loss of $2\text{H}_2\text{O}$: 4.2 or 3.3 % and for loss of 2BPSP: 54.2 %. Found: 6.1 % (from $\sim 20^\circ\text{C}$ to $\sim 200^\circ\text{C}$) and 51.9 % (from $\sim 200^\circ\text{C}$ to $\sim 300^\circ\text{C}$), respectively (Appendix 4, Figure A.4.2). μ_{eff} (Evans) = 1.7 ± 0.1 B. M.

2.10 Synthesis of Mononuclear Ru(II) Dithioether Complexes

2.10.1 *Trans-RuCl₂(BCyTE)₂·2H₂O* (MW = 724.59 g/mol)

Conc. HCl (100 μL) was added to a solution of $\text{RuCl}_3 \cdot 3\text{H}_2\text{O}$ (100 mg, 0.4 mmol) in EtOH (30 mL), and the mixture was refluxed for 5 h. 1,2-Bis(cyclohexylthio)ethane (BCyTE, 198 mg, 0.8 mmol) was added and the mixture was refluxed for a further 6 h. The resulting red precipitate was collected by filtration and dried *in vacuo*. Elemental analysis was performed on the isolated precipitate. Yield 223 mg (81 %). Anal. Calcd for $\text{C}_{28}\text{H}_{52}\text{Cl}_2\text{S}_4\text{Ru} \cdot 2\text{H}_2\text{O}$: C, 46.39; H, 7.78. Found: C, 46.82; H, 7.43 %. Crystals suitable for X-ray analysis were grown by recrystallization of the complex from DMF/ CH_2Cl_2 (500 μL /2 mL) and were found to contain 2 CH_2Cl_2 solvates per molecule. The ^1H -NMR spectrum of

the title complex is a complicated pattern of broad peaks in the range of δ 1.20-3.35. Attempts to assign the ^1H NMR spectrum using ^{13}C , 2D-COSY and ^1H decoupling experiments were unsuccessful. The broad nature of the proton signals presumably results from the rotation of each of the cyclohexyl rings. UV-Vis (CH_2Cl_2) 438 (3.55), 400 (3.53), 280 (3.74), 236 (4.31).

2.10.2 *Trans-RuCl₂(BPhTE)₂* ($MW = 664.75 \text{ g/mol}$)¹⁷

The synthesis of the red complex was as described above in Section 2.10.1, but using 1,2-bis(phenylthio)ethane (BPhTE, 188 mg, 0.8 mmol). The product was then dissolved in minimum CH_2Cl_2 and was purified by column chromatography using neutral alumina with CH_2Cl_2 as eluant. The CH_2Cl_2 was removed by rotary evaporation. Yield 184 mg (73 %). Anal. Calcd for $\text{C}_{28}\text{H}_{28}\text{Cl}_2\text{RuS}_4$: C, 50.59; H, 4.24. Found: C, 50.82; H, 4.11 %. Crystals suitable for X-ray analysis were formed by slow evaporation of a DMF solution of the complex. ^1H -NMR (CDCl_3 , 400 MHz) δ 7.65 (br s, 8H, *o*- C_6H_5), 7.28 (br s, 4H, *p*- C_6H_5), 7.12 (br s, 8H, *m*- C_6H_5), 3.07 (br s, 8H, CH_2CH_2). UV-Vis (CH_2Cl_2) 410 (3.50), 298 (4.55), 268 (4.54).

A preliminary experiment to attempt oxidation of the coordinated BPhSE by *in situ* generation of dimethyldioxirane was unsuccessful as no ν_{SO} was detected in the crude reaction product, and no colour change of the reaction solution was observed (the details will be discussed in Chapter 6).

2.11 Synthesis of Dinuclear Ru(III)/Ru(III) Dithioether Complexes

2.11.1 $[RuCl_2(BETP)]_2(\mu-Cl)_2$ ($MW = 743.50$ g/mol)

Conc. HCl (500 μ L) was added to a solution of $RuCl_3 \cdot 3H_2O$ (500 mg, 2 mmol) in EtOH (30 mL), and the mixture was refluxed for 5 h. 3,7-Dithianonane (BETP, (1,3-bis(ethylthio)propane), 600 mg, 4 mmol) was added and the mixture was refluxed for a further 6 h. The volume of the resulting dark-brown solution was reduced until the solution became oily. Acetone (25 mL) was added and a purple-brown precipitate formed. Crystals suitable for X-ray analysis were formed by slow evaporation of a solution of the complex in CH_2Cl_2 . Yield 178 mg (24 %). Anal. Calcd for $C_7H_{16}Cl_3RuS_2$: C, 22.62; H, 4.34. Found: C, 22.38; H, 4.30 %. UV-Vis (CH_2Cl_2) 454 (3.42), 376 (3.49), 268 (4.53). μ_{eff} (Gouy) = 3.8 ± 0.1 B. M.

2.11.2 $[RuCl_2(BPTP)]_2(\mu-Cl)_2$ ($MW = 799.61$ g/mol)

The procedure used for the production of X-ray quality crystals was as described in Section 2.11.1, but using $RuCl_3 \cdot 3H_2O$ (100 mg, 0.4 mmol) and 4,8-dithiaunadecane (BPTP, (1,3-bis(propylthio)propane), 147 mg, 0.8 mmol) and only 15 mL of acetone was added. Yield 83 mg (52 %). Anal. Calcd for $C_9H_{20}Cl_3RuS_2$: C, 27.04; H, 5.04. Found: C, 27.51; H, 5.08 %. UV-Vis (CH_2Cl_2) 448 (2.62), 374 (2.61), 252 (3.44). μ_{eff} (Gouy) = 3.0 ± 0.1 B. M.

2.11.3 $[RuCl_2(BBTP)]_2(\mu-Cl)_2$ ($MW = 855.72$ g/mol)

The procedure used was identical to that described in Section 2.11.1, but using $RuCl_3 \cdot 3H_2O$ (100 mg, 0.4 mmol) and 5,9-dithiatridecane (BBTP, (1,3-bis(butylthio)propane),

160 mg, 0.8 mmol), and only 15 mL of acetone was added. Yield 43 mg (25 %). Anal. Calcd for $C_{11}H_{24}Cl_3RuS_2$: C, 30.88; H, 5.65. Found: C, 30.70; H, 5.52 %. UV-Vis (CH_2Cl_2) 454 (3.51), 376 (3.57), 268 (4.68). μ_{eff} (Gouy) = 3.2 ± 0.1 B. M.

2.11.4 $[RuCl_2(BPeTP)]_2(\mu-Cl)_2$ (MW = 911.82 g/mol)

The method described above for the other Ru(III)/Ru(III) complexes was used with $RuCl_3 \cdot 3H_2O$ (100 mg, 0.4 mmol), 6,10-dithiapentadecane (BPeTP, (1,3-bis(pentylthio)propane), 190 mg, 0.8 mmol) and a final addition of acetone (15 mL). Yield 100 mg (55 %). Anal. Calcd for $C_{13}H_{28}Cl_3RuS_2$: C, 34.25; H, 6.19. Found: C, 34.34; H, 6.25 %. UV-Vis (CH_2Cl_2) 434 (3.41), 396 (3.45), 266 (4.86), 216 (4.83). μ_{eff} (Gouy) = 3.4 ± 0.1 B. M.

2.12 References for Chapter 2

- 1 Evans, D.F. *J. Chem. Soc.* 1959, 2003.
- 2 Sur, S. K. *J. Mag. Reson.* 1989, 82, 169.
- 3 (a) Carlin, R. L. *Magnetochemistry* Springer-Verlag, Berlin, 1986, p. 3;
(b) Selwood, P. W. *Magnetochemistry* (2nd ed.), Interscience Publishers, Inc., New York, 1956, p. 78;
(c) CRC Handbook of Chemistry and Physics (66th ed.), (eds. R. C. Weast, M. J. Astle and W. H. Beyer), CRC Press, Inc., Boca Raton, 1985-1986, p. E-121.
- 4 Morgan, S. T.; Ledbury, W. *J. Chem. Soc.* 1922, 121, 2882.
- 5 Hartley, F. R.; Murray, S. G.; Levason, W.; Soutter, H. E.; McAuliffe, C. A. *Inorg. Chim. Acta* 1979, 35, 265.
- 6 Cattalini, L.; Michelon, G.; Marangoni, G.; Pelizzi, G. *J. Chem. Soc. Dalton Trans.* 1979, 96.
- 7 Hull, M.; Bargar, T. W. *J. Org. Chem.* 1975, 40, 3152.
- 8 (a) Bell, E. V.; Bennett, G. M. *J. Chem. Soc.* 1927, 1798;
(b) Bennett, G. M.; Statham, F. S. *J. Chem. Soc.* 1931, 1684.
- 9 Yapp, D. T. T. Ph. D. Dissertation, University of British Columbia, Vancouver, B. C., 1993.
- 10 Yapp, D. T. T.; Rettig, S. J.; James, B. R.; Skov, K. A. *Inorg. Chem.* 1997, 36, 5635.
- 11 Judd, R. J.; Cao, R.; Biner, M.; Armbruster, T.; Bürgi, H-B.; Merbach, A. E.; Ludi, A. *Inorg. Chem.* 1995, 34, 5080.
- 12 James, B. R.; McMillan, R. S. *Inorg. Nucl. Chem. Lett.*, 1975, 11, 837.
- 13 (a) Evans, I. P.; Spencer, A.; Wilkinson, G. *J. Chem. Soc. Dalton Trans.* 1973, 204;
(b) McMillan, R. S.; Mercer, A.; James, B. R.; Trotter, J. *J. Chem. Soc. Dalton Trans.* 1975, 1006.
- 14 Alessio, E.; Mestroni, G.; Nardin, G.; Attia, W. M.; Calligaris, M.; Sava, G.; Zorzet, S. *Inorg. Chem.* 1988, 27, 4099.

- 15 (a) Jaswal, J.; Rettig, S. J.; James, B. R. *Can. J. Chem.* 1990, 68, 1808;
(b) Alessio, E.; Balducci, G.; Lutman, A.; Mestroni, G.; Calligaris, M.; Attia, W.
M. *Inorg. Chim. Acta* 1992, 203, 205.
- 16 Calligaris, M.; Faleschini, P.; Todone, F.; Alessio, E.; Geremia, S. *J. Chem. Soc. Dalton Trans.* 1995, 1653.
- 17 Chatt, J.; Leigh, G. J.; Storace, A. P. *J. Chem. Soc. (A)* 1971, 1380.

Chapter 3

Structural Properties of Sulfoxide and Thioether Complexes of Ruthenium

3.1 General Introduction

Early work by Cotton and Francis in sulfoxide chemistry was initiated partly by trade literature, commercial availability, favourable solvent properties of DMSO, and the resemblance of sulfoxides to phosphine oxides as the latter were used as extracting agents.¹ Davies' interest in the coordination chemistry of sulfoxides originated mainly because of the excellent solvation properties of DMSO.² DMSO (b. p. 189 °C) is a convenient solvent in laboratory and industrial use because of its resistance to hydrolysis and thermal decomposition. Reactions involving alkylation, cyclization, condensation and ether formation are more selective and provide higher yields when using DMSO as the solvent.³ The coordination chemistry of sulfoxides has been studied since the early 1960s (and sulfoxides are capable of acting as Lewis bases), when sulfoxides were recognized as being potential ambidentate ligands, coordinating to specific metals via either oxygen or sulfur.² The sulfur-oxygen bond in sulfoxides is very polar making sulfoxides good acceptors for hydrogen bonding.⁴ Transition-metal complexes of sulfoxides are useful as reactive intermediates in preparative coordination chemistry and homogeneous catalysis.⁵ The bioinorganic chemistry of Ru sulfoxide complexes as chemotherapeutic agents has also been investigated (Chapter 1).

3.2 Structural Properties of the S-O Moiety in Sulfoxides

Sulfoxides $R_1-S(O)-R_2$ have an S-atom in an oxidation state (4) intermediate to that found in sulfides R_1-S-R_2 (2) and sulfones $R_1-S(O)_2-R_2$ (6), while the geometry about the S-atom is distorted trigonal pyramid with the S-atom sp^3 hybridized (Figure 3.1(1)).

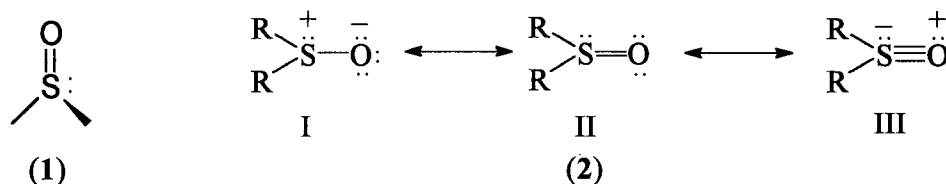


Figure 3.1. Structure (1) and resonance forms (2) of a sulfoxide.

The sulfoxide moiety is non-fluctual around room temperature, allowing for the isolation of chiral sulfoxides,⁶ while their racemization is possible by thermal treatment or by photochemical methods.⁷

The bond angles within free DMSO (Table 3.1) illustrate the trigonal pyramid geometry of the molecule, with the average C-S-O (107°) and C-S-C (98°) angles deviating from 109° because of the lone electron pair on the S-atom and the double bond character present in the sulfur-oxygen bond.⁸ The C-S-C bond angle is invariably smaller than the O-S-C bond angles in metal-sulfoxide complexes regardless of the type of side-groups, this being attributed to the repulsion between the bulkier sulfur-oxygen bonding double pair, the S lone-pair and the S-C bonding pair electrons.¹⁴ The sulfur-oxygen bond length is in the range 1.47 to 1.531 Å (Table 3.1),⁹⁻¹¹ while a bond length of 1.51 Å (estimated from S-N bond lengths) is considered consistent with a bond order of ~ 2.0 .¹²

A valence-bond description can be used to illustrate the bonding nature of sulfoxides. The sulfoxide structure is considered to be a hybrid of three resonance forms with form II the normal representation (Figure 3.1(2)).²

X-ray emission spectroscopic studies on sulfoxides indicate that the sulfur-oxygen bond is polarized with the S-atom having net positive charge.¹³ Calligaris and Carugo stated that the average value of the S-O bond length, 1.492 Å (*cf.* the estimated bond length of 1.51 Å¹²), is consistent with double bond character in the S-O bond and is shorter than the 1.66 Å expected for a single bond.¹⁴

Table 3.1. Selected Bond Lengths and Bond Angles for DMSO in the Gaseous and Solid States.

	Bond Lengths (Å)		Bond Angles (°)		
State	S-O	C-S	C-S-C	C-S-O	Ref.
Gaseous	1.47 ^a	1.82 ^a	100(5)	107(5)	10
Solid at 5°C ^a	1.531	1.775-1.821	97.4	106.7-106.8	9
Solid at -60°C	1.471(8)	1.801(96)- 1.812(14)	97.86(54)	107.04(57)- 107.43(56)	11

^a E.s.d. not given.

3.3 Metal-Sulfoxide Bonding

Sulfoxides are ambidentate and can coordinate either through the S- or O-atom. Initial observations suggested that DMSO coordinated to “harder” metals via oxygen and to “softer” metals via the sulfur.¹⁵ However, the “hardness” or “softness” of a metal ion can be

affected by the nature of the coordinated ligands, and steric effects can force O-bonding even in softer metal ions.¹⁴ In addition, the introduction of highly electronegative substituents with ancillary ligands lowers the electron charge density on the metal, this also favouring O-bonding.¹⁴

In mixed-ligand complexes the preferred coordinating atom of sulfoxides is determined in part by the ability of other ligands at the metal centre to compete for electron density.¹⁶ The presence of strong π -electron acceptors withdraws electron density from the metal, and causes "softer" metals to become "harder". This reduction in electron density at the metal may be accompanied by a change in coordination of the ligand from a "soft" to a "hard" donor atom to optimize orbital overlap.¹⁶ The "hardness" or "softness" of a metal is a qualitative indication of the degree of diffuseness and size of its atomic orbitals, the more diffuse and the larger the orbital, the "softer" the metal is.¹⁵ Metal-ligand orbital overlap with "hard" acids is more favourable with the less diffuse (*i.e.* "hard") donor orbitals of oxygen, while "soft" acids have better orbital overlap with the more diffuse donor orbitals of sulfur.^{2,15}

Steric constraints may cause coordination of sulfoxides through the O-atom to "softer" metals in some metal-sulfoxide systems, as coordination through the O-atom is less sterically demanding than through the sulfur.^{17,25} For example, electronic and steric factors have been used to rationalize the existence of the following two complexes in which sulfoxide coordinates to "softer" metals via oxygen; *cis*-[Pd(DMSO)₂(DMSO)₂]²⁺ and Pd(Ph₂P(CH₂)₂PPh₂)₂(DMSO)²⁺.^{17,18}

Valence bond rationalizations utilizing the different resonance forms of the free sulfoxides are satisfactory in explaining much of the structural data determined for metal-

DMSO complexes (*e.g.* Table 3.2), while steric constraints also play roles in determining whether sulfoxides coordinate through the S- or O-atom. Rationalizations of this type also encompass the initial empirical observation that coordination of sulfoxides occurred in "softer" metals via sulfur, and via oxygen in "harder" metals.¹⁴

A value of 1.531 Å for the sulfur-oxygen bond length for non-coordinated DMSO was obtained after correction for thermal motion whereas most of the sulfur-oxygen bond lengths reported for metal complexes refer to uncorrected values.¹⁴ For comparison of sulfur-oxygen bond lengths, Calligaris and Carugo have used the average value of 1.492(1) Å for a wide range of non-coordinated sulfoxides (excluding low temperature and gas phase values, and data for H-bonded sulfoxides).¹⁴ The sulfur-oxygen bond length of 1.492(1) Å will be used for further comparisons.

3.3.1 Sulfur-Bonded Metal-Sulfoxide Complexes

According to the hard-soft-acid-base theory, in soft metal-ion complexes, diffuse orbitals of acceptor atoms interact favourably with diffuse orbitals on the S-atoms, thus favouring S-bonding.¹⁵ However, certain soft metal ions (Ag^+ , Cd^{2+} and Hg^{2+}) exhibit O-bonding even in the absence of sterically hindering or π acceptor ligands, suggesting that a particular electronic structure is necessary that favours S-bonding over O-bonding, probably involving π back-bonding from the metal orbitals to the S-atom orbitals.¹⁴ Davies suggests that for Ru(II)-DMSO complexes, the Ru-S bond has a partial double bond character because of the $d\pi$ - $d\pi$ back donation from the metal to the sulfur.² Selected structural data for some metal-DMSO complexes are listed in Table 3.2 and show that the geometries of the sulfoxide

Table 3.2. Selected Structural Data for Selected Transition Metal-DMSO Complexes.

Complex	S-O Bond (Å)	C-S-O Angle (°)	Ref.
<i>trans</i> -FeCl ₂ (DMSO) ₄ ⁺	1.541(6)	103.5(4)-103.7(4)	19,20
<i>trans</i> -CuCl ₂ (DMSO) ₂	1.531(4)	103.9(3)-104.7(3)	21
<i>cis</i> -Pt ₂ (DMSO) ₂	1.454(9)-1.469(6)	107.6(5)-110.3(5)	22
<i>cis</i> -RuCl ₂ (DMSO) ₃ (DMSO)	1.557(4); ^a 1.483(5), 1.485(5) ^b	101.6(3)- 104.2(3); ^a 106.0(4)- 107.7(4) ^b	23
<i>mer</i> -Rh(py) ₂ Cl ₃ (DMSO)	1.48(1)	108.0(8)-110.6(8)	24
<i>mer</i> -RuCl ₃ (DMSO) ₂ (DMSO)	1.545(4); ^a 1.474(4)- 1.484(4) ^b	102.4(2), 102.7(3); ^a 107.5(2)- 109.3(2) ^b	25
[Ru ₂ (μ-Cl)(μ-H)(μ-DMSO)Cl ₂ (DMSO) ₄] 2CH ₂ Cl ₂	1.442(5)- 1.486(4); ^b 1.532(4) ^c	<i>d</i>	26
[Ru ₂ Cl(DMSO) ₅](μ-Cl) ₃	1.467(3)-1.479(3)	105.7(2)-107.2(2)	27
[Ru ₂ (μ-Cl)(μ-DMSO)Cl ₃ (DMSO) ₃ (CO) ₂]	1.455(7)-1.480(5); 1.508(5) ^c	<i>d</i>	28
[Ru(O ₂ CCH ₃) ₄ (DMSO) ₂][PF ₆] ₂	1.517(5), 1.523(6)	105.5(5)-108.0(4)	29
<i>cis</i> -[CrCl(en) ₂ (DMSO)]ZnCl ₄ ^e	1.537(5)	101.6(4)-103.9(3)	30
<i>cis</i> -[OsCl ₂ (DMSO) ₄]	1.467(4)-1.483(3)	105.3(2)-107.1(2)	31

^a O-bonded. ^b S-bonded. ^c Bridging. ^d Data not given. ^e en = ethylenediamine.

remain essentially unchanged from that of the free ligand. However, effects of coordination are most evident in the sulfur-oxygen bond length (in DMSO) as this is lengthened to 1.517(5)-1.557(4) Å (see Tables 3.1 and 3.2).

Valence bond arguments imply that donation from resonance form III could account for S-bonding (Figure 3.1(2)), but structural data on the coordinated sulfoxides indicate that the S-atom upon coordination becomes more positive than in the free ligand (it has been shown that an increase in the degree of oxidation of sulfur, accompanied by an

increase in effective positive charge, leads to a displacement of the K absorption edge in the X-ray spectrum towards higher energies).^{13d}

Donation from form II, however, leaves a positive charge on the S-atom and is more consistent with X-ray spectral data,¹³ with the sulfur-oxygen bond order closer to two than three.² The sulfur-oxygen bond environment is directly affected by coordination through the S-atom, as an sp^3 orbital of sulfur is directly involved in the sulfur-metal bond. Donation of electron density from oxygen to sulfur through $p\pi-d\pi$ overlap compensates for the depletion of electron density at the sulfur. The coordination of the sulfoxide, via the S-atom, to the metal results in an increase in the sulfur-oxygen bond order, and a decrease in the sulfur-oxygen bond length, for example, as in the S-bonded complexes listed in Table 3.2.²

3.3.2 Oxygen-Bonded Metal-Sulfoxide Complexes

Generally, O-bonding is observed in metal complexes having "hard" metal ions and/or strong π accepting ancillary ligands, or in order to avoid a *trans* arrangement of S-bonded sulfoxides (in softer metals).¹⁴ The structural data for O-bonded DMSO ligands within the complexes listed in Table 3.2 indicate that the geometry of the sulfoxide changes little upon coordination. The average C-S-O bond angle (103°) is slightly smaller than that of $\sim 107^\circ$ found in free DMSO (Table 3.1), which indicates that the ligand retains its "trigonal pyramid" geometry upon coordination to a metal centre. The sulfur-oxygen bond lengths in O-bonded sulfoxide complexes (1.517(5)-1.557(4) Å, Table 3.2) are longer than that found in free DMSO (1.492(1) Å). Davies had concluded earlier that the sulfur-oxygen bond length changes little on such coordination.²

Calligaris and Carugo suggest that a hybrid of resonance forms I and II predominates, with structure I accounting for coordination of sulfoxides through the O-atom (Figure 3.1(2)).¹⁴ Transfer of electron density from the negative oxygen to the metal is not expected to affect the positive charge on the sulfur.² The O-atom within the S^+-O^- resonance form can be considered to be sp^2 hybridized; then overlap of one oxygen sp^2 orbital with the sp^3 hybridized S-atom results in a single sulfur-oxygen σ -bond, leaving the two sp^2 lone pairs on the oxygen for coordination to the metal.^{2,5} The interaction between the remaining lone-pair p-orbital of the O-atom and the vacant d-orbitals of the S-atom ($p\pi-d\pi$) is not affected directly by the coordination environment of the oxygen. Coordination to a weak Lewis acid should have a small effect on the π overlap, while coordination to a strong Lewis acid should decrease the overlap and result in a decrease in the S-O bond order.

Experimental data support this reasoning with S-O bond lengths for O-bonded DMSO in Ru, Fe, Cu, and Cr complexes in the range 1.517(5)-1.557 Å (Table 3.2) which are longer than the bond length in free DMSO (1.492(1) Å).

3.3.3 Bridging DMSO Metal Complexes

The structural data for bridging DMSO ligand complexes (Table 3.2) indicate again that the sulfoxide geometry does not change much upon coordination. Bridging S-O bond lengths are 1.532(4) Å²⁶ and 1.508(5) Å²⁸ (Table 3.2) and are longer compared to the bond length of free DMSO 1.492(1) Å. Of note, the bridged S-O bond lengths are intermediate between those of S- and O-bound Ru(II)-sulfoxide complexes.²⁸

3.4 NMR and IR Spectroscopic Methods for the Determination of Sulfur- or Oxygen-Bonding in Metal Complexes

The presence of sulfur- and/or oxygen-bonded sulfoxides in metal-sulfoxide complexes can often be detected using two standard spectroscopic methods.

3.4.1 ^1H NMR Spectroscopy

^1H NMR shifts of the α -protons of free sulfoxide change upon coordination of the sulfoxide and can indicate the presence of either S- or O-bonding, the peaks generally shifting downfield. The magnitude of the shift depends upon the coordination mode, with larger effects being observed upon coordination via the S-atom than the O-atom. Free DMSO in CDCl_3 has a single ^1H resonance at δ 2.62 for the equivalent methyl groups.³² In *cis*- $\text{RuCl}_2(\text{DMSO})_3(\text{DMSO})$, the methyl resonance of the O-bonded DMSO is shifted downfield to δ 2.75, while the methyl resonances of the S-bonded DMSO are shifted further and fall in the range δ 3.00-3.52.³²

Generally, O-bonding of sulfoxides results in small chemical shifts of the α -protons ($\leq \delta$ 0.5) while larger shifts $\delta \sim 1$ are seen for coordination through the S-atom, and this trend is observed for the β - and γ -protons although the extent of these effects decreases as the protons become further removed from the S-atom.²

Using the bonding model shown in Figure 3.1(2), coordination of the sulfoxide via the O-atom occurs through the sp^2 orbitals of oxygen, and hence the electron density in the carbon-sulfur bond, which involves sp^3 orbitals from the S-atom, is affected only to a small degree. The α -protons are consequently only deshielded to a small degree, which is reflected in the small downfield shift observed in the ^1H NMR spectrum. In contrast, coordination

through the sulfur involves the sp^3 orbitals of the S-atom, which results in direct withdrawal of electron density from the C-S bond and a greater deshielding effect.

The inequivalence of diastereomeric α -CH₂ protons of a coordinated sulfoxide such as diethylsulfoxide³³ is observed in the ¹H NMR spectrum as a complicated pattern of peaks. This pattern is only observed for S-bonded sulfoxides and not for O-bonded sulfoxides.³³ The ¹H signal observed for the α -protons of O-bonded diethylsulfoxide is simpler than that observed for the α -protons of S-bonded diethylsulfoxide.³⁴ However, in the case of coordinated TMSO, a greater inequivalence is observed for the β - than the α -CH₂ protons in the ¹H NMR spectrum.³⁵

3.4.2 IR Spectroscopy

Upon coordination of sulfoxide, a greater shift is observed in ν_{SO} , the sulfur-oxygen IR stretching frequency, in O-bonded than in S-bonded sulfoxides; a shift to a higher ν_{SO} is observed for S-bonded sulfoxides, and a lower ν_{SO} for O-bonded. These changes are useful indications of the bonding mode. Examples of complexes with S- and/or O-bonded sulfoxides (with their respective ν_{SO} assignments) are tabulated in Table 3.3. Coordination via the S-atom results in both a shorter sulfur-oxygen bond and higher ν_{SO} due to donation of electron density from the O-atom to compensate for the withdrawal of electron density from the S-atom by the metal (Figure 3.1(2)). In the case of O-bonded sulfoxides, donation of electron density occurs through one sp^2 orbital of the oxygen (Figure 3.1(2)), and this results in changes in the sulfur-oxygen bond and ν_{SO} . A bridging sulfoxide, with coordination via both S- and O-atoms,^{26,28} has the characteristics of both S- and O-bonding; ν_{SO} of μ -DMSO shows

a coordination shift of 45 cm⁻¹ (Table 3.3), reflecting relatively minor changes in the sulfur-oxygen bond, consistent with structural data (see Section 3.3.3).

Table 3.3. The Sulfur-oxygen Stretching Frequencies of S-bonded, O-bonded and Bridging DMSO Ru Complexes.^{a,b}

Complex	v _{SO} (cm ⁻¹)			Ref.
	S-bonded	O-bonded	Bridging	
<i>cis</i> -RuCl ₂ (DMSO) ₃ (DMSO) ^c	1115	960		32
<i>cis</i> -RuBr ₂ (DMSO) ₃ (DMSO)	1111.5	924		36
<i>trans</i> -RuCl ₂ (DMSO) ₄	1086			36,37
<i>trans</i> -RuBr ₂ (DMSO) ₄ ^d	1082			38
<i>mer</i> -RuCl ₃ (DMSO) ₂ (DMSO)	1127,1107	912		25
[Ru ₂ (O ₂ CCH ₃) ₄ (DMSO) ₂](PF ₆)		1006		29
[Ru ₂ (μ-Cl)(μ-DMSO)(DMSO) ₃ Cl ₃ (CO) ₂]	1141,1107		1010	28

^a In KBr, unless stated otherwise. ^b v_{SO} free DMSO, 1055 cm⁻¹ in Nujol (ref. 34). ^c NaCl, Nujol or hexachlorobutadiene mulls. ^d Nujol mulls between CsBr windows.

3.5 Disulfoxides and Their Metal Complexes

In this thesis work, several disulfoxides were synthesized by oxidation of the corresponding dithioethers by the methods of Hull and Bargar³⁹ and Bennett *et al.*,⁴⁰ and were characterized by elemental analysis, melting point, and IR and ¹H NMR spectroscopies (Section 2.4 and Table 3.4). Of note, a comprehensive review by Madesclaire includes several methods for oxidizing sulfides to the corresponding sulfoxides,⁴¹ and recently Rakivumar *et*

al. reported a selective conversion of sulfides to sulfoxides using 30 % H_2O_2 in $\text{CF}_3\text{CH}(\text{OH})\text{CF}_3$.⁴² The disulfoxides used in this thesis work were synthesized as mixtures of diastereomers (the *RR/SS* pair, and the *meso RS/SR*) but use of several recrystallizations yielded one diastereomer (Section 2.4).³⁹ As reported, repeat recrystallizations can be used to separate the diastereomers,^{43,44} while separation of the enantiomeric forms of 1,2-bis(phenylsulfinyl)ethane has been achieved by column chromatography on lactose.^{45,46} Zipp and Madan stated that "previous studies have indicated that the sole product obtained from the DMSO oxidation is the higher melting isomer, now identified as the racemic mixture of the *RR* and *SS* forms";⁴⁷ however, X-ray crystal structural analyses of $\text{RS}(\text{O})(\text{CH}_2)_2\text{S}(\text{O})\text{R}$; R = methyl (BMSE),⁴³ propyl (BPSE) and phenyl (BPhSE)⁴⁴ suggest that generally the higher melting isomer is that of the *meso* form (vs. the *rac* form) (Table 3.4).⁴⁸

Attempts, during this thesis work, to crystallize the disulfoxides to obtain X-ray structural analyses were not successful; attempts included variation of solvent combinations and temperatures, and sublimation methods. For example, some "crystals" of BPSP were found not to be single crystals and were apparently characteristic of "soft thread"; attempts by Calligaris to crystallize BPSP have also been unsuccessful.⁴⁹ Svinning *et al.* have reported that crystals of the β form (the lower melting isomer) of *rac*-BMSE were "clusters of interpenetrating needles that were easily shattered or deformed".⁴³

Table 3.4. The Melting Points and ν_{SO} (cm^{-1}) for Disulfoxides.^a

Compound	M. p. ($^{\circ}\text{C}$)	Ref.	ν_{SO} (cm^{-1}) (KBr)
BMSE(<i>RS</i>)	158-162 ^b and 165-166 ^c ; 163-164; ^c 169-170; ^c 174-175 ^d	50; 40a; 39; 43	1018 (ref. 39) ^e
BMSE(<i>rac</i>)	117-119 ^b and 118-120 ^f ; 128-130; ^c 132-133 ^d	50; 40a; 43	1018 (ref. 39) ^e
BESE	142-145; ^g 149-149.5; ^c 148-149; 150 ^h	47; 39; tw; 40b	1019 (ref. 39); 1015 (tw)
BPSE	161-162.5; ⁱ 162-164	39; tw	1012 (ref. 39); 1010 (tw)
BBSE	172-173	tw	1014
BPeSE	134-135	tw	1014, 1073, 1100
BCySE	172-174	tw	1018
BHSE	176.5-177.5	tw	1016, 1114
BPhSE(<i>RS</i>)	166-167 ^{i,k}	48; 44	1033 (ref. 44)
BPhSE(<i>SS</i>)	120-122; ^j 122-123 ^k	48; 44	1037 (ref. 44)
BPhSE	165-170	tw	1035, 1089
BMSP	117-118 ^l	39	1050
BESP	127-130	tw	1016, 1047
BPSP	140-143	tw	1021, 1075
BBSP	146-148	tw	1021
BPeSP	125-129	tw	1026
BPhSP	137-140	tw	1021, 1040, 1084

^a tw, this work. The superscripts ^{b-d} and ^{g-l} indicate the recrystallization solvents that were used in each case. ^b EtOH/ethyl acetate. ^c EtOH. ^d Acetone/ethyl acetate. ^e The value 1018 cm^{-1} is assumed to be quoted for a crude product (m. p. 125-164 $^{\circ}\text{C}$). ^f Recrystallized from the mother liquor using ethyl acetate and toluene. ^g Benzene. ^h Ethyl acetate. ⁱ Benzene/hexane 3:2. ^j Chloroform and petroleum ether. ^k CHCl_3 /light petroleum and ethanol. ^l THF.

3.5.1 Disulfoxide Complexes

For the higher melting diastereomer of *meso*-BMSE (see Section 3.5), the range of the sulfur-oxygen bond lengths was 1.501(2)-1.515(2) Å.⁴³

Madan *et al.* synthesized a series of complexes with formulations $[M(L)_3](ClO_4)_2$ ($M = Mn^{2+}$, Fe^{2+} , Co^{2+} , Ni^{2+} , Cu^{2+} , Zn^{2+} and Cd^{2+}), $M(L)Cl_2$ ($M = Pt^{2+}$ and Pd^{2+}) ($L = 2,5$ -dithiahexane 2,5-dioxide, *i.e.* BMSE), and $[ML_n](ClO_4)_2$ ($n = 3$, $M = Mn^{2+}$, Co^{2+} , Ni^{2+} and Zn^{2+} ; $n = 2$, $M = Cu^{2+}$; and $L = BMSP$, BMSB (1,4-bis(methylsulfinyl)butane) and BESE), as characterized by elemental analyses, IR and magnetic measurements.^{47,51} IR spectroscopy suggested that the disulfoxides were generally O-bonded, except for the Pt^{2+} and Pd^{2+} complexes.

Previous work in this laboratory by Yapp *et al.* led to the isolation of the *cis* complexes $RuCl_2(BMSP)_2$ and $RuCl_2(BESE)_2$, and the *trans* complexes $RuCl_2(BMSE)_2$ and $RuCl_2(BPSE)_2$, shown by X-ray crystallography to contain solely S-bonded disulfoxide.^{52,53} The sulfur-oxygen bond length of coordinated BMSE had shortened to an average of 1.47 Å (Table 3.6, see p. 85).

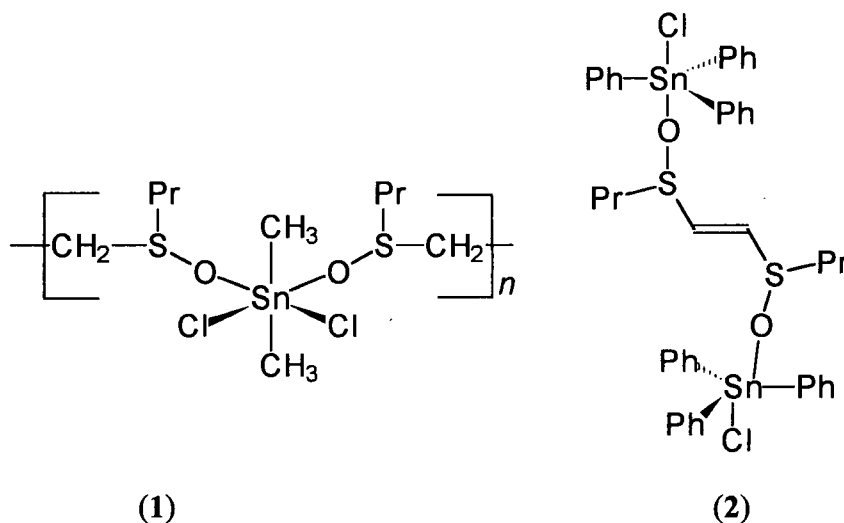


Figure 3.2. Structures of *catena*-poly[*cis*-Cl₂-*trans*-(CH₃)₂Sn(IV)](μ -O, O'-*meso*-BPSE) (1) and [SnCl-*cis*-Ph₃]₂(μ -O, O'-*rac*-1,2-bis(*n*-propylsulfinyl)ethylene) (2).

De Azevedo Jr. *et al.* have structurally characterized *cis*-PtCl₂(BPSE) with S-bonded disulfoxide, and a sulfur-oxygen bond length of 1.45(2)-1.46(1) Å,⁵⁴ while Carvalho *et al.* have structurally characterized *catena*-poly[*cis*-Cl₂-*trans*-(CH₃)₂Sn](μ -O, O'-*meso*-BPSE) with a sulfur-oxygen bond length of 1.520(3) Å (Figure 3.2(1)); the increase in S-O bond length is consistent with O-bonded sulfoxides (Section 3.3.2) compared to the shorter S-O bond lengths observed for S-bonded sulfoxides (Section 3.3.1).⁵⁵ Filgueiras *et al.* have structurally characterized the complex [SnCl-*cis*-Ph₃]₂(μ -O, O'-*rac*-1,2-bis(*n*-propylsulfinyl)ethylene) with a sulfur-oxygen bond length of 1.488(6) Å (Figure 3.2(2)).⁵⁶

Musgrave and Kent synthesized a series of complexes with formulations [M(L)₃](ClO₄)₂ (M = Co²⁺, Ni²⁺ and Cu²⁺; L = O-bonded *meso*- and *rac*-bis(phenylsulfinyl)methane (BPhSM), and *meso*- and *rac*-1,2-bis(phenylsulfinyl)ethane (BPhSE)) and M(L)Cl₂ (M = Pt²⁺; L = S-bonded *meso*- and *rac*-BPhSE) as characterized by elemental analyses, IR spectroscopy, while the ligands were characterized by NMR

spectroscopy.⁵⁷ The authors assigned (perhaps incorrectly) the α -BPhSM (m. p. 196 °C) as the racemic mixture and β -BPhSM (m. p. 104 °C) as the *meso* compound by NMR spectroscopy. They incorrectly quoted a report by Taddei⁴⁵ and, therefore, incorrectly assigned the α -BPhSE (higher melting isomer) and β -BPhSE (lower melting isomer) as the racemic mixture and *meso* isomer, respectively.⁵⁷ Taddei's findings⁴⁵ were later confirmed by Cattalini *et al.*⁴⁴ by X-ray structural analyses for *meso*- and *rac*-(BPhSE). The range of the sulfur-oxygen bond lengths determined for BPhSE (*RS* and *SS*) is 1.487(2)-1.494(6) Å,⁴⁴ and in the S-bound complexes *cis*-PtCl₂(*meso*-BPhSE) and *cis*-PtCl₂(*rac*-BPhSE) these were shortened to 1.461(8)-1.470(8) Å and 1.40(2)-1.46(1) Å, respectively.⁴⁴ In the complex [SnClPh₃]₂(*meso*-BPhSE), in which BPhSE acts as a bridge between the two tin centres, the sulfur-oxygen bond length is 1.525(4) Å (Figure 3.3(1)).⁴⁸ Within [PtCl₂(PEt₃)]₂(μ -*S,S*-*meso*-BPhSE), where BPhSE bridges two Pt centres via the S-atoms, the sulfur-oxygen bond length is 1.475(9) Å (Figure 3.3(2)).⁵⁸

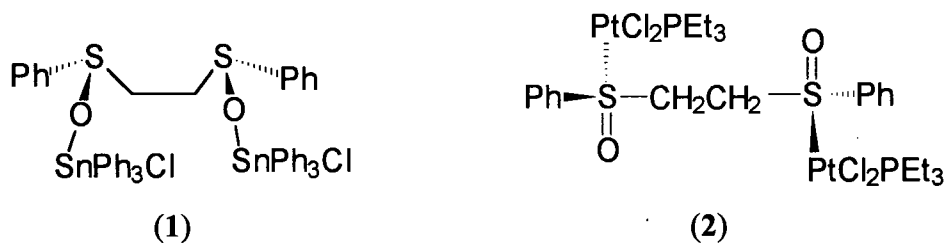


Figure 3.3. Structures containing μ -BPhSE.

A corresponding distance of 1.46 Å has been reported for the S-bound complex *cis*-PtCl₂(*rac-cis*-1,2-bis(phenylsulfinyl)ethylene).⁵⁹

Khiar *et al.* have synthesized Fe(III) complexes containing O-bound (*SS*)-bis(*p*-tolylsulfinyl)methane and (*SS*)-2,2-bis(*p*-tolylsulfinyl)propane ligands, respectively (Figure 3.4(1)), although no characterization data were presented.⁶⁰

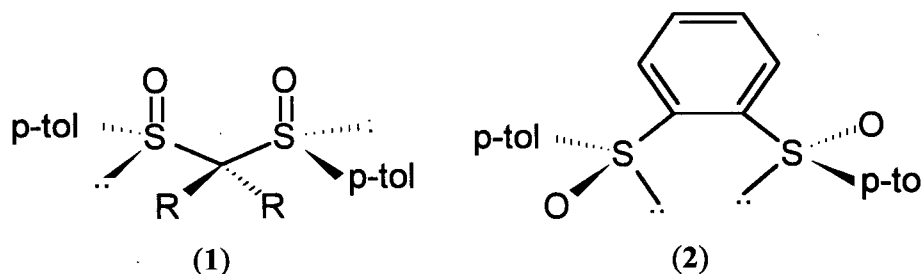


Figure 3.4. (1) $R = H$, (*SS*)-bis(*p*-tolylsulfinyl)methane; and $R = CH_3$, (*SS*)-2,2-bis-*p*-tolylsulfinylpropane. (2) (*SS*)-1,2-bis(*p*-tolylsulfinyl)benzene.

Tokunoh *et al.* synthesized (*SS*)-1,2-bis(*p*-tolylsulfinyl)benzene (BTSB, Figure 3.4(2)), and the corresponding $[Rh(BTSB)(cod)](ClO_4)$, *trans*- $RuCl_2(BTSB)_2$ and *cis*- $PdCl_2(BTSB)$ complexes, containing S-bound sulfoxide. The Pd(II) complex was characterized by X-ray crystallography; the crystal structure is centrosymmetric thus implying the presence of both enantiomers.⁶¹ The sulfur-oxygen bond lengths of the Pd(II) complex are 1.461(12) Å compared to that of 1.481(1) Å for the free disulfoxide. The authors suggest that the relatively small change in the S-O bond length (complexed vs. free BTSB) was because the electron deficiency of the S-atom may be compensated for by π -back donation from the aryl groups of BTSB rather than by the O-atom.⁶¹

Previous work in this laboratory has included the synthesis and characterization of chiral sulfoxides, for example, *R*-methyl *p*-tolyl sulfoxide (MPTSO), and chiral disulfoxides, for example, dios, bdios and ddios (see Figure 3.5), and their Rh (O-bonded)⁶² and Ru (mainly

S-bonded) complexes which were studied as catalysts for asymmetric hydrogenation of prochiral olefins.⁶³

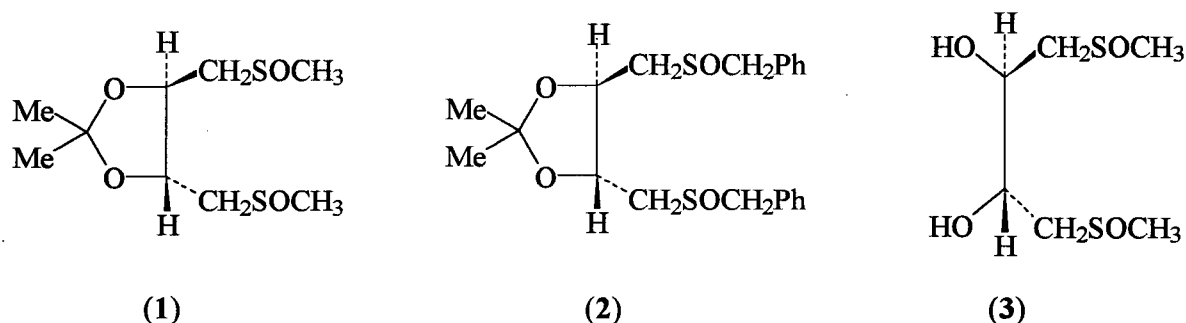


Figure 3.5. Structures of dios ((2*R*3*R*)-2,3-*O*-isopropylidene-2,3-dihydroxy-1,4-bis(methylsulfinyl) butane monohydrate) (1), bdios ((2*R*3*R*)-2,3-*O*-isopropylidene-2,3-dihydroxy-1,4-bis(benzylsulfinyl) butane monohydrate) (2), and ddios ((2*R*3*R*)-2,3-dihydroxy-1,4-bis(methylsulfinyl) butane (3). Adapted from ref. 63b.

Various methods have been utilized to maximize the optical purities of chiral sulfoxides, including electrochemical asymmetric oxidation of unsymmetric sulfides to the corresponding chiral sulfoxides using poly(amino-acid)-coated electrodes,⁶⁴ and chloroperoxidase catalyzed oxidations in *t*-butyl alcohol/water mixtures.⁶⁵ Of note, a review by Allin includes thirty-seven references for the synthesis of chiral sulfoxides via nucleophilic displacement at the S-atom.⁶⁶

3.6 Mononuclear, Bidentate Disulfoxide Complexes of Ruthenium(II)

Previous workers in this laboratory have used *cis*-RuCl₂(DMSO)₄ and *cis*-RuCl₂(TMSO)₄ as precursors for the synthesis of RuCl₂(sulfoxide)₂(nitroimidazole)₂ complexes, but their configurations were not easily resolved because of the number of possible isomers that could be formed.⁶⁷ The range of sulfoxides was then extended to include disulfoxides in order to reduce the number of possible isomers formed in these exchange

reactions, and the four complexes *cis*-RuCl₂(BMSP)₂, *cis*-RuCl₂(BESE)₂, *trans*-RuCl₂(BMSE)₂ and *trans*-RuCl₂(BPSE)₂ were synthesized (via "Ru-blue" solutions, Section 3.8.1, p.104) and structurally characterized.^{52,53}

One of the first goals for this thesis work was to extend the range of the Ru disulfoxide complexes to include the geometrical isomers of the previously characterized complexes, especially as the *trans* Ru-disulfoxide complexes exhibited greater *in vitro* biological activity than the *cis* complexes.⁵² A logical step to attempt to synthesize such isomers was to use the precursors *cis*- and *trans*-RuCl₂(DMSO)₄ in sulfoxide-exchange reactions to give *cis*-RuCl₂(BMSE)₂ and *cis*-RuCl₂(BPSE)₂, and *trans*-RuCl₂(BESE)₂ and *trans*-RuCl₂(BMSP)₂, respectively, and then study their *in vitro* biological activity. However, a reaction of *cis*-RuCl₂(DMSO)₄ with BPSE gave *trans*-RuCl₂(BPSE)₂ (Section 2.7.3), and reactions of *trans*-RuCl₂(DMSO)₄ and K₃[RuCl₆] with BESE both gave *cis*-RuCl₂(BESE)₂ (Section 2.7.1) as characterized by ¹H NMR spectroscopy.

During this thesis work, the Trieste group published a molecular mechanics investigation of the stereochemistry of Ru-bis-chelating disulfoxide complexes,⁶⁸ and concluded that *trans*-RuCl₂(BMSE)₂, *cis*-RuCl₂(BESE)₂ and *trans*-RuCl₂(BPSE)₂ corresponded to the lowest strain diastereomers (Figure 3.6). The minimum energy structure found a *cis*-isomer (Figure 3.6(1)) for the diastereomer containing *meso*-BESE ligands (*i.e.* *cis*-RuCl₂(BESE)₂) and this required *trans* S-atoms with the same *R* or *S* chirality.⁶⁸

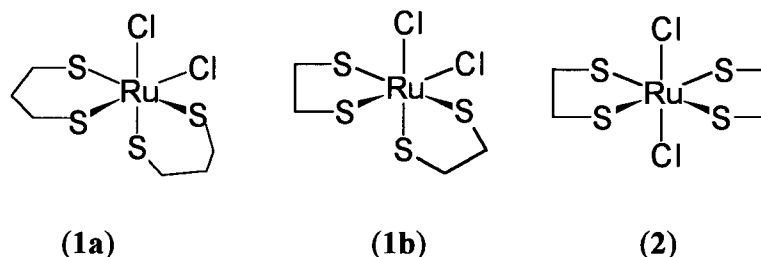


Figure 3.6 General structure for (1a) *cis*-RuCl₂(BMSP)₂ and (1b) *cis*-RuCl₂(BESE)₂ and (2) *trans*-RuCl₂(BMSE)₂ and *trans*-RuCl₂(BPSE)₂; S[^]S = chelating disulfoxide.

The lowest energy form of *trans*-systems (2) is with mutually *trans* S-atoms of opposite chirality. Analogous stereomers have been observed in the crystal structures of both *trans*-RuCl₂(BMSE)₂ and *trans*-RuCl₂(BPSE)₂, where again only S-bonding was found.^{53,68}

During the course of the present work, the water-soluble complex [RuCl(BESE)(H₂O)]₂(μ-Cl)₂ was synthesized and structurally characterized, and its reaction with two equivalents of BESE gave the complex *trans*-RuCl₂(BESE)₂.

The mononuclear, bis-chelating Ru disulfoxide complexes isolated during this present work have the general formula *cis*-RuCl₂(disulfoxide)₂ (with the exception of the complex *trans*-RuCl₂(BESE)₂), and they all contain only S-bonded disulfoxides as indicated by ν_{SO} data (Table 3.5, p. 83) and confirmed by X-ray crystallography in all but one case (*cis*-RuCl₂(BPSeSE)₂). No conductivity was observed for any of these complexes in chlorinated solvents. As well, a Ru(II)/Ru(III), mixed-valence complex [RuCl(BPSP)]₂(μ-Cl)₃ and a series of Ru(II)/Ru(II) chelating disulfoxide complexes (with [RuCl(BESE)(H₂O)]₂(μ-Cl)₂ structurally characterized) were isolated during the present work (Sections 3.7 and 3.8). Again, all these complexes contain only S-bonded sulfoxides.

Of note, the *in situ* reduction of both the $\text{RuCl}_3 \cdot 3\text{H}_2\text{O}$ “green solutions” and the Ru(III) precursor $[\text{RuCl}_6]^{3-}$ to the Ru(II) product was possibly due to the disulfoxide acting as a reductant, which is correspondingly oxidized to the sulfone; this might account for the relatively low isolated yield ($\sim 25\%$), as only a 2:1 sulfoxide:Ru ratio was used. Higher yields might result by using increased sulfoxide concentration. Evidence for this redox process will be discussed in Section 3.9, p. 126.

Table 3.5. IR Data (KBr) for $\nu_{\text{SO}}(\text{cm}^{-1})$ Free and $\nu_{\text{SO}}(\text{cm}^{-1})$ Bound, in Chelating Disulfoxide Complexes of Ru.

Complex	IR $\nu_{\text{SO}}(\text{cm}^{-1})$ free	IR $\nu_{\text{SO}}(\text{cm}^{-1})$ bound
<i>trans</i> - $\text{RuCl}_2(\text{BMSE})_2^a$	1018 (ref. 39)	1109 ^a
<i>cis</i> - $\text{RuCl}_2(\text{BESE})_2^a$	1019 (ref. 39); 1015	1128; ^a 1092, 1122
<i>trans</i> - $\text{RuCl}_2(\text{BESE})_2 \cdot \text{H}_2\text{O}^b$	1019 (ref. 39); 1015	1093, 1119
<i>trans</i> - $\text{RuCl}_2(\text{BPSE})_2^a$	1012 (ref. 39); 1010	1128; ^a 1094 ^c
<i>cis</i> - $\text{RuCl}_2(\text{BBSE})_2^b$	1014	1081, 1126
<i>cis</i> - $\text{RuCl}_2(\text{BPSe})_2$	1014, 1073, 1100	1081, 1128
<i>cis</i> - $\text{RuCl}_2(\text{BCySE})_2^b$	1018	1046, 1100
<i>cis</i> - $\text{RuCl}_2(\text{BMSP})_2^a$	1050	1085 ^a
<i>cis</i> - $\text{RuCl}_2(\text{BESP})_2^b$	1016, 1047	1042, 1088
$[\text{RuCl}(\text{BESE})(\text{H}_2\text{O})]_2(\mu\text{-Cl})_2^b$	1019	1042, 1071, 1118
$[\text{RuCl}(\text{BPSE})(\text{H}_2\text{O})]_2(\mu\text{-Cl})_2$	1012	1048, 1083, 1119
$[\text{RuCl}(\text{BBSE})(\text{H}_2\text{O})]_2(\mu\text{-Cl})_2$	1014	1046, 1098, 1116
$[\text{RuCl}(\text{BPSP})]_2(\mu\text{-Cl})_3^b$	1021, 1075	1053, 1084

^a Indicates data taken from refs. 52 and 53 for the 4 complexes, all of which were characterized by X-ray analysis; otherwise data represent this thesis work. ^b Complexes characterized by X-ray analysis. ^c Formulated with one H_2O .

3.6.1 *Cis-RuCl₂(BESE)₂ and Trans-RuCl₂(BESE)₂·H₂O*

The reaction of BESE with K₃[RuCl₆] gave the yellow *cis* complex in 36 % yield. The ¹H NMR spectrum in CDCl₃ corresponds well to that reported,^{52,53} with two distinctive triplets at δ 1.45 and 1.30 of equal integration for the methyls. Attempts to photolyze *cis*-RuCl₂(BESE)₂ to the *trans* isomer, following a report on photo-induced isomerization of *cis*-to *trans*-RuCl₂(DMSO)₄,³⁶ were unsuccessful (Section 2.7.1).

The reaction of [RuCl(BESE)(H₂O)]₂(μ-Cl)₂ with 2 equivalents of BESE gave the *trans* complex in 33 % yield. The ¹H NMR spectrum (D₂O) of the free ligand consists of multiplets at δ 3.30 (CH₂CH₂), 2.92 (CH₃CH₂), and a triplet at 1.23 (CH₃), which in this complex are shifted downfield to a coalesced peak at δ 3.70 (for the CH₂ protons) and a multiplet at δ 1.45 (CH₃), respectively; the ¹H solution spectrum (D₂O), which does not change over 3 weeks, shows equivalent methyl groups (*cf.* data for the *cis* complex), consistent with the *trans* geometry determined crystallographically. Crystals of a non-solvated species were grown by slow evaporation of an H₂O solution of the complex. This complex crystallizes in a centrosymmetric space group with the Ru-atom on a centre of symmetry, and is thus achiral; the ORTEP diagram is shown in Figure 3.7. The structural data are similar to those of *trans*-RuCl₂(BMSE)₂ and *trans*-RuCl₂(BPSE)₂ (Table 3.6). The key bond lengths and angles are essentially the same as those for the other Ru(II) bis-chelating disulfoxide complexes. The molecule has a slightly distorted octahedral geometry at the Ru with *trans* angles of 180.0 ° and *cis* angles that range from 85.42(3)-90.88(3) ° (Table 3.7). The sulfur-oxygen bond lengths for *cis*-RuCl₂(BESE)₂, *trans*-RuCl₂(BESE)₂ and

[RuCl(BESE)(H₂O)]₂(μ -Cl)₂ average about 1.48 Å and show that there is not much of a change in the sulfur-oxygen bond distance in the three complexes (see Table 3.7).

Table 3.6. Selected Bond Lengths (Å) and Bond Angles (°) for Some *trans*-RuCl₂(S-S)₂ Complexes.^a

Bond or Angle	<i>trans</i> -RuCl ₂ (BMSE) ₂	<i>trans</i> -RuCl ₂ (BPSE) ₂
Ru-Cl	2.402(2), 2.405(2)	2.4077(8)
Ru-S	2.305(2)-2.319(2)	2.300(4), 2.319(3)
S-O	1.453(6)-1.495(7)	1.44(1), 1.47(1)
C-S	1.717(7)-1.855(7)	1.74(1)-1.911(6)
Ru-S-O	118.4(3)-120.4(3)	118.1(5), 120.6(5)
O-S-C	103.9(3)-110.8(4)	99.5(6)-114.8(6)
C-S-C	98.1(3)-106.3(3)	89.3(6), 112.1(6)
S-C-C ^b	107.1(4)-112.5(4)	108.3(3)-109.0(4)
S-C-C ^c		109(1)-116.2(9)
Ru-S-C ^b	102.7(3)-105.6(3)	100.4(2)-106.5(2)
Ru-S-C ^c	113.9(2)-115.7(3)	114.5(6)-117.8(4)

^a Data taken from refs. 52 and 53. ^b Bonds involving backbone carbons. ^c The C-atom of an alkyl substituent.

Table 3.7. Selected Bond Lengths (Å) and Bond Angles (°) for [RuCl(BESE)(H₂O)]₂(μ-Cl)₂·H₂O, *trans*-RuCl₂(BESE)₂ and *cis*-RuCl₂(BESE)₂.

Bond or Angle	[RuCl(BESE)(H ₂ O)] ₂ (μ-Cl) ₂ ·H ₂ O	<i>Trans</i> -RuCl ₂ (BESE) ₂	<i>Cis</i> -RuCl ₂ (BESE) ₂ ^a
Ru-Cl ^b	2.4098(10); ^c 2.4636(10) ^d		
Ru-Cl ^e	2.4006(10) ^c	2.4018(7)	2.4217(8)- 2.4486(8) ^d
Ru-S	2.1985(10); ^c 2.1958(10) ^f	2.3212(9), 2.3288(7)	2.2712(8)- 2.2738(8); ^c 2.2973(8)- 2.3076(8) ^d
Ru-O	2.140(3) ^d		
S-O	1.475(3), 1.496(2)	1.479(2)-1.480(2)	1.470(2)-1.479(2)
C-S	1.803(4)-1.805(4)	1.797(3)-1.809(3)	1.796(3)-1.814(3)
<i>cis</i> angles	82.11(3)-95.11(4)	85.42(3)-90.88(3)	87.19(3)-92.08(3)
<i>trans</i> angles	171.77(4)-178.01(8)	180.0	176.92(3)- 178.54(3)
Ru-Cl-Ru	96.83(3), 97.89(3)		
C-S-C	99.3(2)-102.9(2)	99.1(2)-101.3(2)	100.0(1)-102.8(1)
O-S-C	104.9(2)-107.4(2)	106.6(1)-108.1(2)	106.3(1)-109.3(1)
Ru-S-O	118.52(13)-119.24(13)	119.31(9)-119.44(9)	116.28(8)- 120.43(8)
S-C-C ^g	106.3(3)-108.6(3)	106.8(2)-110.9(2)	106.5(2)-111.0(2)
S-C-C ^h	111.6(3)-114.1(4)	111.1(2)-112.2(2)	111.3(2)-112.0(2)
Ru-S-C ^g	105.56(12)-107.43(13)	103.5(1)-104.9(1)	103.0(1)-104.8(1)
Ru-S-C ^h	115.47	115.7(1)-116.6(1)	113.4(1)-117.3(1)

^a Data taken from refs. 52 and 53. ^b Bridging. ^c *Trans* to Cl. ^d *Trans* to S. ^e Terminal. ^f *Trans* to O. ^g Backbone. ^h End substituents.

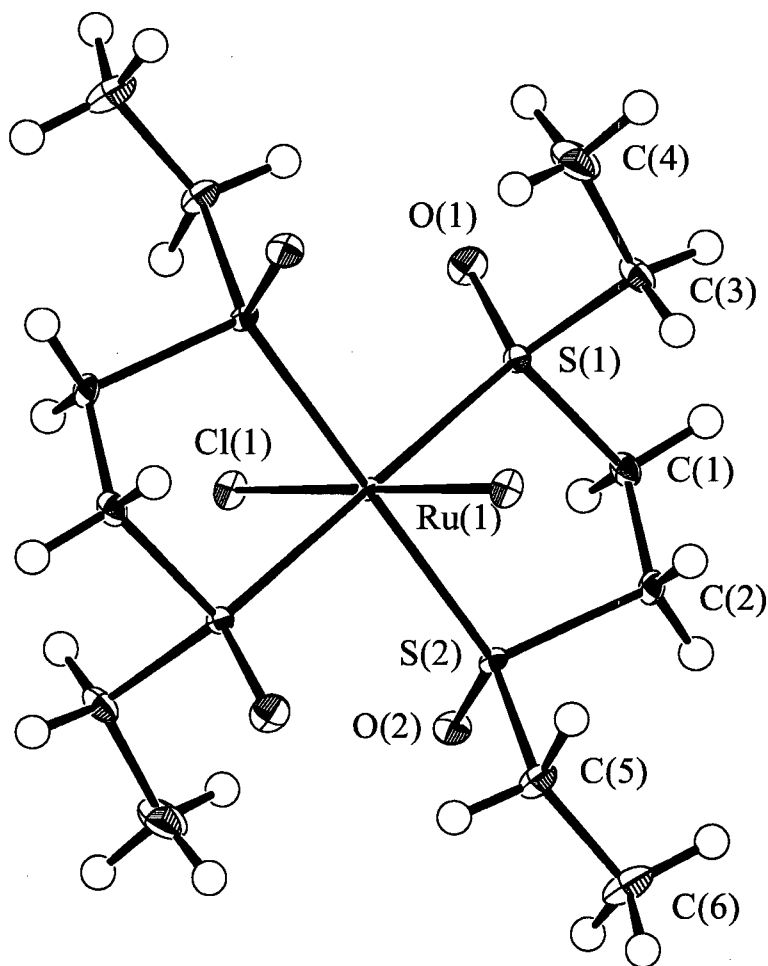


Figure 3.7. An ORTEP drawing of *trans*-RuCl₂(BESE)₂ with 50 % probability thermal ellipsoids shown (crystal data given in Appendix 1.1). For the data of Table 3.8, S(4) and S(3) are taken as *trans* to S(2) and S(1), respectively.

Table 3.8. The Relative Configurations of the S-atoms in Chelating Disulfoxide Complexes of Ru in Refs. 52 and 53 and those depicted in Figures 3.7-3.10, 3.12 and 3.18.

Complex	S(1)	S(2)	S(3)	S(4)
<i>trans</i> -RuCl ₂ (BMSE) ₂ ^a	R	S	S	R
<i>cis</i> -RuCl ₂ (BESE) ₂ ^{a,b}	R ^c	S ^d	R ^c	S ^d
<i>trans</i> -RuCl ₂ (BESE) ₂ ^b	S	R	R	S
<i>trans</i> -RuCl ₂ (BPSE) ₂ ^{a,b}	S	R	R	S
<i>cis</i> -RuCl ₂ (BBSE) ₂ ·EtOH ^b	R ^c	R ^d	S ^c	R ^d
<i>cis</i> -RuCl ₂ (BCySE) ₂ ·EtOH·1/3 MeOH ^b	R ^c	S ^d	R ^c	S ^d
<i>cis</i> -RuCl ₂ (BMSP) ₂ ^{a,b}	R ^c	S ^d	R ^c	S ^d
<i>cis</i> -RuCl ₂ (BESP) ₂ ·EtOH·H ₂ O ^b	S ^c	R ^d	S ^c	R ^d
[RuCl(BESE)(H ₂ O)] ₂ (μ-Cl) ₂ ·H ₂ O ^b	S ^c	R ^e		
[RuCl(BPSP)] ₂ (μ-Cl) ₃ ·2H ₂ O·2.5CH ₂ Cl ₂ ^b	S ^c	R ^c	R ^c	S ^c

^a Data taken from refs. 52 and 53; otherwise data are from this thesis work. ^b Unit cell contains both enantiomers. ^c *Trans* to Cl. ^d *Trans* to S. ^e *Trans* to O.

3.6.2 *Trans*-RuCl₂(BPSE)₂·H₂O

The reaction of BPSE with *cis*-RuCl₂(DMSO)₄ gave the yellow title complex in 47 % yield. The ¹H NMR spectrum in CDCl₃ compare well with data reported in the literature for the structurally characterized *trans* complex with one signal at δ 1.10 assigned to the methyls.^{52,53} Attempts to photolyze *trans*-RuCl₂(BPSE)₂ to the *cis* isomer (refer to Section 3.6.1) were not successful as monitored by ¹H NMR spectroscopy.

3.6.3 *Cis-RuCl₂(BBSE)₂*

The title compound was synthesized from $\text{RuCl}_3 \cdot 3\text{H}_2\text{O}$ and precipitated in an analytically pure form with 21 % yield. ^1H NMR data are consistent with S-bonded sulfoxides with the *cis* geometry shown crystallographically. The ^1H NMR spectrum of the free ligand in CDCl_3 consists of multiplets at δ 3.20 and 3.00 ($\text{S(O)CH}_2\text{CH}_2\text{S(O)}$), 2.75 ($\text{CH}_2\text{S(O)}$), 1.72 ($\text{CH}_3\text{CH}_2\text{CH}_2$), 1.45 (CH_3CH_2), and a triplet at δ 0.95 (CH_3), all of which in the complex are shifted downfield (multiplets) to δ 3.60 ($\text{CH}_2\text{S(O)CH}_2$), 1.55 ($\text{CH}_3\text{CH}_2\text{CH}_2$) and 0.98 (CH_3); no free disulfoxide was observed. The crystal structure (Figure 3.8) is comparable to that of *cis*- $\text{RuCl}_2(\text{BESE})_2$ ^{52,53} in having slightly distorted octahedral geometry at the Ru centre with *trans* angles that range from 173.01(3) to 177.46(3) °, and *cis* angles that range from 85.79(3) to 96.22(3) ° (Table 3.9). Selected bond lengths and bond angles are tabulated in Table 3.9 and are comparable to those of *cis*- $\text{RuCl}_2(\text{BCySE})_2 \cdot \text{EtOH} \cdot 1/3\text{MeOH}$, *cis*- $\text{RuCl}_2(\text{BESE})_2$ (Table 3.7), and *cis*- $\text{RuCl}_2(\text{BESP})_2$ and $-\text{RuCl}_2(\text{BMSP})_2$ (Table 3.10); the key bond lengths and angles are basically similar in all these *cis* complexes. Within *cis*- $\text{RuCl}_2(\text{BBSE})_2 \cdot \text{EtOH}$ three S-atoms have the relative *R* configuration and one S-atom has the *S* configuration (Table 3.8); this is the only complex with S(1) and S(2) showing the same relative configuration. The synthesis of this complex could be plausible by starting with a mixture of the *meso* and *rac* ligands but the sharp melting point (Table 3.4) implies only one diastereomer of the ligand was present. This complex is chiral, with approximate C_2 symmetry, but the crystal structure is centrosymmetric and contains an equal number of the two enantiomers. Figure 3.8 depicts the Δ isomer in which the *trans* S-atoms (S(2) and S(4)) both have the *R* configuration. The unit cell contains the EtOH molecule H-bonded to both an O-atom and a Cl-atom of the

complex. The H-O, and the H-Cl distances are 2.12 and 2.71 Å, respectively, which are 0.58 and 0.19 Å shorter than the sum of the van der Waals radii of an O- and an H-atom (2.70 Å), and a Cl- and an H-atom (2.90 Å), respectively.⁷⁰ The interactions appear to be strong.

Table 3.9. Selected Bond Lengths (Å) and Bond Angles (°) of *cis*-RuCl₂(BBSE)₂·EtOH and *cis*-RuCl₂(BCySE)₂·EtOH·1/3 MeOH.

Bond or Angle	<i>cis</i> -RuCl ₂ (BBSE) ₂ ·EtOH	<i>cis</i> - RuCl ₂ (BCySE) ₂ ·EtOH·1 /3 MeOH
Ru-Cl	2.4159(8), 2.4288(7) ^a	2.4201(13), 2.4344(13) ^a
Ru-S	2.32892(9), 2.3035(9); ^a 2.2674(7), 2.2906(8) ^b	2.3364(13), 2.3484(13); ^a 2 .2719(13), 2.2988(13) ^b
S-O	1.477(2), 1.482(2); ^a 1.468(2), 1.480(2) ^b	1.444(4), 1.464(4); ^a 1.469 (3), 1.470(3) ^b
C-S	1.794(3)-1.838(4)	1.782(5)-1.842(5)
<i>cis</i> angles	85.79(3)-96.22(3)	86.27(5)-96.50(5)
<i>trans</i> angles	173.01(3)-177.46(3)	176.38(5)-178.01(5)
Ru-S-O	116.88(9)-118.59(8)	117.5(2)-119.8(2)
O-S-C	105.91(13)-109.23(15)	106.5(2)-107.9(2)
C-S-C	101.28(4)-102.8(2)	100.0(2)-104.5(2)
S-C-C ^c	106.3(2)-112.2(2)	106.7(4)-109.6(3)
S-C-C ^d	111.5(2)-113.2(2)	106.3(3)-113.4(4)
Ru-S-C ^c	102.72(12)-105.92(10)	101.5(2)-104.3(2)
Ru-S-C ^d	113.85(10)-119.29(10)	116.0(2)-118.2(2)

^a *Trans* to S. ^b *Trans* to Cl. ^c Bonds involving backbone carbons. ^d The C-atom of an alkyl substituent.

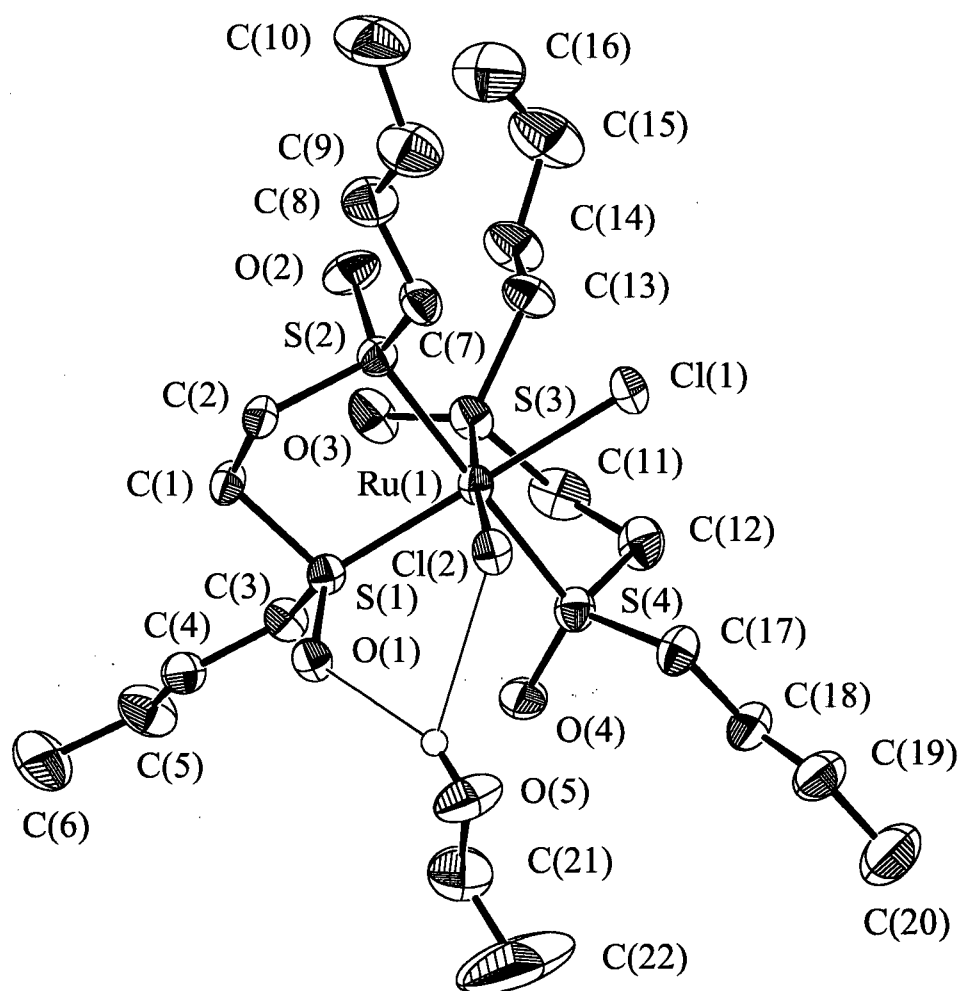


Figure 3.8. An ORTEP drawing of the Δ configuration of *cis*- $\text{RuCl}_2(\text{BBSE})_2 \cdot \text{EtOH}$ with 50 % probability thermal ellipsoids shown; H-atoms (except for that of EtOH) are omitted for clarity (crystal data given in Appendix 1.2).

3.6.4 *Cis-RuCl₂(BPeSE)₂*

The title compound was synthesized from $\text{RuCl}_3 \cdot 3\text{H}_2\text{O}$, purified using column chromatography, and obtained in only 9 % yield; ν_{SO} data (Table 3.5) imply S-bonded sulfoxides. The ^1H NMR spectrum (CDCl_3) of the free ligand consists of multiplets at δ 3.20 and 3.10 ($\text{S(O)CH}_2\text{CH}_2\text{S(O)}$), 2.80 ($\text{CH}_2\text{S(O)}$), 1.80 ($\text{CH}_3\text{CH}_2\text{CH}_2\text{CH}_2$), 1.40 ($\text{CH}_3\text{CH}_2\text{CH}_2$), and a triplet at 0.93 (CH_3), these being shifted to δ 3.70 ($\text{CH}_2\text{S(O)CH}_2$), 2.30 and 1.85 ($\text{CH}_2\text{CH}_2\text{S(O)}$), 1.45 ($\text{CH}_3\text{CH}_2\text{CH}_2$) and 0.90 (CH_3) (all multiplets), respectively, in the coordinated ligand, and no free disulfoxide was observed. The signal for the methyls was observed as one multiplet (presumably 2 overlapping triplets), compared to the two triplet signals observed for *cis*- $\text{RuCl}_2(\text{BESE})_2$ (Section 2.7.1). Crystals were obtained by slow evaporation of an $\text{EtOH}/\text{CH}_2\text{Cl}_2$ solution of the complex and were subjected to X-ray analysis, but excessive thermal motion exhibited by the long pentyl side chains prevented an accurate determination of the structure; however, *cis* geometry was established.⁶⁹

3.6.5 *Cis-RuCl₂(BCySE)₂*

The reaction of $\text{RuCl}_3 \cdot 3\text{H}_2\text{O}$ and BCySE gave the title complex in 30 % yield, with no purification steps being required. The ^1H NMR spectrum of the free ligand consists of peaks at δ 3.60 (CH_2CH_2), 2.56, 2.15 (H_2), 1.69 (H_1), 1.35 ($\text{H}_{3,4}$) (see Figure 2.1, in Section 2.3.11, for the proton labelling), while the ^1H spectrum of the title complex is a complicated pattern of overlapping multiplets between δ 1.0-4.4 (see Section 2.7.6, Chapter 2). The complicated spectrum is due to the inequivalence of the cyclohexyl rings oriented in the *cis* geometry. Crystals of the complex with one EtOH and one third MeOH solvate molecules

were grown by slow evaporation of the preparative reaction solution. This complex is chiral, has approximate C_2 symmetry with the pair of mutually *trans* S-atoms (S(2) and S(4)) having the same chirality. The complex crystallizes in a centrosymmetric space group which contains equal numbers of the two enantiomers. An ORTEP diagram shown in Figure 3.9 depicts the Λ isomer in which the *trans* S-atoms both have the *S* configuration. The molecule has a slightly distorted octahedral geometry at the Ru with *trans* angles ranging from 176.38(5) to 178.01(5) ° and *cis* angles from 86.27(5) to 96.50(5) ° (Table 3.9). Selected bond lengths and bond angles (Table 3.9) are comparable to those of *cis*-RuCl₂(BBSE)₂·EtOH (Table 3.9) and *cis*-RuCl₂(BESE)₂ (Table 3.7). The key bond lengths and angles are again similar to those found in the other *cis* Ru(II) bis-chelating disulfoxide complexes. Each disulfoxide has opposite chiralities at the two chiral S-atoms (Table 3.8). The unit cell of *cis*-RuCl₂(BCySE)₂·EtOH·1/3MeOH contains a MeOH molecule on a three-fold axis and one poorly resolved EtOH molecule in a general position. The thermal motion of the cyclohexyl rings was generally large, even at the low temperature used in the structural determination (crystal data are given in Appendix 1.3).

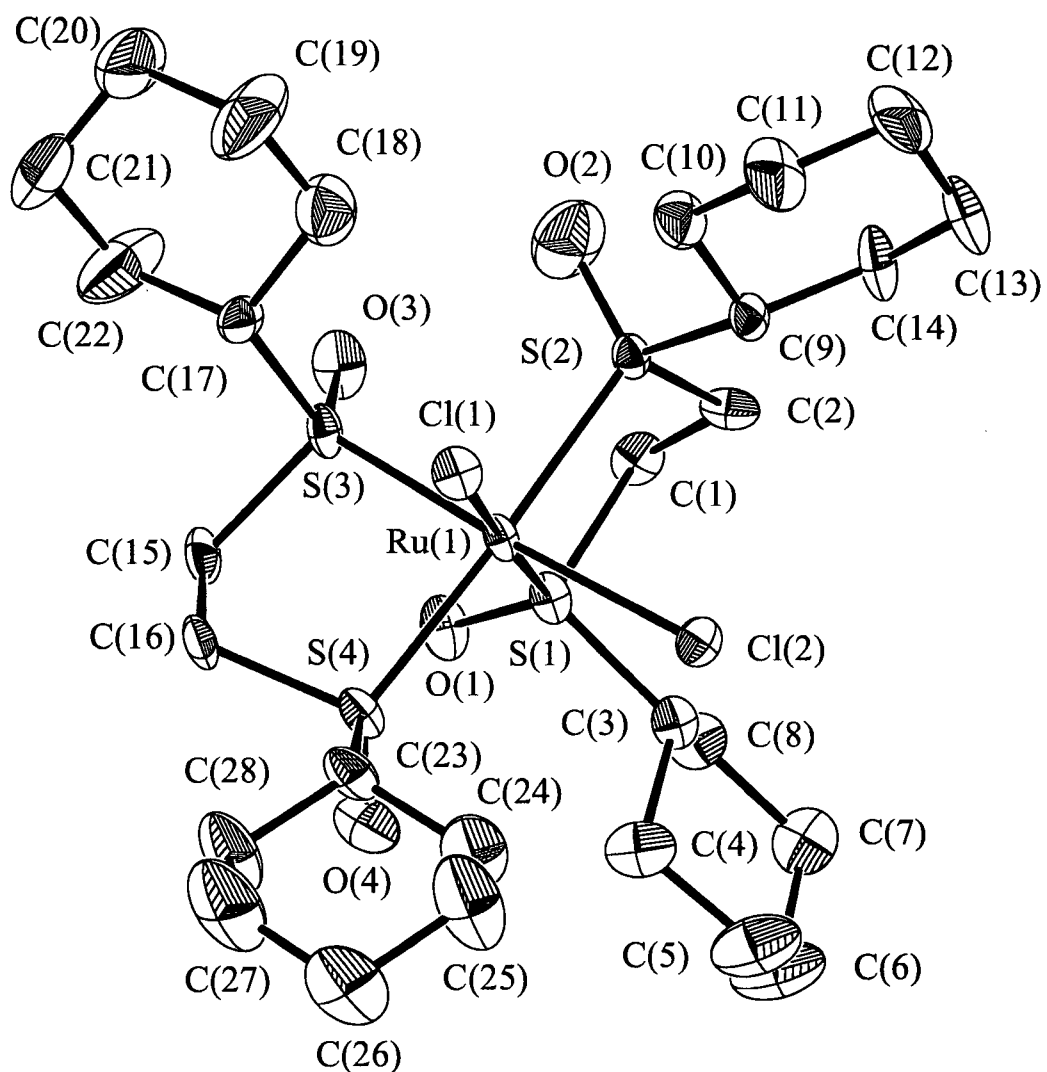


Figure 3.9. An ORTEP drawing of the Λ configuration of $cis\text{-RuCl}_2(\text{BCySE})_2 \cdot \text{EtOH} \cdot 1/3\text{MeOH}$ with 50 % probability thermal ellipsoids shown; H-atoms are omitted for clarity (crystal data given in Appendix 1.3).

3.6.6 *Cis-RuCl₂(BESP)₂*

The reaction of BESP with $\text{RuCl}_3 \cdot 3\text{H}_2\text{O}$ gave a yellow product in 36 % yield after purification by column chromatography. The ^1H NMR spectrum in CDCl_3 of the free ligand consists of multiplets at δ 2.90 ($\text{CH}_2\text{S}(\text{O})\text{CH}_2$), 2.45 ($\text{CH}_2\text{CH}_2\text{CH}_2$) and a triplet at 1.35 (CH_3), which in the complex are shifted downfield to δ 3.45, 2.75, 2.10 and 1.45 (multiplets), respectively (the multiplet at δ 2.45 splits into the two multiplets at δ 2.75 and 2.10). The ^1H NMR data are consistent with the structurally determined *cis* configuration. No free disulfoxide was observed in CDCl_3 solution in the ^1H NMR spectrum. The crystal structure of the *cis*- $\text{RuCl}_2(\text{BESP})_2 \cdot \text{EtOH} \cdot \text{H}_2\text{O}$ (Figure 3.10) is similar to that of *cis*- $\text{RuCl}_2(\text{BMSP})_2$.^{52,53} Selected bond lengths and angles are tabulated in Table 3.10 and are given together with those of *cis*- $\text{RuCl}_2(\text{BMSP})_2$. The key bond lengths and angles are basically similar to those found in the other *cis* Ru(II) bis-chelating disulfoxide complexes. The molecule has a slightly distorted octahedral geometry at Ru with *trans* angles that range from 171.64(4) to 176.35(4) ° and *cis* angles that range from 84.96(3) to 97.57(4) °. The complex crystallizes in a centrosymmetric space group and contains an equal number of the two enantiomers. Figure 3.10 depicts the Δ isomer in which the *trans* S-atoms (S(2) and S(4)) both have the *R* configuration. The unit cell contains a water molecule H-bonded to an O-atom of the sulfur-oxygen moiety of the disulfoxide ligand and to the EtOH solvate (Figure 3.11). The average H-O distance is 1.89 Å, which is 0.81 Å shorter than the sum of the van der Waals radii of an H- and an O-atom (2.70 Å), suggesting a strong interaction between the water molecule, the complex and the EtOH solvate.⁷⁰

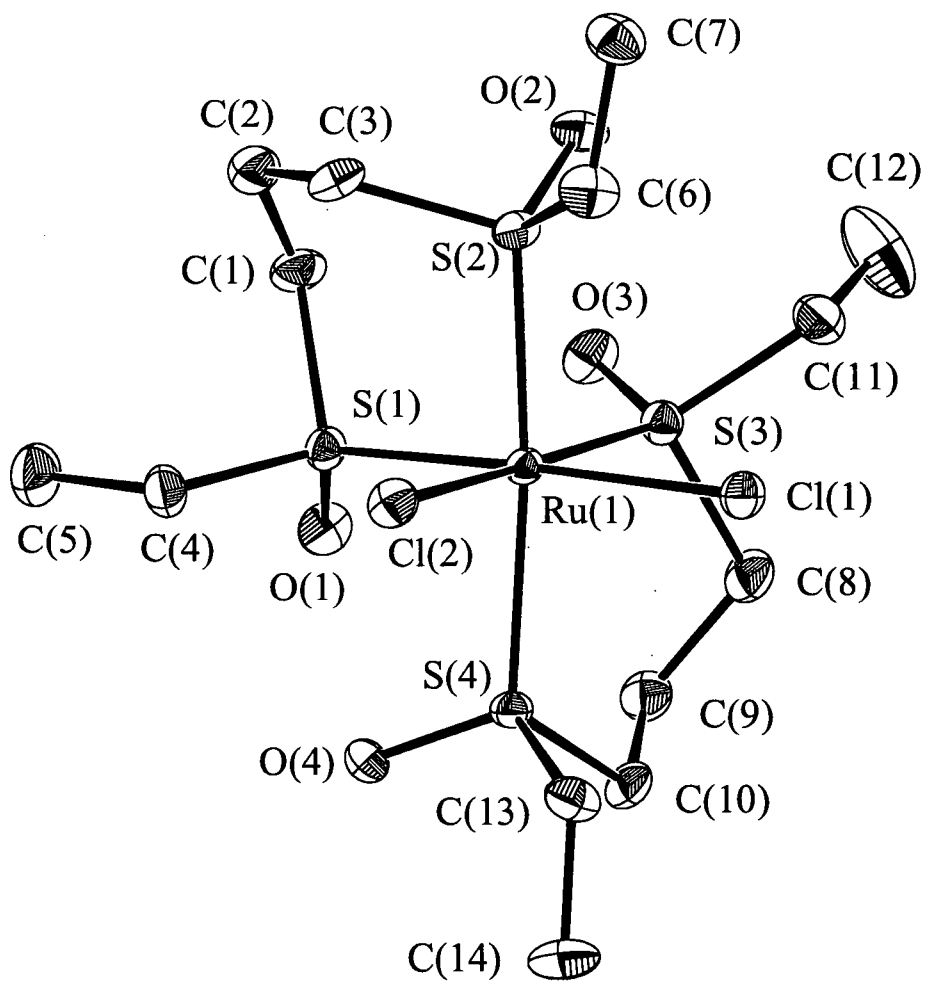


Figure 3.10. An ORTEP drawing of the Δ configuration of cis - $RuCl_2(BESP)_2 \cdot EtOH \cdot H_2O$ with 50 % probability thermal ellipsoids shown; H-atoms are omitted for clarity (crystal data given in Appendix 1.4).

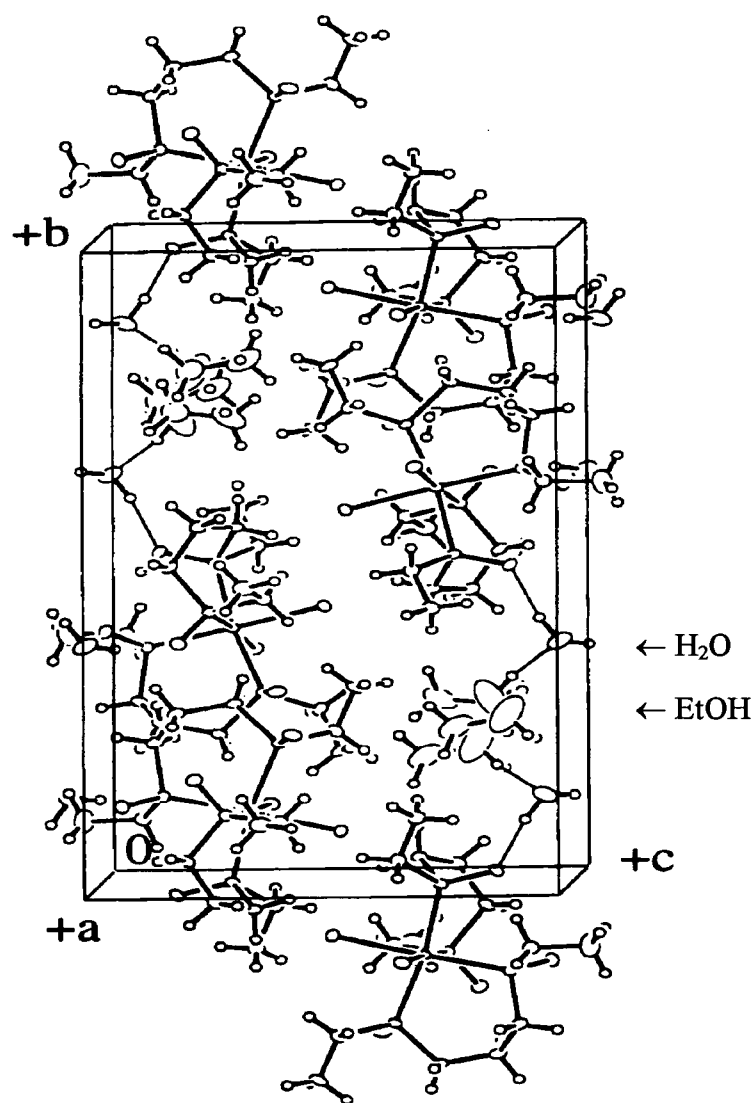


Figure 3.11. The unit cell of *cis*-RuCl₂(BESP)₂·EtOH·H₂O showing the EtOH and H₂O solvate molecules (crystal data given in Appendix 1.4).

Table 3.10. Selected Bond Lengths (Å) and Bond Angles (°) of *cis*-RuCl₂(BESP)₂·EtOH·H₂O and *cis*-RuCl₂(BMSP)₂.

Bond or Angle	<i>cis</i> -RuCl ₂ (BESP) ₂ ·EtOH·H ₂ O	<i>cis</i> -RuCl ₂ (BMSP) ₂ ^a
Ru-Cl	2.4167(8), 2.4310(10) ^b	2.4354(7), 2.4395(7) ^b
Ru-S	2.3311(10), 2.3528(10), ^b 2.2766(8), 2.2905(10) ^c	2.3518(7), 2.3569(7), ^b 2.2682(6), 2.2710(6) ^c
S-O	1.489(2), 1.490(3), ^b 1.479(2), 1.481(3) ^c	1.473(2), 1.480(2), ^b 1.476(2), 1.480(2) ^c
C-S	1.791(4)-1.820(3)	1.773(3)-1.801(3)
<i>cis</i> angles	84.96(3)-97.57(4)	83.42(2)-97.55(2)
<i>trans</i> angles	171.64(4)-176.35(4)	174.21(2)-178.42(2)
Ru-S-O	113.38(10)-117.94(11)	113.91(8)-116.51(9)
C-S-O	106.3(2)-107.8(2)	104.9(1)-107.1(1)
C-S-C	98.4(2)-102.5(2)	98.9(2)-100.6(1)
S-C-C ^d	112.2(3)-116.5(3)	114.4(2)-115.6(2)
S-C-C ^e	111.9(3)-112.8(3)	
C-C-C	111.7(3)-117.1(3)	113.1(3), 113.4(2)
Ru-S-C ^d	109.03(13)-115.79(13)	115.3(1)-115.80(9)
Ru-S-C ^e	112.45(14)-115.12(12)	111.2(1)-113.6(1)

^a Data taken from refs. 52 and 53. ^b *Trans* to S. ^c *Trans* to Cl. ^d Bonds involving backbone carbons. ^e The C-atom of an alkyl substituent.

3.7 Dinuclear Ru(II)/Ru(II) Chelating Disulfoxide Complexes

Previous work in this laboratory involved the synthesis of *cis*-RuCl₂(BESE)₂,^{52,53} while one initial goal of this thesis was to synthesize the corresponding *trans* isomer by utilizing *trans*-RuCl₂(DMSO)₄ as a precursor or photolysis of *cis*-RuCl₂(BESE)₂. These attempts, however, led to the isolation of *cis*-RuCl₂(BESE)₂ (Section 3.6.1).

During the course of this work, Geremia *et al.* reported the topological analysis of bis-chelate disulfoxide metal complexes and the results of molecular mechanical calculations on RuCl₂(BMSE)₂. They implied that *cis*-RuCl₂(BESE)₂ was the lowest strain energy diastereomer of a series of possible isomeric forms,⁶⁸ thus suggesting that attempts to synthesize the corresponding *trans* isomer would likely lead to the isolation of *cis*-RuCl₂(BESE)₂, at least as the thermodynamic product.

The reported procedure for the synthesis of *cis*-RuCl₂(BESE)₂ involved the reaction of two equivalents of BESE with one equivalent of RuCl₃·3H₂O.^{52,53} However, in the present studies, on reduction of the amount of ligand to one equivalent, the interesting water-soluble, dinuclear complex [RuCl(BESE)(H₂O)]₂(μ-Cl)₂ was obtained. Then the reaction of one equivalent of [RuCl(BESE)(H₂O)]₂(μ-Cl)₂ with two equivalents of BESE led to the isolation of *trans*-RuCl₂(BESE)₂ as shown by ¹H NMR spectroscopy and X-ray crystallographic analysis (Section 3.6.1).

3.7.1 Characterization of $[\text{RuCl}(\text{BESE})(\text{H}_2\text{O})]_2(\mu\text{-Cl})_2$, $[\text{RuCl}(\text{BPSE})(\text{H}_2\text{O})]_2(\mu\text{-Cl})_2$ and $[\text{RuCl}(\text{BBSE})(\text{H}_2\text{O})]_2(\mu\text{-Cl})_2$

Reaction of one equivalent of BESE, BPSE and BBSE with $\text{RuCl}_3 \cdot 3\text{H}_2\text{O}$ resulted in the isolation of $[\text{RuCl}(\text{BESE})(\text{H}_2\text{O})]_2(\mu\text{-Cl})_2$, $[\text{RuCl}(\text{BPSE})(\text{H}_2\text{O})]_2(\mu\text{-Cl})_2$ and $[\text{RuCl}(\text{BBSE})(\text{H}_2\text{O})]_2(\mu\text{-Cl})_2$ in 60, 46 and 61 % yield, respectively. The ν_{SO} data are consistent with S-bonded sulfoxides (Section 3.4.2, Table 3.5), later confirmed for $[\text{RuCl}(\text{BESE})(\text{H}_2\text{O})]_2(\mu\text{-Cl})_2$ by X-ray crystallography. The solution ^1H NMR spectra of all three complexes in D_2O generally reveal small downfield shifts from the resonances of the free ligand protons, again consistent with S-bonding (Section 3.4.1). The values of "equilibrium" conductivity for these complexes in water ($\sim 10^{-4}$ M, Λ_{M} 358, 282 and 497, respectively) correspond to those of a 2:1-3:1, 2:1 and 3:1 electrolyte, respectively, when these conductivity values are compared to the equivalent conductances of salts.⁷¹

A titration of $[\text{RuCl}(\text{BESE})(\text{H}_2\text{O})]_2(\mu\text{-Cl})_2$ with NaOH in water showed that two equivalents of a standardized NaOH solution were required to titrate 1 equivalent of $[\text{RuCl}(\text{BESE})(\text{H}_2\text{O})]_2(\mu\text{-Cl})_2$ (see Table 3.11), suggesting the loss of 2 equivalents of H^+ from $[\text{RuCl}(\text{BESE})(\text{H}_2\text{O})]_2(\mu\text{-Cl})_2$. Of note, the measured equivalent conductance of 10^{-3} M HCl was ~ 430 (literature data at 25°C give ~ 420 ⁷²) and this value was reduced to ~ 350 upon addition of 10^{-3} M *cis*- $\text{RuCl}_2(\text{BESE})_2$ (the molar conductance of an equilibrated 10^{-3} M aqueous solution of *cis*- $\text{RuCl}_2(\text{BESE})_2$ is ~ 33.9 ⁵³). The conductivity data are thus consistent with the loss of 2 equivalents of H^+ and 2 equivalents of Cl^- per $[\text{RuCl}(\text{BESE})(\text{H}_2\text{O})]_2(\mu\text{-Cl})_2$ (see p.101).

Table 3.11. Titration data for $[\text{RuCl}(\text{BESE})(\text{H}_2\text{O})]_2(\mu\text{-Cl})_2$ using NaOH.

[NaOH] (mM)	Volume used (mL, mmol)	$[\text{RuCl}(\text{BESE})(\text{H}_2\text{O})]_2(\mu\text{-Cl})_2$ (mg, mmol)
5.80 (± 0.09)	1.96 (± 0.15), 1.13 (± 0.08) $\times 10^{-2}$	4.22 (± 0.05), 5.67 (± 0.06) $\times 10^{-3}$

^1H NMR data on $[\text{RuCl}(\text{BESE})(\text{H}_2\text{O})]_2(\mu\text{-Cl})_2$ in aqueous solution suggest that this complex loses 2 Cl^- per complex. The equilibrium ^1H NMR spectrum of the complex in D_2O (under air) does not change upon addition of up to three equivalents of AgNO_3 . Upon addition of two equivalents of AgNO_3 , added dropwise, to a solution of $[\text{RuCl}(\text{BESE})(\text{H}_2\text{O})]_2(\mu\text{-Cl})_2$ in D_2O , a precipitate formed immediately, but the resulting ^1H NMR spectrum of the solution (*i.e.* the solution obtained from the filtered heterogeneous mixture) was the same as that of the equilibrium spectrum of $[\text{RuCl}(\text{BESE})(\text{H}_2\text{O})]_2(\mu\text{-Cl})_2$ in D_2O . One more equivalent of AgNO_3 was added dropwise to the filtrate. No further precipitate was observed, and the resulting ^1H NMR was identical to that of the equilibrium ^1H NMR of $[\text{RuCl}(\text{BESE})(\text{H}_2\text{O})]_2(\mu\text{-Cl})_2$.

These water-soluble, complexes were tested *in vitro* for cytotoxicity, accumulation and DNA-binding properties in Chinese hamster ovary cells with the results presented in Chapter 4.

Crystals of the BESE complex containing one H_2O solvate molecule were grown by slow evaporation of a saturated aqueous solution of $[\text{RuCl}(\text{BESE})(\text{H}_2\text{O})]_2(\mu\text{-Cl})_2$. The structure is shown in Figure 3.12, and selected bond lengths and angles, together with those of *cis*- and *trans*- $\text{RuCl}_2(\text{BESE})_2$, are given in Table 3.7.

The complex crystallizes in a centrosymmetric space group with a centre of symmetry and is thus achiral. The asymmetric unit consists of two independent half-molecules and a water molecule (Figure 3.13). The H(33)-O(4) and H(34)-Cl(2) distances are 1.81 and 2.28 Å, respectively, which are 0.89 and 0.62 Å less than the sum of the van der Waals radii of an H- and an O-atom (2.70 Å), and that of an H-atom and a Cl-atom (2.90 Å), respectively, an indication of strong H-bond interactions between the H₂O and the complex. The complex has Ru-Cl-Ru bridging angles of 96.83(3) and 97.89(3)°. Thus the Ru atoms are further apart than expected for an ideal cofacial bioctahedron (for which $M-X_{\text{terminal}} = M-X_{\text{bridging}}$, $X-M-X$ angles = 90° and the $M-X_{\text{bridging}}-M$ angles = 70.53° (given by $\cos \theta/2 = (2/3)^{1/2}$)⁷³; M = metal and X = ligand)⁷⁴ and no Ru-Ru interaction was detected out to 3.90 Å; there is no metal-metal bond. The usual range found for a Ru-Ru bond is ~ 2.28-3.04 Å as exemplified by: 2.281 Å for Ru₂(O₂CC₃H₇)₄Cl,⁷⁵ 2.540 Å for [Ru₂(μ-H)₃(PMe₃)₆][BF₄],⁷⁶ 2.728 Å for [Ru(μ-OOCCH₂CH₂CH₃)(CO)₂(P(^tBu)₃)₃]₂,⁷⁷ 2.743 Å for [Ru₂(Et₂dtc)₅][BF₄] (Et₂dtc = N,N-diethyldithiocarbamate, S₂CNEt₂)⁷⁸ 2.80 Å for [Ru(H)₂Cl(Ptol₃)₂]₂ (Ptol₃ = *p*-tris(tolylphosphine),⁷⁹ 2.811 Å Ru₂H₄(PMe₃)₆,⁷⁶ and 2.827-3.034 Å for Ru₆C(CO)₁₇.⁸⁰ The *cis* angles at the Ru range from 82.11(3)° to 95.11(4)° and the *trans* angles range from 171.77(4)° to 178.01(8)°.

The BPSE and BBSE complexes presumably have the corresponding dinuclear, dichloro-bridged structures.

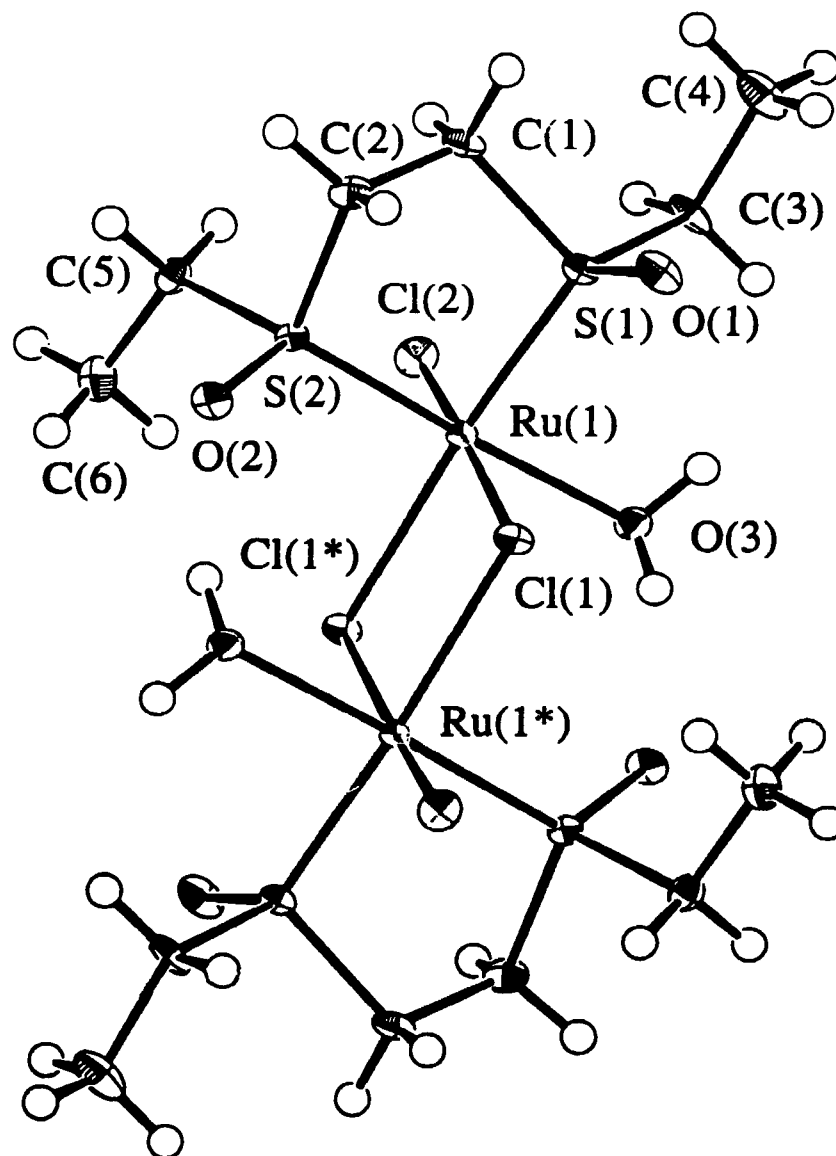


Figure 3.12. An ORTEP drawing of $[\text{RuCl}(\text{BESE})(\text{H}_2\text{O})]_2(\mu\text{-Cl})_2$ with 50 % probability thermal ellipsoids (crystal data given in Appendix 1.5).

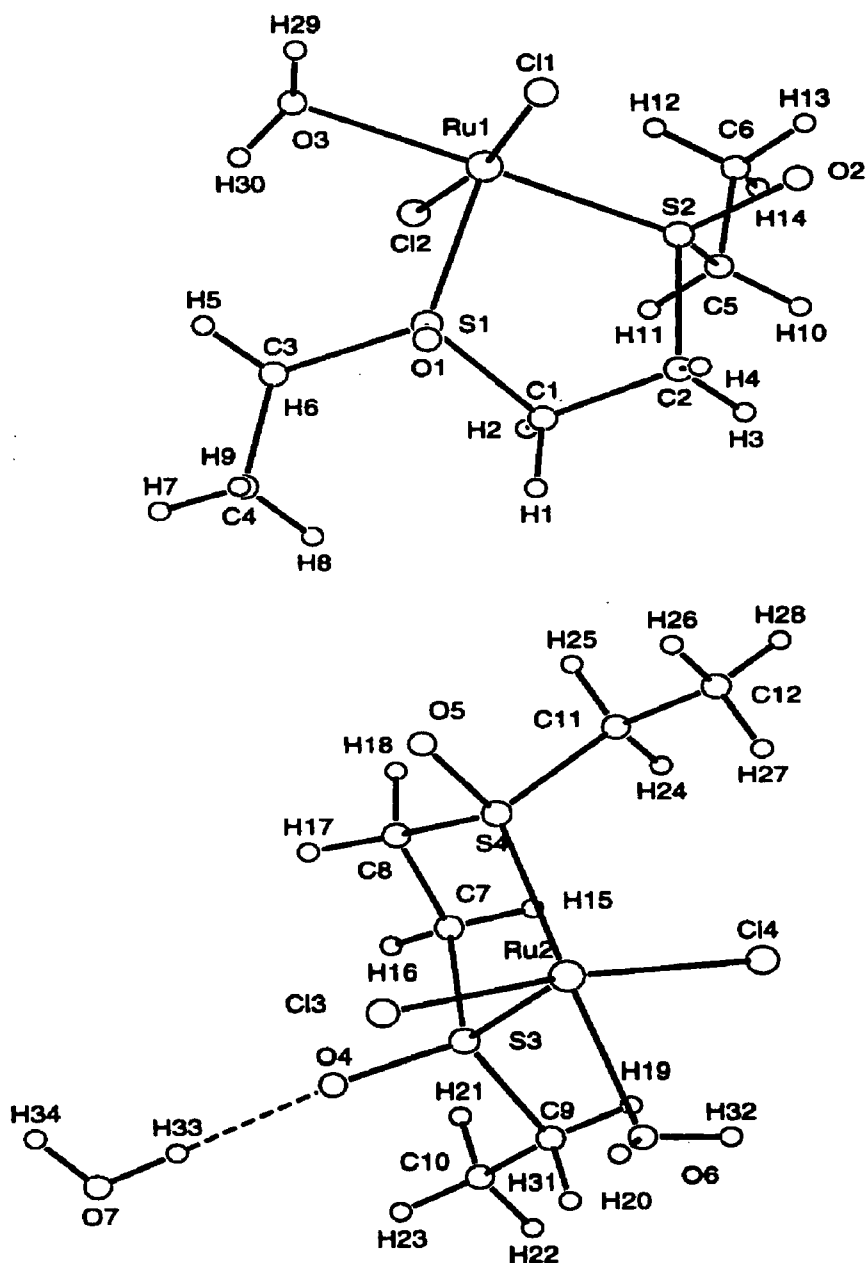


Figure 3.13. Diagram of $[\text{RuCl}(\text{BESE})(\text{H}_2\text{O})]_2(\mu\text{-Cl})_2$ showing the H_2O solvate (crystal data given in Appendix 1.5).

3.8 A Mixed-Valence Ru(II)/Ru(III) Chelating Disulfoxide Complex

Previous synthetic reactions using 2 equivalents of disulfoxide and $\text{RuCl}_3 \cdot 3\text{H}_2\text{O}$ gave mononuclear Ru(II) bis-disulfoxide complexes (Section 3.6). However, reaction of 2 equivalents of BPSP with $\text{RuCl}_3 \cdot 3\text{H}_2\text{O}$ led to the isolation of the first known type of a mixed-valence Ru(II)/Ru(III), chelating disulfoxide complex, $[\text{RuCl}(\text{BPSP})]_2(\mu\text{-Cl})_3$, which contains three bridging chlorides. Of major interest, the species was readily soluble in water. This complex was tested *in vitro* for cytotoxicity, accumulation and DNA-binding properties in Chinese hamster ovary cells with the results presented in Chapter 4.

3.8.1 Introduction

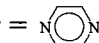
Diruthenium complexes form the largest group of any mixed-valence systems,⁸¹ and Ru has been the transition metal of choice to study electron transfer or exchange reactions because it is relatively inexpensive and forms stable Ru(II) and Ru(III) coordination complexes.⁸¹

Allen and Hush have described the physical properties of mixed-valence compounds,⁸² which contain an element in two different oxidation states and often exhibit unusually intense colouration unrelated to the colours of either of the individual metal ions. Homonuclear intervalence transfer absorption is a result of light absorption causing the transfer of an electron from a lower to a higher oxidation state of the same element,⁸² the probability being smaller the larger the internuclear distance. These electron transfer absorptions may occur in the UV, visible or near-IR regions.⁸² Mixed-valence complexes have been classified into three types (Table 3.12).⁸¹⁻⁸⁵

Table 3.12. Classes of Mixed-valence Complexes.^a

Class I	Class II	Class III
metal ions in ligand fields of very different symmetry and/or strength (<i>i.e.</i> tetrahedral vs. octahedral)	metal ions in ligand fields of nearly identical symmetry	III-A: metal ions indistinguishable but grouped into polynuclear clusters III-B: metal ions indistinguishable
no mixed-valence transitions in the visible region	one or more mixed-valence transitions in the visible region or near IR	III-A: one or more mixed-valence transitions in the visible region III-B: absorption edge in the IR, opaque with metallic reflectivity in the visible region
no coupling between metal ions (completely valence trapped)	weak coupling between metal ions (valence trapped)	strong coupling between metal ions (delocalized valency)
exhibits properties observable only for isolated mononuclear M and M ⁺ complexes (M = metal centre, M ⁺ = one electron oxidation product)	exhibits slightly perturbed M and M ⁺ characteristics, and may also manifest properties not associated with isolated units	properties of the (M-M) ⁺ unit are discerned

^a Based on data in refs. 81-85.

Examples of Ru mixed-valence complexes include Ru red, $[(\text{NH}_3)_5\text{Ru}-\text{O}-\text{Ru}(\text{NH}_3)_4-\text{O}-\text{Ru}(\text{NH}_3)_5]^{6+}$,⁸⁶ "Ru blues",⁸⁷⁻⁹¹ and the now classic Creutz-Taube ion, $[(\text{NH}_3)_5\text{Ru}-(\mu\text{-pyr})-\text{Ru}(\text{NH}_3)_5]^{5+}$ (pyr = )^{81,85,92}. "Ru blue" solutions, well known as synthetic precursors to many Ru(II) and Ru(III) complexes,⁸⁸ appear to contain several species. Mercer and Dumas have identified three of these as being dinuclear Ru(II)/Ru(III) species of the type $\text{Ru}_2\text{Cl}_{3+n}^{(2-n)+}$, where $n = 0, 1$ or 2 .⁸⁷ Rose and Wilkinson isolated green salts from the blue solutions and have proposed that such solutions may contain the anion RuCl_3^- and the cluster $[\text{Ru}_4\text{Cl}_{12}]^{4-}$,⁸⁹ while Bino and Cotton later structurally characterized a green, mixed-valent

complex $[\text{Ru}_3\text{Cl}_{12}]^{4-}$ containing a linear arrangement of Ru(III)-Ru(II)-Ru(III).⁹⁰ Bottomley and Tong suggested that the species responsible for one "Ru blue" solution was the mixed-valence dimer $[\text{Ru}_2(\text{NH}_3)_6\text{Cl}_4(\text{H}_2\text{O})]\text{Cl}$, formed either by reduction of chloroammine-complexes of Ru(III) or by reaction of ammine complexes of Ru(II) with acids.⁹¹

Gibson *et al.* reported that mixed-valence chloroammine complexes of Ru, like cisplatin, induced filamentation in *E. coli* (Section 1.3.1).⁹³ $[\text{Ru}_2(\text{NH}_3)_6\text{Cl}_3](\text{BPh}_4)_2$ ⁹⁴ has been structurally characterized as a trichloro-bridged bioctahedral dimer, with a Ru-Ru distance of 2.753 Å and an average Ru-Cl-Ru angle of 70.2°; the related complex $[(\text{NH}_3)_3\text{RuBr}_3\text{Ru}(\text{NH}_3)_3](\text{ZnBr}_4)$ ⁹⁵ has a Ru-Ru distance of 2.852 Å and an average Ru-Br-Ru angle of 68.5°. Other characterized trichloro-bridged Ru(II)/Ru(III) complexes include $\text{Ru}_2\text{Cl}_5(\text{P}^n\text{Bu}_3)_4$ ⁷⁴ and the series $[\text{RuCl}(\text{P-P})]_2(\mu\text{-Cl})_3$ (P-P = chiraphos, diop or $\text{PPh}_2(\text{CH}_2)_n\text{PPh}_2$, $n = 3$ or 4; Figure 3.14)⁹⁶. A Ru-Ru distance of 3.25 Å (*i.e.* no Ru-Ru bond) and an average Ru-Cl-Ru angle of 83.4° were determined for $[\text{RuCl}(\text{chiraphos})]_2(\mu\text{-Cl})_3$.⁹⁶ Thorburn *et al.* stated that the X-ray data do not distinguish between a weakly interacting system and a completely delocalized system, but did suggest that $[\text{RuCl}(\text{chiraphos})]_2(\mu\text{-Cl})_3$ would be best formulated as a valence-delocalized, class III A system (Table 3.12).⁹⁶

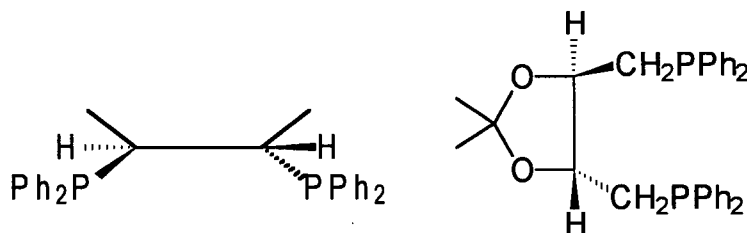


Figure 3.14. Structures of *SS*-chiraphos and *RR*-diop.

Yapp in this laboratory reported the mixed-valence sulfoxide complexes $\text{Ru}_2\text{Cl}_5(\text{Et}_2\text{SO})_4$, $\text{Ru}_2\text{Cl}_5(\text{Pr}_2\text{SO})_5$ and $\text{Ru}_2\text{Cl}_5(\text{Bu}_2\text{SO})_5$.⁵² Based on IR and ^1H NMR spectroscopies, $\text{Ru}_2\text{Cl}_5(\text{Et}_2\text{SO})_4$ was proposed to be a trichloro-bridged dimer with all terminal S-bonded sulfoxides arranged symmetrically around the Ru centres, whereas $\text{Ru}_2\text{Cl}_5(\text{Pr}_2\text{SO})_5$ and $\text{Ru}_2\text{Cl}_5(\text{Bu}_2\text{SO})_5$ were tentatively assigned with four S- and one O-bonded sulfoxides to be dichloro-bridged (*e.g.* $\text{Cl}(\text{Pr}_2\text{SO})_3\text{Ru}(\text{II})(\mu\text{-Cl})_2\text{Ru}(\text{III})\text{Cl}_2(\text{Pr}_2\text{SO})_2$).⁵²

Of interest, mixed-valent Pt complexes, the so-called "Pt blues", have been studied as a potentially useful class of anti-cancer drugs. These complexes, which may be obtained by reaction of cisplatin⁹⁷ with pyrimidine bases,^{99,100} are characterized by high solubility in aqueous solutions, low toxicity, minimal kidney toxicity and high anti-tumour activity as compared to cisplatin.⁹⁸ Insights into Pt blue chemistry were the structural determinations and detailed characterizations of the dimeric *cis*-diammineplatinum α -pyridone blue (average oxidation state 2.25) and *cis*-diammineplatinum(II)methylthymine (see Figures 3.15 and 3.16 for the structures of α -pyridone and methylthymine, and $[(\text{NH}_3)_4\text{Pt}_2(\text{C}_5\text{H}_4\text{NO})_2]_2(\text{NO}_3)_5 \cdot \text{H}_2\text{O}$ ⁹⁹ and $[(\text{NH}_3)_2\text{Pt}(\text{C}_6\text{H}_7\text{N}_2\text{O}_2)_2\text{Pt}(\text{NH}_3)_2](\text{NO}_3)_2 \cdot \text{H}_2\text{O}$,¹⁰⁰ respectively). Related Pt(II) creatinine blues (see Figures 3.15 and 3.16)¹⁰¹ and a mixed-valence octanuclear Pt blue complex (average oxidation state 2.25) with bridging acetamido or 2-fluoroacetamido ligands (see Figure 3.16)¹⁰² are also known.

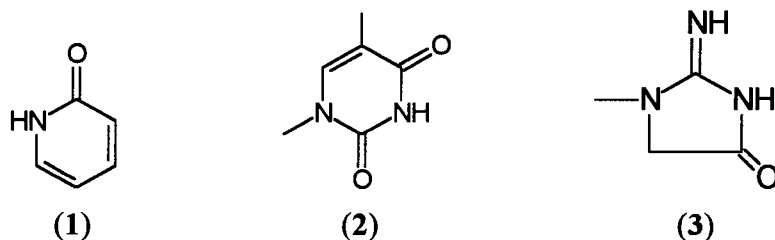


Figure 3.15. Structures of α -pyridone (1), 1-methylthymine (2) and creatinine (3).

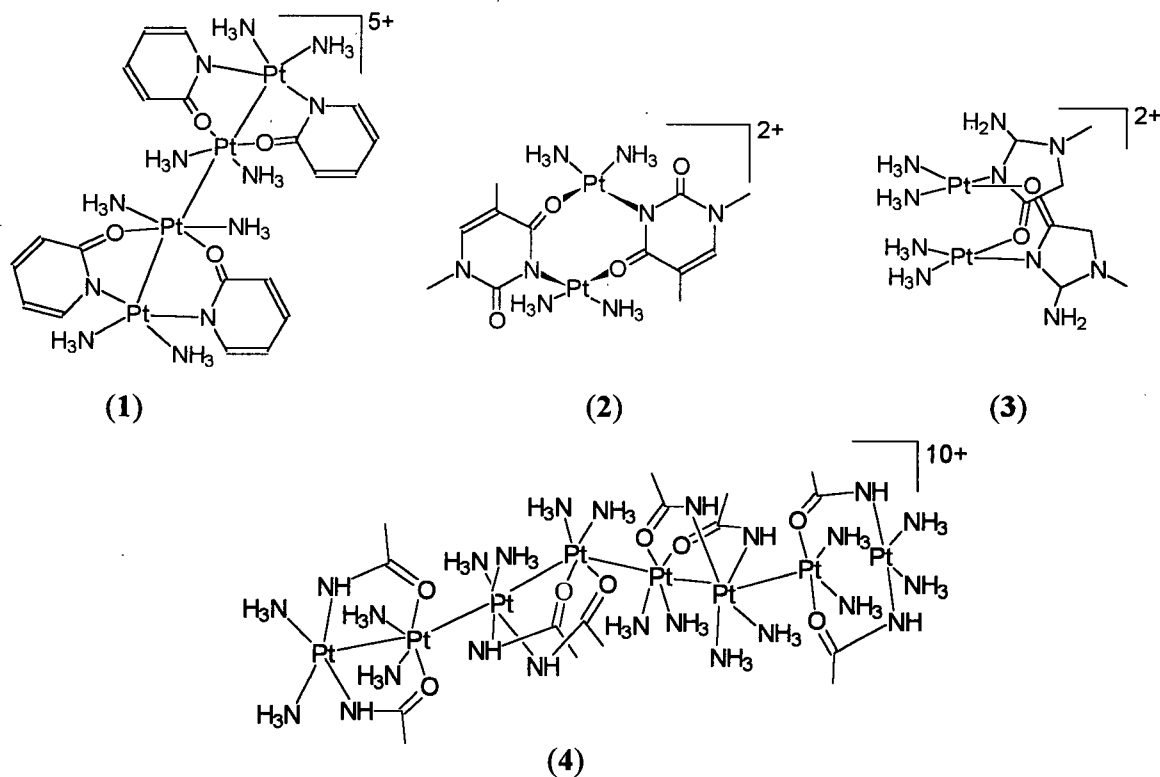


Figure 3.16. Structures of $[(\text{NH}_3)_4\text{Pt}_2(\text{C}_5\text{H}_4\text{NO})_2](\text{NO}_3)_5 \cdot \text{H}_2\text{O}$ (1), $[(\text{NH}_3)_2\text{Pt}(\text{C}_6\text{H}_7\text{N}_2\text{O}_2)_2\text{Pt}(\text{NH}_3)_2](\text{NO}_3)_2 \cdot \text{H}_2\text{O}$ (2), $[\text{Pt}_2(\text{NH}_3)_4(\text{C}_4\text{H}_7\text{N}_3\text{O})_2](\text{NO}_3)_2$ (3), and $[(\text{NH}_3)_2\text{Pt}(\text{CH}_3\text{CONH})_2\text{Pt}(\text{NH}_3)_2]_4(\text{NO}_3)_{10} \cdot 4\text{H}_2\text{O}$ (4) adapted from refs. 99-102.

3.8.2 $[\text{RuCl}(\text{BPSP})]_2(\mu\text{-Cl})_3$

Reaction of $\text{RuCl}_3 \cdot 3\text{H}_2\text{O}$ with two equivalents of BPSP in EtOH led to the isolation in 15 % yield of the unexpected dinuclear, mixed-valence complex $[\text{RuCl}(\text{BPSP})]_2(\mu\text{-Cl})_3$

containing three bridging chloride ligands. A possible explanation for the low yield could be that some of the "green solution" containing Ru(II) (formed from $\text{RuCl}_3 \cdot 3\text{H}_2\text{O}$ with concomitant oxidation of EtOH to acetaldehyde) was oxidized *in situ* to Ru(III) with reduction of disulfoxide to dithioether; a distinctive thioether odour was detected during the workup of the reaction solution (see Section 3.9, p. 126 for discussion of this redox chemistry). ν_{SO} data for the title complex indicated S-bonded sulfoxides (see Section 3.4.2, Table 3.5) and this was later confirmed by X-ray crystallography (Figure 3.18). The ^1H NMR spectrum in CDCl_3 of the free ligand consists of multiplets at δ 3.00 ($\text{CH}_2\text{CH}_2\text{CH}_2$), 2.90 ($\text{CH}_2\text{CH}_2\text{CH}_3$), 2.20 ($\text{CH}_2\text{CH}_2\text{CH}_2$), 1.70 (CH_2CH_3) and a triplet at 1.07 (CH_3), while for the complex (an equilibrated solution in D_2O) these appear more downfield (with the exception of the methyl multiplet at 0.90) as broad signals at δ 3.72, 3.20, 2.44, 1.72 and 0.90, respectively (see Figure 3.21, p. 118); the ^1H spectrum in CDCl_3 consists of two broad peaks at δ 2.18 and 1.10. These data suggest that the Ru(II)/Ru(III) centres are delocalized, as broad resonances were observed in the ^1H NMR spectrum. No transitions were observed in the near-IR region (800–2000 nm). The complex exhibited no conductivity in CHCl_3 , but in H_2O the molar conductivity (per mole of dimer) increased to a steady value of 234 after 20 min, the value corresponding to that of a 2:1 electrolyte (based on the equivalent conductance of salts (see Section 3.7.1); however, evidence suggests the solution contains 2H^+ and 2Cl^- produced from each mole of dimer (Section 3.8.3), although the equivalent conductance of 10^{-3} M HCl at 25°C is $\sim 420^{72}$ and is much greater than that observed for $[\text{RuCl}(\text{BPSP})]_2(\mu\text{-Cl})_3$ (but see p. 100 that shows that the conductivity of the HCl solution is decreased considerably in the presence of a 'neutral' Ru disulfoxide complex). The solution μ_{eff} value, determined by a

modified Evans' method (see Figure 3.17, and Section 2.2.3), was 1.7 ± 0.1 B. M. consistent with one unpaired electron per molecule.

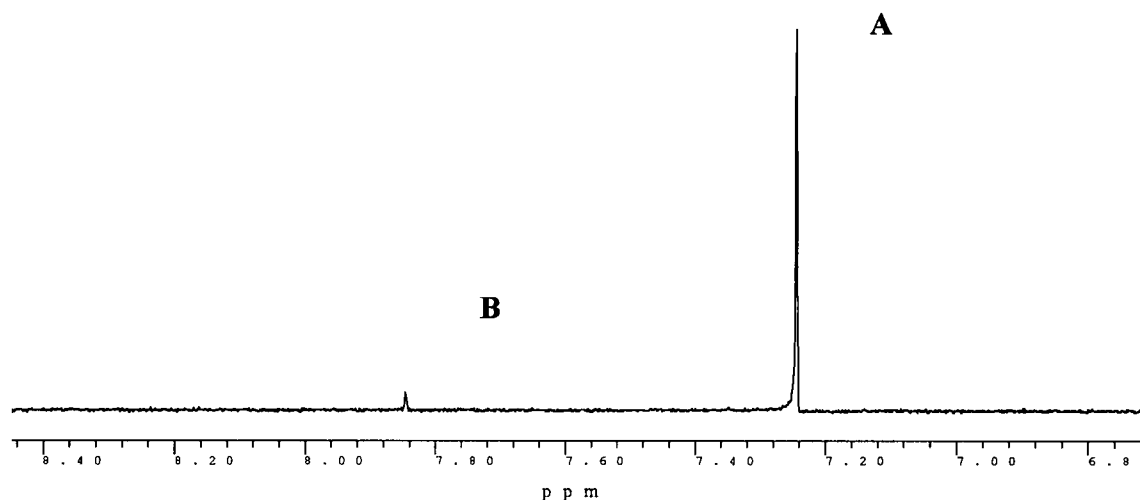


Figure 3.17. The ¹H NMR (200 MHz, CDCl₃) spectrum showing the paramagnetic shift caused by [RuCl(BPSP)]₂(μ-Cl)₃ (8.8×10^{-2} M) of the residual CHCl₃ relative to that of the reference CHCl₃. (A = residual CHCl₃ in CDCl₃, and B = residual CHCl₃ peak shifted by [RuCl(BPSP)]₂(μ-Cl)₃).

An X-ray diffraction study of a single crystal of [RuCl(BPSP)]₂(μ-Cl)₃, obtained from a saturated solution of CH₂Cl₂, showed the dinuclear, triply chloro-bridged geometry (Figures 3.18 and 3.19). The complex crystallizes in an acentric space group containing a glide plane and thus enantiomers are present in the crystal structure. Figure 3.18 depicts one of the enantiomers. Selected bond lengths and bond angles for the observed two asymmetric units are given in Tables 3.13 and 3.14, respectively; crystallographically the two Ru-atoms are indistinguishable, consistent with the description as a delocalized Ru(II)/Ru(III) system.

The bond lengths are in fact comparable to those found in $[\text{RuCl}(\text{BESE})(\text{H}_2\text{O})]_2(\mu\text{-Cl})_2$ where, for example, Ru-Cl is 2.4636(10) Å (bridging, *trans* to S) and Ru-S is 2.1985(10) Å.

The coordination geometry about each Ru is irregular octahedral with *cis* angles that range from 79.21(5)-97.46(6)° and *trans* angles that range from 168.66(6)-174.70(6)° (Table 3.14). The bridging chloride Cl(1) *trans* to terminal chlorides has a shorter Ru-Cl distance (2.3877(14)-2.4081(15) Å) compared to those of the bridging chloro ligands *trans* to sulfur (2.444(2)-2.4882(15) Å) (Table 3.13). This results from a weaker *trans* influence of the chloro ligands and produces a wider Ru-Cl(1)-Ru angle (84.69(5) and 85.01(5)°) compared to the other two Ru-Cl-Ru (81.25(5)-82.61(5)°). The range of the bridging angles and the Ru-Ru distance (3.2300(6) and 3.2321(6) Å) are outside those observed for a Ru-Ru bonded system (Section 3.7.1).

The crystallographic and ^1H NMR spectral data taken together suggest that $[\text{RuCl}(\text{BPSP})]_2(\mu\text{-Cl})_3$ is best formulated as a valence-delocalized class III system.

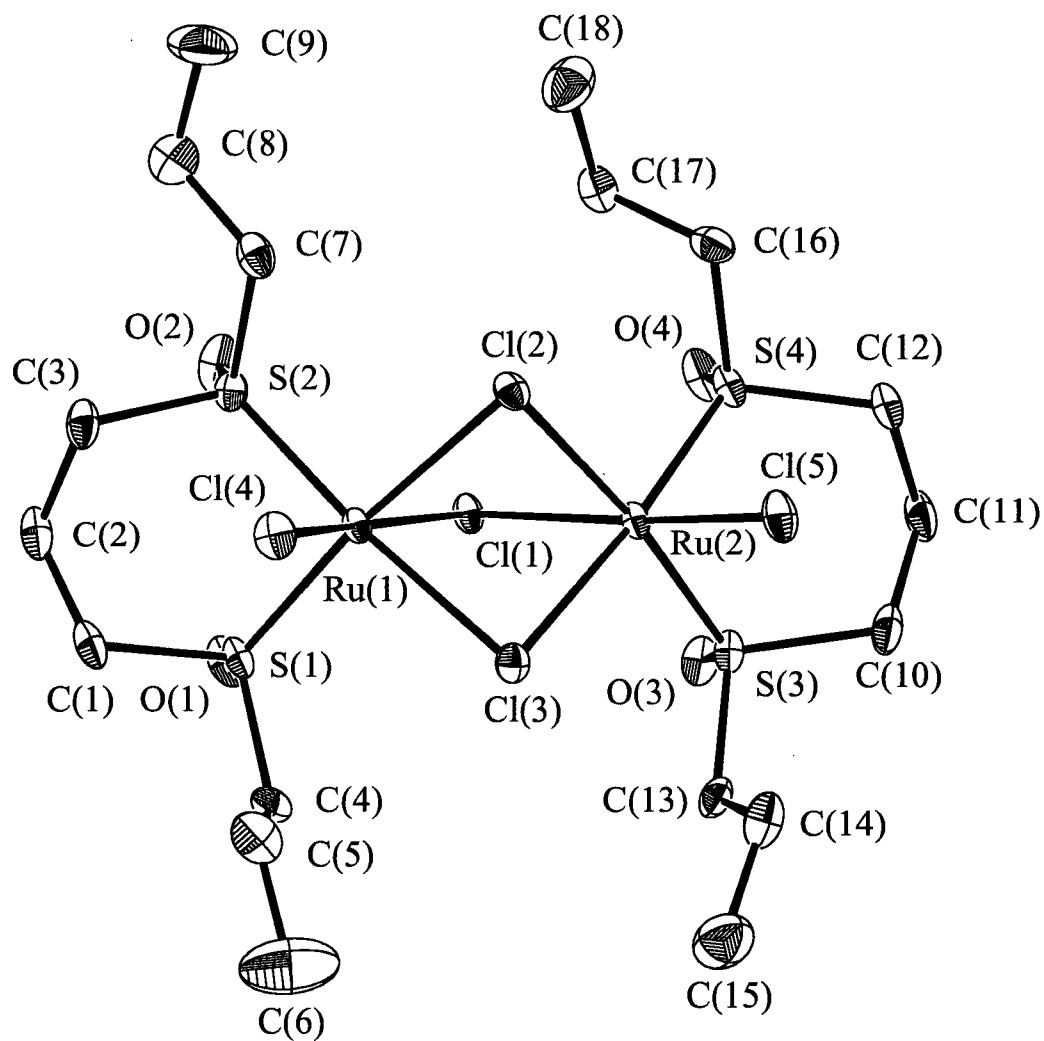


Figure 3.18. An ORTEP drawing of one of the $[\text{RuCl}(\text{BPSP})]_2(\mu\text{-Cl})_3$ units with 50 % probability thermal ellipsoids shown; H-atoms are omitted for clarity (crystal data given in Appendix 1.6).

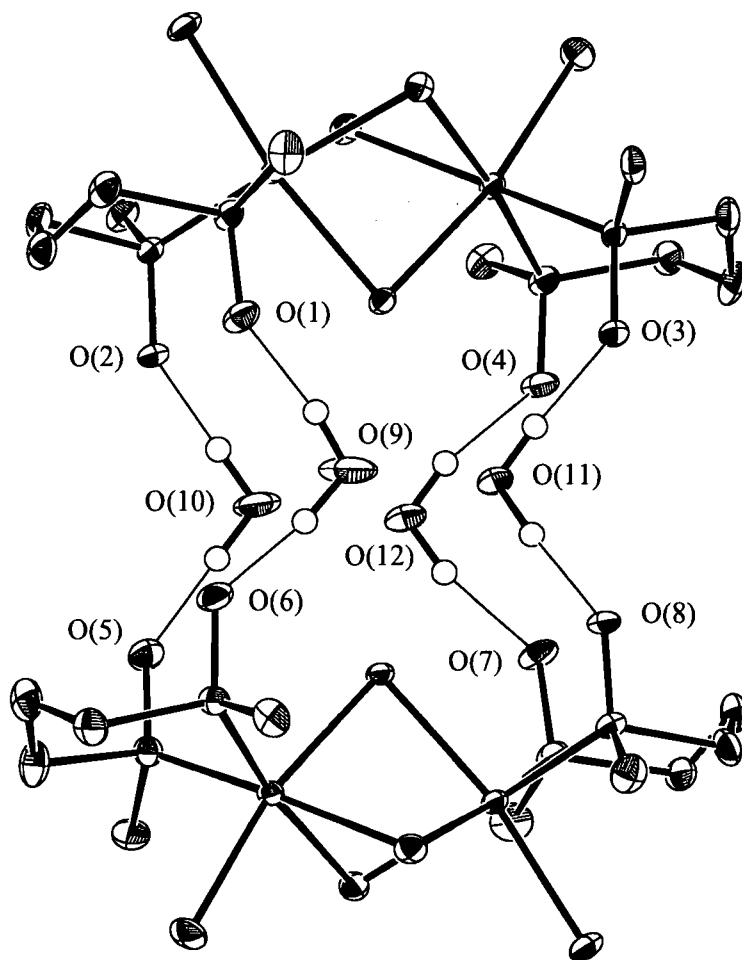


Figure 3.19. A diagram of $[\text{RuCl}(\text{BPSP})]_2(\mu\text{-Cl})_3$ showing short H-bonds connecting two asymmetric units via four H_2O molecules (the CH_2Cl_2 atoms are not shown) (crystal data given in Appendix 1.6).

Table 3.13. Selected Bond Lengths for the Two Asymmetric Units of $[\text{RuCl}(\text{BPSP})]_2(\mu\text{-Cl})_3$.

Bond	Length (Å)
Ru-Cl ^a	2.3877(14)-2.4081(15); ^b 2.444(2)-2.4882(15) ^c
Ru-Cl ^d	2.377(2)-2.3903(15)
Ru-S	2.204(2)-2.2093(15)
S-O	1.474(5)-1.501(4)
C-S	1.776(6)-1.809(6)

^a Bridging. ^b *Trans* to Cl. ^c *Trans* to S. ^d Terminal.

Table 3.14. Selected Bond Angles for the Two Asymmetric Units of $[\text{RuCl}(\text{BPSP})]_2(\mu\text{-Cl})_3$.

Bond angle	Angle (°)	Bond angle	Angle (°)
<i>cis</i> angles	79.21(5)-97.46(6)	Ru-S-O	117.1(2)-119.7(2)
<i>trans</i> angles	168.66(6)-174.70(6)	S-C-C ^a	109.5(4)-112.8(5)
Ru-Cl-Ru	81.25(5)-82.61(5) ^c 84.69(5) and 85.01(5) ^d	S-C-C ^b	110.7(4)-117.6(5)
C-S-C	100.3(3)-102.3(3)	Ru-S-C ^a	110.6(2)-112.7(2)
O-S-C	104.2(3)-107.0(3)	Ru-S-C ^b	111.3(2)-115.8(2)

^a Backbone. ^b End substituents. ^c *Trans* to sulfur. ^d *Trans* to chloride.

Crystals of the complex were found to contain 2 H₂O and 2.5 CH₂Cl₂ solvate molecules per molecule. The range of the H-O distances (H-atoms of the water molecules and the O-atoms of the sulfoxides) is 1.61-1.76 Å, which is 0.94-1.09 Å shorter than the sum

of the van der Waals radii of an H- and an O-atom (2.70 Å) (Figure 3.19).⁷⁰ This suggests a strong interaction between the solvate water molecules and the two asymmetric units. The range of the H-Cl distances (H-atoms of the sulfoxides and the Cl-atoms of CH₂Cl₂) is 2.77-2.93 Å (not illustrated), the average being shorter than the sum of the van der Waals radii of an H- and a Cl-atom (2.90 Å),⁷⁰ thus implying relatively weak interactions between the CH₂Cl₂ solvates and the complex. The chiralities at the S-atoms on each of the BPSP ligands are *R* and *S*, respectively (Table 3.8).

Of interest, during the preparation of this thesis, Geremia *et al.* reported a structure consisting of parallel layers of [Cu(BPSP)₂(ClO₄)]_{*n*}⁺ cations intercalated by *n*[ClO₄]⁻ anions with the O-atoms of BPSP acting as a bridge linking the Cu atoms.¹⁰³

3.8.3 Chemical Behaviour of [RuCl(BPSP)]₂(μ-Cl)₃ in Aqueous Solutions

In view of the potential biological interest of the water-soluble Ru(II)/Ru(III) complex [RuCl(BPSP)]₂(μ-Cl)₃, its chemical behaviour in aqueous solutions was studied. The proposed mechanism for the chemical behaviour in aqueous solution is summarized in Figure 3.20, with supporting data being given subsequently (the experimental details are given in Appendix 2).

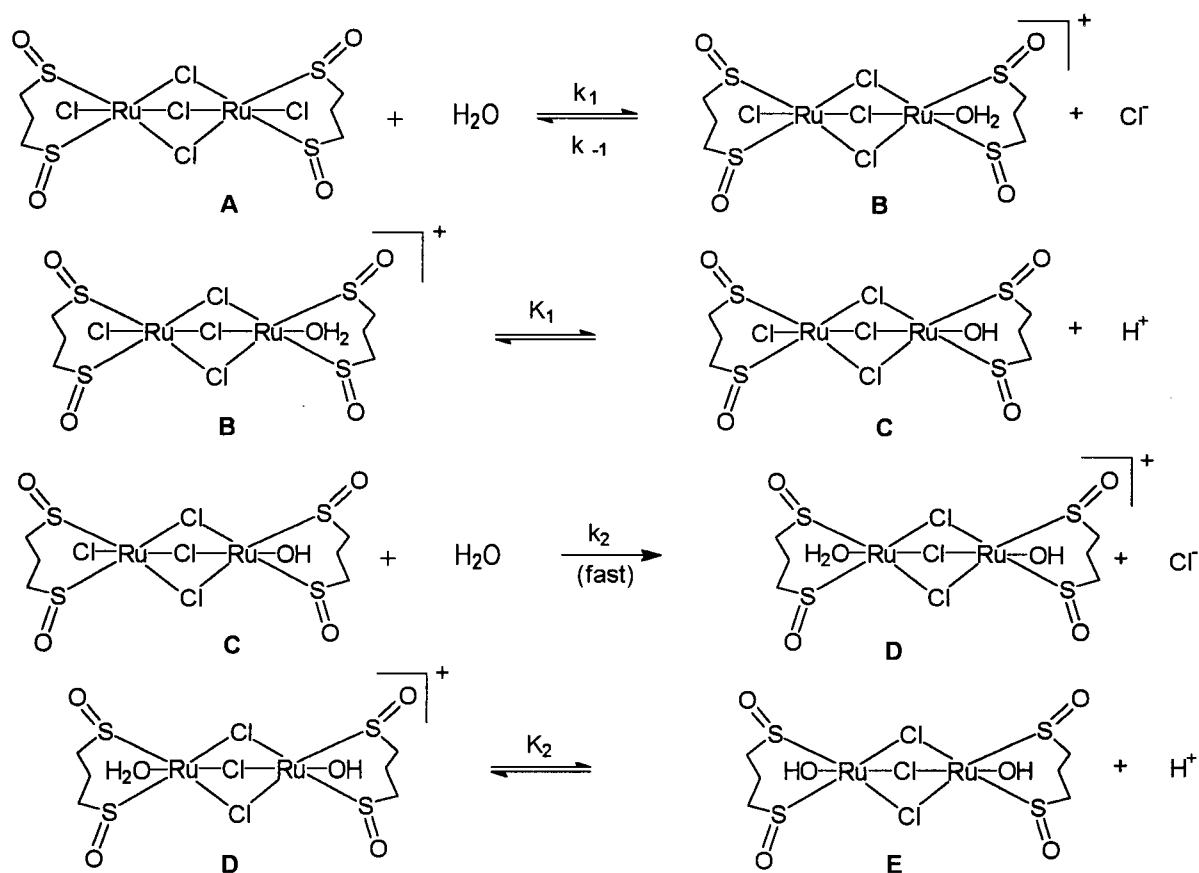


Figure 3.20. Proposed mechanism for the behaviour of $[\text{RuCl}(\text{BPSP})]_2(\mu\text{-Cl})_3$ in aqueous solution; the two Ru(II)/Ru(III) centres are not distinguished crystallographically, and loss of the chlorides is assumed to be from the terminal positions (the propyl groups of BPSP are omitted for clarity).

The equilibrium ^1H NMR spectrum of the complex in D_2O (under air) does not change upon addition of up to three equivalents of AgNO_3 . Upon addition of two equivalents of AgNO_3 , added dropwise, to a solution of $[\text{RuCl}(\text{BPSP})]_2(\mu\text{-Cl})_3$ in D_2O , a precipitate formed immediately, but the resulting ^1H NMR spectrum of the heterogeneous mixture was the same as that of the equilibrium spectrum of $[\text{RuCl}(\text{BPSP})]_2(\mu\text{-Cl})_3$ in D_2O (Figure 3.21), suggesting that the two terminal chlorides dissociate in D_2O . The D_2O solution containing the AgCl precipitate was then filtered and one more equivalent of AgNO_3 was added dropwise to

the filtrate. No further precipitate was observed, and the resulting ^1H NMR (Figure 3.21B) was identical to that in Figure 3.21A.

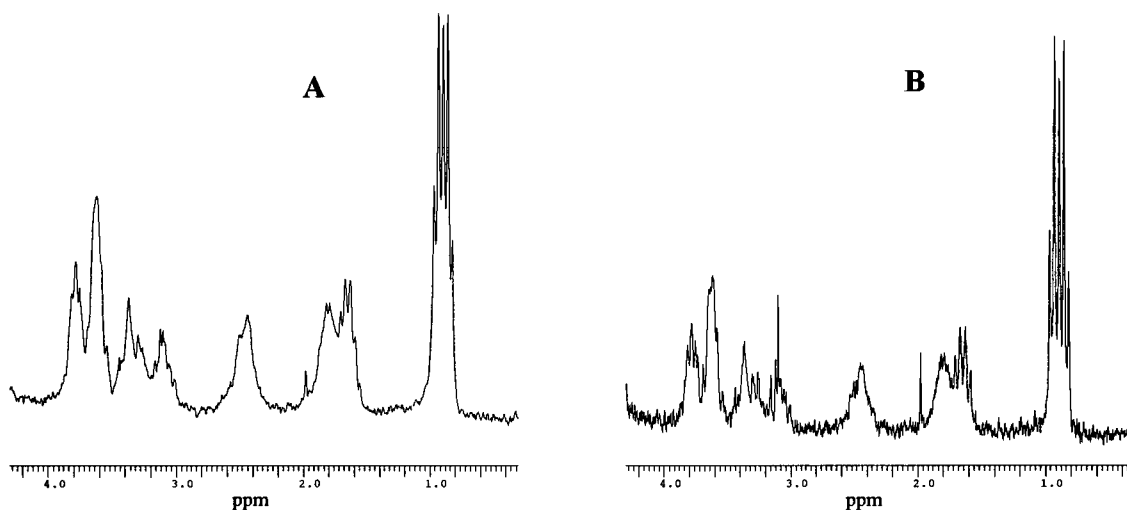


Figure 3.21. ^1H NMR spectra of equilibrated $[\text{RuCl}(\text{BPSP})]_2(\mu\text{-Cl})_3$ in D_2O (after 2 h) (A) and immediate spectrum of $[\text{RuCl}(\text{BPSP})]_2(\mu\text{-Cl})_3$ (2.02×10^{-3} M) after addition of two or three equivalents of AgNO_3 in D_2O (B).

A titration of $[\text{RuCl}(\text{BPSP})]_2(\mu\text{-Cl})_3$ with NaOH in water showed that two equivalents of a standardized NaOH solution were required to titrate 1 equivalent of $[\text{RuCl}(\text{BPSP})]_2(\mu\text{-Cl})_3$ (see Table 3.15), suggesting the loss of 2 equivalents of H^+ from $[\text{RuCl}(\text{BPSP})]_2(\mu\text{-Cl})_3$.

Table 3.15. Titration data for $[\text{RuCl}(\text{BPSP})]_2(\mu\text{-Cl})_3$ using NaOH .

$[\text{NaOH}]$ (mM)	Volume used (mL, mmol)	$[\text{RuCl}(\text{BPSP})]_2(\mu\text{-Cl})_3$ (mg, mmole)
$2.23 (\pm 0.09)$	$3.32 (\pm 0.13), 7.5 (\pm 0.3) \times 10^{-3}$	$3.10 (\pm 0.05), 3.74 (\pm 0.06) \times 10^{-3}$

^1H NMR studies and pH measurements in H_2O are consistent with the loss of two H^+ and two Cl^- ions on dissolution of $[\text{RuCl}(\text{BPSP})]_2(\mu\text{-Cl})_3$ in H_2O while conductivity measurements are somewhat inconclusive (p. 110).

$[\text{RuCl}(\text{BPSP})]_2(\mu\text{-Cl})_3$ is yellow-orange in solution; in CH_3CN no conductivity was observed and the spectrum was time invariant, with absorption maxima at 286, 324 and 424 nm, while dissolution in H_2O leads to a final product (≥ 20 min) with absorption maxima at 282, 318 and 450 nm, the colour then remaining yellow-orange and invariant with time. An example of the spectral changes observed for $[\text{RuCl}(\text{BPSP})]_2(\mu\text{-Cl})_3$ in aqueous solution is shown in Figure 3.22 (the initial spectrum was recorded 30 s after dissolution of the sample). The aqueous solution system was well-behaved in that isosbestic points at λ 268, 336 and 396 nm were observed as the UV-Vis spectrum changed with time (Figure 3.22). Absorbance changes were then monitored as a function of time at $\lambda = 362$ nm (Figure 3.23). An example of a pseudo-first-order rate plot is shown in Figure 3.24 and the pseudo-first-order rate constants, k_{obs} , obtained were found to be directly dependent on the concentration of H_2O from 22.2–55.6 M (in mixtures of $\text{H}_2\text{O}/\text{CH}_3\text{CN}$, Table 3.16, Figure 3.25). For reactions run in 0.25 M aqueous NaCl, 0.1 M aqueous toluene-4-sulfonic acid, and under N_2 , the measured k_{obs} values were 5.34×10^{-3} , $5.22 \times 10^{-3} \text{ s}^{-1}$ and 5.33×10^{-3} respectively (Table 3.16 and Figure 3.25); the data reveal an independence of the reaction on added $[\text{Cl}^-]$, $[\text{H}^+]$ and show that the solutions are not air-sensitive.

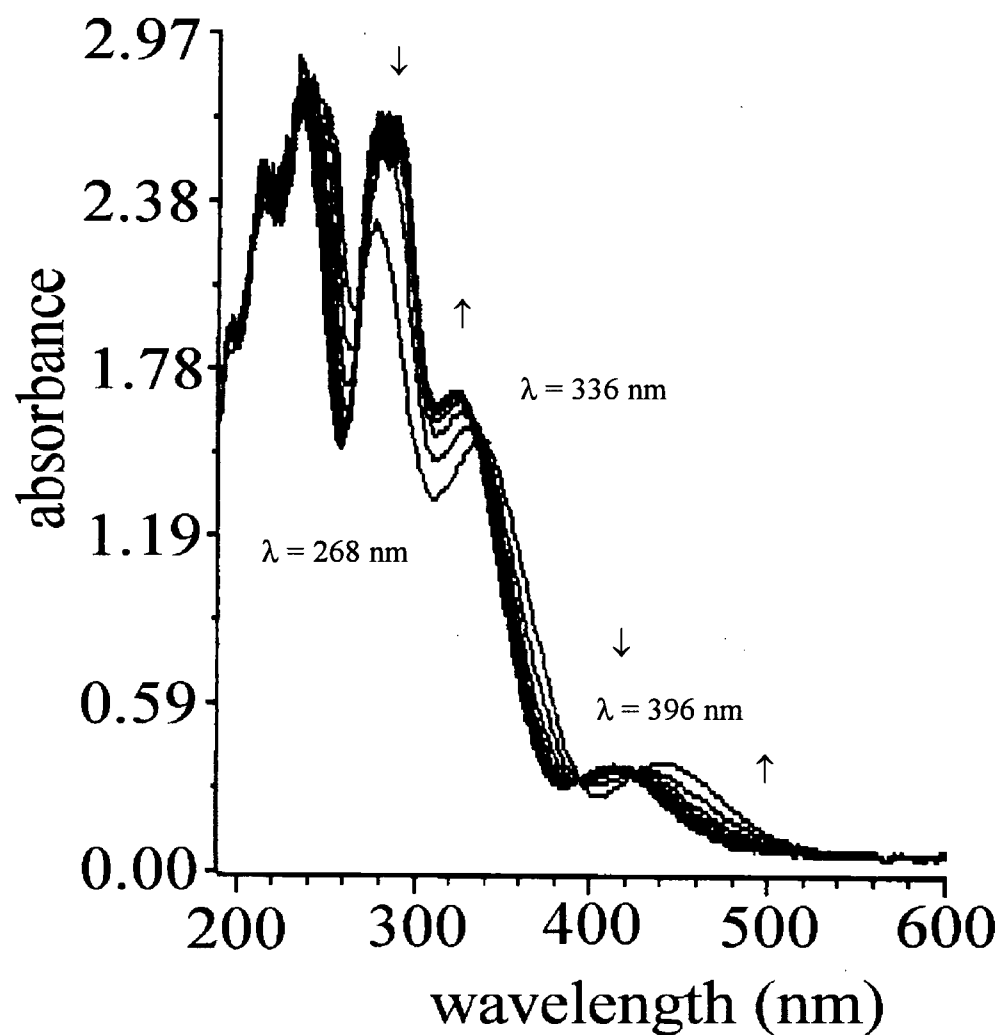


Figure 3.22. A representative spectrum of the UV-Vis spectral changes (200-600 nm region, 1 cm cell) of $[\text{RuCl}(\text{BPSP})]_2(\mu\text{-Cl})_3$ (2.96×10^{-4} M) in an aqueous solution at 27 °C as a function of time (half life $t_{1/2} = 120$ s, for the pseudo-first order process, see Figure 3.24); isosbestic points are observed at the noted wavelengths.

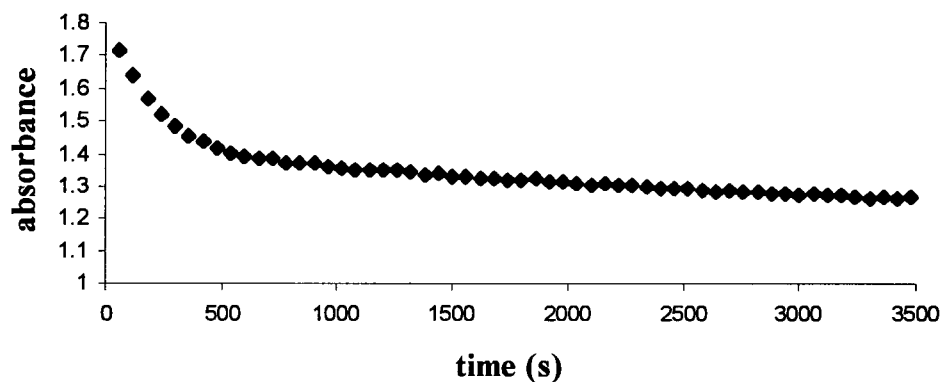


Figure 3.23. Absorption spectral changes at $\lambda = 362$ nm as a function of time for the reaction of $[\text{RuCl}(\text{BPSP})]_2(\mu\text{-Cl})_3$ in H_2O (55.6 M) at 27°C .

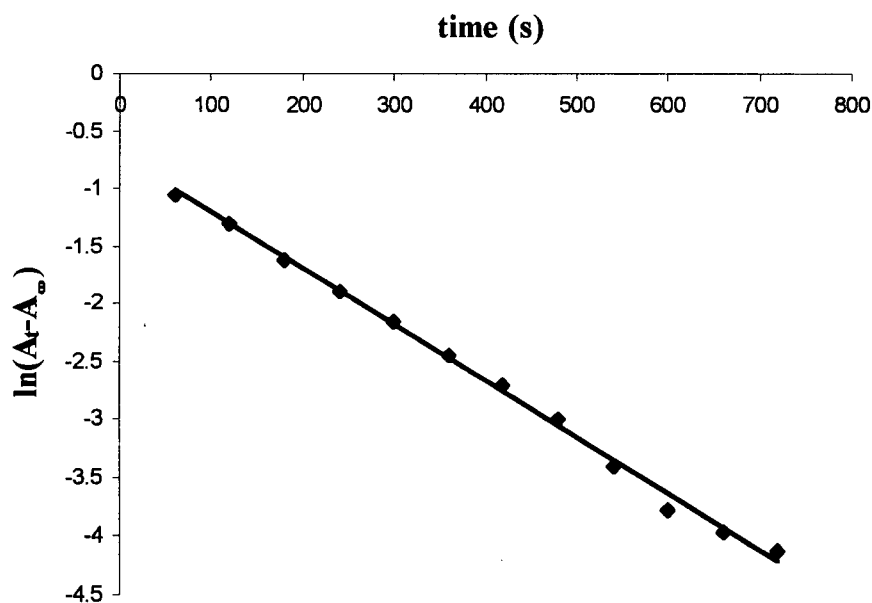


Figure 3.24. A representative rate-plot analyzed for a first-order dependence on $[\text{RuCl}(\text{BPSP})]_2(\mu\text{-Cl})_3$; A_t and A_∞ represent the absorbance at 362 nm at times t and ∞ , respectively, at 27°C .

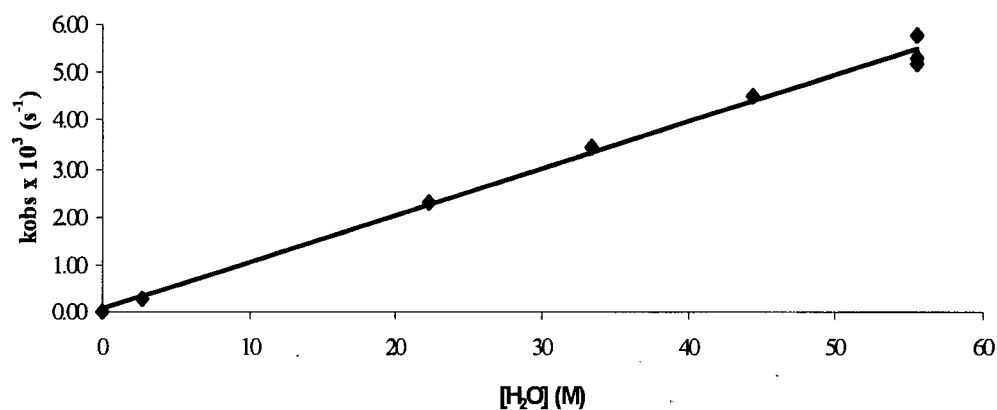


Figure 3.25. The dependence of the pseudo-first-order rate constant, k_{obs} , on $[\text{H}_2\text{O}]$ at 27 °C; including the k_{obs} values obtained from reactions run in 0.25 M aqueous NaCl and 0.1 M aqueous toluene-4-sulfonic acid (in $\text{H}_2\text{O}/\text{CH}_3\text{CN}$ solutions, see Table 3.16).

As the reaction rate is independent of added chloride and added protons, the rate-law for the stepwise process outlined in Figure 3.20 (p. 117) becomes simply $k_1[\text{A}][\text{H}_2\text{O}]$: the independence on $[\text{Cl}^-]$ implies k_{-1} is negligible, while the independence on $[\text{H}^+]$ implies that K_1 and K_2 are sufficiently large that variation of the $[\text{H}^+]$ during any single kinetic run does not change the concentration of any kinetically significant species, in this case **C** and **D**. Of note, $[\text{Cl}^-]$ and $[\text{H}^+]$ production should also be governed kinetically by k_1 .

Under pseudo first-order conditions, with excess H_2O , the rate = $k_{\text{obs}}[\text{A}]$ where $k_{\text{obs}} = k_1[\text{H}_2\text{O}]$; the second-order rate-constant k_1 was determined from Figure 3.25 to be $9.82 \times 10^{-5} \text{ M}^{-1} \text{ s}^{-1}$ at 27 °C, and was essentially independent of the concentration of $[\text{RuCl}(\text{BPSP})_2(\mu\text{-Cl})_3]$ from $(1.48\text{-}14.8) \times 10^{-4} \text{ M}$ (Figure 3.26).

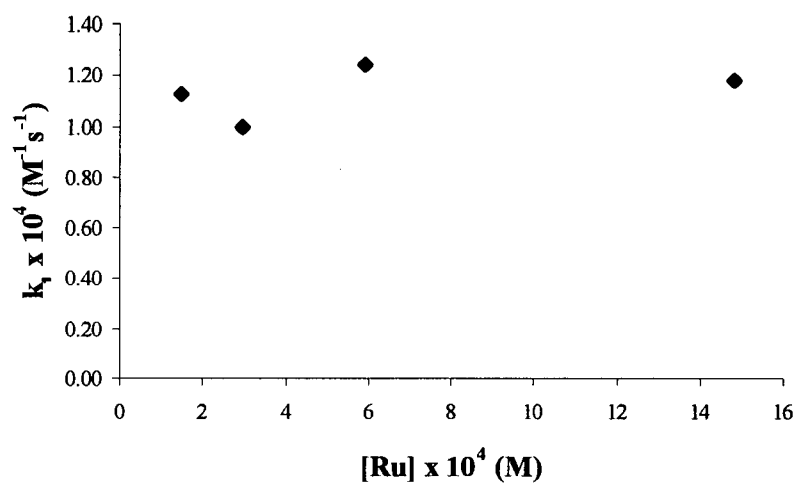


Figure 3.26. The dependence of the second-order rate constant k_1 on $[\text{RuCl(BPSP)}]_2[(\mu\text{-Cl})_3]$ in H_2O (22.2 M) at 27 °C. ($\text{Ru} = [\text{RuCl(BPSP)}]_2(\mu\text{-Cl})_3$).

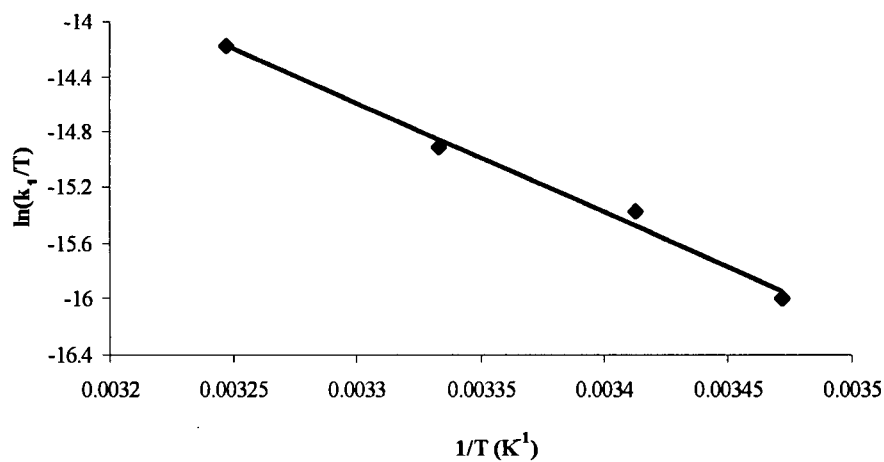


Figure 3.27. Eyring plot for the temperature dependence of the rate constant k_1 for the reaction of $[\text{RuCl(BPSP)}]_2(\mu\text{-Cl})_3$ (2.96×10^{-4} M) with H_2O (22.2 M).

The temperature dependence data for k_1 were obtained at a single concentration of $[\text{RuCl}(\text{BPSP})]_2(\mu\text{-Cl})_3$, 2.96×10^{-4} M, with 22.2 M H_2O in acetonitrile (3:2 V/V). An Eyring plot (Figure 3.27) of the data from 15–35 °C (Table 3.16) gave a straight line from which the activation parameters $\Delta H^\ddagger = 65 \pm 7 \text{ kJ mol}^{-1}$ and $\Delta S^\ddagger = -105 \pm 21 \text{ J mol}^{-1}\text{K}^{-1}$ were determined. These data, taken together with the second-order rate-law, are consistent with an associative process for the k_1 step.

Of note, Alessio *et al.* have studied the chemical behaviour of $\text{Na}[\text{trans-RuCl}_4(\text{DMSO})_2]$ and *mer*- $\text{RuCl}_3(\text{DMSO})_2(\text{DMSO})$ in aqueous solution (Section 1.4.2).²⁵ These two complexes turned greenish grey in a few hours at 25 °C and the authors attributed this, and a noted pH drop of the solutions, to the formation of polymeric Ru(III) species probably with hydroxo or μ -oxo bridges.^{25,104} Chloride concentrations up to 0.3 M did not significantly influence the rates of these processes in solution, but a strong acid dependence was observed down to $\text{pH} < 3$.²⁵ At this stage, such polymer formation from the mixed-valence Ru(II)/Ru(III) system seem unlikely. Attempts to isolate the product from an aqueous solution were unsuccessful; only an oily residue was obtained.

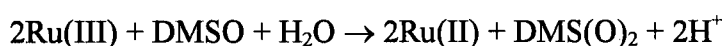
Table 3.16. Kinetic Data for the Hydration Reaction of $[\text{RuCl}(\text{BPSP})]_2(\mu\text{-Cl})_3$ in H_2O .^a

$[[\text{RuCl}(\text{BPSP})]_2(\mu\text{-Cl})_3]$ (M)	$[\text{H}_2\text{O}]$ (M)	T (°C)	k_{obs} (s^{-1})	k_1 ($\text{M}^{-1}\text{s}^{-1}$)
2.96×10^{-4}	55.6	27	5.82×10^{-3}	1.05×10^{-4}
2.96×10^{-4}	44.4	27	4.54×10^{-3}	1.02×10^{-4}
2.96×10^{-4}	33.3	27	3.46×10^{-3}	1.04×10^{-4}
2.96×10^{-4}	2.8	27	2.94×10^{-4}	1.05×10^{-4}
2.96×10^{-4}	22.2	27	2.30×10^{-3}	1.04×10^{-4}
2.96×10^{-4}	22.2	35	4.78×10^{-3}	2.15×10^{-4}
2.96×10^{-4}	22.2	27	2.22×10^{-3}	1.00×10^{-4}
2.96×10^{-4}	22.2	20	1.37×10^{-3}	6.17×10^{-5}
2.96×10^{-4}	22.2	15	7.20×10^{-4}	3.24×10^{-5}
5.92×10^{-4}	22.2	27	2.75×10^{-3}	1.24×10^{-4}
1.48×10^{-4}	22.2	27	2.51×10^{-3}	1.13×10^{-4}
1.48×10^{-3}	22.2	27	2.62×10^{-3}	1.18×10^{-4}
2.96×10^{-4}	55.6 [0.05-0.25M Cl^-]	27	5.34-5.62 \times 10^{-3}	0.96-1.01 \times 10^{-4}
2.96×10^{-4}	55.6 [0.1 M H^+]	27	5.22×10^{-3}	9.39×10^{-5}
2.96×10^{-4}	55.6 (under N_2)	27	5.33×10^{-3}	9.59×10^{-5}

^a In mixtures of $\text{H}_2\text{O}/\text{CH}_3\text{CN}$.

3.9 Dithioether Complexes of Ru

Previous workers in this laboratory have isolated $\text{RuX}_3(\text{thioether})_3$ complexes (thioether = DMS or TMS; X = Cl or Br) from reactions of $\text{RuCl}_3 \cdot 3\text{H}_2\text{O}$ with acidified DMSO or TMSO.^{35a,37} The reported synthetic procedures for these complexes were similar to those which gave the anionic complexes^{25,37,105} with protonated DMSO and TMSO as associated cations, *trans*- $[(\text{DMSO})_2\text{H}]^+[\text{RuCl}_4(\text{DMSO})_2]^-$ and *trans*- $[(\text{TMSO})\text{H}]^+[\text{RuCl}_4(\text{TMSO})_2]^-$, respectively, except that a higher reaction temperature was used (130-140 vs. 70-80 °C); formation of the thioether was attributed to redox processes involving Ru(III) and the sulfoxide.^{35a,37} Commercially available $\text{RuCl}_3 \cdot 3\text{H}_2\text{O}$ analyzes well for such a composition, but actually consists of a mixture of Ru(III) and Ru(IV) species of which the latter is thought to be a hydroxo species.^{106,107} Of note, Lipponer *et al.* have recently described three methods of purifying $\text{RuCl}_3 \cdot 3\text{H}_2\text{O}$ to yield solutions of pure Ru(III).¹⁰⁸ The exact mechanistic steps leading to the reduction of the sulfoxide are not known, but there is some evidence to indicate that the following reactions may play a role:



The reduction of Ru(III) to Ru(II) with accompanying oxidation of DMSO to the sulfone was initially suggested by Ledlie *et al.*,¹⁰⁹ and the Trieste group subsequently detected the presence of dimethyl sulfone (in a stoichiometric amount) in the reduction of *mer*- $\text{RuCl}_3(\text{DMSO})_3$ (in DMSO under Ar) to *trans*- $\text{RuCl}_2(\text{DMSO})_4$.²⁵ Evidence for the second equilibrium (R = Bu) was reported by Ledlie *et al.* and under highly acidic conditions the reaction is likely pushed to

the right-hand side generating the Ru(III)-thioether.¹⁰⁹ The ligand sets on Ru during this process, however, remain undefined, and more studies are required before the mechanistic steps in this new route to thioether complexes are more fully understood.

3.9.1 Literature Data

As discussed in Section 3.6, reactions of disulfoxides with Ru precursors gave mainly $\text{RuCl}_2(\text{disulfoxide})_2$ complexes of a preferred *cis*- or *trans*-geometry regardless of the nature of the precursor. The goal of synthesizing $\text{RuCl}_2(\text{dithioether})_2$ complexes was to determine the *cis*- or *trans*-geometry, and then oxidize the coordinated dithioethers to the disulfoxides to determine if the geometry was retained.

Chatt *et al.* reported that $\text{RuCl}_3 \cdot 3\text{H}_2\text{O}$ reacted with mono-(S), di-(SS), or tri-organic sulfides (SSS) to give complexes with the formulations *mer*- $[\text{RuCl}_3\text{S}_3]$, $[\{\text{RuCl}_3(\text{SS})_{1.5}\}_n]$ and *trans*- $[\text{RuX}_2(\text{SS})_2]$ ($\text{X} = \text{Cl}$ or Br), or $[\text{RuCl}_3(\text{SSS})]$, respectively.¹¹⁰ The authors state that in the series of $[\{\text{RuCl}_3(\text{RSCH}_2\text{CH}_2\text{SR})_{1.5}\}_n]$ complexes ($\text{R} = \text{Me}$, Et , Pr or Ph); ‘these complexes are at least dinuclear although they are too insoluble for molecular weight determination’ and it is ‘likely that one sulfide molecule is chelating and one bridging’.¹¹⁰ The authors also reported the isolation of $\text{RuCl}_2(\text{RSCH}_2\text{CH}_2\text{SR})_2$ species ($\text{R} = \text{Ph}$) during attempts to isolate Ru(III) complexes and suggested that $\text{RSCH}_2\text{CH}_2\text{SR}$ ($\text{R} = \text{Ph}$) is more strongly reducing than the thioethers with $\text{R} = \text{Me}$, Et or Pr ; *trans* geometry was suggested based on IR data.¹¹⁰

Within related complexes, Lucas *et al.* have reported on the Pt or Pd complexes $\text{MX}_2\cdot\text{BBTE}$ ($\text{M} = \text{Pd}$ and $\text{X} = \text{Cl}$ or I , and $\text{M} = \text{Pt}$ and $\text{X} = \text{Cl}$ with $\text{BBTE} = 1,2$ -bis(benzylthio)ethane).¹¹¹ Hartley *et al.* have reported on the Pd or Pt complexes *cis*- $[\text{MLX}_2]$ and $[\text{ML}_2](\text{ClO}_4)_2$ ($\text{X} = \text{Cl}$, Br or I ; $\text{L} = (\text{a}) \text{RS}(\text{CH}_2)_n\text{SR}$, $\text{R} = \text{Me}$ or Ph , and $n = 2$ or 3 ; (b) *cis*- $\text{RSCH}=\text{CHSR}$, $\text{R} = \text{Me}$, Ph or $o\text{-C}_6\text{H}_4(\text{SR}')_2$ ($\text{R}' = \text{Me}$ or Ph). With $\text{L} = \text{PhS}(\text{CH}_2)_n\text{SPh}$, $n = 6$ or 8 , polymeric $[\text{PdLX}_2]_n$ species were obtained, while with $n = 12$ *trans*- PdLX_2 ($\text{X} = \text{Cl}$ or Br) and *trans*- PtLCl_2 were formed.¹¹² The complexes $[\text{M}(\text{MeSCH}_2\text{SMe})\text{X}_2]$ ($\text{M} = \text{Pd}$ or Pt ; $\text{X} = \text{Cl}$, Br or I), $[\text{Rh}(\text{PhSCH}_2\text{SPh})_3\text{Cl}_3]$, $[\text{Ir}(\text{PhSCH}_2\text{SPh})_3\text{Cl}_3]$ and $\text{Ru}(\text{PhSCH}_2\text{SPh})_2\text{Cl}_3\cdot\text{EtOH}$ have also been reported.¹¹³ None of the above was characterized structurally. Song *et al.* have structurally characterized the complex $\text{Rh}_2\text{Cl}_2(\text{CO})_2(\text{bis}(\text{ethylthio})\text{methane})_2$ ¹¹⁴ and Shao *et al.* have reported the use of $\text{RSCH}_2\text{CH}_2\text{SR}$ ($\text{R} = n\text{-C}_3\text{H}_7$, $n\text{-C}_5\text{H}_{11}$, $n\text{-C}_8\text{H}_{17}$ and Ph) as reagents used in the extraction of Ag .¹¹⁵

This thesis work reveals that reactions of BPhTE and BCyTE with $\text{RuCl}_3\cdot 3\text{H}_2\text{O}$ gave mononuclear *trans*- $\text{Ru}(\text{II})$ complexes (Section 3.9.2), whereas the longer chain dithioethers 3,7-dithianonane, 4,8-dithiaundecane, 5,9-dithiatridecane, and 6,10-dithiapentadecane gave the dinuclear $\text{Ru}_2(\text{III})$ complexes $[\text{RuCl}_2(\text{BETP})]_2(\mu\text{-Cl})_2$, $[\text{RuCl}_2(\text{BPTP})]_2(\mu\text{-Cl})_2$, $[\text{RuCl}_2(\text{BBTP})]_2(\mu\text{-Cl})_2$ and $[\text{RuCl}_2(\text{BPETP})]_2(\mu\text{-Cl})_2$ (Section 3.9.3), respectively.

Schenk *et al.* have reported that Ru-thioether complexes can be directly converted with dimethyldioxirane to the corresponding sulfoxide complexes; for example, $[\text{RuCp}(\text{chiraphos})(\text{SR/R}')]\text{PF}_6$ gave $[\text{RuCp}(\text{chiraphos})(\text{SOR/R}')]\text{PF}_6$ (Cp = cyclopentadienyl; R/R' = Me/Ph, Me/Pr, Me/Bz, Et/Bz or Me/Cy),¹¹⁶ and this led to the idea of such an alternative oxidation route to different geometrical isomers of the known disulfoxide Ru complexes. However, an initial attempt to oxidize *trans*- $\text{RuCl}_2(\text{BPhTE})_2$ using dimethyldioxirane was unsuccessful; no ν_{SO} was detected in an isolated crude product (Section 2.10.2). Of note, Schenk *et al.* noted that “conversions of the thioether to the sulfoxide drop sharply when both substituents at sulfur are sterically more demanding” (*e.g.* SR/R' = Et/Bz) and “using a large excess of dimethyldioxirane in this case leads to increased decomposition”.¹¹⁶

3.9.2 The Mononuclear Ru(II) Dithioether Complexes: *Trans*- $\text{RuCl}_2(\text{BCyTE})_2 \cdot 2\text{H}_2\text{O}$ and *Trans*- $\text{RuCl}_2(\text{BPhTE})_2$

Reaction of $\text{RuCl}_3 \cdot 3\text{H}_2\text{O}$ with BCyTE gave the complex *trans*- $\text{RuCl}_2(\text{BCyTE})_2$. Its ^1H NMR spectrum in CDCl_3 is a complicated pattern of broad peaks between δ 1.20–3.35 that could not be assigned by using ^{13}C , 2D-COSY and ^1H NMR decoupling experiments; the broad signals presumably result from the rotation of the cyclohexyl rings. An ORTEP of the complex is shown in Figure 3.28, and the unit cell showing 2 CH_2Cl_2 solvate molecules is shown in Figure 3.29. Selected bond lengths and angles are given in Table 3.17. No significant H-bonding interactions are evident with the solvate molecules. The Ru–Cl bond length in the centrosymmetric structure is 2.4262(6) Å, while the Ru–Cl bond lengths (*trans* to

S) for the disulfoxide complex $cis\text{-RuCl}_2(\text{BCySE})_2$ are 2.4201(13) and 2.4344(13) Å, indicating that the *trans* influence of the sulfoxide moiety is similar to that of Cl⁻. The Ru-S bond lengths of 2.3629(9) and 2.3646(9) Å for the dithioether complex and are longer than those for $cis\text{-RuCl}_2(\text{BCySE})_2$ (2.3364(13) and 2.3484(13) Å).

The isolation of $trans\text{-RuCl}_2(\text{BCyTE})_2$ implies that the suggestion by Chatt *et al.* that $\text{PhSCH}_2\text{CH}_2\text{SPh}$ is a more strongly reducing thioether is not valid in a general sense (Section 3.9.1).

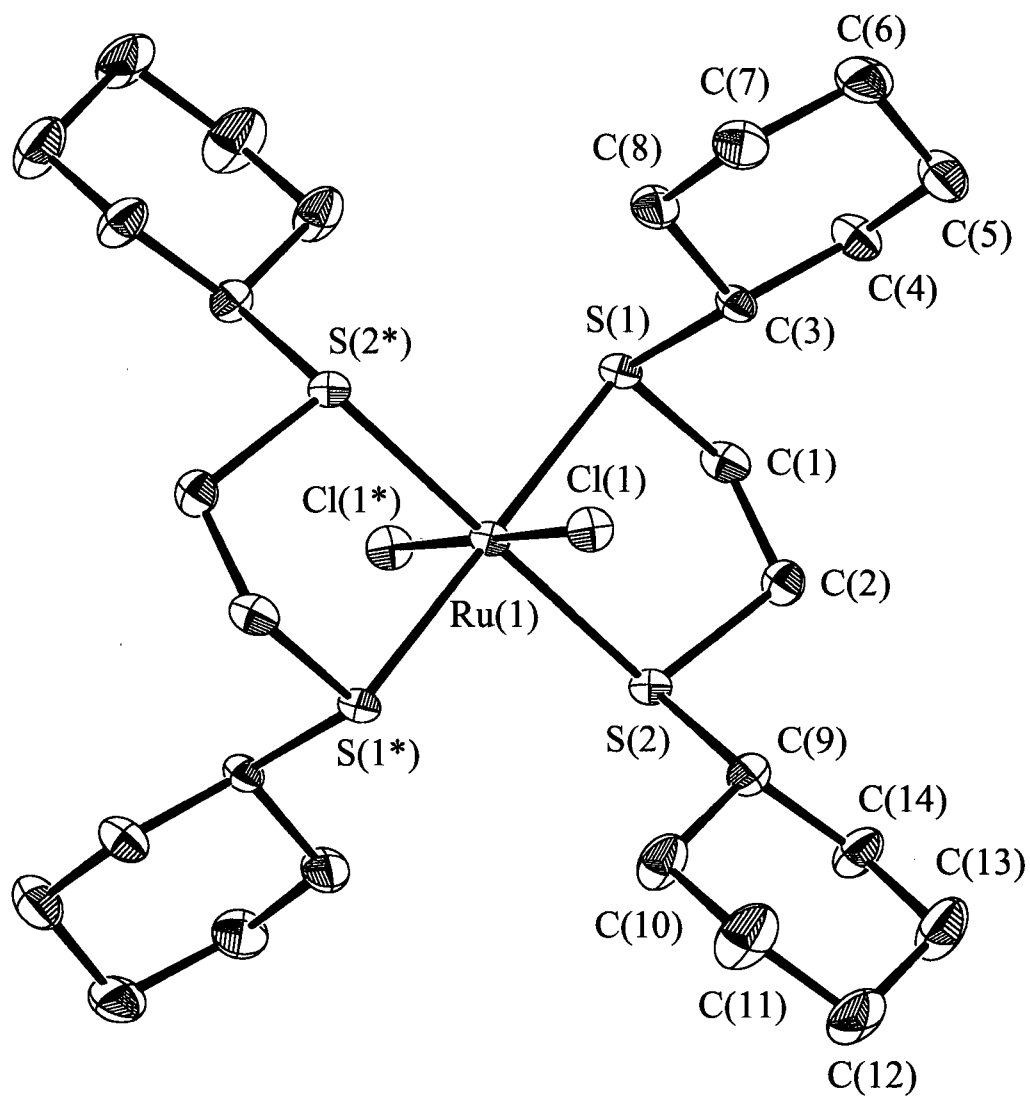


Figure 3.28. An ORTEP drawing of *trans*-RuCl₂(BCyTE)₂·2CH₂Cl₂ with 50 % probability shown; H-atoms are omitted for clarity (the CH₂Cl₂ molecules are not shown) (crystal data are given in Appendix 1.7).

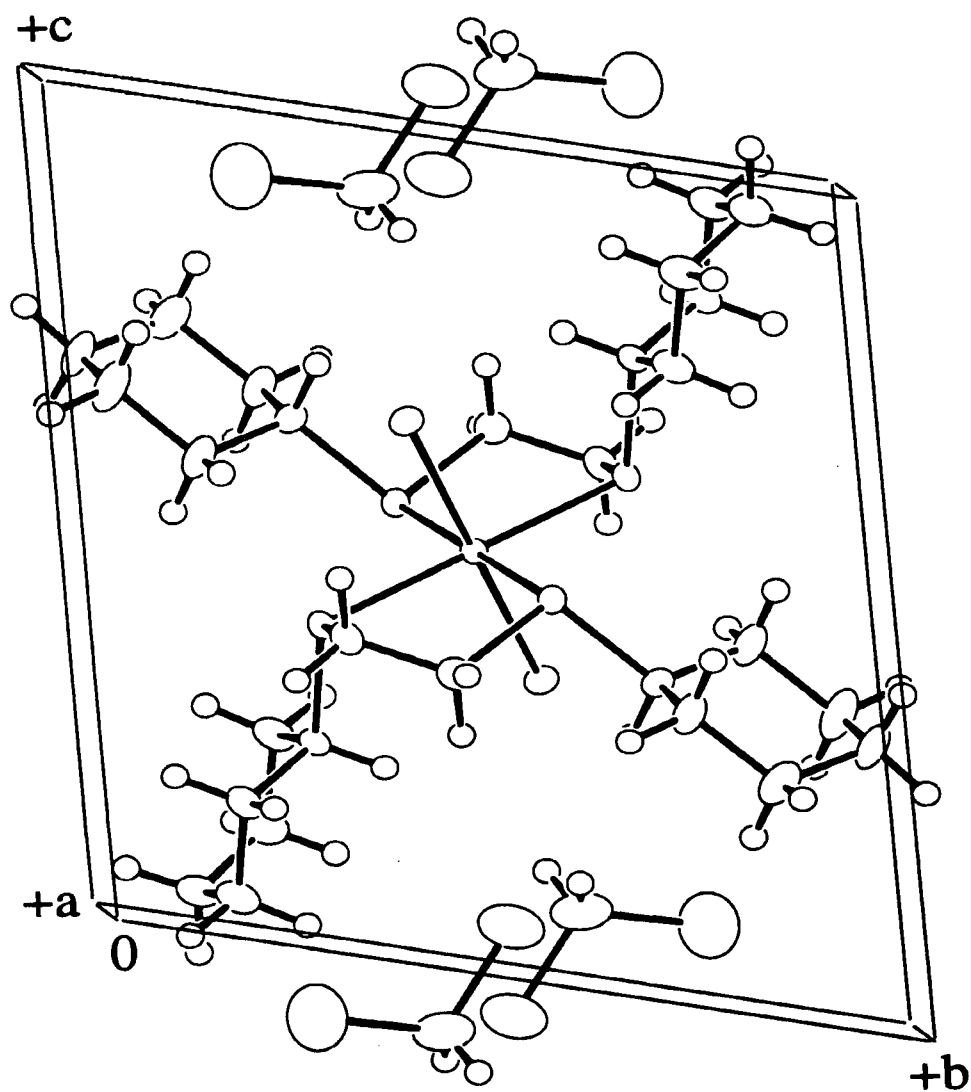


Figure 3.29. The unit cell of *trans*-RuCl₂(BCyTE)₂·2CH₂Cl₂ showing the 2 CH₂Cl₂ solvate molecules (crystal data given in Appendix 1.7).

Table 3.17. Selected Bond Lengths (Å) and Angles (°) for *trans*-RuCl₂(BCyTE)₂·2CH₂Cl₂ and *trans*-RuCl₂(BPhTE)₂.

Bond or angle	<i>trans</i> -RuCl ₂ (BCyTE) ₂ ·2CH ₂ Cl ₂	<i>trans</i> -RuCl ₂ (BPhTE) ₂
Ru-Cl	2.4262(6)	2.4244(8), 2.4266(8)
Ru-S	2.3629(6), 2.3646(7)	2.3424(7), 2.3594(8)
C-S	1.813(3)-1.840(3)	1.815(4)-1.836(4), ^a 1.777(3)-1.799(3) ^b
<i>cis</i> angles	84.14(2)-95.86(2)	83.65(3)-98.09(3)
<i>trans</i> angles	180.0	167.66(3)-178.13(4)
C-S-C	97.89(11), 104.30(11)	98.52(15)-102.22(15)
S-C-C ^a	110.4(2), 112.3(2)	106.8(2)-108.9(2)
S-C-C ^c	105.5(2)-112.6(2)	118.2(3)-124.3(3)
Ru-S-C ^a	101.76(9), 104.13(9)	102.61(11)-104.14(10)
Ru-S-C ^c	110.98(9), 117.26(9)	117.01(10)-120.96(11)

^a Backbone C-atoms. ^b Phenyl rings. ^c End substituents.

Reaction of RuCl₃·3H₂O and BPhTE gave the complex *trans*-RuCl₂(BPhTE)₂ (confirming the geometry of the complex previously suggested by Chatt *et al.*, Section 3.9.1). The ¹H NMR spectrum in CDCl₃ of the free ligand consists of a singlet at δ 3.10 assigned to the CH₂CH₂ backbone and a multiplet centred at δ 7.15 due to the phenyl protons; the ¹H signals for the aromatic protons of the coordinated dithioether are split into three signals at δ 7.65, 7.28 and 7.12 assigned to the *o*-, *p*- and *m*-protons, respectively. The assignments are based on the resonance structures of the phenyl ring with a thioether (Figure 3.30). These

resonance structures show that the S-atom removes electron density from the *o*- and *p*-positions and results in downfield shifts of these signals, while the protons at the *m*-positions are not affected directly.

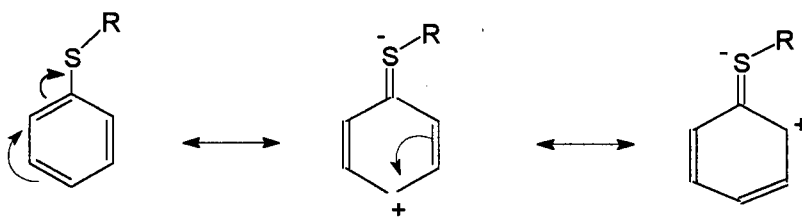


Figure 3.30. Resonance structures of a phenyl ring with a thioether.

The structure of the complex is shown in Figure 3.31, and selected bond lengths and angles are given in Table 3.17. The Ru-Cl bond lengths are 2.4244(8) and 2.4266(8) Å for this bis-chelating dithioether complex (Table 3.17).

No conductivity was observed for these *trans*-bis(dithioether) complexes in CH₂Cl₂ solution.

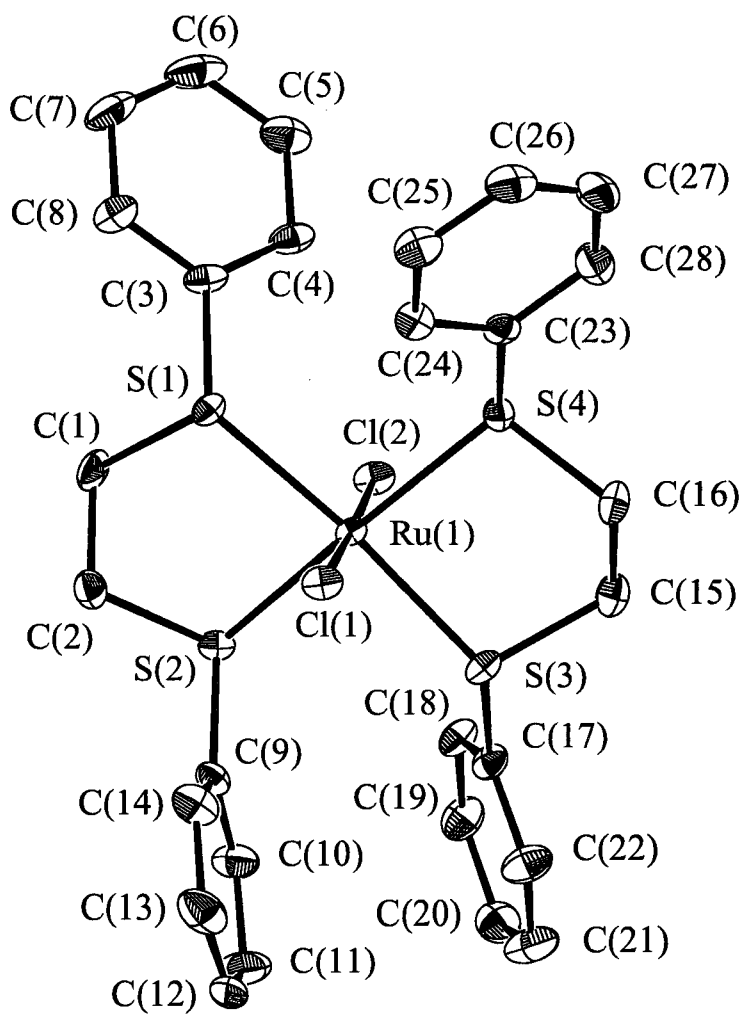


Figure 3.31. An ORTEP drawing of *trans*-RuCl₂(BPhTE)₂ with 50 % probability thermal ellipsoids shown; H-atoms are omitted for clarity (crystal data are given in Appendix 1.8).

3.9.3 Dinuclear Ru(III)/Ru(III) Dithioether Complexes: $[\text{RuCl}_2(\text{BETP})]_2(\mu\text{-Cl})_2$, $[\text{RuCl}_2(\text{BPTP})]_2(\mu\text{-Cl})_2$, $[\text{RuCl}_2(\text{BBTP})]_2(\mu\text{-Cl})_2$ and $[\text{RuCl}_2(\text{BPeTP})]_2(\mu\text{-Cl})_2$

Reactions of 3,7-dithianonane, 4,8-dithiaundecane, 5,9-dithiatridecane, and 6,10-dithiapentadecane with $\text{RuCl}_3 \cdot 3\text{H}_2\text{O}$ gave the dark purple-brown, dinuclear $\text{Ru}_2(\text{III})$ complexes $[\text{RuCl}_2(\text{BETP})]_2(\mu\text{-Cl})_2$, $[\text{RuCl}_2(\text{BPTP})]_2(\mu\text{-Cl})_2$, $[\text{RuCl}_2(\text{BBTP})]_2(\mu\text{-Cl})_2$ and $[\text{RuCl}_2(\text{BPeTP})]_2(\mu\text{-Cl})_2$, respectively, while crystals of $[\text{RuCl}_2(\text{BETP})]_2(\mu\text{-Cl})_2$ and $[\text{RuCl}_2(\text{BPTP})]_2(\mu\text{-Cl})_2$ suitable for X-ray analysis were obtained by slow evaporation of a solution of the respective complex in CH_2Cl_2 . Both complexes (Figures 3.32 and 3.33) have two bridging Cl-atoms, each Ru(III) centre also having two terminal Cl-atoms. The Ru-Cl bond lengths for the terminal Cl-atoms for $[\text{RuCl}_2(\text{BETP})]_2(\mu\text{-Cl})_2$ and $[\text{RuCl}_2(\text{BPTP})]_2(\mu\text{-Cl})_2$ are 2.3258(7) Å and 2.3213(9) Å (*trans* to Cl) and 2.3501(8) Å and 2.3579(10) Å (*trans* to S), respectively, (Table 3.18), suggesting a small *trans* influence of S (vs. Cl). The Ru-Cl bond lengths for the bridging Cl-atoms are 2.3915(7) Å and 2.4617(7) Å for $[\text{RuCl}_2(\text{BETP})]_2(\mu\text{-Cl})_2$, and 2.3833(9) Å and 2.4605(9) Å for $[\text{RuCl}_2(\text{BPTP})]_2(\mu\text{-Cl})_2$. The two Ru-S bond lengths are 2.3201(8) and 2.3677(8) Å for $[\text{RuCl}_2(\text{BETP})]_2(\mu\text{-Cl})_2$, and 2.3311(10) and 2.3564(11) Å for $[\text{RuCl}_2(\text{BPTP})]_2(\mu\text{-Cl})_2$. $[\text{RuCl}_2(\text{BETP})]_2(\mu\text{-Cl})_2$ and $[\text{RuCl}_2(\text{BPTP})]_2(\mu\text{-Cl})_2$ have bridging angles of 95.86(3)° and 97.02(3)°, respectively, and there are no Ru-Ru bonds (usually considered in the range 2.28-3.034 Å, see Section 3.7.1).

Elemental analyses of $[\text{RuCl}_2(\text{BBTP})]_2(\mu\text{-Cl})_2$ and $[\text{RuCl}_2(\text{BPeTP})]_2(\mu\text{-Cl})_2$ show a formulation consistent with the structurally characterized dinuclear, dichloro-bridged $\text{Ru}_2(\text{III})$ species described above. The solid-state magnetic susceptibilities of $[\text{RuCl}_2(\text{BETP})]_2(\mu\text{-Cl})_2$,

$[\text{RuCl}_2(\text{BPTP})]_2(\mu\text{-Cl})_2$, $[\text{RuCl}_2(\text{BBTP})]_2(\mu\text{-Cl})_2$ and $[\text{RuCl}_2(\text{BPeTP})]_2(\mu\text{-Cl})_2$ were $\mu_{\text{eff}} = 3.8$, 3.1, 3.2 and 3.4 ± 0.1 B. M., respectively, showing in 1 unpaired electron/Ru(III) center in each case, and are consistent with no interaction between the metal centres.

No conductivity was observed for these dimeric Ru(III)/Ru(III) complexes in CH_2Cl_2 solution. The complexes are insoluble in water.

Table 3.18. Selected Bond Lengths (Å) and Bond Angles (°) for $[\text{RuCl}_2(\text{BETP})]_2(\mu\text{-Cl})_2$ and $[\text{RuCl}_2(\text{BPTP})]_2(\mu\text{-Cl})_2$.

Bond or Angle	$[\text{RuCl}_2(\text{BETP})]_2(\mu\text{-Cl})_2$	$[\text{RuCl}_2(\text{BPTP})]_2(\mu\text{-Cl})_2$
Ru-Cl ^a	2.3258(7), ^b 2.3501(8) ^c	2.3213(9), ^b 2.3579(10) ^c
Ru-Cl ^d	2.3915(7), 2.4617(7)	2.3833(9), 2.4605(9)
Ru-S	2.3201(8), 2.3677(8)	2.3311(10), 2.3564(11)
C-S	1.808(3)-1.823(3)	1.806(4)-1.821(4)
<i>cis</i> angles	84.14(3)-96.74(3)	82.98(3)-97.50(3)
<i>trans</i> angles	172.05(3)-175.81(3)	173.32(4)-175.93(4)
C-S-C	99.78(15), 100.54(15)	99.0(2), 100.6(2)
S-C-C ^e	112.9(2), 117.3(2)	112.0(3), 117.5(3)
S-C-C ^f	110.7(2), 112.5(3)	111.3(3), 112.8(3)
Ru-S-C ^e	110.16(11), 111.62(11)	110.27(14), 112.80(14)
Ru-S-C ^f	107.85(11), 110.65(10)	109.73(13), 110.74(13)
Ru-Cl-Ru	95.86(3)	97.02(3)

^a Terminal Cl. ^b *Trans* to Cl. ^c *Trans* to S. ^d Bridging Cl. ^e Backbone C-atoms. ^f End substituents.

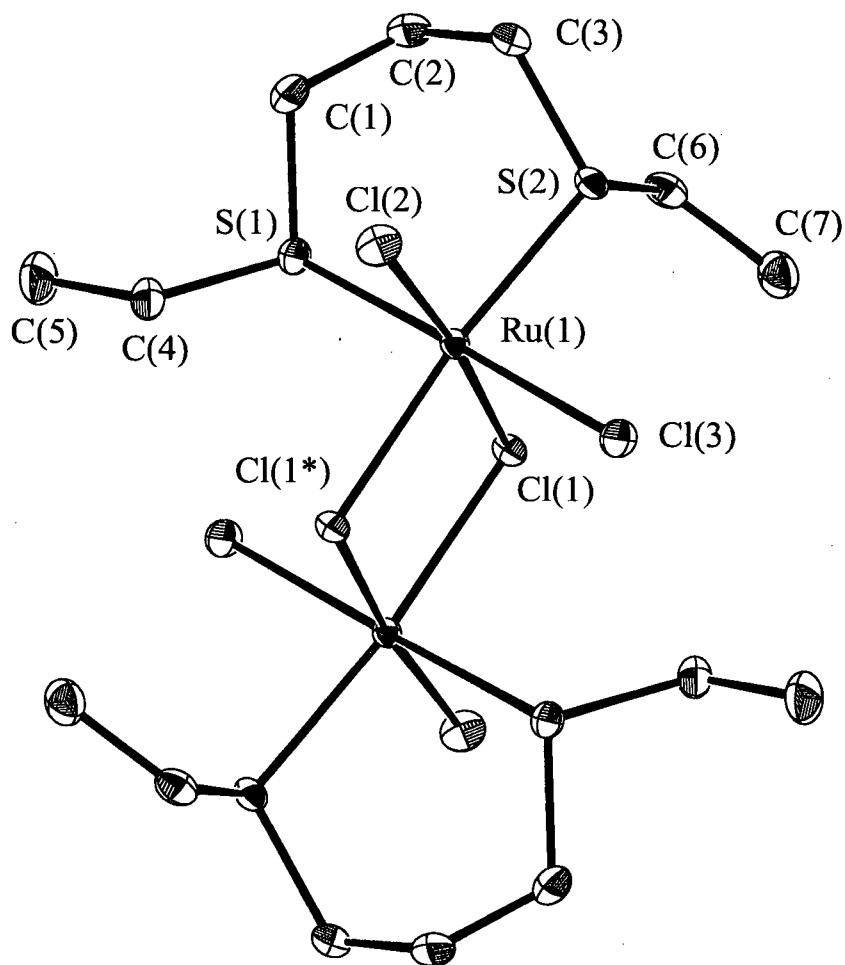


Figure 3.32. An ORTEP drawing of $[\text{RuCl}_2(\text{BETP})]_2(\mu\text{-Cl})_2$ with 50 % probability thermal ellipsoids shown; H-atoms are omitted for clarity (crystal data are given in Appendix 1.9).

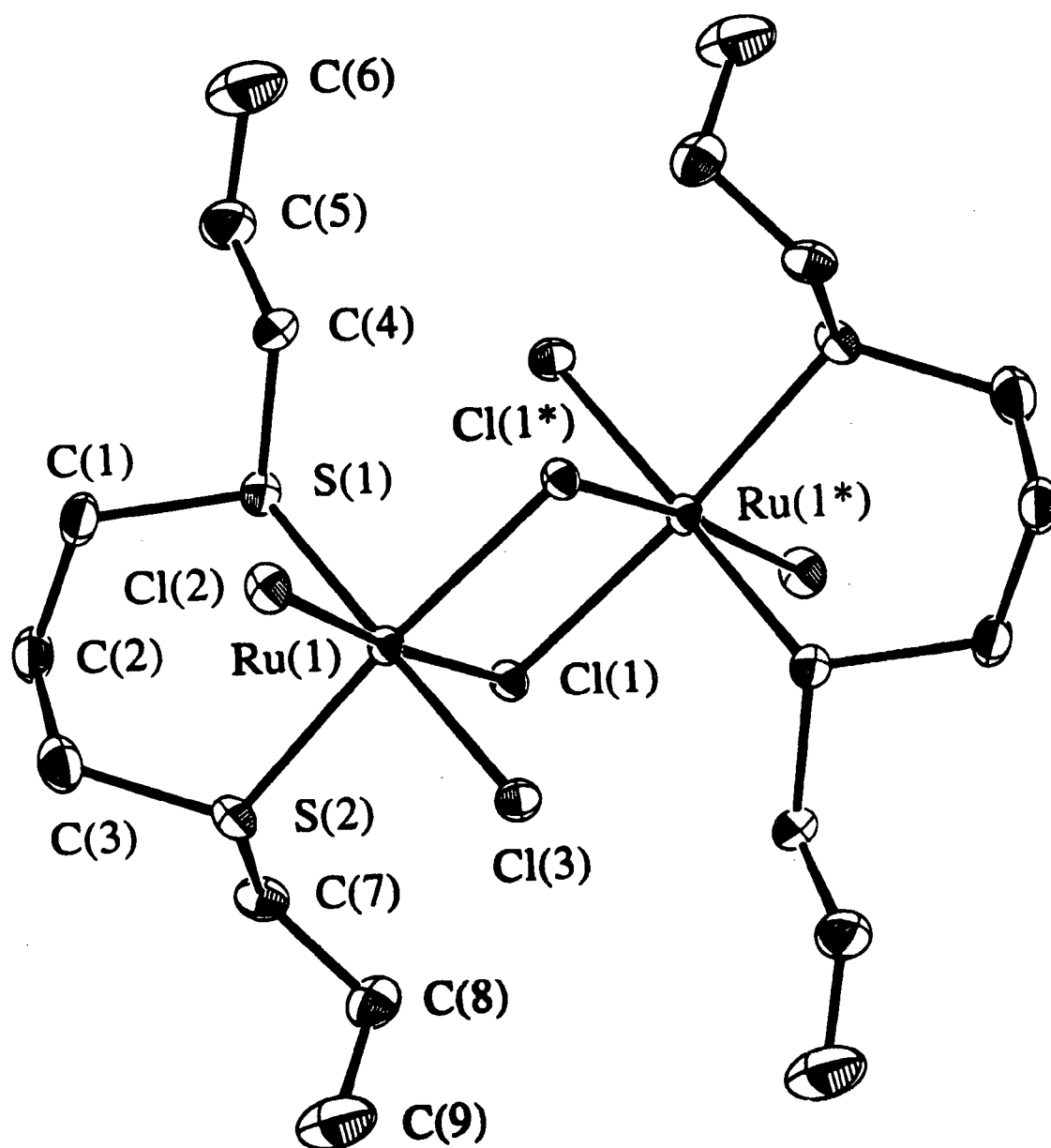


Figure 3.33. An ORTEP drawing of $[\text{RuCl}_2(\text{BPTP})]_2(\mu\text{-Cl})_2$ with 50 % probability thermal ellipsoids shown. The H-atoms are omitted for clarity (crystal data are given in Appendix 1.10).

3.10 *Mer*-RuCl₃(DPSO)₂(DPSO)

According to literature data, *mer*-[MCl₃(sulfoxide-S)₂(sulfoxide-O)] (M = Ru(III) or Rh(III)) have been isolated with the sulfoxides = DMSO, TMSO, Me(Ph)SO and ⁿPr₂SO.^{105,117} Previous work in this group has included the synthesis and structural characterization of two complexes with Ph₂SO (DPSO): *mer*-[RhCl₃(DPSO)(DPSO)(ⁱPrOH)]¹¹⁷ and *mer*-[RuCl₃(DPSO)(DPSO)(MeOH)]⁵² (see Figure 3.34).

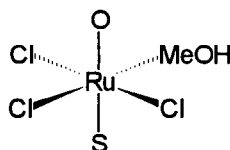


Figure 3.34. Structure of *mer*-[RuCl₃(DPSO)₂(DPSO)(MeOH)]; O and S are O- and S-bonded DPSO, respectively.

These results perhaps suggest that coordination of three DPSO ligands may be prevented sterically as the electronic properties of the S-O moiety of DPSO have been considered to be “similar to those of the other sulfoxides”.¹¹⁸ The crystal structure of DPSO¹¹⁹ reveals approximate pyramidal geometry at each S-atom with a sulfur-oxygen bond length of 1.47 Å indicating some double bond character in this bond. The coordination of a third DPSO is not, in fact, restricted as shown here by reaction of excess DPSO with RuCl₃·3H₂O to generate *mer*-RuCl₃(DPSO)₂(DPSO); the Trieste group independently synthesized and characterized this complex during the course of this present thesis work.¹¹⁸

3.10.1 Characterization of *Mer-Cis-RuCl₃(DPSO)₂(DPSO)*

As noted above, the title complex was synthesized by reacting excess DPSO with $\text{RuCl}_3 \cdot 3\text{H}_2\text{O}$, and crystals were obtained following the addition of ether to a reduced-volume reaction solution. Strong IR ν_{SO} bands were observed in the solid state at 922 cm^{-1} attributed to O-bonded DPSO, and at 1063 and 1129 cm^{-1} attributed to S-bonded DPSO (the Trieste group report ν_{SO} (DPSO) at 919 cm^{-1} and (DPSO) at 1128 cm^{-1}).¹¹⁸ ^1H NMR spectral data (Section 2.6.3) consisted of a broad peak centred at $\delta\ 8.80$, and sharp peaks that correspond to those of free DPSO. Very similar ^1H NMR data have been observed for *mer*- $[\text{RuCl}_3(\text{DPSO})(\text{DPSO})(\text{MeOH})]$.⁵² The solution magnetic susceptibility of the complex $\mu_{\text{eff}} = 2.33\text{ B. M.}$ corresponds to one unpaired electron.

The X-ray analysis revealed the presence of two O-bonded and one S-bonded DPSO ligands in a *mer*-geometry (Figure 3.35); the S-bonded sulfoxide is *trans* to an O-bonded one. This is the first example of a Ru complex showing more O- than S-bonded sulfoxides (*cf.* *mer-trans*- $[\text{RuCl}_3(\text{DMSO})_2(\text{DMSO})]$)^{25, 118}

Table 3.19 summarizes geometrical data for the complex, and the related *mer*- $[\text{RuCl}_3(\text{DPSO})(\text{DPSO})(\text{MeOH})]$.⁵² The Ru-Cl bond distance *trans* to oxygen is $2.305(1)\text{ \AA}$ which is shorter than the mutually *trans* Cl-atoms, $2.338(1)$ and $2.324(1)\text{ \AA}$; in *mer*- $[\text{RuCl}_3(\text{DPSO})(\text{DPSO})(\text{MeOH})]$ (Figure 3.34) the Ru-Cl bond distance *trans* to the O-atom of MeOH is $2.301(1)\text{ \AA}$ and the mutually *trans* Ru-Cl bonds are $2.3165(9)$ and $2.339(1)\text{ \AA}$.⁵² These data suggest that DPSO and MeOH (*trans* to Cl) have a similar *trans* influence, which is somewhat less than that of Cl. As expected, the Ru(III)-Cl bond lengths are shorter than those found in Ru(II)/Cl/sulfoxide complexes (typically 2.39 - 2.45 \AA , Section 3.6), because of

the electrostatic effect of the greater charge on Ru(III).¹²⁰ In both DPSO complexes, the Ru-O distance *trans* to S is 0.02 to 0.03 Å longer than the Ru-O bond *trans* to Cl, because of the greater *trans* influence of S vs. Cl. The Ru-S bond lengths (*trans* to an O-atom) in the tris- and bis(DPSO) complexes are 2.251(1) and 2.2391(9) Å, respectively. These Ru-S bonds are shorter than those found for example, in *trans*-[(TMSO)H]⁺[RuCl₄(TMSO)₂]⁻ (2.3219(8) Å).¹⁰⁵ A similar situation is found within Ru(II)/DMSO systems where the shorter Ru-S bonds are those in which the S-atoms are *trans* to O (e.g. 2.248 Å in *cis*-RuCl₂(DMSO)₄) while those *trans* to Cl or S are longer (e.g. 2.277 Å in *cis*-RuCl₂(DMSO)₄ and 2.353 Å in *trans*-RuCl₂(DMSO)₄).^{23,36,37} The sulfur-oxygen bond lengths of the O-bonded DPSO are 1.524(3) (*trans* to Cl) and 1.544(3) Å (*trans* to S) in the *tris* DPSO complex, slightly longer than that found in *mer*-[RuCl₃(DPSO)(DPSO)(MeOH)] 1.529(2) Å (*trans* to S)⁵². The sulfur-oxygen bond distance in the S-bonded DPSO is 1.472(3) Å, the same as that of free DPSO;¹¹⁹ however, the sulfur-oxygen bond length found for the S-bonded DPSO in *mer*-[RuCl₃(DPSO)(DPSO)(MeOH)] is just longer at 1.486(2) Å,⁵² and the increase was considered to be due to the interaction between the oxygen of the S-bonded DPSO and the hydroxyl proton of the bound MeOH.⁵²

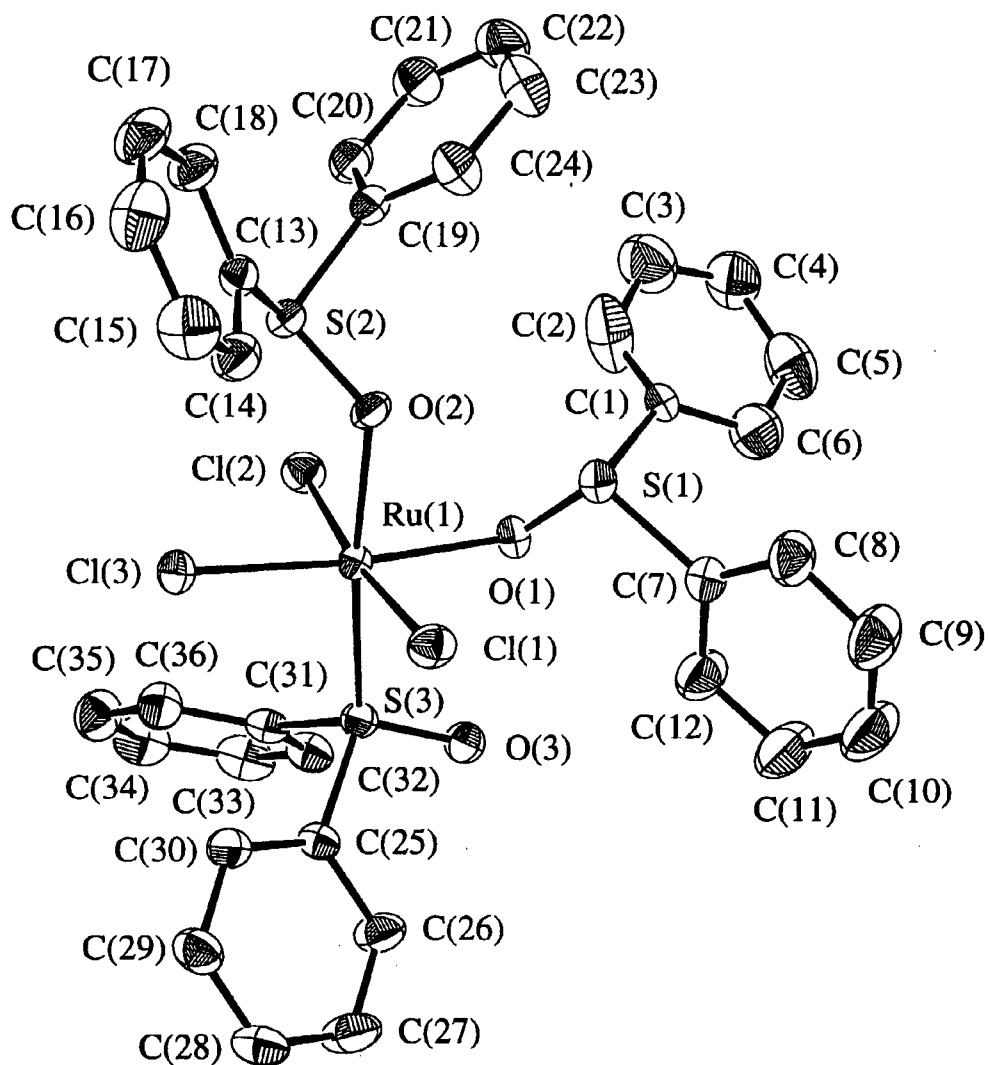


Figure 3.35. An ORTEP diagram of *mer-cis*-[RuCl₃(DPSO)₂(DPSO)] showing 50 % thermal ellipsoids; the H-atoms are omitted for clarity (crystal data are given in Appendix 1.11).

Table 3.19. Selected Bond Lengths (Å) and Bond Angles (°) for *mer-cis*-[RuCl₃(DPSO)₂(DPSO)] and *mer*-[RuCl₃(DPSO)(DPSO)(MeOH)].

Bond or Angle	<i>mer-cis</i> -[RuCl ₃ (DPSO) ₂ (DPSO)]		<i>mer</i> -[RuCl ₃ (DPSO)(DPSO)(MeOH)](ref. 52)
	this work	Ref. 118	
Ru-Cl	2.338(1), 2.324(1); ^a 2.305(1) ^b	2.307(2), 2.337(2); ^a 2.307(2) ^b	2.3165(9), 2.339(1); ^a 2.301(1) ^b
Ru-S	2.251(1) ^b	2.251(2) ^b	2.2391(9) ^b
Ru-O	2.090(3), ^a 2.111(3) ^c	2.091(6), ^a 2.114(5) ^c	2.094(3), ^a 2.122(2) ^c
S-O	1.524(3), ^a 1.472(3), ^b 1.544(3) ^c	1.522(6), ^a 1.463(7), ^b 1.546(6) ^c	1.486(2), ^b 1.529(2) ^c
Cl-Ru-Cl	172.63(5)	172.54(9)	172.03(4)
<i>trans</i>			
Cl-Ru-O	173.70(9)	174.0(2)	175.02(8)
<i>trans</i>			
S-Ru-O <i>trans</i>	173.65(9)	173.5(2)	171.84(7)
Cl-Ru-O <i>cis</i>	86.82(9)-89.57(9)	86.3(1)-89.7(1)	85.93(9)-86.82(9)
Cl-Ru-Cl <i>cis</i>	93.02(4)-93.22(5)	93.17(8)-93.19(8)	92.11(4)-94.84(4)
Cl-Ru-S <i>cis</i>	91.18(5)-98.86(4)	91.19(7)-98.88(8)	90.31(3)-99.06(4)
O-Ru-S <i>cis</i>	87.42(9)	87.1(2)	85.61(8)
O-Ru-O <i>cis</i>	86.5(1)	86.6(2)	86.8(1)

^a *Trans* to Cl. ^b *Trans* to O. ^c *Trans* to S.

3.11 Macrocyclic Thioether, DMSO Complexes of Ruthenium

Interest in the coordination chemistry of macrocyclic thioethers has stemmed from the observation that these can bind to a range of transition metal ions to form stable complexes.¹²¹ In this present work, the goal was to synthesize and characterize Ru/sulfoxide/macrocyclic thioether complexes and study how the macrocycle might affect the *in vitro* properties of the Ru sulfoxide moiety, particularly the cytotoxicity, accumulation and DNA-binding properties with respect to Chinese hamster ovary cells (Chapter 4).

3.11.1 3,6,9,14-Tetrathiabicyclo[9.2.1]tetradeca-11,13-diene [L]

This structurally characterized macrocyclic thioether ligand¹²² (Figure 3.36) was used as purchased from Aldrich; the structure shows the thiophene moiety to be placed 60 ° relative to the plane of the three S-atoms of the macrocycle, all the S-atoms lying in *exocyclic* positions with respect to the macrocyclic cavity. Inclusion of the thiophene sub-unit imposes limitations on the possible orientations of the S-atom electron pairs and on the size and shape of the cavity. Several metal complexes of this macrocyclic thioether are known, for example, with Cu(I),¹²³ Cu (II)¹²³ and Pd(II).¹²⁴

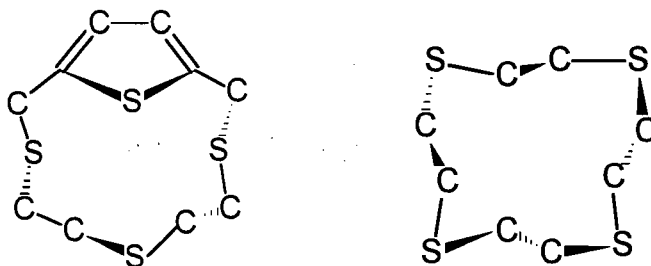


Figure 3.36. 3,6,9,14-Tetrathiabicyclo[9.2.1]tetradeca-11,13-diene (L), and 1,4,7,10-tetrathiacyclododecane (12-S-4); H-atoms omitted. Adapted from refs. 122 and 125, respectively.

3.11.2 $RuCl_2(DMSO)(L)$

A Ru(II) complex containing ligand L, $RuCl_2(DMSO)(L)$, was synthesized by sulfoxide displacement from *cis*- $RuCl_2(DMSO)_4$ and structurally characterized (Figure 3.37, Tables 3.20 and 3.21).

Three S-atoms of the ligand coordinate in a *fac*-arrangement. Two five-membered rings are formed, one involving the S-atom of the thiophene and S(2) of the macrocycle, and the other involving the S(2)- and S(3)-atoms. One eight-membered ring is formed between the S-atom of the thiophene, the Ru and S(3)-atom of the macrocycle. The S-bound DMSO is *trans* to S(3) of the macrocycle, Cl(2) is *trans* to S(2), and Cl(1) is *trans* to the thiophene S. The complex has slightly distorted octahedral geometry at the Ru(II) centre with *trans* angles ranging from 171.63(8)-175.80(9)°, and *cis* angles ranging from 82.27(8)-100.25(8)° (Table 3.20). The Ru-S bond lengths (macrocycle) are 2.320(2) and 2.300(2) Å *trans* to Cl, and 2.375(2) Å *trans* to S (Table 3.21). The eight-membered chelate ring of S(1)-Ru-S(3) spans an angle of 100.25(8)°, and the five-membered chelate rings span angles of 85.64(9) and 88.42(7)°. The sulfur-oxygen bond length is 1.479(8) Å, and the Ru-S(DMSO) bond (*trans*

to S) is 2.290(2) Å. The two Ru-Cl bond lengths are 2.400(2) and 2.430(2) Å. The crystallographic data show that the macrocycle changes remarkably little upon coordination.

The solid state IR spectrum of the complex exhibits a strong ν_{SO} at 1083 cm^{-1} of the S-bonded DMSO (free DMSO ν_{SO} 1055 cm^{-1}). The ^1H NMR spectrum ($\text{DMSO-}d_6$) exhibits a multiplet centred at δ 7.1 assigned to the olefinic protons, and a complex pattern centred between δ 2.7-4.5 presumably because of the overlap of the resonances of the H-atoms of the macrocycle with those of the S-bound DMSO.

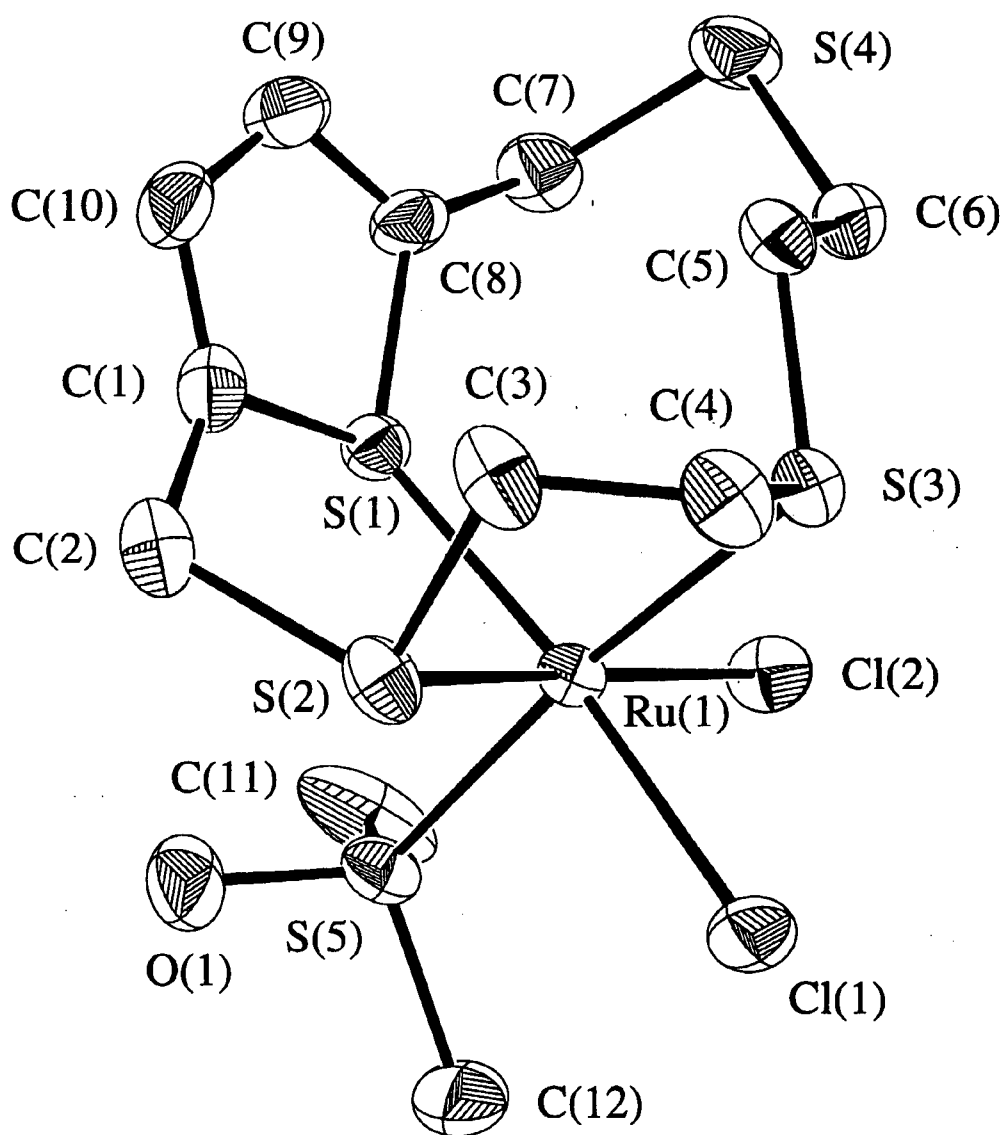


Figure 3.37. An ORTEP diagram of $\text{RuCl}_2(\text{DMSO})(\text{L})$ showing 50 % thermal ellipsoids; the H-atoms are omitted for clarity (crystal data are given in Appendix 1.12).

Table 3.20. Comparison of Selected Bond Angles (°) of L and RuCl₂(DMSO)(L).

Bond angle	L (ref. 122)	RuCl ₂ (DMSO)(L)
C(1)-S(1)-C(8)	91.7(3)	92.3(5)
C(2)-S(2)-C(3)	101.7(3)	97.3(5)
C(4)-S(3)-C(5)	101.2(3)	101.9(4)
C(6)-S(4)-C(7)	102.4(3)	100.7(4)
S(1)-C(1)-C(10)	109.8(4)	111.0(7)
S(1)-C(1)-C(2)	120.6(5)	115.4(7)
C(10)-C(1)-C(2)	129.5(5)	133.0(9)
C(1)-C(10)-C(9)	115.2(5)	112.8(9)
C(10)-C(9)-C(8)	111.6(5)	115.2(10)
S(1)-C(8)-C(9)	111.6(4)	108.1(8)
S(1)-C(8)-C(7)	119.2(4)	122.4(7)
C(9)-C(8)-C(7)	128.8(5)	129.4(9)
S(2)-C(2)-C(1)	115.3(5)	110.3(7)
S(2)-C(3)-C(4)	112.2(4)	109.6(6)
S(3)-C(4)-C(3)	111.8(4)	111.7(6)
S(3)-C(5)-C(6)	114.2(5)	106.6(6)
S(4)-C(6)-C(5)	114.7(5)	113.9(6)
S(4)-C(7)-C(8)	112.8(4)	114.2(7)
<i>cis</i> angles		82.27(8)-100.25(8)
<i>trans</i> angles		171.63(8)-175.80(9)
S(1)-Ru-S(3)		100.25(8)
S(2)-Ru-S(3)		88.42(7)
S(1)-Ru-S(2)		85.64(9)

Table 3.21. Comparison of Selected Bond Lengths (Å) of L and RuCl₂(DMSO)(L).

Bond	L (ref. 122)	RuCl ₂ (DMSO)(L)
S(1)-C(1)	1.737(5)	1.764(9)
S(1)-C(8)	1.721(5)	1.749(5)
S(2)-C(2)	1.805(8)	1.82(1)
S(2)-C(3)	1.816(7)	1.846(10)
S(3)-C(4)	1.814(6)	1.822(9)
S(3)-C(5)	1.800(7)	1.808(9)
S(4)-C(6)	1.800(8)	1.784(10)
S(4)-C(7)	1.840(8)	1.81(1)
C(1)-C(10)	1.344(9)	1.32(1)
C(1)-C(2)	1.485(8)	1.48(1)
C(10)-C(9)	1.406(9)	1.44(2)
C(9)-C(8)	1.363(8)	1.36(1)
C(8)-C(7)	1.505(8)	1.50(1)
C(3)-C(4)	1.529(9)	1.49(1)
C(5)-C(6)	1.53(1)	1.57(1)
Ru-Cl(1)		2.400(2)
Ru-Cl(2)		2.430(2)
Ru-S(1)		2.320(2)
Ru-S(2)		2.300(2)
Ru-S(3)		2.375(2)
Ru-S(5)		2.290(2)
S-O		1.479(8)

3.11.3 1,4,7,10-Tetrathiacyclododecane (12-S-4)

This macrocyclic thioether ligand^{125,126} (Figure 3.36) was used as purchased from Aldrich. In the solid state, 12-S-4 adopts a square conformation with the S-atoms at the corners, giving a structure with the terminal S-atoms forming two “bracket” units, and all eight C-S bonds assume mutually gauche placements in order to minimize S...S repulsions by incorporating an *exo* formation where the S-atoms point out of the macrocyclic ring.^{125,127} These observations explain the tendency for tetrathia-macrocycles to bind to metal ions in an *exo* manner.¹²⁵ Complexes with Ni(II),¹²⁶ Cu(I),¹²⁸ Cu(II)¹²⁸ and Pt(II)¹²⁹ are known.

3.11.4 [Ru(12-S-4)(DMSO)(H₂O)][OTf]₂

The Ru(II) complex of 12-S-4 was synthesized by sulfoxide displacement from *cis*-RuCl₂(DMSO)₄, followed by Cl⁻ abstraction by utilization of AgOTf. The six-coordinate complex has a slightly distorted octahedral geometry (Figure 3.38, Tables 3.22 and 3.23) with *trans* angles that range from 166.83(2)-178.17(5) ° and *cis* angles that range from 84.29(2)-100.72(2) ° (Table 3.22). The Ru-S(macrocycle) bond lengths range from 2.2903(6)-2.3907(6) Å. The S-bound DMSO ligand is *trans* to S(2) and has a Ru-S bond length of 2.3011(6) Å; the sulfur-oxygen bond length is 1.494(2) Å. The Ru-O bond length is 2.193(2) Å which is comparable to others found within Ru(II)-aqua complexes (*e.g.* values for [RuCl(BESE)(H₂O)]₂(μ-Cl)₂ (Table 3.7), RuCl₂(PPh₃)(P-N)(H₂O)·2C₆H₆,¹³⁰ RuCl₂(PPh₃)(P-N)(H₂O)·1.5C₆H₆,¹³⁰ and RuCl₂(P(*p*-tolyl)₃)(P-N)(H₂O)¹³⁰ (P-N = [*o*-(N,N-dimethylamino)phenyl]diphenylphosphine) are 2.140(3), 2.238(3), 2.187(2) and 2.252(4) Å, respectively). The coordinated H₂O is H-bonded to the O-atoms of the two triflate anions.

The average H...O distance is 1.905 Å is 0.795 Å shorter than the sum of the van der Waals radii of an H- and an O-atom (2.70 Å)⁷⁰ and indicates a strong interaction between the bound H₂O molecule and the two triflate anions. Tables 3.22 and 3.23 compare selected bond angles and bond lengths, respectively, of free 12-S-4 with those of the complex [Ru(12-S-4)(DMSO)(H₂O)][OTf]₂. The crystallographic data show that the macrocycle does not change much upon coordination.

A strong ν_{SO} band was observed in the solid state IR spectrum of the complex at 1082 cm⁻¹ attributed to the S-bonded DMSO. The ¹H NMR spectrum (MeOD) shows a complex pattern for the protons of the complex centred at δ 3.1 presumably because of the presence of the diastereomeric H-atoms of the macrocycle and the methyl groups of the S-bound DMSO. This complex was tested *in vitro* for cytotoxicity, accumulation and DNA-binding properties in Chinese hamster ovary cells with the results presented in Chapter 4.

Table 3.22. Comparison of Selected Bond Angles (°) of 12-S-4 and [Ru(12-S-4)(DMSO)(H₂O)][OTf]₂.

Bond angle	12-S-4 (ref.125)	[Ru(12-S-4)(DMSO)(H ₂ O)][OTf] ₂
C(8)-S(1)-C(1)	101.3(2)	101.5(1)
C(3)-S(2)-C(2)	102.2(3)	106.1(1)
C(4)-S(3)-C(5)	100.7(3)	100.6(1)
C(7)-S(4)-C(6)	100.8(2)	106.4(1)
<i>cis</i> angles		84.29(2)-100.72(2)
<i>trans</i> angles		166.83(2)-178.17(5)

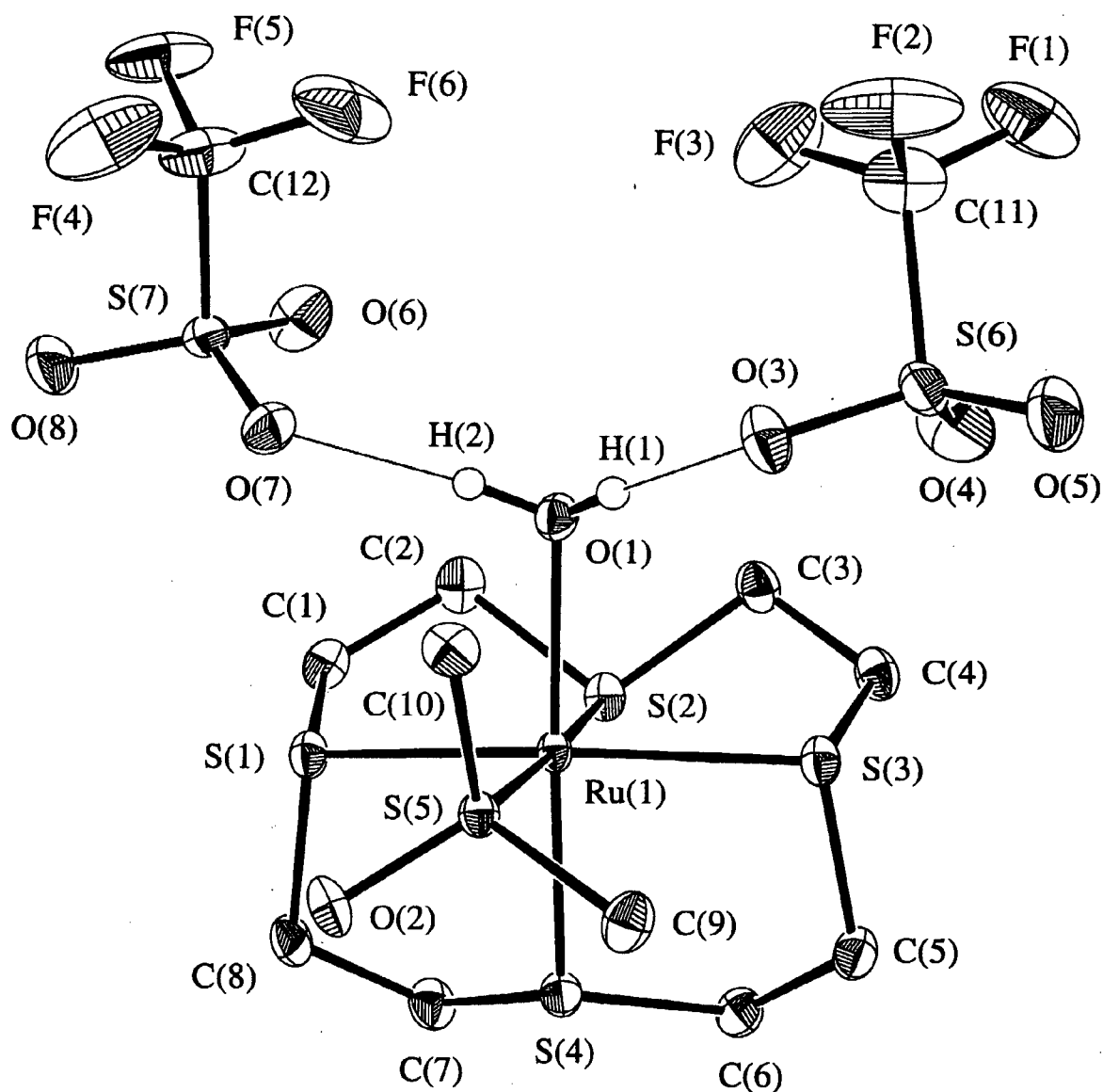


Figure 3.38. An ORTEP diagram of $[\text{Ru}(12\text{-S-4})(\text{DMSO})(\text{H}_2\text{O})][\text{OTf}]_2$ showing 50 % thermal ellipsoids; the H-atoms are omitted for clarity (crystal data are give in Appendix 1.13).

Table 3.23. Comparison of Selected Bond Lengths (Å) of 12-S-4 and [Ru(12-S-4)(DMSO)(H₂O)][OTf]₂.

Bond	12-S-4 (ref. 125)	[Ru(12-S-4)(DMSO)(H ₂ O)][OTf] ₂
S(1)-C(1)	1.826(5)	1.864(3)
S(1)-C(8)	1.806(5)	1.860(3)
S(2)-C(3)	1.801(6)	1.823(3)
S(2)-C(2)	1.808(6)	1.822(3)
S(3)-C(4)	1.815(6)	1.872(3)
S(3)-C(5)	1.820(5)	1.851(3)
S(4)-C(6)	1.825(5)	1.836(3)
S(4)-C(7)	1.817(5)	1.837(3)
C(7)-C(8)	1.505(8)	1.528(4)
C(1)-C(2)	1.528(8)	1.525(4)
C(3)-C(4)	1.504(8)	1.526(4)
C(5)-C(6)	1.508(8)	1.533(4)
Ru-S(1)		2.3852(6)
Ru-S(2)		2.3708(6)
Ru-S(3)		2.3907(6)
Ru-S(4)		2.2903(6)
Ru-S(5)		2.3011(6)
Ru-O		2.193(2)
S-O		1.494(2)

3.12 References for Chapter 3

- 1 Cotton, F. A.; Francis, R. *J. Am. Chem. Soc.* 1960, 82, 2986.
- 2 Davies, J. A. *Adv. Inorg. Chem. Radiochem.* 1981, 24, 115.
- 3 Sze, K. H.; Brion, C. E.; Tronc, M.; Bodeur, S.; Hitchcock, A. P. *Chem. Phys.* 1988, 121, 279.
- 4 Kagan, H. B.; Ronan, B. *Rev. Heteroatom. Chem.* 1992, 7, 92.
- 5 Reynolds, W. L. *Prog. Inorg. Chem.* 1970, 12, 1.
- 6 Rayner, D. R.; Miller, E. G.; Bickart, P.; Gordon, A. J.; Mislow, K. *J. Am. Chem. Soc.* 1966, 88, 3138.
- 7 Jacobus, J.; Mislow, K. *J. Am. Chem. Soc.* 1967, 89, 5228.
- 8 Bhandary, K. K.; Manohar, H.; Venkatesan, K. *Indian J. Pure Appl. Phys.* 1976, 14, 771.
- 9 Thomas, R.; Shoemaker, C. B.; Eriks, K. *Acta Cryst.* 1966, 21, 12.
- 10 Bastiansen, O.; Viervoll, H. *Acta Chem. Scand.* 1948, 2, 702.
- 11 Viswamitra, M. A.; Kannan, K. K. *Nature* 1966, 209, 1016.
- 12 Bennett, M. J.; Cotton, F. A.; Weaver, D. L.; Williams, R. J.; Watson, W. H. *Acta Cryst.* 1967, 23, 788.
- 13 (a) Coulson, C. A.; Zauli, C. *Mol. Phys.* 1963, 6, 525;
 (b) Sato, T.; Takahashi, Y.; Yabe, K. *Bull. Chem. Soc. Jap.* 1967, 40, 298;
 (c) Takahashi, Y.; Yabe, K.; Sato, T. *Bull. Chem. Soc. Jap.* 1970, 42, 2707;
 (d) Nikolaev, A. V.; Torgov, V. G.; Andrievskii, V. N.; Gal'tsova, E. A.; Gilbert, E. N.; Kotlyarovskii, I. L.; Mazalov, L. N.; Mikhailov, V. A.; Cheremisina, I. M. *Russ. J. Inorg. Chem.* 1970, 15, 685 and references therein.
- 14 Calligaris, M.; Carugo, O. *Coord. Chem. Rev.* 1996, 153, 83.
- 15 (a) Pearson, R. G. *J. Am. Chem. Soc.* 1963, 85, 3533;
 (b) Pearson, R. G. *J. Chem. Educ.* 1987, 64, 561;
 (c) Pearson, R. G. *Coord. Chem. Rev.* 1990, 100, 403;
 (d) Pearson, R. G. Chemical Hardness - An Historical Introduction, in *Structure and Bonding* (ed. K. D. Sen), Springer-Verlag, Berlin, 1993, 80, p. 1.

- 16 Burmeister, J. L.; Basolo, F. Inorganic Linkage Isomerism of the Thiocyanate Ion, in *Hard and Soft Acids and Bases* (ed. R. G. Pearson), Dowden, Hutchinson and Ross Inc., Stroudsburg, Pennsylvania, 1973, p. 300.
- 17 Davies, J. A. Hartley, F. R.; Murray, S. G. *J. Chem. Soc. Dalton Trans.* 1979, 1705.
- 18 Wayland, B. B.; Schramm, R. F. *Inorg. Chem.* 1969, 8, 971.
- 19 Bennett, M. J.; Cotton, F. A.; Weaver, D. L. *Nature* 1966, 212, 286.
- 20 Bennett, M. J.; Cotton, F. A.; Weaver, D. L. *Acta Cryst.* 1967, 23, 581.
- 21 Willet, R. D.; Chang, K. *Inorg. Chim. Acta* 1970, 4, 447.
- 22 Melanson, R.; Rochon, F. D. *Can. J. Chem.* 1975, 53, 2371.
- 23 Mercer, A.; Trotter, J. *J. Chem. Soc. Dalton Trans.* 1975, 2480.
- 24 Colamarino, P.; Orioli, P. *J. Chem. Soc. Dalton Trans.* 1976, 845.
- 25 Alessio, E.; Balducci, G.; Calligaris, M.; Costa, G.; Attia, W. M.; Mestroni, G. *Inorg. Chem.* 1991, 30, 609.
- 26 Tanase, T.; Aiko, T.; Yamamoto, Y. *J. Chem. Soc. Dalton Trans.* 1996, 2341.
- 27 (a) Calligaris, M.; Faleschini, P.; Alessio, E. *Acta Cryst.* 1993, C49, 663;
(b) Ghosh, P.; Pramanik, A. *Acta Cryst.* 1995, C51, 824.
- 28 Geremia, S.; Mestroni, S.; Calligaris, M.; Alessio, E. *J. Chem. Soc. Dalton Trans.* 1998, 2447.
- 29 Drysdale, K. D.; Beck, E. J.; Cameron, T. S.; Robertson, K. N.; Aquino, M. A. S. *Inorg. Chim. Acta* 1997, 256, 243.
- 30 House, D. A.; Steel, P. J. *Inorg. Chim. Acta* 1998, 269, 229.
- 31 McDonagh, A. M.; Humphrey, M. G.; Hockless, D. C. R. *Aust. J. Chem.* 1998, 51, 807.
- 32 (a) Evans, I. P.; Spencer, A., Wilkinson *J. Chem. Soc. Dalton Trans.* 1973, 204;
(b) McMillan, R. S.; Mercer, A.; James, B. R.; Trotter, J. *J. Chem. Soc. Dalton Trans.* 1975, 1006.
- 33 Kitching, W.; Moore, C. J.; Doddrell, D. *Aust. J. Chem.* 1969, 22, 1149.
- 34 Kitching, W.; Moore, C. J.; Doddrell, D. *Inorg. Chem.* 1970, 9, 541.

- 35 (a) Yapp, D. T. T.; Jaswal, J. S.; Rettig, S. J.; James, B. R.; Skov, K. A. *Inorg. Chim. Acta* 1990, 177, 199;
(b) Jaswal, J. S.; Yapp, D. T. T.; Rettig, S. J.; James, B. R.; Skov, K. A. *J. Chem. Soc., Chem. Commun.* 1992, 1528.
- 36 Alessio, E.; Mestroni, G.; Nardin, G.; Attia, W. M.; Calligaris, M.; Sava, G.; Zorzet, S. *Inorg. Chem.* 1988, 27, 4099.
- 37 Jaswal, J. S.; Rettig, S. J.; James, B. R. *Can. J. Chem.* 1990, 68, 1808.
- 38 Oliver, J. D.; Riley, D. P. *Inorg. Chem.* 1984, 23, 156.
- 39 Hull, M.; Bargar, T. W. *J. Org. Chem.* 1975, 40, 3152.
- 40 (a) Bell, E. V.; Bennett, G. M. *J. Chem. Soc.* 1927, 1798;
(b) Bennett, G. M.; Statham, F. S. *J. Chem. Soc.* 1931, 1684.
- 41 Madesclaire, M. *Tetrahedron* 1986, 42, 5459.
- 42 Ravikumar, K. S.; Bégué J-P.; Bonnet-Delpon, D. *Tetrahedron Lett.* 1998, 39, 3141.
- 43 Svinning, T.; Mo, F.; Bruun, T. *Acta Cryst.* 1976, B32, 759.
- 44 Cattalini, L.; Michelon, G.; Marangoni, G.; Pelizzi, G. *J. Chem. Soc. Dalton Trans.* 1979, 96.
- 45 Taddei, F. *Boll. Sci. Fac. Chim. Ind. Bologna* 1968, 26, 107.
- 46 Personal communication from S. Colonna.
- 47 Zipp, A. P.; Madan, S. K. *Inorg. Chim. Acta* 1977, 22, 49, and references therein.
- 48 Zhu, F. C.; Shao, P. X.; Yao, X. K. Wang, R. J.; Wang, H. G. *Inorg. Chim. Acta* 1990, 171, 85.
- 49 Calligaris, M. Personal communication to B. R. James.
- 50 Nieuwenhuyse, H.; Louw, R. *J. Chem. Soc., Perkins I* 1973, 839.
- 51 Madan, S. K.; Hull, C. M.; Herman, L. J. *Inorg. Chem.* 1968, 7, 491.
- 52 Yapp, D. T. T. Ph. D. Dissertation, University of British Columbia, Vancouver, 1993.
- 53 Yapp, D. T. T.; Rettig, S. J.; James, B. R.; Skov, K. A. *Inorg. Chem.* 1997, 36, 5635.

- 54 De Azevedo Jr., W. F.; Mascarenhas, Y. P.; De Sousa, G. F.; Filgueiras, C. A. L. *Acta Cryst.* 1995, *C51*, 619.
- 55 Carvalho, C. C.; Francisco, R. H. P.; Gambardella, M. T. do P.; de Sousa, G. F.; Filgueiras, C. A. L. *Acta Cryst.* 1996, *C52*, 1627.
- 56 Filgueiras, C. A. L.; Holland, P. R.; Johnson, B. F. G.; Raithby, P. R. *Acta Cryst.* 1982, *B38*, 2684.
- 57 Musgrave, T. R.; Kent, G. D. *J. Coord. Chem.* 1972, *2*, 23.
- 58 Francisco, R. H. P.; Gambardella, M. T. P.; Rodrigues, A. M. G. D.; de Souza, G. F.; Filgueiras, C. A. L. *Acta Cryst.* 1995, *C51*, 604.
- 59 Filgueiras, C. A. L.; Holland, P. R.; Johnson, B. F. G.; Raithby, P. R. *Acta Cryst.* 1982, *B38*, 954.
- 60 Khiar, N.; Fernández, I.; Alcudia, F. *Tetrahedron Lett.* 1993, *34*, 123.
- 61 Tokunoh, R.; Sodeoka, M.; Aoe, K.; Shibasaki, M. *Tetrahedron Lett.* 1995, *36*, 8035.
- 62 James, B. R.; Morris, R. H.; Reimer, K. J. *Can. J. Chem.* 1977, *55*, 2353.
- 63 (a) McMillan, R. S. Ph. D. Dissertation, University of British Columbia, Vancouver, 1976;
(b) James, B. R.; McMillan, R. S. *Can. J. Chem.* 1977, *55*, 3927;
(c) James, B. R.; McMillan, R. S.; Morris, R. H.; Wang, D. K. W. Ruthenium and Rhodium Hydrides Containing Chiral Phosphine or Chiral Sulfoxide Ligands, and Catalytic Asymmetric Hydrogenation in *Advances in Chemistry Series, No. 167 Transition Metal Hydrides* (ed. R. Bau), American Chemical Society, Washington, 1978, p. 122.
- 64 Komori, T.; Nonaka, T. *J. Am. Chem. Soc.* 1984, *106*, 2656.
- 65 van Deurzen, M. P. J.; Remkes, I. J.; van Rantwijk, F.; Sheldon, R. A. *J. Mol. Cat. A: Chemical* 1997, *117*, 329.
- 66 Allin, S. M. *Organosulfur Chem.* 1998, *2*, 41.
- 67 (a) Chan, P. K. L.; Chan, P. K. H.; Frost, D. C.; James, B. R.; Skov, K. A. *Can. J. Chem.* 1988, *66*, 117;

- (b) Chan, P. K. L.; James, B. R.; Frost, D. C.; Chan, P. K. H.; Hu, H-L.; Skov, K. A. *Can. J. Chem.* 1989, 67, 508;
- 68 Geremia, S.; Vicentini, L.; Calligaris, M. *Inorg. Chem.* 1998, 37, 4094.
- 69 Rettig, S. J. Private communication.
- 70 Huheey, J. E. *Inorganic Chemistry* (3rd ed.), Harper & Row, New York, 1983, p. 269.
- 71 (a) Huheey, J. E. *Inorganic Chemistry* (3rd ed.), Harper & Row, New York, 1983, p. 362;
- (b) Geary, W. J. *Coord. Chem. Rev.* 1971, 7, 110.
- 72 Glasstone, S. *Textbook of Physical Chemistry* (2nd ed.), MacMillan and Co. Limited, London, 1951, p. 892.
- 73 Chioccola, G.; Daly, J. J. *J. Chem. Soc. (A)* 1968, 1981.
- 74 Cotton, F. A.; Ucko, D. A. *Inorg. Chim. Acta* 1972, 6, 161.
- 75 (a) Bennett, M. J.; Caulton, K. G.; Cotton, F. A. *Inorg. Chem.* 1969, 8, 1;
- (b) Cotton, F. A. *Chem. Soc. Rev.* 1975, 4, 27.
- 76 Jones, R. A.; Wilkinson, G.; Colquhoun, I. J.; McFarlane, W.; Galas, A. M. R.; Hursthouse, M. B. *J. Chem. Soc. Dalton Trans.* 1980, 2480.
- 77 Schumann, H.; Opitz, J.; Pichardt, J. *J. Organomet. Chem.* 1977, 128, 253.
- 78 Mattson, B. M.; Heiman, J. R.; Pignolet, L. H. *Inorg. Chem.* 1976, 15, 564.
- 79 Dekleva T. W.; Thorburn, I. S.; James, B. R., *Inorg. Chim. Acta* 1985, 100, 49.
- 80 Sirigu, A.; Bianchi, M.; Benedetti, E. *J. Chem. Soc., Chem. Commun. (D)* 1969, 596.
- 81 Crutchley, R. J. *Adv. Inorg. Chem.* 1994, 41, 273.
- 82 Allen, G. C.; Hush, N. S. *Prog. Inorg. Chem.* 1967, 8, 357.
- 83 Robin, M. B.; Day, P. *Adv. Inorg. Chem. Radiochem.* 1967, 10, 247.
- 84 Shriver, D. E.; Atkins, P. W.; Langford, C. H. *Inorganic Chemistry*, W. H. Freeman and Company, New York, 1990, p. 461.
- 85 Creutz, C. *Prog. Inorg. Chem.* 1983, 30, 1.
- 86 Clausen III, C. A.; Prados, R. A.; Good, M. L. *Inorg. Nucl. Chem. Lett.* 1971, 7, 485.

- 87 Mercer, E. E.; Dumas, P. E. *Inorg. Chem.* 1971, 10, 2755.
- 88 (a) Gilbert, J. D.; Rose, D.; Wilkinson, G. *J. Chem. Soc. (A)* 1970, 2765;
(b) Seddon, E. A.; Seddon, K. R. *The Chemistry of Ruthenium*, Elsevier, Amsterdam, 1984, p. 310.
- 89 Rose, D.; Wilkinson, G. *J. Chem. Soc. (A)* 1970, 1791.
- 90 Bino, A.; Cotton, F. A. *J. Am. Chem. Soc.* 1980, 102, 608.
- 91 Bottomley, F.; Tong, S. B. *Can. J. Chem.* 1971, 49, 3739.
- 92 Creutz, C.; Taube, H. *J. Am. Chem. Soc.* 1969, 91, 3988.
- 93 Gibson, J. F.; Poole, R. K.; Hughes, M. N.; Rees, J. F. *Arch. Microbiol.* 1984, 139, 265.
- 94 Hughes, M. N.; O'Reardon, D.; Poole, R. K.; Hursthouse, M. B.; Thornton-Pett, M. *Polyhedron* 1987, 6, 1711.
- 95 Beattie, J. K.; Del Favero, P.; Hambley, T. W.; Hush, N. S. *Inorg. Chem.* 1988, 27, 2000.
- 96 Thorburn, I. S.; Rettig, S. J.; James, B. R. *Inorg. Chem.* 1986, 25, 234.
- 97 Rosenberg, B.; Van Camp, L.; Krigas, T. *Nature* 1969, 205, 698.
- 98 Rosenberg, B. *Cancer Chemother. Rep.* 1975, 59, 589.
- 99 Barton, J. K.; Szalda, D. J.; Rabinowitz, H. N.; Waszczak, J. V.; Lippard, S. J. *J. Am. Chem. Soc.* 1979, 101, 1434.
- 100 Lock, C. J. L.; Persie, H. J.; Rosenberg, B.; Turner, G. *J. Am. Chem. Soc.* 1978, 100, 3371.
- 101 Geraldes, C. F. G. C.; Aragon-Salgado, M.; Martin-Gil, J. *Polyhedron*, 1991, 10, 799.
- 102 Matsumoto, K.; Sakai, K.; Nishio, K.; Tokisue, Y.; Ito, R.; Nishide, T.; Shichi, Y. *J. Am. Chem. Soc.* 1992, 114, 8110.
- 103 Geremia, S.; Calligaris, M.; Mestroni, S. *Inorg. Chim. Acta* 1999, 292, 144.
- 104 Taqui Khan, M. M.; Ramachandraiah, G.; Prakash Rao, A. *Inorg. Chem.* 1986, 25, 665.
- 105 Alessio, E.; Milani, B.; Mestroni, G.; Calligaris, M.; Faleschini, P.; Attia, W. M. *Inorg. Chim. Acta* 1990, 177, 255.

- 106 Halpern, J.; James, B. R. *Can. J. Chem.* 1966, 44, 495.
- 107 Hui, B. C.; James, B. R. *Can. J. Chem.* 1974, 52, 348.
- 108 Lipponer, K-G.; Vogel, E.; Keppler, B. K. *Metal-Based Drugs* 1996, 3, 243.
- 109 Ledlie, M. A.; Allum, K. G.; Howell, I. V.; Pitkethley, C. R. *J. Chem. Soc. Perkin I* 1976, 1734.
- 110 Chatt, J.; Leigh, G. J.; Storace, A. P. *J. Chem. Soc. (A)* 1971, 1380.
- 111 Lucas, C. R.; Liu, S.; Newlands, M. J.; Gabe, E. J. *Can. J. Chem.* 1990, 68, 1357.
- 112 Hartley, F. R.; Murray, S. G.; Levason, W.; Soutter, H. E.; McAuliffe, C. A. *Inorg. Chim. Acta* 1979, 35, 265.
- 113 Murray, S. G.; Levason, W.; Tuttlebee, H. E. *Inorg. Chim. Acta* 1981, 51, 185.
- 114 Song, H.; Haltiwanger, R. C.; Rakowski-DuBois, M. *Organometallics* 1987, 6, 2021.
- 115 Shao, P.; Yao, X.; Wang, H.; Wang, W.; Liu, B.; Li, M.; Luo, L.; Xu, D. *Gaodeng Xuexiao Huaxue Xuebao* 1991, 12, 143 (from Chem. Abstr. 1998, 115, 190904).
- 116 Schenk, W. A.; Frisch, J.; Dürr, M.; Burzlaff, N.; Stalke, D.; Fleischer, R.; Adam, W.; Pechtl, F.; Smerz, A. K. *Inorg. Chem.* 1997, 36, 2372.
- 117 James, B. R.; Morris, R. H. *Can. J. Chem.* 1980, 58, 399.
- 118 Calligaris, M.; Faleschini, P.; Todone, F.; Alessio, E.; Geremia, S. *J. Chem. Soc. Dalton Trans.* 1995, 1653.
- 119 Abrahams, S. C. *Acta Cryst.* 1957, 10, 417.
- 120 Stynes, H. C.; Ibers, J. A. *Inorg. Chem.* 1971, 10, 2304.
- 121 (a) DeSimone, R. E.; Glick, M. D. *Inorg. Chem.* 1978, 17, 3574;
(b) Schröder, M. *Pure Appl. Chem.* 1988, 60, 517.
- 122 Lucas, C. R.; Shuang, L.; Newlands, M. J.; Charland, J-P.; Gabe, E. J. *Can. J. Chem.* 1988, 66, 1506.
- 123 (a) Lucas, C. R.; Liu, S.; Newlands, M. J.; Charland, J-P.; Gabe, E. J. *Can. J. Chem.* 1989, 67, 639;
(b) Lucas, C. R.; Liu, S.; Thompson, L. K. *Inorg. Chem.* 1990, 29, 85;
(c) Lucas, R. C.; Shuang, L.; Newlands, M. J.; Charland, J-P.; Gabe, E. J. *Can. J. Chem.* 1988, 66, 1506.

- 124 Liu, S.; Lucas, C. R.; Newlands, M. J.; Charland, J-P. *Inorg. Chem.* 1990, 29, 4380.
- 125 Wolf Jr., R. E.; Hartman, J. R.; Storey, J. M. E.; Foxman, B. M.; Cooper, S. R. *J. Am. Chem. Soc.* 1987, 109, 4328.
- 126 (a) Rosen, W.; Busch, D. H. *J. Am. Chem. Soc.* 1969, 91, 4694;
(b) Rosen, W.; Busch, D. H. *Inorg. Chem.* 1970, 9, 262.
- 127 Robinson, G. H.; Sangokoya, S. A. *J. Am. Chem. Soc.* 1988, 110, 1494.
- 128 Gorewit, B. V.; Musker, W. K. *J. Coord. Chem.* 1976, 5, 67.
- 129 Blake, A. J.; Holder, A. J.; Reid, G.; Schröder, M. *J. Chem. Soc. Dalton Trans.* 1994, 627.
- 130 Ma, E. S. F. Ph. D. Dissertation, University of British Columbia, Vancouver, 1999.

Chapter 4

Preliminary *In Vitro* Examination of Water-soluble Ru Sulfoxide Complexes

4.1 Introduction

As outlined in Chapter 1, preliminary investigation into the *in vitro* activity of water-soluble ruthenium bis-chelating sulfoxide complexes was suggested by reports of the anti-tumour activity of *cis*- and *trans*- $\text{RuCl}_2(\text{DMSO})_4$,¹ and other Ru-DMSO complexes.^{2,3} These reports show that Ru-sulfoxide complexes exhibit anti-leukaemic,⁴ anti-metastatic⁵ and anti-neoplastic⁶ activity without appreciable toxicities to the murine host. In addition, the complex $\text{Na}[\text{trans-RuCl}_4(\text{DMSO})(\text{Im})]$ exhibits no cytotoxicity in tumour cells; however, it does reduce lung metastasis formation to less than 10 % of that seen in controls.⁷ Studies of reactions between *cis*- and *trans*- $\text{RuCl}_2(\text{DMSO})_4$ and DNA have shown that these complexes accumulate in cells⁸ and bind to bases,⁹ nucleosides,^{10,11} and nucleotides.¹²⁻¹⁴ Durig *et al.*¹⁵ and Gibson *et al.*¹⁶ have studied the ability of Ru complexes to induce filamentous growth in *E. coli*, which is an indication of possible DNA damage, suggesting interaction between the complex and DNA (Section 1.3.1). Previous work in this laboratory has suggested that *trans*- $\text{RuCl}_2(\text{disulfoxide})_2$ ^{8,17} complexes accumulate in cells and bind to DNA to a greater degree than *cis*- $\text{RuCl}_2(\text{disulfoxide})_2$ complexes (chelating disulfoxide = BMSE, BESE, BPSE and BMSP, see Chapter 1). The ability of these complexes to traverse the cell membrane and to bind to DNA are two important considerations, as DNA is considered to be a main target for anti-tumour activity. For example, $\text{Na}[\text{trans-RuCl}_4(\text{DMSO})(\text{Im})]$ interacts with nucleic acids which results in a reduction of nucleic acid activity (Chapter 1).⁷ Complexes which accumulate in the cell and bind to DNA may also exhibit toxicity which is relevant.

The toxicities, accumulation and DNA-binding characteristics in Chinese hamster ovary (CHO) cells (under oxic and hypoxic conditions) of selected Ru-sulfoxides are presented in this chapter. The five complexes, discussed in Chapter 3 and listed in Table 4.1 were selected for *in vitro* studies because of solubility in aqueous solutions.

Table 4.1. Water-soluble Ru sulfoxide complexes studied *in vitro*.^a

Complex	Conc. (mM) ^b
[Ru(12-S-4)(DMSO)(H ₂ O)][OTf] ₂	1.5, 3.0 and 5.0
[RuCl(BPSP)] ₂ (μ-Cl) ₃	0.1, 0.5, 1.2 and 1.4
[RuCl(BESE)(H ₂ O)] ₂ (μ-Cl) ₂	0.1, 0.5, 0.64 and 1.4
[RuCl(BPSE)(H ₂ O)] ₂ (μ-Cl) ₂	0.25 and 0.42
[RuCl(BBSE)(H ₂ O)] ₂ (μ-Cl) ₂	0.16, 0.5 and 0.89

^a See Chapter 3, Sections 3.7, 3.8 and 3.11.4 for formulations of the complexes.

^b Concentrations of the complex used in buffered aqueous solutions, chosen in relation to the amount of complex available for repeat experiments (at least two experiments, same concentrations) and in a range for possible toxicity.

4.2 Tumour Hypoxia, Radiotherapy and Progression

One characteristic of many solid tumour masses is a poor blood supply which results in inadequate levels of both oxygen and nutrients in regions of the tumour.¹⁸ The degree of hypoxia within tumours varies according to the proximity of blood vessels in a rapidly growing tumour in which development of vasculature does not keep up with cell proliferation and where rapid replication of cancer cells deplete O₂.^{19,20} If the cells are too far from the capillaries for effective delivery of nutrients and oxygen and for elimination for

wastes, necrotic regions can result. Hypoxia can also be the result of periodic suspension of blood flow because of irregularities and occlusions in the tumour vasculature and the high interstitial pressure of tumours with poorly developed lymphatic systems.^{19a,b} Normal or malignant tissue that is poorly supplied with oxygen at the time of conventional radiotherapy (e.g. ionizing radiation such as X-rays) is much less damaged by a given dose of radiation than the same well-oxygenated tissue. Thus hypoxic mammalian tissue may only be one-half to one-third as sensitive to radiation compared to well-oxygenated tissue.²¹ Radiotherapy may remove the oxygenated areas of a tumour while the hypoxic areas, being radioresistant and not having received as much radiation damage, become reoxygenated, and recommence growth and regenerate the tumour.¹⁹

Hypoxia also has an effect on malignant progression and the responsiveness to therapy of advanced cervical tumours.²² Höckel *et al.* have studied the effect of hypoxia on metastasis and survival probabilities of patients. Those with hypoxic tumours exhibited relatively inferior survival probability compared with those with non-hypoxic cervical cancers. The authors suggest that tumour oxygenation acts as a prognostic indicator of malignant progression in terms of tumour metastasis (as well as radioresistance) in advanced cervical cancers.²²

Radiotherapy is effective against localized neoplasms but is not effective toward a widely disseminated disease (*e.g.* leukemia), mainly because a curative dose will cause too much damage to the surrounding healthy tissue.¹⁹ There are certain clinical situations in which the use of radiotherapy is limited by a radioresistant neoplasm or by a tumour that has invaded radiosensitive normal tissue. Again, a curative dose of radiation may cause excessive damage to normal tissue.

Hypoxic cells of solid neoplasms may be unresponsive to conventional chemotherapy.¹⁹ The proliferation patterns of hypoxic tumour cells probably differ from those of the oxic cells, in that many hypoxic cells are non-cycling or are cycling with prolonged and abnormal cell cycle times. Such cells would have reduced sensitivities to cycle-active chemotherapeutic agents.¹⁹ As well, hypoxic cells are found in regions of vascular deficiency and may not be exposed to the chemotherapeutic agents which are mainly distributed through the vascular system.

4.3 Experimental

All media, buffer solutions and drug solutions were sterilized by filtration through a 0.22 μm filter (Nalgene) before cell suspensions were added. All flasks and humidifiers were sterilized in a BBMC Century 21 Laboratory Sterilizer.

4.3.1 Media

An alpha-modification of Eagle's minimum essential medium (Gibco) was used in all procedures involving the maintenance or incubation of CHO cells. Three different forms of the medium were used, α -/-, α +/- and α +/+ depending on the requirements of the procedure.

To make α -/- medium, one packet of α -medium powder and 10,000 units of penicillin/streptomycin antibiotic (Gibco) were added to 10 L of doubly distilled water and the solution was stirred for 2 h at r.t. and pH adjusted to 7.3. Preparation of α +/+ medium involved the addition of fetal bovine serum (Gibco) to a final concentration of 10 % and NaHCO_3 (20 g/10 L) was added to the solution before filtration; then the pH was adjusted to 7.3 with 4 M aq. NaOH. Preparation of α +/- medium involved the addition of 10 % (v/v) of fetal bovine serum to α -/- medium buffered with 10 mM HEPES. All media were stored at 4 °C.

4.3.2 Phosphate Buffer Saline Solution

To prepare the phosphate buffer saline solution (PBS), NaCl (160 g), KCl (4 g), Na_2HPO_4 (23 g) and KH_2PO_4 (4 g) were dissolved in distilled water (20 L); the solution was stored at r.t. and cooled to 4 °C before use.

4.3.3 Methylene Blue Solution

Methylene blue (2 g, Sigma) was dissolved in H_2O (1 L) and the solution allowed to stand for 1 h prior to filtration. This solution was used for fixing and staining colonies after incubation to assess colony forming ability. The methylene blue solution was filtered after use in toxicity experiments and re-used several times before being discarded.

4.3.4 Tris-EDTA (TE) Solutions

Stock solutions of TE (0.5 M Tris-HCl, Sigma and 50 mM EDTA, Sigma) were prepared, and the pH of the solutions adjusted to 8.0 with 4 M NaOH. The stock solutions were then diluted to the final concentration of 10 μ M Tris-HCl and 1 μ M EDTA.

4.3.5 TNE Solutions

TNE was prepared from stock solutions and had a final composition of 10 mM Tris-HCl (Sigma), 150 mM NaCl and 10 mM EDTA (Sigma), with the final pH of the solution being adjusted to 8.0.

4.3.6 TNE-Equilibrated Phenol

Pure phenol (250 mL, 99 %, Aldrich) was liquefied by heating in a water-bath (60 °C) and saturated with an equal volume of 0.5 M Tris-HCl (250 mL, pH 8.00, Sigma), the two phases then being allowed to separate. The aqueous layer was discarded and the process repeated with fresh Tris-HCl solutions until the pH of the aqueous layer was about 7.0. The final wash consisted of equal volumes of TNE and phenol. The TNE-equilibrated phenol was then transferred into 50 mL polypropylene tubes and stored at -20 °C in darkness. The frozen stock was thawed to r.t. just prior to use in the DNA-extraction experiments.

4.3.7 Cell Preparation

The cells used for *in vitro* experiments were obtained from a Chinese hamster ovary (CHO) cell line, chosen for its rapid growth cycle and high plating efficiency. The cells (1.3 x 10⁵ cells/mL) were routinely grown in α +/- medium (~60 mL) (Section 4.3.1), and the cell

suspensions were maintained in spinner culture flasks at 37 °C in an Associated Biomedic Systems "Incu-cover" incubator under an atmosphere of 95 % air/5 % CO₂ (Canadian Liquid Air Co. Ltd.). Spinner flasks were diluted twice a week, and 1×10^5 cells were plated in T-75 flasks (Falcon) once a week as backups in the event that the spinner culture was contaminated. The cell cultures were diluted daily to a cell count of about 1×10^5 cells/mL to maintain an exponential growth phase cell population (doubling time was about 13-14 h); higher cell suspensions were prepared if a larger number of cells was required the following day. The cell suspension (cells/mL) was determined using a Coulter Cell Counter from Coulter Electronics Inc., Hialeah, Florida.

4.3.8 Atomic Absorption Spectroscopy

A Varian "SpectrAA 300" atomic absorption spectrometer, controlled by a Compaq Deskpro 386s computer, was used to analyze for the Ru atoms. A Ru hollow cathode lamp, λ 265.9 nm (Varian), was used as the source. The samples were dried, ashed and atomized in graphite tube furnaces (Varian). Corrections for background absorption were done using a technique, developed by Varian, based on the Zeeman effect. Calibration of the spectrometer was completed by using Ru standards (Sigma). A reslope was performed after every fifth sample to ensure that buildup on the pyrolytic graphite surface did not cause significant variations in the calibration. The furnace parameters used in the drying, ashing, and atomization stages of the analysis are tabulated below in Table 4.2.

Table 4.2. Furnace parameters used in AAS for Ru, at λ 265.9 nm.

Step No.	Temp. (°C)	Time (s)	Gas Flow	Gas Type	Read Command
1	90	20.0	3.0	Ar	No
2	100	5.0	3.0	Ar	No
3	120	15.0	3.0	Ar	No
4	500	15.0	3.0	Ar	No
5	1100	5.0	3.0	Ar	No
6	1100	10.0	3.0	Ar	No
7	1100	0.5	0.0	Ar	No
8	2800	0.9	0.0	Ar	Yes
9	2800	2.0	0.0	Ar	Yes
10	2800	2.0	3.0	Ar	No

4.3.9 Cell Incubation Procedures

The required number of cells was harvested from the culture solution using a centrifuge (Sorvall RC-3, 600 rpm, 80 g at 4 °C for 7 min, where g = gravity = relative centrifugal factor = $28.38(R)(N/1000)^2$, R = 23.11 cm and N = rpm). The cells were then resuspended in α +/- medium and added to solutions of the complexes previously made up in the same media. The incubation conditions and sampling frequencies were varied depending on the experiment being performed. The cells were incubated with solutions of the complexes (10 mL) at a cell suspension of about $3.0 - 3.7 \times 10^5$ cells/mL in standard Erlenmeyer flasks

fitted with a modified rubber stopper to introduce a flow of gas (through a syringe needle) and made for easy sampling (through a stoppered glass tube). The solutions were maintained at 37 °C in a Labline Instruments "Orbit Shaker Bath" which is a modified water-bath designed to rotate the flasks continuously but gently. For assessment under hypoxic conditions, N₂ was passed over the flasks for 1 h before introduction of the cells into the flasks, which contained solutions of the complexes, and this was maintained during the experiment (oxygen-free N₂ (Linde Specialty Gas, Union Carbide)). For aerobic experiments, air (filtered through a cotton plug) was passed over the suspensions and this prevented build up of CO₂ due to cellular respiration. Both gases were humidified in a glass bubbler filled with sterile water maintained at 37 °C.

4.3.10 Cell Toxicity Assays Under Oxic and Hypoxic Conditions

The toxicities of the complexes in CHO cells under air and under N₂ were measured by comparing the plating efficiency of cells as a function of concentration (2 h) with those incubated in control solutions. CHO cell suspensions (approximately 3.5×10^5 cells/mL in α +/-) with the appropriate complex were incubated for a period of 2 h at 37 °C. Thereafter, samples (1 mL) were taken from each flask, diluted immediately in fresh α -/- media (10 mL, 0 °C), and pelleted. The supernatant was decanted and the cells resuspended in fresh α -/- medium (10 mL, 0 °C). An aliquot (2 mL) of this cell suspension was then diluted in PBS (10 mL, 0 °C), and the cell suspension determined using the Coulter Counter.

Aliquots of this cell solution (typically 10, 100, and 1000 μ L) were then plated onto Petri dishes (Falcon), prepared previously by filling with α +/+ medium (5 mL) and left to

equilibrate in a tray incubator (National Inc.) maintained at 37 °C with a 95 % air/5 % CO₂ gas flow. The dishes were then incubated in the tray incubator for 7 days for the cells to form colonies. The α +/+ medium was then discarded, and the colonies stained with methylene blue solution for ~7 min; the stain was then decanted, and the dishes rinsed with cold water. The number of colonies per dish was counted, and the plating efficiency (PE = number of colonies/number of cells plated) was calculated.

4.3.11 Cell Accumulation Assays

The remaining 9 mL cell solution from the cell toxicity studies (2 h, 37 °C, Section 4.3.10) were pelleted by centrifugation and the supernatant discarded (2 h). The cells were then washed twice with PBS (10 mL, 0 °C) to remove unbound complex, and then resuspended in PBS (7.5 mL, 0 °C). At this point the samples were vortexed and then separated into three portions into polypropylene tubes: a 3 mL fraction was used for cell accumulation, 4 mL for the DNA-binding assay (Section 4.3.12) and the remaining 0.5 mL to determine the population of cells (200 μ L of the cell suspension being added to 20 mL of PBS).

The cells for the accumulation assay were pelleted, the supernatant decanted, and the cell pellet air-dried overnight at 37 °C. Concentrated HNO₃ (50 μ L) was then added to the cell pellet, and the acid mixture vortexed vigorously and left at 37 °C overnight to enhance digestion of the cell pellet. TE buffer (250 μ L, pH 8.0) was then added to the digested cell solutions, and the mixtures analyzed for Ru content using atomic absorption. The analytical

results were first calculated as ng Ru/mL and then expressed as ng (Ru)/10⁶ cells (using the cell counts).

4.3.12 DNA-Binding Assays

The 4 mL sample obtained from the toxicity assay (Section 4.3.10) was pelleted, the supernatant decanted, and 1 mL of a solution made up of 10 mL TNE, 0.2 mL RNase (10 mg/mL, Sigma), 0.2 mL 10 % S.D.S (sodium dodecyl sulfate, Sigma) and 0.2 mL Proteinase K (10 mg/mL, Sigma) was then added while the pellet was vortexed. The samples were stored at 37 °C overnight to ensure the cells were fully digested. The following day, each sample was sonicated for ~ 8 s and then extracted with washes (2 x 1 mL) of TNE-equilibrated phenol. The samples were centrifuged (5 min at 1000 rpm, 200 g) to ensure that the separation between the aqueous and organic layer was well defined. The samples were then washed (2 x 1 mL) with CHCl₃ containing 4 % *iso*-amyl alcohol. The DNA was precipitated by adding 99.5 % EtOH (2 mL), vortexing and cooling the solution to -20 °C for at least 2 h. The precipitated DNA was pelleted by centrifugation (30 min at 3000 rpm, 2300 g, 4 °C), the supernatant decanted and the pelleted DNA air-dried. The dried DNA was then re-hydrated in 200 µL of TE and analyzed for Ru content using atomic absorption; the amount of Ru bound was normalized to the amount of DNA present which was determined by measuring the optical density (OD) of the re-hydrated DNA solutions using a dilution of 20 µL with 980 µL TE at 260 nm. The analytical results were first calculated as ng (Ru)/mL and then expressed as ng (Ru)/mg (DNA).

4.4 *In Vitro* Studies of Five Ru Sulfoxides (Table 4.1): Preliminary Results in CHO Cells

4.4.1 Toxicity of Ru Sulfoxides in CHO Cells under Oxic and Hypoxic Conditions

A study was undertaken to determine whether the presence of oxygen might affect the toxicity of the Ru sulfoxide complexes. The toxicity of the complexes in CHO cells was measured as PE, after an incubation time of 2 h in the solutions of the complexes (Section 4.3.10). The toxicity is expressed in terms of the PE as a function of concentration. None of the complexes listed in Table 4.1 exhibited significant toxicity in CHO cells, after an incubation time of 2 h at the concentrations tested under oxic or hypoxic conditions (see Figure 4.1 for an example).

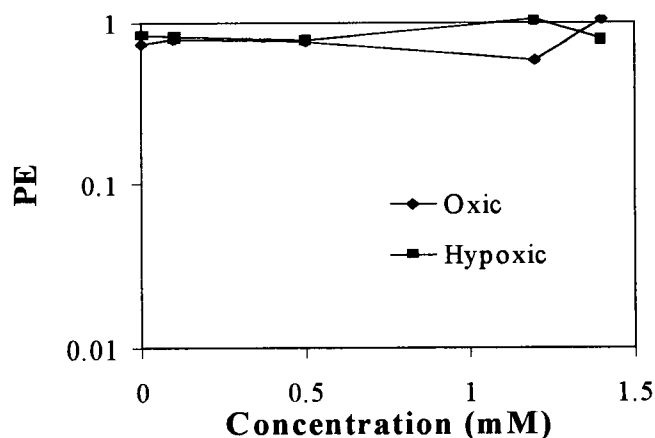


Figure 4.1. The absence of toxicity of $[\text{RuCl}(\text{BPSP})]_2(\mu\text{-Cl})_3$ in CHO cells.

Similar results were obtained by Yapp *et al.* in that no significant toxicity was observed for Ru sulfoxide complexes of the type *cis*- and *trans*- $\text{RuCl}_2(\text{sulfoxide})_4$ and

$\text{RuCl}_2(\text{disulfoxide})_2$ (sulfoxide = DMSO and TMSO, 1.0 mM; disulfoxide = BMSE (1.0 mM), BESE (0.5 mM), BPSE (0.5 mM) and BMSP (1.0 mM)) toward CHO cells *in vitro*.^{8,17}

4.4.2 Ruthenium Accumulation Under Oxidic and Hypoxic Conditions

Simultaneously, the effect of oxidic or hypoxic conditions on the accumulation of the Ru sulfoxide complexes was examined. The results indicate the gross amount of Ru present (up to 2 h) in the whole cell (expressed at ng (Ru)/ 10^6 cells), and are presented as a plot of ng (Ru)/ 10^6 cells vs. concentration (mM) (Figure 4.2(A)); the accumulation (of Ru) plots of the individual complexes are presented in Appendix 4). The errors were calculated using the average of repeat experiments (a minimum of 2) performed (*e.g.* control $\pm 20\%$). The results indicate that Ru does accumulate in CHO cells but there is no difference for these complexes between accumulation under oxidic or hypoxic conditions. Yapp *et al.* observed linear profiles for the accumulation of selected Ru-sulfoxide complexes in CHO cells for periods up to 6 h,^{8,17} implying that the accumulation had not yet reached equilibrium or that the complex was being bound irreversibly to some cellular component.

The accumulation of Ru (ng (Ru)/ 10^6 cells) was estimated for 0.5 mM concentration for each of the complexes studied and was compared to those of the Ru-sulfoxides previously studied by Yapp *et al.*^{8,17} For a comparison, these values were estimated assuming a linear response for accumulation over the concentration range up to 1.0 mM to facilitate this preliminary comparison (Figure 4.3(A)).

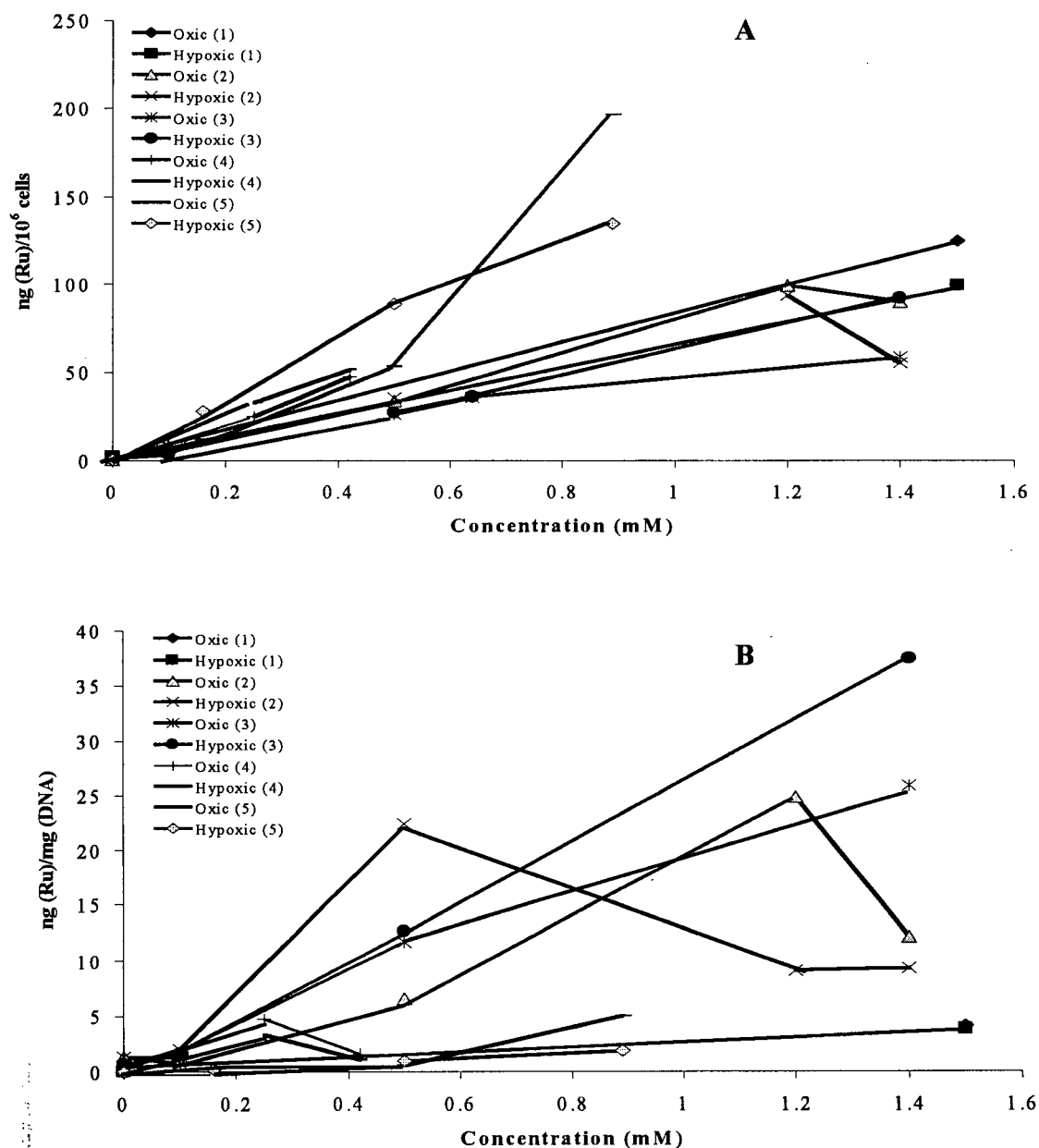


Figure 4.2. Accumulation of Ru (A) and Ru-DNA-binding (B) in CHO cells after 2 h incubation with $[\text{Ru}(12\text{-S-4})(\text{DMSO})(\text{H}_2\text{O})][\text{OTf}]_2$ (1), $[\text{RuCl}(\text{BPSP})]_2(\mu\text{-Cl})_3$ (2), $[\text{RuCl}(\text{BESE})(\text{H}_2\text{O})]_2(\mu\text{-Cl})_2$ (3), $[\text{RuCl}(\text{BPSE})(\text{H}_2\text{O})]_2(\mu\text{-Cl})_2$ (4), $[\text{RuCl}(\text{BBSE})(\text{H}_2\text{O})]_2(\mu\text{-Cl})_2$ (5).

Comparison of accumulation of Ru in CHO cells shows that the mononuclear Ru bis-disulfoxide complexes^{8,17} generally accumulate to a lesser degree relative to the corresponding dinuclear Ru sulfoxides (9-12), with the exception of *trans*-RuCl₂(BPSE)₂ (6) which exhibits a higher accumulation than [RuCl(BPSE)(H₂O)]₂(μ-Cl)₂ (11). [Ru(12-S-4)(DMSO)(H₂O)][OTf]₂ (8), [RuCl(BPSP)]₂(μ-Cl)₃ (9) and [RuCl(BPSE)(H₂O)]₂(μ-Cl)₂ (11) accumulate in CHO cells to a similar extent under both oxic and hypoxic conditions. [RuCl(BESE)(H₂O)]₂(μ-Cl)₂ (10) also accumulates in CHO cells to a similar extent under both oxic and hypoxic conditions; however, relatively less than that of 8, 9, 11 or 12. [RuCl(BBSE)(H₂O)]₂(μ-Cl)₂ (12) exhibits the greatest degree of accumulation under hypoxic conditions. Although (10) exhibits only moderate cellular accumulation, however, it is ~10 times greater than the accumulation of the corresponding mononuclear complex, *cis*-RuCl₂(BESE)₂ (5).

4.4.3 DNA-binding Under Oxic and Hypoxic Conditions

The extent of Ru binding to DNA, and the possible enhancement in hypoxic conditions, were examined. The results are presented as the gross amount of Ru bound to the extracted DNA (expressed at ng (Ru)/mg (DNA)) vs. concentration (mM) (Figure 4.2(B); the Ru-DNA-binding plots of the individual complexes are presented in Appendix 5). Again, the errors were calculated using the average of repeat experiments (a minimum of 2) performed (*e.g.* control \pm 20 %). Ru appears to bind to DNA without significant difference between DNA-binding under oxic or hypoxic conditions. The DNA-binding of Ru studied for complexes $[\text{RuCl}(\text{BPSP})]_2(\mu\text{-Cl})_3$ and $[\text{RuCl}(\text{BPSE})(\text{H}_2\text{O})]_2(\mu\text{-Cl})_2$ decreased at high concentrations possibly because of incomplete extraction of the DNA using the protocol described in Section 4.3.12.

As with the cell accumulation, the binding of Ru to DNA (ng (Ru)/mg DNA) was estimated for 0.5 mM concentration (see Section 4.4.2) for a period of 2 h for each of the complexes studied. The findings are compared to complexes 1-7 of Yapp *et al.*^{8,17} (Figure 4.3(B) (studied only under oxic conditions after an incubation period of 4 h).

Figure 4.3(B) shows that the complexes 9-12 from this present study exhibit greater binding of Ru to DNA than the previously studied Ru-sulfoxide complexes.^{8,17}

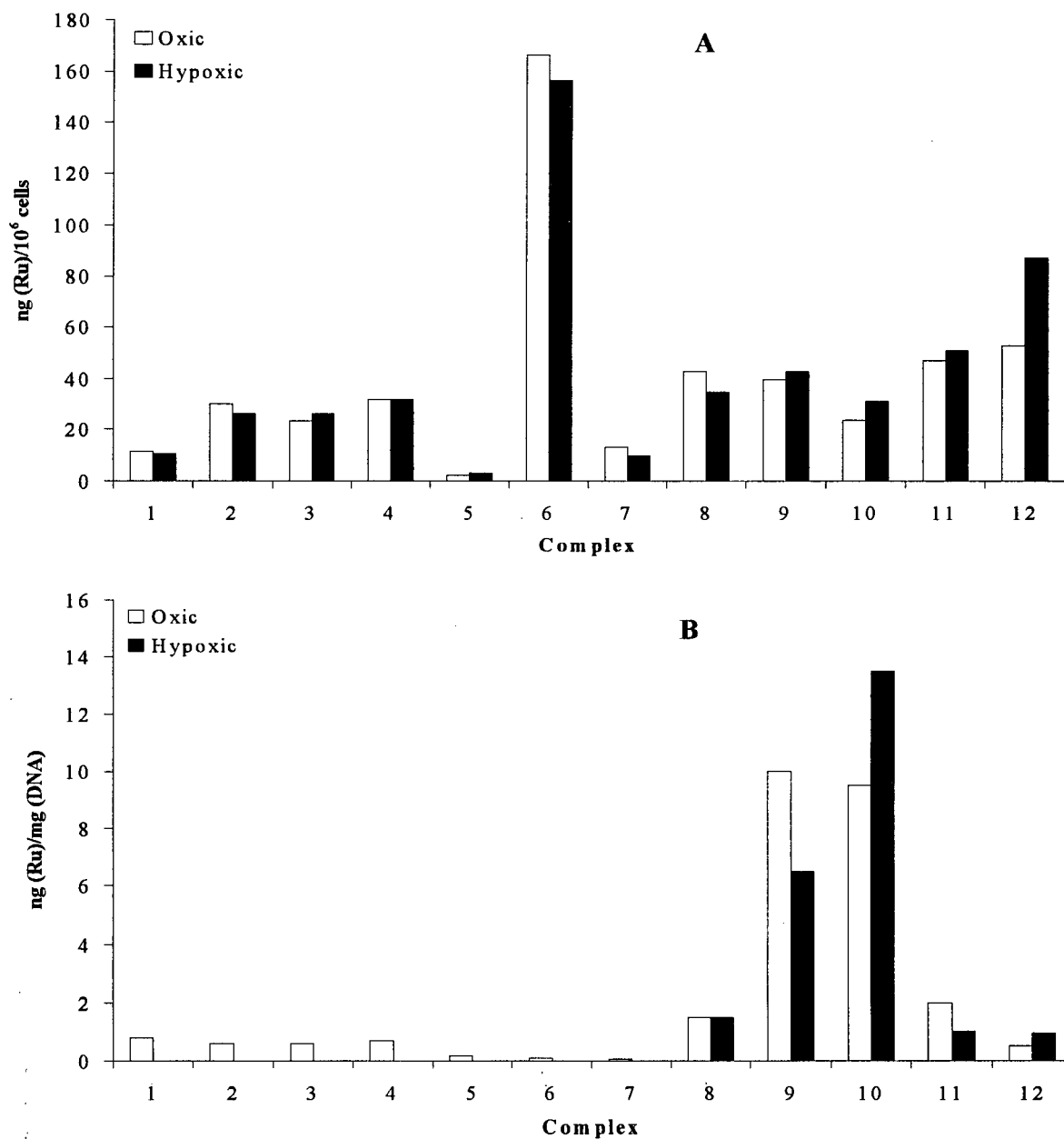


Figure 4.3. Accumulation (A) and DNA-binding (B) with 0.5 mM of Ru complex. 1 = *cis*-RuCl₂(DMSO)₄, 2 = *trans*-RuCl₂(DMSO)₄, 3 = *cis*-RuCl₂(TMSO)₄, 4 = *trans*-RuCl₂(BMSE)₂, 5 = *cis*-RuCl₂(BESE)₂, 6 = *trans*-RuCl₂(BPSE)₂, 7 = *cis*-RuCl₂(BMSP)₂, 8 = [Ru(12-S-4)(DMSO)(H₂O)][OTf]₂, 9 = [RuCl(BPSP)]₂(μ-Cl)₃, 10 = [RuCl(BESE)(H₂O)]₂(μ-Cl)₂, 11 = [RuCl(BPSE)(H₂O)]₂(μ-Cl)₂, 12 = [RuCl(BBSE)(H₂O)]₂(μ-Cl)₂. (Data for 1-7 taken from refs. 8 and 17; for 1-7 (B) a 4 h incubation period was used and a 2 h incubation period was used for 8-12 (B)).

Although $[\text{Ru}(\text{12-S-4})(\text{DMSO})(\text{H}_2\text{O})][\text{OTf}]_2$ (**8**) and $[\text{RuCl}(\text{BPSP})]_2(\mu\text{-Cl})_3$ (**9**) show similar whole cell accumulation at 0.5 mM (Section 4.4.2), DNA-binding of **8** is much less than that of **9**. It is interesting to note that greater uptake is not necessarily reflected in greater DNA-binding. This suggests that **8** accumulates elsewhere in the cell while **9** shows some binding to DNA.

While $[\text{RuCl}(\text{BESE})(\text{H}_2\text{O})]_2(\mu\text{-Cl})_2$ (**10**) exhibits somewhat less accumulation than **9** (Section 4.4.2), the DNA-binding of the two complexes is similar with **10** binding somewhat to a greater extent than **9** at 0.5 mM. Complex **10** exhibits greater accumulation than *cis*- $\text{RuCl}_2(\text{BESE})_2$ (**5**) in the whole cell by a factor of ~ 10 (Section 4.4.2) and the DNA-binding of **10** is ~ 100 times greater than for **5** (under oxic conditions). The DNA-binding of **10** is the highest (hypoxic conditions) of all the complexes studied.

While $[\text{RuCl}(\text{BPSE})(\text{H}_2\text{O})]_2(\mu\text{-Cl})_2$ (**11**) exhibited moderate accumulation and $[\text{RuCl}(\text{BBSE})(\text{H}_2\text{O})]_2(\mu\text{-Cl})_2$ (**12**) exhibited the highest accumulation (Section 4.4.2), the DNA-binding of these two complexes is relatively small. The data suggest that these complexes accumulate in the cell, but not by extensive binding to DNA. Of note, **11** exhibits DNA-binding that is ~ 10 times greater than that of the corresponding mononuclear complex, *trans*- $\text{RuCl}_2(\text{BPSE})_2$ (**6**), yet the latter exhibits greater accumulation (Section 4.4.2). This suggests that **6** accumulates in the whole cell but exhibits less DNA binding.

4.5 Conclusions

The biological assays present a preliminary survey of the biological activity of these five complexes. The complexes do enter CHO cells, bind to DNA, but are non-toxic at the concentrations tested. Furthermore, no hypoxic selectivity was observed in CHO cells with respect to the toxicity, cell accumulation and DNA-binding assays. A high degree of DNA-binding (*e.g.* with $[\text{RuCl}(\text{BPSP})]_2(\mu\text{-Cl})_3$ and $[\text{RuCl}(\text{BESE})(\text{H}_2\text{O})]_2(\mu\text{-Cl})_2$) does not necessarily depend on an equally high degree of accumulation in whole cells. While there are insufficient data to rationalize the *in vitro* behaviour of the complexes, the results do suggest future studies.

Yapp *et al.*^{8,17} have shown previously that *trans* Ru bis-chelating disulfoxide and DMSO complexes exhibit more accumulation and DNA-binding than *cis* complexes. The new data show that the dinuclear Ru sulfoxides generally accumulate to a greater degree than the *trans* complexes (with the exception of *trans*- $\text{RuCl}_2(\text{BPSE})_2$) and *cis*- or *trans*- $\text{RuCl}_2(\text{DMSO})_4$, both of which have shown anti-tumour effects and binding to DNA without appreciable toxicity to the murine host (Chapter 1). The new complexes bind to DNA up to 270 times more than the complexes studied by Yapp *et al.*,^{8,17} and ~ 16 and ~ 23 times more than *cis*- and *trans*- $\text{RuCl}_2(\text{DMSO})_4$, respectively.

The *in vitro* results suggest that these water-soluble, Ru sulfoxide complexes, which are non-toxic toward CHO cells but yet show binding to DNA, may possess anti-tumour activity similar to that of complexes studied by Sava *et al.*,¹ Alessio *et al.*,² and Mestroni³.

4.6 References for Chapter 4

- 1 Sava, G. Ruthenium Compounds in Cancer Therapy, in *Metal Compounds in Cancer Therapy* (ed. S Fricker), Chapman and Hall, London, 1994, p. 80.
- 2 Alessio, E.; Balducci, G.; Calligaris, M.; Costa, G.; Attia, W. H.; Mestroni, G. *Inorg. Chem.* 1991, *30*, 609.
- 3 Mestroni, G. The Development of Tumour-Inhibiting Ruthenium Dimethylsulfoxide Complexes, in *Metal Complexes in Cancer Chemotherapy* (ed. B. K. Keppler), VCH, Weinheim, 1993, p. 157.
- 4 Coluccia, M.; Sava, G.; Loseto, F.; Nassi, A.; Boccarelli, A.; Giordano, D.; Alessio, E.; Mestroni, G. *Eur. J. Cancer* 1993, *29*, 1873.
- 5 (a) Sava, G.; Pacor, S.; Mestroni, G.; Alessio, E. *Clin. Exp. Metastasis* 1992, *10*, 273;
(b) Gagliardi, R.; Sava, G.; Pacor, S.; Mestroni, G.; Alessio, E. *Clin. Exp. Metastasis* 1994, *12*, 93;
(c) Sava, G.; Capozzi, I.; Clerici, K.; Gagliardi, G.; Alessio, E.; Mestroni, G. *Clin. Exp. Metastasis* 1998, *16*, 371.
- 6 (a) Sava, G.; Zoret, S.; Giraldi, T.; Mestroni, G.; Zassinovich, G. *Eur. J. Cancer Clin. Oncol.* 1984, *20*, 841;
(b) Pacor, S.; Sava, G.; Ceschia, V.; Bregant, F.; Mestroni, G.; Alessio, E. *Chem. Biol. Interactions* 1991, *78*, 223.
- 7 Sava, G.; Capozzi, I.; Bergamo, A.; Gagliardi, R.; Cocchietto, M.; Masiero, L.; Onisto, M.; Alessio, E.; Mestroni, G.; Garbisa, S. *Int. J. Cancer* 1996, *68*, 60.
- 8 Yapp, D. T. T. Ph. D. Dissertation, University of British Columbia, Vancouver, 1993.
- 9 Khan, B. T.; Mehmood, A. *J. Inorg. Nucl. Chem.* 1978, *40*, 1938.
- 10 Alessio, E.; Xu, Y.; Cauci, S.; Mestroni, G.; Quadrifoglio, F.; Viglino, P.; Marzilli, L. *G. J. Am. Chem. Soc.* 1989, *111*, 7068.
- 11 Davey, J. M.; Moerman, K. L.; Ralph, S. F.; Kanitz, R.; Sheil, M. M. *Inorg. Chim. Acta* 1998, *281*, 10.
- 12 Sherman, S. E.; Lippard, S. J. *Chem. Rev.* 1987, *87*, 1153.

- 13 Esposito, G.; Cauci, S.; Fogolari, F.; Alessio, E.; Scocchi, M.; Quadrifoglio, F.; Viglino, P. *Biochem.* 1992, *31*, 7094.
- 14 Tian, Y-N.; Yang, P.; Li, Q-S.; Guo, M-L.; Zhao, M-G. *Polyhedron* 1997, *16*, 1993.
- 15 Durig, J. R.; Danneman, J.; Behnke, W. D.; Mercer, E. E. *Chem. Biol. Interact.* 1976, *13*, 287.
- 16 Gibson, J. F.; Poole, R. K.; Hughes, M. N.; Rees, J. F. *Arch. Microbiol.* 1984, *139*, 265.
- 17 Yapp, D. T. T.; Rettig, S. J.; James, B. R.; Skov, K. A. *Inorg. Chem.* 1997, *36*, 5635.
- 18 (a) Vaupel, P.; Fortmeyer, H. P.; Runkel, S.; Kallinowski, F. *Cancer Res.* 1987, *47*, 3496;
(b) Vaupel, P.; Kallinowski, F.; Okunieff, P. *Cancer Res.* 1989, *49*, 6449.
- 19 (a) Denny, W. A.; Wilson, W. R. *J. Med. Chem.* 1986, *29*, 879;
(b) Chaplin, D. J. *Int. J. Radiat. Oncol. Biol. Phys.* 1992, *22*, 685;
(c) Brown, J. M.; Giaccia, A. J. *Int. J. Radiat. Biol.* 1994, *65*, 95.
- 20 Kennedy, K. A.; Teicher, B. A.; Rockwell, S.; Sartoelli, A. C. *Biochem. Pharmacol.* 1980, *29*, 1.
- 21 Gray, L. H.; Conger, A. D.; Ebert, M.; Hornsey, S.; Scott, O. C. A. *Br. J. Radiol.* 1953, *26*, 638.
- 22 Höckel, M.; Schlenger, K.; Aral, B.; Mitze, M.; Schäffer, U.; Vaupel, P. *Cancer Res.* 1996, *56*, 4509.

Chapter 5

Metallation of Free-base Porphyrins

5.1 Introduction

Water-soluble porphyrins have potential to interact with biological systems and can be involved, for example, in double-stranded cleavage of DNA, photochemical oxidations, photodynamic therapy, and photoinduced intramolecular electron- and energy transfer.¹ The radiosensitizing properties of metalloporphyrins^{2,3} and the anti-tumour activity of certain ruthenium complexes (see Sections 1.3 and 1.4 and ref. 4) have been reported. Porphyrins have been shown to accumulate at tumours,⁵ and ruthenium(II) complexes have been shown to bind to DNA (see Sections 1.3 and 1.4). Combining the accumulating properties of porphyrins at a tumour and the binding properties of a ruthenium(II) centre to DNA provides an approach to Ru(porphyrin) systems that offer potential for both radiosensitizing and chemotherapeutic activity (see Section 1.3.2).

5.1.1 Metalloporphyrins as Hypoxic Radiosensitizers

Water-soluble porphyrins have been reported to accumulate at tumour tissue⁵ (although this remains controversial), and compounds containing methylpyridinium, sulfonato or carboxylato substituents, and their metal complexes, have been reported to be moderate radiosensitizers.² Synthetic, water-soluble porphyrins and their metalloporphyrin derivatives with Co(III), Cu(II), Ru(II) and Pt(II) have been synthesized and evaluated as hypoxic agents, especially as cytotoxins and radiosensitizers.³ Of the porphyrins studied, the Co(III) complexes exhibited some selective toxicity and radiosensitizing activity toward CHO cells.³

Ru(II) porphyrins were included in the study³ as complexes of Ru have been recognized for their anti-tumour activity.^{6,7}

5.2 Ruthenium Porphyrins

Fleischer *et al.* synthesized the first Ru porphyrin in 1969 (reported as $[\text{Ru}(\text{TPhP})\text{Cl}(\text{CO})]^\dagger$) by bubbling CO through an EtOH solution of $\text{RuCl}_3 \cdot 3\text{H}_2\text{O}$ for 3 h, then adding a glacial acetic acid solution of H_2TPhP and refluxing the solution for 21 h;⁸ however, in 1971 Chow and Cohen reformulated the material correctly as $\text{Ru}(\text{TPhP})(\text{CO})$, after a synthesis using either $\text{Ru}_3(\text{CO})_{12}$ or $[\text{RuCl}_2(\text{CO})_3]_2$ as the precursor with H_2TPhP in refluxing acetic acid or propionic acid under N_2 for 24 h.⁹

Synthetic methods for the insertion of Ru into porphyrins remain largely based on modifications of the original procedures.⁸⁻¹⁰ These all produce stable Ru(II) carbonyl species, which are formed by the interaction of the free base porphyrin, $\text{H}_2(\text{Porp})$, with the ruthenium precursors $\text{Ru}_3(\text{CO})_{12}$ or $\text{RuCl}_3 \cdot 3\text{H}_2\text{O}$, either in the presence or absence of a CO atmosphere. The thermolysis of $\text{Ru}_3(\text{CO})_{12}$ in the presence of $\text{H}_2(\text{Porp})$ remains the most common method of synthesis.¹¹

Massoudipour and Pandey have synthesized $\text{Ru}(\text{TPhP})(\text{CO})(\text{EtOH})$ utilizing $\text{RuCl}_3 \cdot 3\text{H}_2\text{O}$ as the metallation agent by refluxing a solution of 50:50 % vol. ethyl glycol/formaldehyde under N_2 until the colour of the solution changed to pale yellow. This solution was reduced in volume and added dropwise to a solution of H_2TPhP over a period of 1 h., with the reaction complete in 30 h.¹²

† TPP and TSPP are normally used as the standard abbreviations for the dianion of 5,10,15,20-tetraphenylporphyrin and -tetrakis(4-sulfonato)phenylporphyrin, respectively, although a more consistent abbreviation for them would be TPhP and TSPhP, as used here.

The only published route to Ru(II) water-soluble porphyrins, *e.g.* the synthesis of $[\text{Ru(II)(TSPhP)(CO)}]^{4-}$ requires refluxing a DMF solution of the free-base, water-soluble porphyrin $[\text{H}_2(\text{TSPhP})]^{4-}$ and $\text{Ru}_3(\text{CO})_{12}$ under Ar for a period of 1-3 weeks,¹³ and by adding 2,4,6-collidine, the reaction time was reduced to 24 h.¹⁴ In addition to the long reaction times, the preparation of the $\text{Ru}_3(\text{CO})_{12}$ precursor requires the stirring of a solution of RuCl_3 under a steady stream of CO for several hours.¹⁵

5.3 A New Route for the Insertion of Ruthenium into Selected Free-base Porphyrins

Work from this group has led to a new, more convenient route to ruthenium(II) water-soluble porphyrin complexes.^{3,16} The reaction time is decreased from 1-3 weeks (see above) to just 24 h and the method does not require an atmosphere of CO at any stage of the preparation, in which the Ru(III) precursor $[\text{Ru(III)(DMF)}_6][\text{OTf}]_3$ ¹⁷ is used. The refluxing of this precursor in DMF in the presence of the free-base, water-soluble porphyrin yields, for example, $\text{Na}_4[\text{Ru(II)(TSPhP)(CO)}] \cdot 4\text{H}_2\text{O}$. The process involves *in situ* reduction of $[\text{Ru(DMF)}_6]^{3+}$, but the nature of this reduction remains unclear.¹⁶ The following non-water-soluble Ru(II)(CO)porphyrin complexes were then synthesized, using $[\text{Ru(III)(DMF)}_6][\text{OTf}]_3$, in this current thesis work: Ru(II)(TPhP)(CO) , Ru(II)(BPhP)(CO) , $\text{Ru(II)(TrPhPyNO)(CO)}$ and Ru(II)(OEP)(CO) (BPhP = dianion of 5,15-bis(phenyl)porphyrin, TrPhPyNO = dianion of 5,10,15-triphenyl-20-(4-pyridyl-*N*-oxide)porphyrin, and OEP = dianion of 2,3,7,8,12,13,17,18-octaethylporphyrin) (Figure 5.1 and Table 5.1).

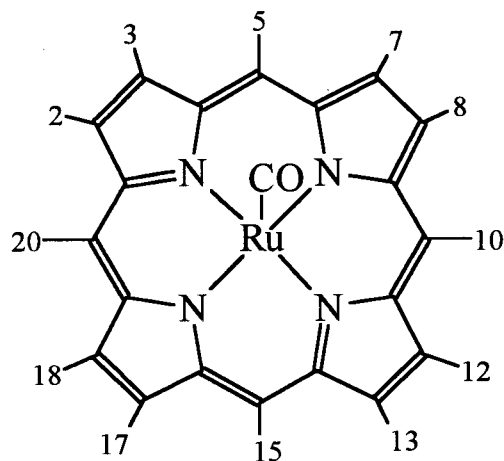


Figure 5.1. Ru(II)(Porp)(CO) species, showing the numbering system.

Table 5.1. Ru(Porp)(CO) species.

Substituent Positions	Porp				
	(TSPhP) ⁴⁻	(TPhP)	(BPhP)	(TrPhPyNO)	(OEP)
5-					H
10-			H		H
15-					H
20-			H		H
2,3,7,8,12,13,17,18-	H	H	H	H	CH ₃ CH ₂

5.4 Experimental

The free-base porphyrin $\text{Na}_4[\text{H}_2\text{TSPHP}] \cdot 15\text{H}_2\text{O}$ was prepared according to a literature procedure.¹⁸ $\text{H}_2(\text{OEP})$ and $\text{H}_2(\text{TPhP})$ were kindly donated by Dr. C. Alexander; $\text{H}_2(\text{BPhP})$, $\text{H}_2(\text{TrPhPyNO})$, $\text{H}_2(\text{TPyP})$, $\text{H}_2(\text{BPhBPyNOP})$, $\text{H}_2(\text{DBrBPhP})$ and $\text{H}_2(\text{PPIXDME})$ were kindly donated by Dr. J. Posakony; and $\text{H}_2(\text{TMP})$ and $\text{H}_2(\text{TPFPhP})$ were kindly donated by Dr. S. Cheng (see Table 5.5 on p. 205 for porphyrin abbreviations). Water was distilled and deionized before use. Silica gel (grade 60, 230-400 mesh) was purchased from BDH. Conc. H_2SO_4 was purchased from Fisher. All other chemicals and reagents used are described in Chapter 2, Section 2.1.

5.4.1 Physical Techniques

The general spectroscopic methods and instrumentation used are described in Chapter 2, Section 2.2. In addition MALDI-TOF was also used as a method of mass spectral analysis. Fluorescence spectroscopic data were obtained using an SLM Aminco 8100 Spectrofluorometer; wavelength maxima, λ_{max} , are given in nm.

5.4.2 Synthesis of Precursors

5.4.2.1 $\text{Na}_4[\text{H}_2\text{TSPHP}] \cdot 15\text{H}_2\text{O}$ ($\text{MW} = 1292.88 \text{ g/mol}$)

$\text{Na}_4[\text{H}_2\text{TSPHP}] \cdot 15\text{H}_2\text{O}$, the free-base porphyrin was synthesized from H_2TPhP and conc. H_2SO_4 according to the procedure reported by Meng *et al.*¹⁸ The purity of the product was determined by UV-Vis and ^1H NMR spectroscopies and TGA. The spectroscopic data are in good agreement with those previously reported.¹⁸ ^1H -NMR ($\text{DMSO}-d_6$, 200 MHz) δ

8.85 (s, 8H, pyrrole *H*), 8.20 (d, 8H, *m*-C₆H₄SO₃⁻), 8.03 (d, 8H, *o*-C₆H₄SO₃⁻), -3.00 (s, 2H, NH). UV-Vis (H₂O) 636 (3.24), 578 (3.79), 550 (3.78), 516 (3.90), 414 (5.03). TGA: Calcd loss of 15H₂O: 20.9. Found: 19.6 % (from ~ 25 to ~ 155°C) (TGA plot is given in Appendix 4, Figure A.4.3).

5.4.2.2 [Ru(DMF)₆][OTf]₃

The synthesis of [Ru(DMF)₆][OTf]₃ was described in Chapter 2, Section 2.5.1.

5.5 Synthesis of Ru(Porp)(CO) Complexes

5.5.1 Na₄[Ru(TSPbP)(CO)]·4H₂O (MW = 1221.95 g/mol)

Na₄[H₂(TSPbP)]·15H₂O (210 mg, 0.205 mmol) was dissolved in DMF (80 mL) and the solution heated to 50 °C under N₂. [Ru(DMF)₆][OTf]₃ (614 mg, 0.622 mmol) was then added and the dark purple solution was heated to reflux under N₂, in the absence of light for 24 h. The resulting dark red solution was concentrated to a minimal volume by rotary evaporation. The product was purified as a purple-red band by column chromatography using silica gel and MeOH as the eluant. The solvent was removed by rotary evaporation, and the purple product was collected and dried *in vacuo* for 1 week. Yield: 133 mg (53 %). Anal. Calcd for C₄₅H₃₂N₄O₁₇S₄Na₄Ru: C, 44.23; H, 2.64; N, 4.58; S, 10.49. Found: C, 44.36; H, 2.70; N, 4.55; S, 10.68%. ¹H-NMR (MeOD-*d*₄, 200 MHz) δ 8.65, 8.60 (s, 4H each, pyrrole *H*), 8.25 (m, 16H, *m*-C₆H₄SO₃⁻ and *o*-C₆H₄SO₃⁻). IR ν_{CO}: 1923, ν_{OH}: 3460. UV-Vis (H₂O) 528 (4.21), 410 (5.43). TGA: Calcd loss of 4H₂O: 5.9 %. Found: 5.1 % (from ~ 37 to ~ 60°C) (TGA plot is given in Appendix 4, Figure A.4.4). The ¹H-NMR, ν_{CO}, and UV-Vis

spectroscopic data are consistent with those previously reported for the $\text{Ru(II)(TSPbP)(CO)}^4$ moiety.^{13,14,16,19} Attempts to analyze this product by mass spectroscopic methods (EI and LSIMS) did not show the parent peak or any other peaks related to the title compound.

5.5.2 Ru(OEP)(CO)(THF) ($MW = 733.96 \text{ g/mol}$)

The procedure used was as given in Section 5.5.1, but using $\text{H}_2(\text{OEP})$ (60 mg, 0.11 mmol), $[\text{Ru}(\text{DMF})_6][\text{OTf}]_3$ (312 mg, 0.316 mmol) and DMF (30 mL), with the reaction time being reduced to 6 h. The product was purified by column chromatography using neutral alumina with CH_2Cl_2 as eluant for unreacted $\text{H}_2(\text{OEP})$, and with 10 % THF/MeOH as eluant for the product. Red crystals suitable for X-ray analysis were obtained from slow evaporation of a saturated solution of the complex in 10 % THF/toluene. Yield: 45 mg (56 %). Anal. Calcd for $\text{C}_{41}\text{H}_{52}\text{N}_4\text{O}_2\text{Ru}$: C, 67.09; H, 7.14; N, 7.63. Found: C, 66.51; H, 7.17; N, 8.40%. $^1\text{H-NMR}$ of a sample left under *vacuo* for 24 h (CDCl_3 , 200 MHz) δ 9.90 (s, 4H, *meso-H*), 4.03 (q, 16H, CH_2CH_3), 1.90 (t, 24H, CH_2CH_3). IR ν_{CO} : 1925. UV-Vis (DMF) 548 (4.76), 518 (4.49), 396 (5.63). Mass spectrum [LSIMS, m/z] 662 $[\text{M}-(\text{THF})]^+$ and 634 $[\text{M}-(\text{THF})-(\text{CO})]^+$. The $^1\text{H-NMR}$, ν_{CO} , and UV-Vis spectroscopic data are consistent with those previously reported for the Ru(II)(OEP)(CO) moiety.^{10,20-22}

5.5.3 $\text{Ru(TPhP)(CO)(H}_2\text{O)}$ ($MW = 759.78 \text{ g/mol}$)

The procedure used was as given in Section 5.5.1, but using $\text{H}_2(\text{TPhP})$ (25 mg, 0.042 mmol), $[\text{Ru}(\text{DMF})_6][\text{OTf}]_3$ (125 mg, 0.126 mmol) and DMF (30 mL). Benzene was used as eluant for unreacted $\text{H}_2(\text{TPhP})$, and 5 % THF/benzene was used as eluant for the product. Yield: 18 mg (51 %). Anal. Calcd for $\text{C}_{45}\text{H}_{28}\text{N}_4\text{ORu}\cdot\text{H}_2\text{O}$: C, 71.14; H, 3.98; N,

7.37. Found: C, 70.65; H, 4.31; N, 7.10%. $^1\text{H-NMR}$ (CDCl_3 , 200 MHz) δ 8.60 (s, 8H, β -pyrrole-*H*), 8.18 and 8.02 (m, 8H, *o*- C_6H_5), 7.65 (m, 12H, *m*- C_6H_5 and *p*- C_6H_5). IR ν_{CO} : 1946, ν_{OH} : 3412. UV-Vis (DMF) 532 (4.72), 412 (5.60). Mass spectrum [LSIMS, m/z] 742 $[\text{M}-(\text{H}_2\text{O})]^+$ and 714 $[\text{M}-(\text{H}_2\text{O})-(\text{CO})]^+$. The ^1H NMR, ν_{CO} , and UV-Vis data are consistent with those previously reported for a complex containing the Ru(II)(TPhP)(CO) moiety.^{9,23-26} Red crystals of the complex Ru(TPhP)(CO)(py) containing a coordinated pyridine suitable for X-ray analysis were obtained by slow evaporation of a saturated solution of the aquo complex in 5 % pyridine/benzene.

5.5.4 Ru(BPhP)(CO)

The procedure used was as given in Section 5.5.1, but using $\text{H}_2(\text{BPhP})$ (4.67 mg, 0.01 mmol), $[\text{Ru}(\text{DMF})_6][\text{OTf}]_3$ (30 mg, 0.03 mmol) and DMF (3 mL). CH_2Cl_2 was used as eluant for unreacted $\text{H}_2(\text{BPhP})$, and 2 % THF/ CH_2Cl_2 was used as eluant for the product. Yield < 2 mg (not determined). $^1\text{H-NMR}$ (CDCl_3 , 200 MHz) δ 10.00 (s, 2H, *meso-H*), 9.13, 8.85 (s, 4H each, β -pyrrole-*H*), 8.25 and 8.02 (m, 2H each, *o*- C_6H_5), 7.95 (m, 6H, *m*- C_6H_5 and *p*- C_6H_5). IR ν_{CO} : 1930. UV-Vis (CH_2Cl_2) 520, 402. Mass spectrum [LSIMS, m/z] 590 $[\text{M}]^+$, 562 $[\text{M}-(\text{CO})]^+$.

5.5.5 Ru(TrPhPyNO)(CO)

The procedure used was as given in Section 5.5.1, but using $\text{H}_2(\text{TrPhPyNO})$ (6.4 mg, 0.01 mmol), $[\text{Ru}(\text{DMF})_6][\text{OTf}]_3$ (30 mg, 0.03 mmol) and DMF (3 mL). CHCl_3 was used as eluant for unreacted $\text{H}_2(\text{TrPhPyNO})$ and 2 % pyridine/ CHCl_3 was used as eluant for the

product. Yield < 2 mg (not determined). IR ν_{CO} : 1935, ν_{NO} : 1251. UV-Vis (CH_2Cl_2) 532, 414. Mass spectrum [LSIMS, m/z] 743 $[\text{M}-(\text{O})]^+$, 715 $[\text{M}-(\text{O})-(\text{CO})]^+$.

5.6 Results and Discussion

Previous work has shown that metallation failed to occur using a 3:1 molar ratio of $[\text{Ru}(\text{DMF})_6][\text{OTf}]_3$ and $\text{H}_2(\text{TSPHP})^{4-}$ in DMF under 1 atm of H_2 .¹⁶ The present work demonstrates that an inert atmosphere and neat DMF are both necessary in order for metallation to occur. Of note, attempts to metallate the free-base porphyrins using DMSO, or DMSO/DMF as the solvent, under N_2 or air did not result in the insertion of Ru.

The metallation reaction involves an *in situ* reduction of Ru(III) to Ru(II). The mechanism of this reduction is unclear,¹⁶ however, CO has been proposed to be the reductant which derives from the decarbonylation of DMF. Such decarbonylation of DMF by Ru-porphyrins to generate carbonyl derivatives has been reported,²⁷ and the mechanisms of reactions in which CO acts as a reductant are well established.²⁸

Baird *et al.*, from this laboratory, have reported the synthesis of $[\text{Ru}(\text{L})_6][\text{OTf}]_2$ complexes (L = an imidazole) utilizing $[\text{Ru}(\text{DMF})_6][\text{OTf}]_3$ as the precursor.²⁹ These reactions carried out in MeOH involve ligand exchange of the DMF ligands of $[\text{Ru}(\text{DMF})_6][\text{OTf}]_3$ with imidazole as well as the *in situ* reduction of Ru(III) to Ru(II). The authors suggest that MeOH and/or imidazoles may be acting as the reducing agent; both these reagents can act as reductants.^{30,31}

5.6.1 $\text{Na}_4[\text{Ru}(\text{TSPHP})(\text{CO})]\cdot 4\text{H}_2\text{O}$

Pawlik *et al.* reported the first water-soluble Ru(II) porphyrin as $\text{Na}_4[\text{Ru}(\text{TSPHP})(\text{CO})]$ formed by reaction of $\text{Ru}_3(\text{CO})_{12}$ with $\text{Na}_4(\text{TSPHP})\cdot 12\text{H}_2\text{O}$ in refluxing DMF under Ar for a period of 1-3 weeks. However, the authors noted that the sodium salt is contaminated by other sodium salts, but addition of a saturated solution of CaCl_2 gave $\text{Ca}_2[\text{Ru}(\text{TSPHP})(\text{CO})]\cdot 12\text{H}_2\text{O}$,¹³ while Yong-Wu and Xing-Min reported the isolation of $\text{Na}_4[\text{Ru}(\text{TSPHP})(\text{CO})]\cdot 12\text{H}_2\text{O}$ from the reaction of $\text{Ru}_3(\text{CO})_{12}$ and the sodium salt quoted as $\text{Na}_4(\text{TSPHP})\cdot 9\text{H}_2\text{O}$.¹⁹ Recently, Hartmann *et al.* reported the characterization of $\text{Na}_4[\text{Ru}(\text{TSPHP})(\text{CO})(\text{EtOH})]$.¹⁴ Ware in this laboratory reported the isolation of the complex $\text{Na}_4[\text{Ru}(\text{TSPHP})(\text{CO})(\text{DMF})]\cdot \text{solvate}$ ¹⁶ (solvate = $2\text{DMF}\cdot 2\text{H}_2\text{O}$ or $6\text{H}_2\text{O}$) by the method described in Section 5.5.1.

During the present work, $\text{Na}_4[\text{Ru}(\text{TSPHP})(\text{CO})]\cdot 4\text{H}_2\text{O}$ was isolated from the reaction between $\text{Na}_4[\text{H}_2\text{TSPHP}]\cdot 15\text{H}_2\text{O}$ and $[\text{Ru}(\text{DMF})_6][\text{OTf}]_3$ (Section 5.5.1). The complex was formulated with four solvate H_2O molecules as elemental and thermal gravimetric analyses provide support for this formulation. The calculated elemental analyses agree well with the determined analyses, while thermal gravimetric analyses of the complex (Section 5.5.1) showed a weight loss corresponding to 3.5 H_2O molecules from the formulated $\text{Na}_4[\text{Ru}(\text{TSPHP})(\text{CO})]\cdot 4\text{H}_2\text{O}$. Of note, Buchler *et al.* reported the use of gel electrophoresis as an efficient method for the separation and analysis of several free-base and metallated water-soluble porphyrins, and the authors report that "results of elemental analyses are not definitive because the substances are strongly hygroscopic".³² The ν_{CO} stretch for the CO ligand was observed at 1923 cm^{-1} (KBr) which compares with the reported values of 1925

cm^{-1} for $\text{Ru}(\text{TSPhP})(\text{CO}) \cdot 12\text{H}_2\text{O}$ (medium not given),¹⁹ 1940 cm^{-1} for $\text{Ca}_2[\text{Ru}(\text{TSPhP})(\text{CO})] \cdot 12\text{H}_2\text{O}$ (medium not given),¹³ 2042 and 1936 cm^{-1} for $\text{Na}_4[\text{Ru}(\text{TSPhP})(\text{CO})(\text{EtOH})]$ (KBr),¹⁴ 2035 , 1959 and 1924 cm^{-1} for $\text{Na}_4[\text{Ru}(\text{TSPhP})(\text{CO})(\text{DMF})] \cdot 2\text{DMF} \cdot 2\text{H}_2\text{O}$ (KBr)¹⁶ and 2027 , 1971 and 1929 cm^{-1} for $\text{Na}_4[\text{Ru}(\text{TSPhP})(\text{CO})(\text{DMF})] \cdot 6\text{H}_2\text{O}$ (KBr).¹⁶ Ware noted that "the solid state IR spectrum of $\text{Na}_4[\text{Ru}(\text{TSPhP})(\text{CO})(\text{DMF})] \cdot \text{solvate}$ (solvate = $6\text{H}_2\text{O}$ or $2\text{DMF} \cdot 2\text{H}_2\text{O}$) shows three ν_{CO} stretches which could indicate the presence of more than one mono-CO complex (e.g. with H_2O as the axial ligand), a trace of some Ru-CO impurity or solid state effects".¹⁶

Hartmann *et al.* tested a series of water-soluble Ru porphyrins ($[\text{Ru}(\text{II})(\text{TMPyP})(\text{CO})(\text{CH}_3\text{OH})](\text{OAc})_4$, $\text{Na}_4[\text{Ru}(\text{II})(\text{TSPhP})(\text{CO})(\text{EtOH})]$ and $[\text{Ru}(\text{II})(p\text{-COOH-PP})(\text{CO})(\text{MeOH})]$ (TMPyP = dianion of *meso*-tetrakis(4-N-methylpyridinium)porphyrin and *p*-COOH-PP = dianion of *meso*-tetrakis(4-carboxylphenyl)porphyrin)) and their Mn and Fe analogues for possible *in vivo* anti-tumour activity using mice bearing P388 leukemia cells, and these results were compared to those for cisplatin.¹⁴ Of the complexes studied, only $\text{Na}_4[\text{Ru}(\text{TSPhP})(\text{CO})(\text{EtOH})]$ exhibited "borderline" anti-tumour activity (0.047 mmol/kg) compared to that of cisplatin (0.013 mmol/kg).¹⁴ Previous biological results, in this laboratory, reported by Ware¹⁶ indicate that $\text{Na}_4[\text{Ru}(\text{TSPhP})(\text{CO})(\text{DMF})]$ does not accumulate in CHO cells as well as, for example, *trans*- $\text{RuCl}_2(\text{BPSE})_2$ (up to $8.81 \times 10^{-6} \text{ ng(Ru)/cell}$ at $50\text{-}200 \text{ }\mu\text{M}$ after 1 h ¹⁶ vs. $175 \times 10^{-6} \text{ ng(Ru)/cell}$ at $500 \text{ }\mu\text{M}$ for 4 h).³³ $\text{Na}_4[\text{Ru}(\text{TSPhP})(\text{CO})(\text{DMF})]$ was shown to be non-toxic toward CHO cells in air at the concentrations tested ($50\text{-}200 \text{ }\mu\text{M}$) which parallels other reports from this laboratory showing that various Co, Cu and Pt porphyrin complexes are also

non-toxic to oxic cells.^{3,34} The complex $\text{Na}_4[\text{Ru}(\text{TSPHP})(\text{DMSO})_2]$, derived from $\text{Na}_4[\text{Ru}(\text{TSPHP})(\text{CO})(\text{DMF})]$, was found to show no radiosensitizing ability toward CHO cells under oxic or hypoxic conditions, and indeed seemed to be weakly radioprotecting.^{3,16}

5.6.2 $\text{Ru}(\text{OEP})(\text{CO})(\text{THF})$

The reaction of $\text{H}_2(\text{OEP})$ with $[\text{Ru}(\text{DMF})_6][\text{OTf}]_3$ led to the isolation of the title complex (Section 5.5.2), which has been made previously via the $\text{Ru}_3(\text{CO})_{12}$ precursor;¹⁰ ν_{CO} observed at 1925 cm^{-1} (KBr) compares with the reported values of 1950 cm^{-1} for $\text{Ru}(\text{OEP})(\text{CO})(\text{THF})$ (medium not given),¹⁰ 1952 cm^{-1} for $\text{Ru}(\text{OEP})(\text{CO})(\text{PPh}_3)$ (medium not given),^{20a} 1917 cm^{-1} for $\text{Ru}(\text{OEP})(\text{CO})$ (in $0.1\text{ M } [\text{nBu}_4\text{N}][\text{PF}_6]$ in CH_2Cl_2),²¹ and 1945 and 1928 cm^{-1} for $\text{Ru}(\text{OEP})(\text{CO})(\text{MeOH})$ (KBr).²² Crystals of $\text{Ru}(\text{OEP})(\text{CO})(\text{THF})$ (Section 5.5.2) were grown by slow evaporation of a 10 % THF/toluene solution of the complex. It was not possible to obtain good elemental analysis or definitive NMR data for the complex because the THF was removed during attempts to remove associated solvent by pumping. Eaton and Eaton have reported ^1H NMR multiplets at $\delta -1.23$ and -0.45 peaks for bound THF in $\text{Ru}(\text{OEP})(\text{CO})(\text{THF})$.¹⁰

Structural data (Figure 5.2 and Table 5.2) show that the molecule has a slightly distorted octahedral geometry at the Ru with *trans* angles that range from $172.66(12)$ to $177.23(12)^\circ$, *cis* N-Ru-N angles from $89.53(10)$ - $89.97(10)^\circ$, *cis* C-Ru-N angles from $89.92(13)$ - $97.41(13)^\circ$, and *cis* O-Ru-N angles from $85.31(10)$ - $87.35(10)^\circ$. The complex possesses a linear binding mode for the CO ligand with a Ru-C-O angle of $176.6(3)^\circ$, a Ru-C bond length of $1.805(4)\text{ \AA}$ and a C-O bond length of $1.144(4)\text{ \AA}$. The Ru-O(2) distance is $2.241(3)\text{ \AA}$ which is somewhat longer than those reported ($2.019(3)\text{ \AA}$ (av.) for the Ru-O

bond in $\text{Ru}(\text{TPhP})(\text{OEt})(\text{EtOH}) \cdot 2\text{EtOH}$,²² and 2.21(2) Å for $\text{Ru}(\text{TPhP})(\text{CO})(\text{EtOH})$ ²⁵) and suggests a weak ligation of THF in the solid state.

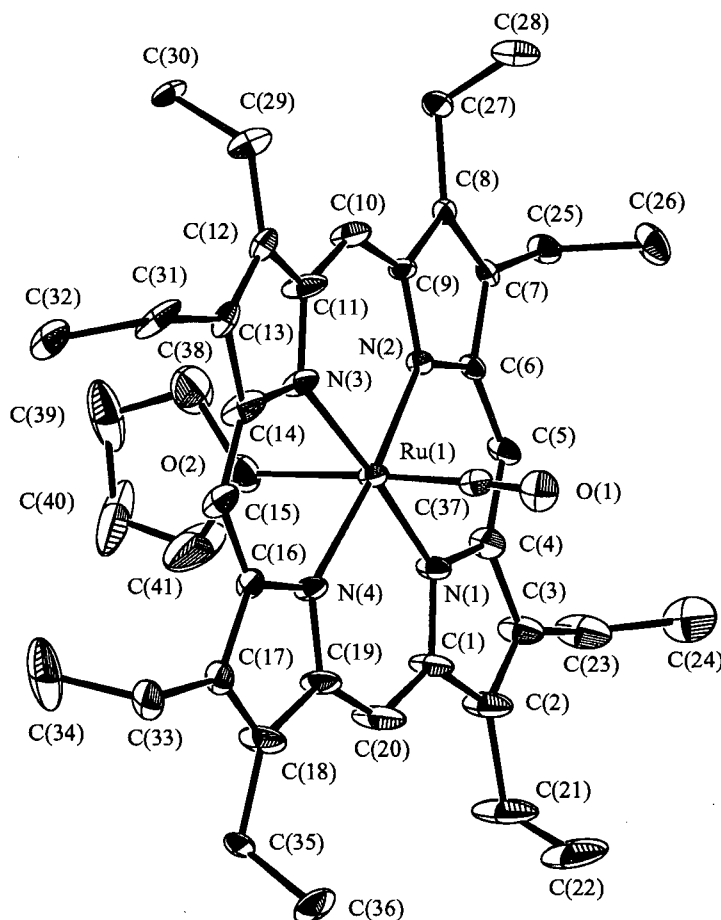


Figure 5.2. An ORTEP diagram of $\text{Ru}(\text{OEP})(\text{CO})(\text{THF})$ showing 50 % thermal ellipsoids; the H-atoms are omitted for clarity (crystal data are given in Appendix 1.14).

Table 5.2. Selected Bond Angles and Lengths for Ru(OEP)(CO)(THF).

Bond	Distance (Å)	Bond angles	Angle (°)
Ru-C	1.805(4)	<i>trans</i> angles	172.66(12)-177.23(12)
Ru-N(porp)	2.052(2)-2.059(2)	<i>cis</i> -N-Ru-N	89.53(10)-89.97(10)
Ru-O	2.241(3)	<i>cis</i> -C-Ru-N	89.92(13)-97.41(13)
C-O	1.144(4)	<i>cis</i> -O-Ru-N	85.31(10)-87.35(10)
		Ru-C-O	176.6(3)

Seyler *et al.* have reported on the reaction of TEMPO (Figure 5.3) with Ru(OEP)(CH₃) to give Ru(OEP)(CO)(TEMPO), the first reported transformation of a CH₃ to a CO within a metal complex.³⁵ The CO ligand is linearly bound with a Ru-C-O angle of 178.6°, a Ru-C bond distance of 1.798(5) Å and a C-O bond distance of 1.150(5) Å. The reported Ru-O distance of 2.348(3) Å is larger than those noted above and suggests a weak ligation of the TEMPO ligand. The ¹H NMR solution spectrum of Ru(OEP)(CO)(TEMPO) revealed no evidence for TEMPO ligation with the Ru(OEP)(CO) moiety in solution.³⁵ Other Ru(OEP) complexes characterized by X-ray crystallography include Ru(OEP)(R₂S)₂ (R₂ = *n*-decylmethyl and Ph₂),³⁶ [Ru(OEP)(R₂S)₂][BF₄] (R₂ = *n*-decylmethyl),³⁷ and Ru(OEP)(CO)(py).³⁸ Funatsu *et al.* have reported the structure of the 'diporphyrin species' Ru(OEP)(CO)(H₂PyP₃P) (H₂PyP₃P = 5-pyridyl-10,15,20-triphenylporphyrin), in which the carbonyl ligand is again linearly coordinated to Ru with the Ru-C-O angle of 179.7(6)°, a Ru-C bond distance of 1.801 Å and a C-O bond distance of 1.165(7) Å.³⁹

[Of interest, TEMPO has been utilized previously in this group to study bond homolysis within Ru(IV)-diaryl/dialkyl porphyrin complexes.⁴⁰ Hanada *et al.* have reported the structure and magnetic properties of a bis(nitroxide)diruthenium (II,III) cation within the mixed cation complex $[\text{Ru}_2(\text{O}_2\text{CCMe}_3)_4(\text{TEMPO})_2][\text{Ru}_2(\text{O}_2\text{CCMe}_3)_4(\text{H}_2\text{O})_2](\text{BF}_4)_2$.⁴¹

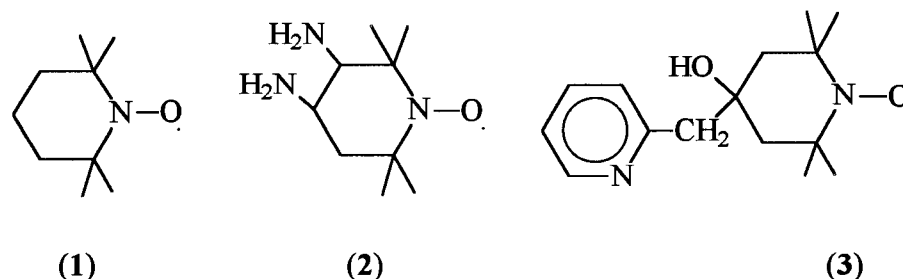


Figure 5.3. Structures of (1) = TEMPO = 2,2,6,6-tetramethylpiperidine-1-oxyl,³⁵ (2) = DAPO = *trans* 3,4,-diamino-2,2,6,6-tetramethyl piperidine-1-oxyl,⁴² (3) = TEMPICOL-2 = 4-hydroxy-4-(2-picolyl)-2,2,6,6-tetramethylpiperidine-1-oxyl.⁴³

More generally, derivatives of TEMPO and associated metal complexes have been studied as novel classes of antioxidants and anticancer agents. Sen' *et al.* have reported the synthesis and anti-tumour activity of the Pt(II) complexes $\text{Pt}(\text{DAPO})\text{X}_2$ (see Figure 5.3).⁴² The toxicity of the Pt complexes was dependent on the nature of X, and in terms of LD_{50} varied between 11 mg/kg ($\text{X} = \text{NO}_3$) and 400 mg/kg ($\text{X}_2 = 1,1\text{-cyclobutanedicarboxylate}$) compared to that of cisplatin, 12 mg/kg. The complex with $\text{X} = \text{Cl}$ (at 4.75 mg/kg) appeared to more efficient than cisplatin (1.88 mg/kg) in suppressing tumour growth (evaluated as an inhibition of growth of tumour diameter) against subcutaneously transplanted adenocarcinoma 755 in mice. Metodiewa *et al.* have reported studies of TEMPICOL-2 (see Figure 5.3) as an anticancer agent, in which administration of the nitroxide to rats bearing 3 day-old Yoshida Sarcoma led to growth inhibition.^{43]}

5.6.3 *Ru(TPhP)(CO)(py)*

The title complex was synthesized 'inadvertently' by reaction of $[\text{Ru}(\text{DMF})_6]^{3+}$ and $\text{H}_2(\text{TPhP})$, followed by crystallization from a pyridine/benzene solution (Section 5.5.3). Structural determination revealed that the molecule was identical to that reported by Little and Ibers in 1973.³⁸ The ν_{CO} value compares with those reported in the literature: 1945 cm^{-1} for $\text{Ru}(\text{TPhP})(\text{CO})$ in KBr^9 or NaCl^{23} , 1945 cm^{-1} for $\text{Ru}(\text{TPhP})(\text{CO})(\text{imidazole})$ in CHCl_3 ,²⁴ 1934 and 1939 cm^{-1} for $\text{Ru}(\text{TPhP})(\text{CO})$ and $\text{Ru}(\text{TPhP})(\text{CO})(\text{py})$, respectively in tetrachloroethane²⁵ and 1922 cm^{-1} for $\text{Ru}(\text{TPhP})(\text{CO})$ in DMSO^{26} . (Table 5.3 shows a comparison of selected bond lengths for the two determined structures of $\text{Ru}(\text{TPhP})(\text{CO})(\text{py})$).

Table 5.3. Comparison of Selected Bond Lengths for $\text{Ru}(\text{TPhP})(\text{CO})(\text{py})$ (Figure 5.4).

Bond	This Work	Ref. 38
Ru-C	1.837(3) Å	1.838(9) Å
Ru-N(porp)	2.057(2)-2.062(2) Å	2.055(6)-2.058(5) Å
Ru-N(py)	2.207(2) Å	2.193(4) Å
C-O	1.151(3) Å	1.141(10) Å

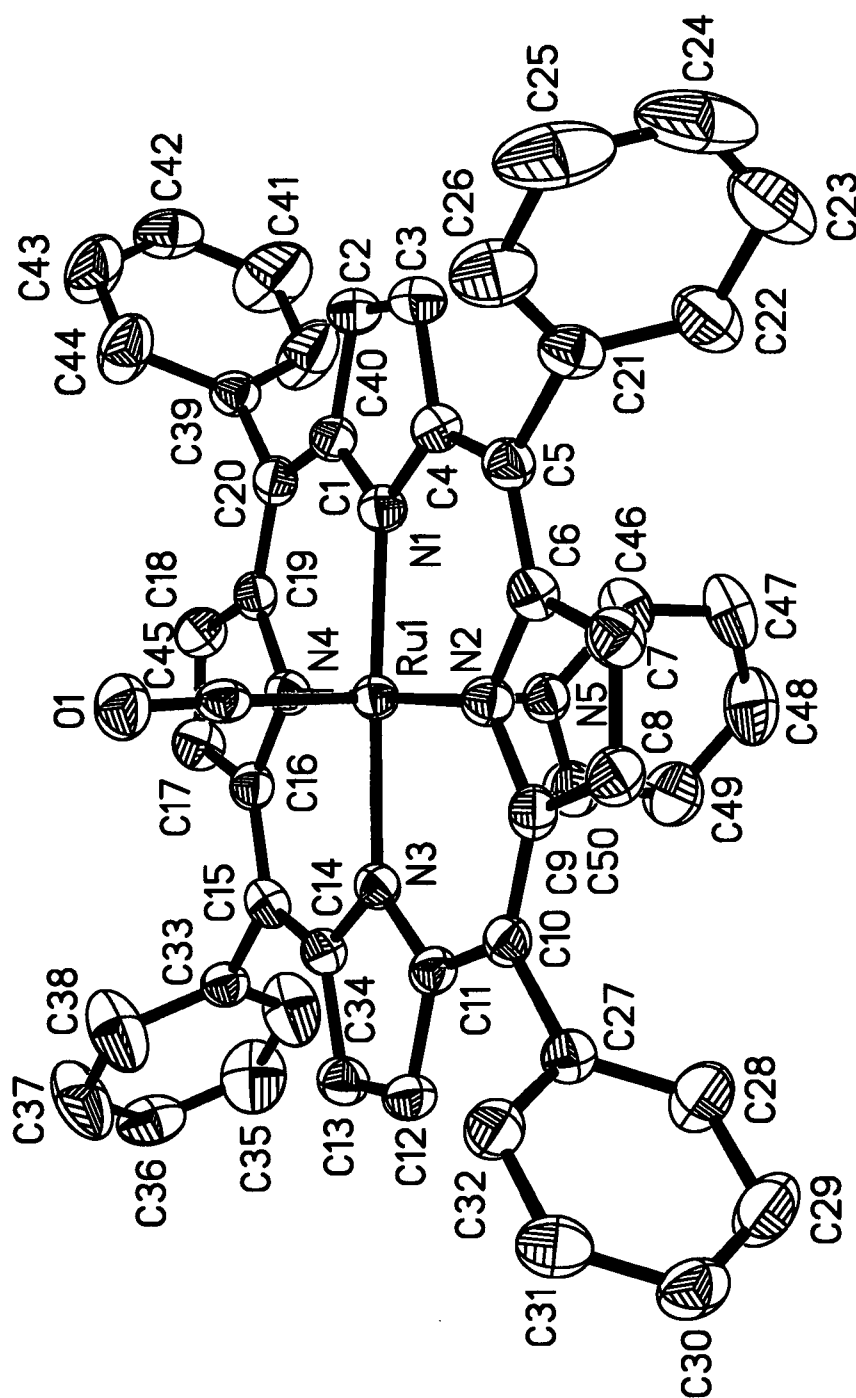


Figure 5.4. An ORTEP diagram of Ru(TPhP)(CO)(py) showing 50 % thermal ellipsoids; the H-atoms have been omitted for clarity (crystal data are given in Appendix 1.15).

5.6.4 *Ru(BPhP)(CO)*

The title complex was synthesized by reaction of $[\text{Ru}(\text{DMF})_6]^{3+}$ and $\text{H}_2(\text{BPhP})$ (Section 5.5.4), and has been partially characterized: ν_{CO} is observed at 1930 cm^{-1} , the mass spectrum shows peaks for $\text{Ru}(\text{BPhP})(\text{CO})$ and $\text{Ru}(\text{BPhP})$, and the ^1H NMR data are consistent with the formulation.

5.6.5 *Ru(TrPhPyNO)(CO)*

The title complex ($\nu_{\text{CO}} 1935$, $\nu_{\text{NO}} 1251\text{ cm}^{-1}$) was synthesized by reaction of $[\text{Ru}(\text{DMF})_6]^{3+}$ and $\text{H}_2(\text{TrPhPyNO})$ (Section 5.5.5). The mass spectrum shows peaks for $\text{Ru}(\text{TrPhPyN})(\text{CO})$ and $\text{Ru}(\text{TrPhPyN})$; the oxidopyridyl groups were deoxygenated using the ionization techniques (EI, LSIMS and MALDI-TOF) and no molecular ion peak was observed. Of note, the free-base porphyrins, 5,15-bis(1-oxido-4-pyridyl)-10-20-diphenylporphyrin and 5,10-bis(1-oxido-4-pyridyl)-15-20-diphenylporphyrin, were deoxygenated under conditions of EI or LSIMS, but were analyzed by MALDI-TOF mass spectrometry which led to less deoxygenation of these porphyrin-N-oxides.⁴⁴

5.7 Fluorescent Properties of Porphyrins

The accumulation of non-metallated (free-base) porphyrins in cells has been previously studied using fluorescence microscopy,^{5a,45} including the water-soluble sodium salt of 5-(1-oxido-4-pyridyl)-10, 15, 20-tris(4-sulfonatophenyl) porphyrin.⁴⁴ Fluorescence from porphyrin chromophores localized in cells was observed when the cells were irradiated with

UV light (330-380 nm, with emission measured at > 420 nm) and in the green region (510-560 nm, with emission measured at > 590 nm).⁴⁴

5.7.1 Fluorescence Spectra of Selected Ru Porphyrins

A qualitative measure of fluorescence was determined for some Ru(Porp)(CO) species. The excitation wavelengths chosen are the absorbance maxima in the UV-Vis spectrum. Fluorescence was observed from the porphyrin chromophores when the samples were irradiated with UV light (300-380 nm, with emission measured at ≥ 570 nm) and with visible light in the violet region (389-421 nm, with emission measured at ≥ 429 nm). The fluorescence data are summarized in Table 5.4. The fluorescence spectrum of $\text{Na}_4[\text{Ru}(\text{TSPbP})(\text{CO})]\cdot 4\text{H}_2\text{O}$ is shown in Figure 5.5 as an example.

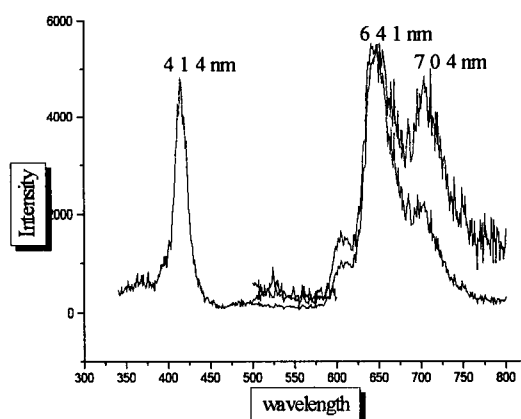


Figure 5.5. Fluorescence spectrum of $\text{Na}_4[\text{Ru}(\text{TSPbP})(\text{CO})]\cdot 4\text{H}_2\text{O}$. The excitation wavelength was 414 nm and emission was measured at 641 and 704 nm.

Table 5.4. Fluorescence wavelengths for selected Ru porphyrins.

Porphyrin	Excitation (λ) nm	Emission (λ) nm
$\text{Na}_4[\text{Ru}(\text{TSPbP})(\text{CO})] \cdot 4\text{H}_2\text{O}^a$	414	641 and 704
$\text{Ru}(\text{OEP})(\text{CO})(\text{THF})^b$	389	429
$\text{Ru}(\text{BPhP})(\text{CO})^c$	315	570 and 633
	406	698
$\text{Ru}(\text{TrPhPyNO})(\text{CO})^c$	421	650

^a DMSO/H₂O. ^b THF/toluene/acetone. ^c CH₂Cl₂/acetone.

5.8 Attempted Metallations

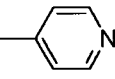
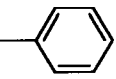
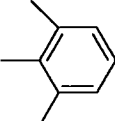
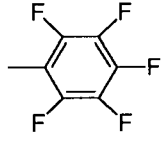
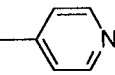
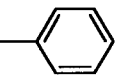
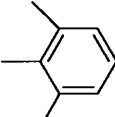
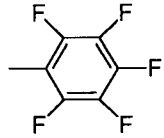
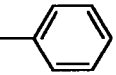
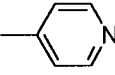
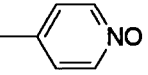
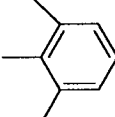
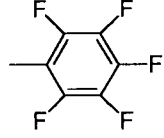
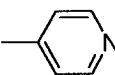
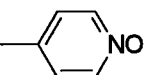
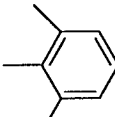
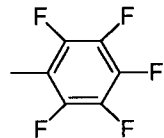
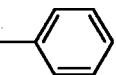
As described in Section 5.6 the metallation, using $[\text{Ru}(\text{DMF})_6][\text{OTf}]_3$, of selected porphyrins has proven to be quite useful and convenient. Several attempts to metallate other porphyrins were unsuccessful. These reactions were monitored by: (a) TLC for the disappearance of $\text{H}_2(\text{Porp})$, (b) UV-Vis spectroscopy by shifts in the spectra, and (c) by IR for the appearance of ν_{CO} . Porphyrins that were not metallated using the $[\text{Ru}(\text{DMF})_6]^{3+}$ precursor are shown in Table 5.5 (for the numbering scheme of the free-base porphyrins refer to Figure 5.1, p. 187).

Ware reported that the metallation of $\text{H}_2(\text{TPyP})$ with $[\text{Ru}(\text{DMF})_6][\text{OTf}]_3$ led to the isolation of an insoluble, red product "Ru(TPyP)" that is likely of a polymeric nature.¹⁶ Shi and Anson exposed graphite electrodes coated with Co(TPyP) to solutions of *fac*- $[\text{Ru}(\text{NH}_3)_3(\text{OH}_2)_3]^{2+}$ and postulated the formation of a polymeric substance containing bridging Ru atoms linked to Co(TPyP) via the nitrogen of the pyridyl group.⁴⁶ During this

present work, the reaction of $\text{H}_2(\text{TPyP})$ and $[\text{Ru}(\text{DMF})_6][\text{OTf}]_3$ (following the methodology described in Section 5.5) resulted in the isolation of an insoluble microcrystalline purple compound that did not analyze well for either “ $\text{Ru}(\text{TPyP})(\text{CO})$ ” or a polymeric “ $\text{Ru}(\text{TPyP})$ ” material.

Alessio *et al.* have reported the design of a “pentamer of vertically linked porphyrins” $(\text{MTPyP})[\text{Ru}(\text{TPhP})(\text{CO})]_4$ ($\text{M} = 2\text{H}^+$ or Zn^{2+}) formed by treating (MTPyP) with $[\text{Ru}(\text{TPhP})(\text{CO})(\text{EtOH})]$.⁴⁷ Of note, the “pentamer” $(\text{H}_2\text{TPyP})[\text{Ru}(\text{TPhP})(\text{CO})]_4$ was considerably more soluble than $\text{H}_2(\text{TPyP})$ in CHCl_3 . The authors have also observed that $(\text{ZnTPyP})[\text{Ru}(\text{TPhP})(\text{CO})]_4$ can interact with the O-atom of DMSO (both free and S-bonded to a metal centre) to form adducts containing the “rare bridging DMSO”.⁴⁷ Funatsu *et al.* have synthesized a series of cyclic Ru porphyrin tetramers including $[\text{Ru}(\text{TrPhPyP})(\text{CO})]_4$,⁴⁸ which represent a class of molecules capable of supramolecular self-assembly. More generally, porphyrin oligomers have assisted in elucidation of important electronic and photochemical consequences for bacteriochlorophyll molecules in photosynthetic reaction centres.⁴⁹ For example, Stibrany *et al.* have reported on a structural and spectroscopic comparison between Zn(II) porphyrin dimers and bacterial photosynthetic reaction centres in bacteriochlorophyll molecules,^{49a} while Kobuke and Miyaji reported the synthesis of porphyrin dimers and oligomers as models of photosynthetic reaction centres,^{49b} and Nagata *et al.* reported the synthesis and spectroscopic properties of trimeric and pentameric porphyrin arrays as models toward the development of synthetic catalysts for photosynthetic charge separation.^{49c}

Table 5.5. Free-Base Porphyrins. 5,10,15,20-tetrapyridylporphyrin (TPyP), 5,10-bis(phenyl)-15,20-bis(4-pyridyl-*N*-oxide)porphyrin (BPhBPyNOP), 5,10,15,20-tetramesitylporphyrin (TMP), 5,10,15,20-tetra(pentafluorophenyl)porphyrin (TPFPhP), 5,15-dibromo-10,20-bisphenylporphyrin (DBrBPhP), and protoporphyrin(IX)dimethylester (PPIXDME).

Substituent Positions	Porp					
	(TPyP)	(BPhBPyNOP)	(TMP)	(TPFPhP)	(DBrBPhP)	(PPIXDME)
5-					Br	H
10-						H
15-					Br	H
20-						H
2,7,12,18-	H	H	H	H	H	CH ₃
3,8-	H	H	H	H	H	CH ₂ =CH
13,17-	H	H	H	H	H	DME ^a

^a DME = CH₃COOCH₂CH₂.

5.9 Conclusions

Work in this laboratory has shown that $[\text{Ru(III)(DMF)}_6][\text{OTf}]_3$ is an effective precursor for the metallation of the water-soluble porphyrin, $\text{H}_2(\text{TSPHP})^{4-}$.¹⁶ The present work has shown that this metallation method is not limited to the water-soluble porphyrin $\text{H}_2(\text{TSPHP})^{4-}$ but applies also to several non-water-soluble porphyrins to give Ru(II)(Porp)(CO) complexes. This method is both convenient and efficient, in that an atmosphere of CO is not required and the reaction times are reduced from 1-3 weeks (using $\text{Ru}_3(\text{CO})_{12}$ as precursor) to a period of 3-24 h.

The *in situ* reduction of the Ru(III) to Ru(II) in this metallation process may involve CO (derived from the DMF) as the reductant (Section 5.6). As well, metallation does not occur in air, implying that Ru(III) is first reduced to Ru(II) and then inserted into the porphyrin to yield Ru(II)(Porp)(CO) . Further work is required to determine the mechanism of this metallation process involving the *in situ* reduction of Ru(III) to Ru(II).

5.10 References for Chapter 5

- 1 Märkel, G.; Reiss, M.; Kreitmeier, P.; Nöth, H. *Angew. Chem. Int. Ed. Engl.* 1995, 34, 2230 and references therein.
- 2 O'Hara, J. A.; Douple, E. B.; Abrams, M. J.; Picker, D. J.; Giandomenico, C. M.; Vollano, J. F. *Int. J. Radiat. Oncol. Biol. Phys.* 1989, 16, 1049.
- 3 James, B. R.; Meng, G. G.; Posakony, J. J.; Ravensbergen, J. A.; Ware, C. J.; Skov, K. A. *Metal-Based Drugs* 1996, 3, 85.
- 4 Jaswal, J. S.; Yapp, D. T. T.; Rettig, S. J.; James, B. R.; Skov, K.; A. J. *Chem. Soc., Chem. Commun.* 1992, 1528 and references therein.
- 5 (a) Kessel, D.; Thompson, P.; Saatio, K.; Nantwi, K. D. *Photochem. Photobiol.* 1987, 45, 787;
(b) Fiel, R. J.; Mark, E.; Button, T.; Gilani, S.; Musser, D. *Cancer Lett.* 1988, 40, 23;
(c) Dougherty, T. J. *Photochem. Photobiol.* 1987, 45, 879;
(d) Miura, M.; Micca, P. L.; Heinrichs, J. C.; Gabel, D.; Fairchild, R. G.; Slatkin, D. N. *Biochem. Pharmacol.* 1992, 43, 467.
- 6 Farrell, N. P. *Transition Metal Complexes as Drugs and Chemotherapeutic Agents*, Kluwer Academic Publishers, Dordrecht, 1989.
- 7 Sava G. Ruthenium Compounds in Cancer Therapy, in *Metal Compounds in Cancer Therapy* (ed. S Fricker), Chapman and Hall, London, 1994, p. 65.
- 8 Fleischer, E. B.; Thorp, R.; Venerable, D. J. *Chem. Soc., Chem. Commun.* 1969, 475.
- 9 Chow, B.; Cohen, I. *Bioinorg. Chem.* 1971, 1, 57.
- 10 Eaton, G. R.; Eaton, S. S. *J. Am. Chem. Soc.* 1975, 97, 235.
- 11 Mlodnicka, T.; James, B. R. Oxidations Catalyzed by Ruthenium Porphyrins, in *Metalloporphyrins Catalyzed Oxidations* (eds. F. Montanari and L. Casella), Kluwer Academic Publishers, Dordrecht, 1994, 17, p. 121.
- 12 Massoudipour, M.; Pandey, K. K. *Inorg. Chim. Acta* 1989, 160, 115.
- 13 Pawlik, M.; Hoq, M. F.; Shepherd, R. E. *J. Chem. Soc., Chem. Commun.* 1983, 1467.

- 14 Hartmann, M.; Robert, A.; Duarte, V.; Keppler, B. K.; Meunier, B. *J. Biol. Inorg. Chem.* 1997, 2, 427.
- 15 Dawes, J. L.; Holmes, J. D. *Inorg. Nucl. Chem. Lett.* 1971, 7, 847.
- 16 Ware, C. J. M. Sc. Dissertation, University of British Columbia, Vancouver, 1994.
- 17 Judd, R. J.; Cao, R.; Biner, M.; Armbruster, T.; Bürgi, H.-B.; Merbach, A. E.; Ludi, A. *Inorg. Chem.* 1995, 34, 5080.
- 18 Meng, G. G.; James, B. R.; Skov, K. A.; Korbelik, M. *Can. J. Chem.* 1994, 72, 2447.
- 19 Yong-Wu, L.; Xing-Min, A. *Acta Chim. Sin.* 1986, 44, 964.
- 20 (a) Barley, M.; Becker, G.; Domazetis, G.; Dolphin, D.; James, B. R. *Can. J. Chem.* 1983, 61, 2389;
(b) Antipas, A.; Buchler, J. W.; Gouterman, M.; Smith, P. D. *J. Am. Chem. Soc.* 1978, 100, 3015.
- 21 Brown, G. M.; Hopf, F. R.; Ferguson, J. A.; Meyer, T. J.; Whitten, D. G. *J. Am. Chem. Soc.* 1973, 95, 5939.
- 22 Collman, J. P.; Barnes, C. E.; Brothers, P. J.; Collins, T. J.; Ozawa, T.; Gallucci, J. C.; Ibers, J. A. *J. Am. Chem. Soc.* 1984, 106, 5151.
- 23 Tsutsui, M.; Ostfeld, D.; Francis, J. N.; Hoffman, L. M. *J. Coord. Chem.* 1971, 1, 115.
- 24 Tsutsui, M.; Ostfeld, D.; Hoffman, L. M. *J. Am. Chem. Soc.* 1971, 93, 1820.
- 25 Bonnet, J. J.; Eaton, S. S.; Eaton, G. R.; Holm, R. H.; Ibers, J. A. *J. Am. Chem. Soc.* 1973, 95, 2141.
- 26 Rillema, D. P.; Nagle, J. K.; Barringer Jr., L. F.; Meyer, T. J. *J. Am. Chem. Soc.* 1981, 103, 56.
- 27 Belani, R. M.; James, B. R.; Dolphin, D.; Rettig, S. J. *Can. J. Chem.* 1988, 66, 2072.
- 28 Sheldon, R. *Chemicals from Synthesis Gas*, Reidel Publishing Co., Dordrecht, 1983, p. 33.
- 29 Baird, I. R.; Rettig, S. J.; James, B. R.; Skov, K. A. *Can. J. Chem.* 1998, 76, 1379.
- 30 Hallman, P. S.; Stephenson, T. A.; Wilkinson, G. *Inorg. Synth.* 1970, 12, 237.
- 31 (a) Collman, J. P.; Gagne, R. R.; Halbert, T. R.; Marchon, J.-C.; Reed, C. A. *J. Am. Chem. Soc.* 1973, 95, 7868;

- (b) Chin, D-H.; Balch, A. L.; La Mar, G. N. *J. Am. Chem. Soc.* 1980, *102*, 1446;
(c) Anderson, C.; Beauchamp, A. L. *Inorg. Chem.* 1995, *34*, 6065.
- 32 Buchler, J. W.; Künzel, F. M.; Mayer, U.; Nawra, M. *Fresenius J. Anal. Chem.* 1994, *348*, 371.
- 33 (a) Yapp, D. T. T. Ph. D. Dissertation, University of British Columbia, Vancouver, 1993;
(b) Yapp, D. T. T.; Rettig, S. J.; James, B. R.; Skov, K. A. *Inorg. Chem.* 1997, *36*, 5635.
- 34 (a) Meng, G. G. Ph.D. Dissertation, University of British Columbia, Vancouver, 1993;
(b) Ravensbergen, J. A. M. M. Sc. Dissertation, University of British Columbia, Vancouver, 1993.
- 35 Seyler, J. W.; Fanwick, P. E.; Leidner, C. R. *Inorg. Chem.* 1992, *31*, 3699.
- 36 James, B. R.; Pacheco, A.; Rettig, S. J.; Ibers, J. A. *Inorg. Chem.* 1988, *27*, 2414.
- 37 Pacheco, A.; James, B. R.; Rettig, S. J. *Inorg. Chem.* 1995, *34*, 3477.
- 38 Little, R. G.; Ibers, J. A. *J. Am. Chem. Soc.* 1973, *95*, 8583.
- 39 Funatsu, K.; Kimura, A.; Imamura, T.; Ichimura, A.; Sasaki, Y. *Inorg. Chem.* 1997, *36*, 1625.
- 40 Ke, M.; Rettig, S. J.; James, B. R.; Dolphin, D. *J. Chem. Soc., Chem. Commun.* 1987, 1110.
- 41 Hanada, M.; Sayama, Y.; Mikuriya, M.; Nukada, R.; Hiromitsu, I.; Kasuga, K. *Bull. Chem. Soc. Jpn.* 1995, *68*, 1647.
- 42 Sen', V. D.; Golubev, V. A.; Volkova, L. M.; Konovalova, N. P. *J. Inorg. Biochem.* 1996, *64*, 69.
- 43 Metodiewa, D.; Skolimowski, J.; Kochman, A.; Gwozdzinski, K.; Glebeska, J. *Anticancer Res.* 1998, *18*, 369.
- 44 (a) Posakony, J. J. Ph.D. Dissertation, University of British Columbia, Vancouver, 1998, p. 94;
(b) Posakony, J. J.; Pratt, R. C.; Rettig, S. J.; James, B. R.; Skov, K. A. *Can. J. Chem.* 1999, *77*, 182.

- 45 (a) Berg, K.; Western, A.; Bommer, J. C.; Moan, J. *Photochem. Photobiol.* 1990, 52, 481;
(b) Woodburn, K. W.; Vardaxis, N. J.; Hill, J. S.; Kaye, A. H.; Phillips, D. R. *Photochem. Photobiol.* 1991, 54, 725;
(c) Berg, K.; Madslien, K.; Bommer, J. C.; Oftebro, R.; Winkelman, J. W.; Moan, J. *Photochem. Photobiol.* 1991, 53, 203;
(d) Karagianis, G.; Hill, J. S.; Stylli, S. S.; Kaye, A. H.; Varadaxis, N. J.; Reiss, J. A.; Phillips, D. R. *Br. J. Cancer* 1996, 73, 514.
- 46 Shi, C.; Anson, F. C. *Inorg. Chim. Acta* 1994, 225, 215.
- 47 Alessio, E.; Macchi, M.; Heath, S.; Marzilli, L. G. *J. Chem. Soc., Chem. Commun.* 1996, 1411.
- 48 Funatsu, K.; Imamura, T.; Ichimura, A.; Sasaki, Y. *Inorg. Chem.* 1998, 37, 1798.
- 49 (a) Stibrany, R. T.; Vasudevan, J.; Knapp, S.; Potenza, J. A.; Emge, T.; Schugar, H. I. *J. Am. Chem. Soc.* 1996, 118, 3980;
(b) Kokube, Y.; Miyaji, H. *J. Am. Chem. Soc.* 1994, 116, 4111;
(c) Nagata, T.; Osuka, A.; Maruyama, K. *J. Am. Chem. Soc.* 1990, 112, 3054.

Chapter 6

Conclusions and Recommendations for Future Work

6.1 General Remarks

This chapter highlights the most significant results obtained from the projects described, specifically the characterizations of water-soluble, dinuclear, Ru-disulfoxide complexes. Suggestions for future investigations are made. Less successful experiments are also considered, including suggestions on how syntheses might be improved. Finally, some comments are made regarding the potential use of water-soluble Ru complexes as chemotherapeutic agents.

6.2 Sulfoxide and Thioether Complexes of Ruthenium

The initial focus of this work was to synthesize geometrical isomers of the *cis* and *trans* forms of some existing Ru bis-chelating, disulfoxide complexes (Chapter 1). However, because of the unsuccessful early attempts of utilizing various Ru precursors (Chapter 2), it was decided to extend the series of disulfoxides (Chapter 2), and to synthesize their corresponding Ru complexes. The successful reactions are discussed in Chapter 3. Reactions of 2 equivalents of disulfoxide with $\text{RuCl}_3 \cdot 3\text{H}_2\text{O}$ generally give the mononuclear *cis*- $\text{RuCl}_2(\text{disulfoxide})_2$ complexes, which contain solely S-bonded sulfoxides as indicated by IR data and established by X-ray crystallography for *cis*- $\text{RuCl}_2(\text{BBSE})_2 \cdot \text{EtOH}$, *cis*- $\text{RuCl}_2(\text{BCySE})_2 \cdot \text{EtOH} \cdot 1/3 \text{ MeOH}$ and *cis*- $\text{RuCl}_2(\text{BESP})_2 \cdot \text{EtOH} \cdot \text{H}_2\text{O}$. With the exception of *cis*- $\text{RuCl}_2(\text{BBSE})_2 \cdot \text{EtOH}$, which contains one *RR* and one *meso* form of BBSE, the coordinated disulfoxides are all the *meso* diastereomers. Of major interest are the water-

soluble, dinuclear, disulfoxide complex $[\text{RuCl}(\text{BPSP})]_2(\mu\text{-Cl})_3$, which represents a new type of mixed-valence species, and a series of $[\text{RuCl}(\text{disulfoxide})(\text{H}_2\text{O})]_2(\mu\text{-Cl})_2$ complexes (disulfoxide = BESE, BPSE or BBSE). The aqueous solution chemistry of $[\text{RuCl}(\text{BPSP})]_2(\mu\text{-Cl})_3$ was studied and the data suggest the formation of a dihydroxy species. However, attempts to isolate this complex were unsuccessful, possibly due to its hygroscopic nature. Such aqueous solution chemistry needs further study.

Reaction of the dinuclear complex $[\text{RuCl}(\text{BESE})(\text{H}_2\text{O})]_2(\mu\text{-Cl})_2$ with 2 equivalents of BESE gave the mononuclear *trans*- $\text{RuCl}_2(\text{BESE})_2$ containing again just S-bonded sulfoxides. The *cis* isomer was described by the Trieste group as the lowest energy diastereomer (Chapter 3, p. 99),¹ implying that the *cis* isomer would likely be isolated in attempts to synthesize the *trans* form, and early attempts to synthesize the *trans* complex via the *trans*- $\text{RuCl}_2(\text{DMSO})_4$ precursor or and photolyzing *cis*- $\text{RuCl}_2(\text{BESE})_2$ yielded only the *cis* isomer. It is not clear why *trans*- $\text{RuCl}_2(\text{BESE})_2$ is isolated by utilizing the dinuclear complex as precursor. The generality of this method to synthesize the unknown geometrical isomers *cis*- $\text{RuCl}_2(\text{BPSE})_2$ and *trans*- $\text{RuCl}_2(\text{BBSE})_2$ from $[\text{RuCl}(\text{BPSE})(\text{H}_2\text{O})]_2(\mu\text{-Cl})_2$ and $[\text{RuCl}(\text{BBSE})(\text{H}_2\text{O})]_2(\mu\text{-Cl})_2$, respectively, should be examined.

Reactions of BPhSE, BHSE, BⁱPSP, BBSP, BPeSP, BPhSP and BMSB with $\text{RuCl}_3 \cdot 3\text{H}_2\text{O}$, utilizing procedures described in Chapter 2, led to yellow, uncharacterized products which by column chromatography yielded several bands or, in the case of BMSB, a product insoluble in common solvents. Elemental analyses for the products obtained from the major chromatography bands and the insoluble products were variable from repeat

reactions. Further investigations into the reactions of the disulfoxides containing $(\text{CH}_2)_2$ and $(\text{CH}_2)_3$ backbones with Ru precursors should be pursued.

An attempt to oxidize 1,3-bis(phenylthio)propane using air/DMSO oxidation led to an oily product, which by TLC, ^1H NMR spectroscopy and ν_{SO} data appeared to be the disulfoxide. Reaction of this oil and $\text{RuCl}_3 \cdot 3\text{H}_2\text{O}$, again utilizing the procedure described in Chapter 2, led to the isolation of red crystals which were submitted for X-ray analysis. The structural diagram shows one coordinated disulfoxide and one 'half-oxidized' dithioether. Large thermal motion prevented an accurate determination of the structure; however, *cis* geometry was established (Figure 6.1). The coordination chemistry of 'half-oxidized' dithioether Ru complexes is intriguing. The oxidation of dithioethers using only one-half of the required oxidizing agent should be examined. Thus a novel series of mixed thioether/sulfoxide Ru complexes could presumably be synthesized and characterized.

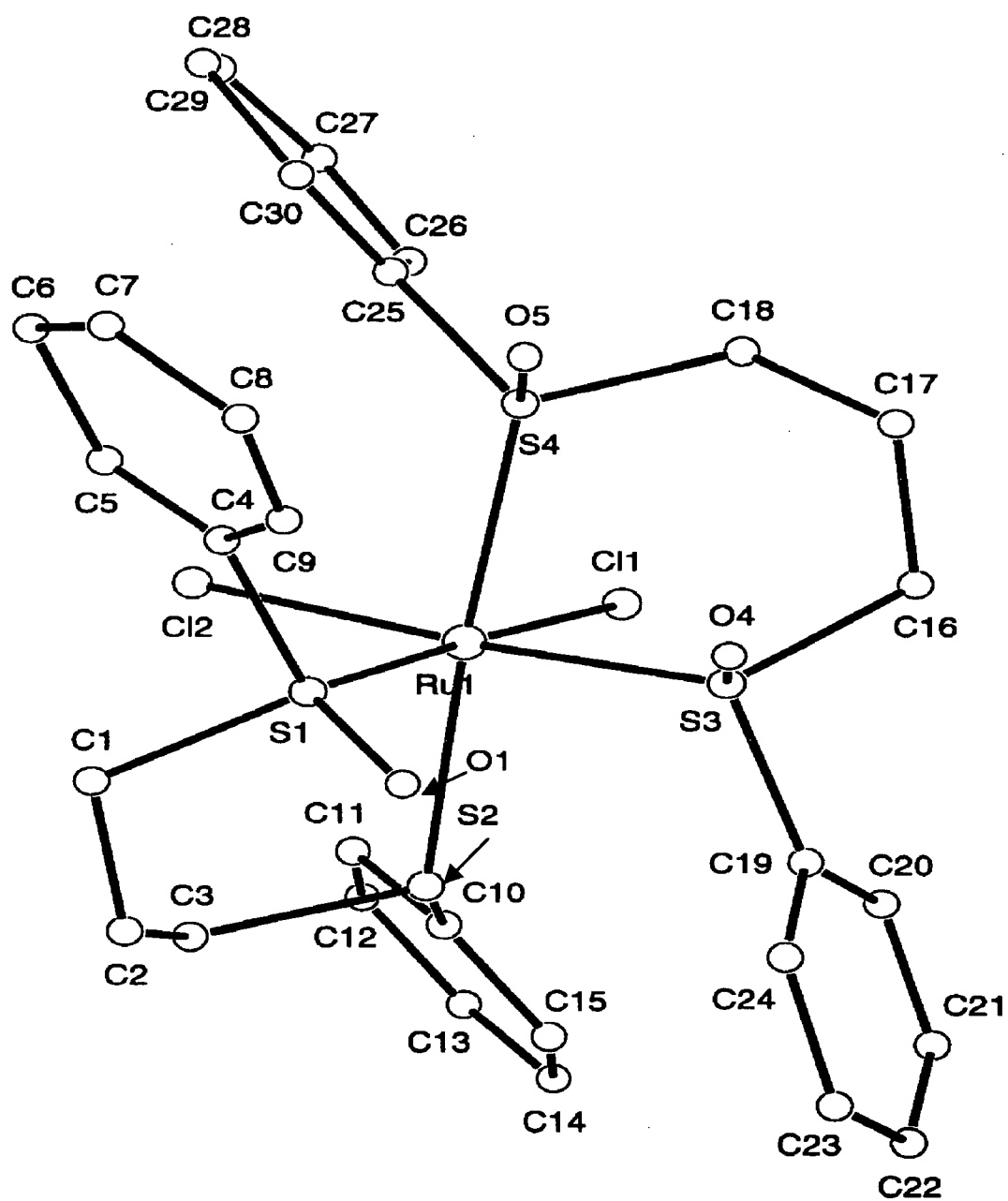


Figure 6.1. Structural diagram of *cis*-RuCl₂(BPhSP)(1-(phenylthio)-3-(phenylsulfinyl)propane).

Most of the disulfoxides synthesized in this work are water-soluble; however, the mononuclear, bis-chelating disulfoxide Ru complexes are all non-water-soluble. Synthesis of disulfoxide ligands incorporating moieties that would render the complexes water-soluble (for example, that shown in Figure 6.2) would seem a worthwhile endeavour.

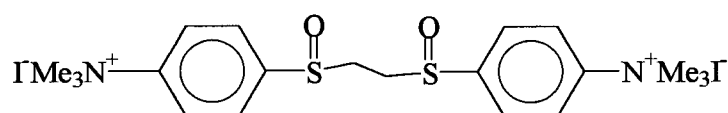


Figure 6.2. A potentially water-soluble disulfoxide.

The disulfoxides in this work were synthesized as mixtures of diastereomers (Chapter 3), thus preventing the determination of the absolute configurations of the S-atoms. Stereospecific syntheses of disulfoxides should be undertaken (Chapter 3, Section 3.5.1), and subsequent reactions with Ru precursors investigated. Such syntheses should result in isolation of complexes with known stereochemistry as opposed to mixtures of diastereomers.

Reactions of dithioethers with $\text{RuCl}_3 \cdot 3\text{H}_2\text{O}$ resulted in isolation of the mononuclear Ru(II) species *trans*- $\text{RuCl}_2(\text{BCyTE})_2$ and $-\text{RuCl}_2(\text{BPhTE})_2$ and the dinuclear Ru(III) complexes $[\text{RuCl}_2(\text{BETP})]_2(\mu\text{-Cl})_2$, $[\text{RuCl}_2(\text{BPTP})]_2(\mu\text{-Cl})_2$, $[\text{RuCl}_2(\text{BBTP})]_2(\mu\text{-Cl})_2$ and $[\text{RuCl}_2(\text{BPETP})]_2(\mu\text{-Cl})_2$. The redox chemistry of these requires study, as complexes of both Ru(II) and Ru(III) were isolated using dialkyldithioethers. Chatt *et al.*² suggested that diphenyldithioether may be a stronger reductant than dialkyldithioethers in reactions with $\text{RuCl}_3 \cdot 3\text{H}_2\text{O}$, as it gives *trans*- $\text{RuCl}_2(\text{BPhTE})_2$; however, the isolation of *trans*- $\text{RuCl}_2(\text{BCyTE})_2$ implies that such a conclusion is not valid in a general sense.

The redox chemistry of the disulfoxide and dithioether systems is of interest and needs study, particularly for the dinuclear Ru(II)/Ru(II) and Ru(II)/Ru(III) disulfoxides, and

the Ru(III)/Ru(III) dithioethers. It should be possible to isolate entire ranges of Ru(II)/Ru(II), Ru(II)/Ru(III) and Ru(III)/Ru(III) complexes for each disulfoxide and dithioether. One possible route to Ru(III)/Ru(III) disulfoxides is via oxidation of coordinated dithioethers (for example, $[\text{RuCl}_2(\text{BPTP})]_2(\mu\text{-Cl})_2$ to give $[\text{RuCl}(\text{BPSP})]_2(\mu\text{-Cl})_3$ or $[\text{RuCl}_2(\text{BPSP})]_2(\mu\text{-Cl})_2$). Oxidation of Ru(II)-thioethers to Ru(II)-sulfoxides has been reported by Schenk *et al.*³ Initial attempts to oxidize *trans*- $\text{RuCl}_2(\text{BPhTE})_2$ using *in situ* dimethyldioxirane were unsuccessful in that no ν_{SO} band was detected in the isolated product (Chapter 3); perhaps the bulky substituents at the sulfur prevent its oxidation. This oxidation should be attempted using complexes with thioethers containing less bulky substituents.

6.3 Metallation of Selected Free-base Porphyrins

$[\text{Ru(III)}(\text{DMF})_6][\text{OTf}]_3$ is an effective precursor for the metallation of the water-soluble porphyrin, $\text{H}_2(\text{TSPhP})^{4-}$.⁴ The present work has shown that this metallation method is not limited to the water-soluble porphyrin $\text{H}_2(\text{TSPhP})^{4-}$ but applies also to several non-water-soluble porphyrins to give Ru(II)(Porp)(CO) complexes.

Earlier work from this laboratory has shown that $\text{Na}_4[\text{Ru}(\text{TSPhP})(\text{DMSO})_2]$ has no radiosensitization activity in CHO cells and that $\text{Na}_4[\text{Ru}(\text{TSPhP})(\text{CO})(\text{DMF})]$ is non-toxic and does not accumulate in CHO cells.^{4,5} The radiosensitizing capability of Ru porphyrins may be improved in principle by the attachment of a nitroimidazole group either to Ru or to the porphyrin ring.⁶ Photochemical studies with nitroimidazoles, misonidazole and metronidazole (see Chapter 1, Section 1.4.3), using photosensitizers such as hematoporphyrin, uroporphyrin, $(\text{H}_2\text{TSPhP})^{4-}$ and its Zn complex, and mono-*L*-aspartyl chlorin *e*₆, have given evidence for Type I photoprocesses,⁷ these yielding the radical cation

of the photosensitizer and radical anion of metronidazole.⁸ The accumulation properties of Ru porphyrins in CHO cells may be improved by the attachment of cationic groups to the porphyrin ring, as James *et al.* have shown enhanced accumulation profiles for cationic porphyrins.^{5,9} H_2TMPyP (TMPyP = dianion of *meso*-tetrakis(4-N-methylpyridinium)porphyrin) has been shown to interact with DNA, and a Mn derivative activated by a water-soluble oxygen-atom donor (potassium monopersulfate, KHSO_5) has been shown to be an efficient DNA-cleaving system.¹⁰ During this present thesis work, the anticancer properties of TEMPO derivatives have been reported.¹¹ The reported isolation of $\text{Ru}(\text{OEP})(\text{CO})(\text{TEMPO})$ encourages a study to coordinate TEMPO (or a related nitroxide derivative) to a cationic, Ru porphyrin.

6.4 Preliminary *In Vitro* Examination Of Water-soluble Ru Sulfoxide Complexes

A preliminary survey of the biological activity of five complexes was presented in Chapter 4. The 5 selected complexes do accumulate in CHO cells, bind to DNA, but are non-toxic at the concentrations tested. Furthermore, no hypoxic selectivity was observed in CHO cells with respect to toxicity, cell accumulation and DNA-binding. A relatively high degree of DNA-binding occurs with these water-soluble complexes, particularly $[\text{RuCl}(\text{BPSP})]_2(\mu\text{-Cl})_3$ and $[\text{RuCl}(\text{BESE})(\text{H}_2\text{O})]_2(\mu\text{-Cl})_2$.

The DNA-binding assays imply that Ru-disulfoxide-DNA adducts are formed, and thus more extensive *in vitro* studies should be undertaken to understand the nature of these interactions. *In vivo* assays should also be undertaken to determine whether these complexes resemble the Ru-DMSO complexes in murine experiments.

Some metal complexes have potential as "carriers" to target radiosensitizers to DNA.¹² The non-toxic, cell accumulating and DNA-binding properties of these complexes might be retained with the addition of a nitroimidazole ligand that would act as the radiosensitizer (see Chapter 1, Section 1.4.3).¹²

For example, Chan *et al.* have shown that the radiosensitizing activities of selected 2- and 4-nitroimidazoles are improved upon coordination using *cis*-RuCl₂(DMSO)₄¹³ and *cis*-RuCl₂(TMSO)₄¹⁴ as precursors. The geometric formulations of some resulting RuCl₂(sulfoxide)₂(L)₂ complexes (sulfoxide = DMSO or TMSO, and L = a nitroimidazole) were not definitely resolved because no crystal structures were determined, and there are several possible isomers within such complexes. The advantage of using chelating disulfoxide ligands would be to reduce the number of possible isomers in the preparation of nitroimidazole complexes. Preliminary attempts to synthesize (in air/H₂O) such complexes using [RuCl(BESE)(H₂O)]₂(μ-Cl)₂, as a precursor, with 2-nitroimidazole, 2-methyl-5-nitroimidazole and imidazole led to water-soluble, red complexes that could not be purified by column chromatography and did not analyze well for C or H content. Of note, Yapp previously isolated red mixtures, from reactions of RuCl₂(disulfoxide)₂ and nitroimidazoles, that could not be purified.^{12a} Follow-up of this chemistry might prove useful for targeting applications.

6.5 References for Chapter 6

- 1 Geremia, S.; Vicentini, L.; Calligaris, M. *Inorg. Chem.* 1998, 37, 4094.
- 2 Chatt, J.; Leigh, G. J.; Storace, A. P. *J. Chem. Soc. (A)* 1971, 1380.
- 3 Schenk, W. A.; Frisch, J.; Dürr, M.; Burzlaff, N.; Stalke, D.; Fleischer, R.; Adam, W.; Prechtel, F.; Smerz, A. K. *Inorg. Chem.* 1997, 36, 2372.
- 4 Ware, C. J. M. Sc. Dissertation, University of British Columbia, Vancouver, 1994.
- 5 James, B. R.; Meng, G. G.; Posakony, J. J.; Ravensbergen, J. A.; Ware, C. J.; Skov, K. A. *Metal-Based Drugs* 1996, 3, 85.
- 6 (a) Posakony, J. J. Ph.D. Dissertation, University of British Columbia, Vancouver, 1998, p. 94;
(b) Posakony, J. J.; Pratt, R. C.; Rettig, S. J.; James, B. R.; Skov, K. A. *Can. J. Chem.* 1999, 77, 182.
- 7 (a) Oschner, M. *Photochem. Photobiol. B: Biol.* 1997, 39, 1;
(b) Dolphin, D. *Can. J. Chem.* 1994, 72, 1005.
- 8 (a) Bazin, M.; Patterson, L. K.; Ronfard-Haret, J. C.; Santus, R. *Photochem. Photobiol.* 1988, 48, 177;
(b) Bazin, M.; Santus, R. *Photochem. Photobiol.* 1986, 43, 235.
- 9 Meng, G. G. Ph.D. Dissertation, University of British Columbia, Vancouver, 1993.
- 10 (a) Pitié, M.; Bernadou, J.; Meunier, B. *J. Am. Chem. Soc.* 1995, 117, 2935 and references therein;
(b) Bigey, P.; Pratviel, G.; Meunier, B. *J. Chem. Soc., Chem. Commun.* 1995, 181.
- 11 (a) Sen', V. D.; Golubev, V. A.; Volkova, L. M.; Konovalova, N. P. *J. Inorg. Biochem.* 1996, 64, 69;
(b) Metodiewa, D.; Skolimowski, J.; Kochman, A.; Gwozdzinski, K.; Glebeska, J. *Anticancer Res.* 1998, 18, 369.
- 12 (a) Yapp, D. T. T. Ph. D. Dissertation, University of British Columbia, Vancouver, 1993;

- (b) Yapp, D. T. T.; Rettig, S. J.; James, B. R.; Skov, K. A. *Inorg. Chem.* 1997, 36, 5635.
- 13 (a) Chan, P. K. L.; Skov, K. A.; James, B. R. *Int. J. Radiat. Biol.* 1987, 52, 49;
(b) Chan, P. K. L.; Chan, P. K. H.; Frost, D. C.; James, B. R.; Skov, K. A. *Can. J. Chem.* 1988, 66, 117.
- 14 Chan, P. K. L.; James, B. R.; Frost, D. C.; Chan, P. K. H.; Hu, H-L.; Skov, K. A. *Can. J. Chem.* 1989, 67, 508.

Appendix 1. Crystallographic Data

Appendix 1.1 Crystallographic Data for *trans*-RuCl₂(BESE)₂

Table A.1 1. Experimental Details for X-ray Crystal Structure of *trans*-RuCl₂(BESE)₂

A. Crystal Data

Empirical Formula	C ₁₂ H ₂₈ Cl ₂ O ₄ RuS ₄
Formula Weight	536.57
Crystal Colour, Habit	yellow, plate
Crystal Dimensions	0.05 x 0.25 x 0.35 mm
Crystal System	monoclinic
Lattice Type	Primitive
Lattice Parameters	a = 10.309(2) Å b = 7.6799(9) Å c = 12.9465(7) Å β = 104.721(1) ° V = 991.4(2) Å ³
Space Group	P2 ₁ /n (# 14)
Z Value	2
D _{calc}	1.797 g/cm ³
F ₀₀₀	548.00
μ(MoKα)	14.94 cm ⁻¹

B. Intensity Measurements

Diffractometer	Rigaku/ADSC CCD
Radiation	MoKα (λ = 0.71069 Å) graphite monochromated
Detector Aperature	94 mm x 94 mm
Data Images	460 exposures at 90.0 seconds
φ oscillation Range (χ = -90)	0.0 - 190.0 °
ω oscillation Range (χ = -90)	-22.0 - 18.0 °
Detector Position	39.18(1) mm
Detector Swing Angle	-10 °
2θ _{max}	60 °
Scan Width	-0.30 °
2θ _{max}	67.0 °
No. of Reflections Measured	Total: 9574 Unique: 2344 (R _{int} = 0.024)
Corrections	Lorentz-polarization Absorption/scaling (trans. factors: 0.7927 - 0.9986)

C. Structure Solution and Refinement

Structure Solution	Direct Methods (SIR92)
Refinement	Full-matrix least-squares
Function Minimized	Σω(F _o ² - F _c ²) ²
Least Squares Weights	ω = 1/σ ² (F _o ²)
p-factor	0.0100
Anomalous Dispersion	All non-hydrogen atoms
No. Observations (I > 0.00σ(I))	2344
No. Variables	162
Reflection/Parameter Ratio	14.47
Residuals (on F ² , all data): R; Rw	0.063; 0.075

Goodness of Fit Indicator	2.57
No. Observations ($I > 3\sigma(I)$)	1928
Residuals (on F, $I > 3\sigma(I)$): R1; R1w	0.033; 0.037
Max Shift/Error in Final Cycle	0.0006
Maximum peak in Final Diff. Map	$0.38 \text{ e}^-/\text{\AA}^3$
Minimum peak in Final Diff. Map	$-0.84 \text{ e}^-/\text{\AA}^3$

Table A.1 2. Bond Angles ($^\circ$) for *trans*-RuCl₂(BESE)₂

atom	atom	atom	angle	atom	atom	atom	angle
Cl(1)	Ru(1)	Cl(1)	180.00	Ru(1)	S(1)	C(1)	104.9(1)
Cl(1)	Ru(1)	S(1)	89.12(3)	Ru(1)	S(1)	C(3)	116.6(1)
Cl(1)	Ru(1)	S(1)	90.88(3)	O(1)	S(1)	C(1)	107.6(1)
Cl(1)	Ru(1)	S(2)	92.27(3)	O(1)	S(1)	C(3)	107.1(2)
Cl(1)	Ru(1)	S(2)	87.73(3)	C(1)	S(1)	C(3)	99.1(2)
Cl(1)	Ru(1)	S(1)	90.88(3)	Ru(1)	S(2)	O(2)	119.44(9)
Cl(1)	Ru(1)	S(1)	89.12(3)	Ru(1)	S(2)	C(2)	103.5(1)
Cl(1)	Ru(1)	S(2)	87.73(3)	Ru(1)	S(2)	C(5)	115.7(1)
Cl(1)	Ru(1)	S(2)	92.27(3)	O(2)	S(2)	C(2)	106.6(1)
S(1)	Ru(1)	S(1)	180.00	O(2)	S(2)	C(5)	108.1(2)
S(1)	Ru(1)	S(2)	85.42(3)	C(2)	S(2)	C(5)	101.3(2)
S(1)	Ru(1)	S(2)	94.58(3)	S(1)	C(1)	C(2)	110.9(2)
S(1)	Ru(1)	S(2)	94.58(3)	S(2)	C(2)	C(1)	106.8(2)
S(1)	Ru(1)	S(2)	85.42(3)	S(1)	C(3)	C(4)	111.1(2)
S(2)	Ru(1)	S(2)	180.00	S(2)	C(5)	C(6)	112.2(2)
Ru(1)	S(1)	O(1)	119.31(9)				

Angles are in degrees. Estimated standard deviations in the least significant figure are given in parentheses.

Table A.1 3. Bond Lengths (\AA) for *trans*-RuCl₂(BESE)₂

atom	atom	distance	atom	atom	distance
Ru(1)	Cl(1)	2.4018(7)	S(1)	C(3)	1.802(3)
Ru(1)	Cl(1)	2.4018(7)	S(2)	O(2)	1.480(2)
Ru(1)	S(1)	2.3288(7)	S(2)	C(2)	1.809(3)
Ru(1)	S(1)	2.3288(7)	S(2)	C(5)	1.797(3)
Ru(1)	S(2)	2.3212(9)	C(1)	C(2)	1.512(5)
Ru(1)	S(2)	2.3212(9)	C(3)	C(4)	1.518(5)
S(1)	O(1)	1.479(2)	C(5)	C(6)	1.518(5)
S(1)	C(1)	1.804(3)			

Distances are in angstroms. Estimated standard deviations in the least significant figure are given in parentheses.

Table A.1 4. Atomic Coordinates for *trans*-RuCl₂(BESE)₂

atom	x	y	z
Ru(1)	0.50000	0.50000	0.50000
Cl(1)	0.55954(8)	0.78088(9)	0.57951(6)
S(1)	0.49825(8)	0.39123(9)	0.66755(6)
S(2)	0.72217(8)	0.40991(9)	0.54113(6)
O(1)	0.4587(2)	0.5070(3)	0.7456(2)
O(2)	0.8297(2)	0.5363(3)	0.5870(2)
C(1)	0.6684(3)	0.3216(4)	0.7255(3)
C(2)	0.7293(3)	0.2437(4)	0.6414(3)
C(3)	0.4137(3)	0.1865(4)	0.6700(3)
C(4)	0.2626(4)	0.2098(5)	0.6371(3)

C(5)	0.7718(3)	0.2886(4)	0.4388(3)
C(6)	0.9153(4)	0.2238(5)	0.4752(3)

Appendix 1.2 Crystallographic Data for *cis*-RuCl₂(BBSE)₂·EtOH

Table A.1 5. Experimental Details for X-ray Crystal Structure of *cis*-RuCl₂(BBSE)₂·EtOH

A. Crystal Data

Empirical Formula	C ₂₂ H ₅₀ Cl ₂ O ₅ RuS ₄
Formula Weight	694.85
Crystal Colour, Habit	yellow, prism
Crystal Dimensions	0.50 x 0.35 x 0.20 mm
Crystal System	orthorhombic
Lattice Type	Primitive
Lattice Parameters	a = 16.1309(3) Å b = 15.7775(7) Å c = 24.9852(4) Å V = 6358.9(5) Å ³
Space Group	Pbca (# 61)
Z Value	8
D _{calc}	1.452 g/cm ³
F ₀₀₀	2912.00
μ(MoKα)	9.52 cm ⁻¹

B. Intensity Measurements

Diffractometer	Rigaku/ADSC CCD
Radiation	MoKα (λ = 0.71069 Å) graphite monochromated
Detector Aperature	94 mm x 94 mm
Data Images	769 exposures of 25.0 seconds
φ oscillation Range (χ = -90)	0.0 - 190.2 °
ω oscillation Range (χ = -90)	-23.0 - 17.8 °
Detector Position	39.21(2) mm
Detector Swing Angle	-10 °
2θ _{max}	60.1 °
No. of Reflections Measured	Total: 58797 Unique: 8641 (R _{int} = 0.036)
Corrections	Lorentz-polarization Absorption/scaling (trans. factors: 0.6880 - 1.0000)

C. Structure Solution and Refinement

Structure Solution	Patterson Methods (DIRDIF92 PATTY)
Refinement	Full-matrix least-squares
Function Minimized	Σω(F _o ² - F _c ²) ²
Least Squares Weights	ω = 1/σ ² (F _o ²)
p-factor	0.0000
Anomalous Dispersion	All non-hydrogen atoms
No. Observations	8641
No. Variables	2317
Reflection/Parameter Ratio	27.26
Residuals (on F ² , all data): R; Rw	0.067; 0.062
Goodness of Fit Indicator	1.75
No. Observations (I > 3σ(I))	4889

Residuals (on F, $I > 3\sigma(I)$): R; R _w	0.040; 0.028
Max Shift/Error in Final Cycle	0.008
Maximum peak in Final Diff. Map	1.62 e ⁻ /Å ³ (near Ru)
Minimum peak in Final Diff. Map	-2.30 e ⁻ /Å ³ (near Ru)

Table A.1 6. Bond Angles (°) for *cis*-RuCl₂(BBSE)₂·EtOH

atom	atom	atom	angle		atom	atom	atom	angle
Cl(1)	Ru(1)	Cl(2)	86.16(3)		Cl(1)	Ru(1)	S(1)	173.01(3)
Cl(1)	Ru(1)	S(2)	90.21(3)		Cl(1)	Ru(1)	S(3)	89.94(3)
Cl(1)	Ru(1)	S(4)	89.11(3)		Cl(2)	Ru(1)	S(1)	87.71(3)
Cl(2)	Ru(1)	S(2)	88.99(3)		Cl(2)	Ru(1)	S(3)	176.04(3)
Cl(2)	Ru(1)	S(4)	93.41(3)		S(1)	Ru(1)	S(2)	86.32(3)
S(1)	Ru(1)	S(3)	96.22(3)		S(1)	Ru(1)	S(4)	94.62(3)
S(2)	Ru(1)	S(3)	91.76(3)		S(2)	Ru(1)	S(4)	177.46(3)
S(3)	Ru(1)	S(4)	85.79(3)		Ru(1)	S(1)	O(1)	116.88(9)
Ru(1)	S(1)	C(1)	104.36(11)		Ru(1)	S(1)	C(3)	119.29(10)
O(1)	S(1)	C(1)	107.40(13)		O(1)	S(1)	C(3)	105.91(13)
C(1)	S(1)	C(3)	101.28(14)		Ru(1)	S(2)	O(2)	117.32(9)
Ru(1)	S(2)	C(2)	103.74(11)		Ru(1)	S(2)	C(7)	115.81(12)
O(2)	S(2)	C(2)	108.17(13)		O(2)	S(2)	C(7)	107.82(15)
C(2)	S(2)	C(7)	102.59(14)		Ru(1)	S(3)	O(3)	118.59(8)
Ru(1)	S(3)	C(11)	105.92(10)		Ru(1)	S(3)	C(13)	123.85(10)
O(3)	S(3)	C(11)	107.06(15)		O(3)	S(3)	C(13)	108.12(14)
C(11)	S(3)	C(13)	101.69(15)		Ru(1)	S(4)	O(4)	118.37(10)
Ru(1)	S(4)	C(12)	102.72(12)		Ru(1)	S(4)	C(17)	114.25(12)
O(4)	S(4)	C(12)	107.84(14)		O(4)	S(4)	C(17)	109.23(15)
C(12)	S(4)	C(17)	102.8(2)		S(1)	C(1)	C(2)	110.0(2)
S(2)	C(2)	C(1)	107.5(2)		S(1)	C(3)	C(4)	111.6(2)
C(3)	C(4)	C(5)	112.4(3)		C(4)	C(5)	C(6)	112.1(3)
S(2)	C(7)	C(8)	111.5(2)		C(7)	C(8)	C(9)	113.3(3)
C(8)	C(9)	C(10)	113.0(4)		S(3)	C(11)	C(12)	112.2(3)
S(4)	C(12)	C(11)	106.3(2)		S(3)	C(13)	C(14)	113.2(2)
C(13)	C(14)	C(15)	111.3(3)		C(14)	C(15)	C(16)	117.7(5)
C(14)	C(15)	C(16a)	125.2(6)		S(4)	C(17)	C(18)	113.5(2)
C(17)	C(18)	C(19)	111.0(3)		C(18)	C(19)	C(20)	113.5(3)
O(5)	C(21)	C(22)	108.4(4)					

Angles are in degrees. Estimated standard deviations in the least significant figure are given in parentheses.

Table A.1 7. Bond Lengths (Å) for *cis*-RuCl₂(BBSE)₂·EtOH

atom	atom	distance		atom	atom	distance
Ru(1)	Cl(1)	2.4159(8)		O(5)	C(21)	1.402(4)
Ru(1)	Cl(2)	2.4288(7)		C(1)	C(2)	1.503(4)
Ru(1)	S(1)	2.2906(8)		C(3)	C(4)	1.516(4)
Ru(1)	S(2)	2.3035(9)		C(4)	C(5)	1.521(4)
Ru(1)	S(3)	2.2674(7)		C(5)	C(6)	1.522(5)
Ru(1)	S(4)	2.2892(9)		C(7)	C(8)	1.515(5)
S(1)	O(1)	1.480(2)		C(8)	C(9)	1.504(5)
S(1)	C(1)	1.802(3)		C(9)	C(10)	1.514(5)
S(1)	C(3)	1.804(3)		C(11)	C(12)	1.501(5)
S(2)	O(2)	1.482(2)		C(13)	C(14)	1.521(4)
S(2)	C(2)	1.797(3)		C(14)	C(15)	1.511(5)
S(2)	C(7)	1.791(3)		C(15)	C(16a)	1.35(1)

S(3)	O(3)	1.468(2)		C(15)	C(16)	1.341(8)
S(3)	C(11)	1.838(4)		C(16a)	C(16)	1.71(1)
S(3)	C(13)	1.794(3)		C(17)	C(18)	1.521(4)
S(4)	O(4)	1.477(2)		C(18)	C(19)	1.503(4)
S(4)	C(12)	1.820(3)		C(19)	C(20)	1.511(5)
S(4)	C(17)	1.793(3)		C(21)	C(22)	1.420(6)

Distances are in angstroms. Estimated standard deviations in the least significant figure are given in parentheses.

Table A.1 8. Atomic Coordinates for *cis*-RuCl₂(BBSE)₂·EtOH

atom	x	y	z	atom	x	y	z
S(1)	0.51156(5)	0.15392(4)	0.43542(3)	C(7)	0.6035(2)	0.1196(2)	0.60824(14)
S(2)	0.55568(5)	0.18151(5)	0.55669(3)	C(8)	0.5624(2)	0.1341(2)	0.6619(2)
S(3)	0.60476(5)	0.33631(4)	0.47490(4)	C(9)	0.6048(3)	0.0887(2)	0.7073(2)
S(4)	0.70447(5)	0.21496(5)	0.40146(4)	C(10)	0.5726(3)	0.1149(3)	0.7617(2)
O(1)	0.51180(12)	0.06875(11)	0.41064(9)	C(11)	0.6678(2)	0.3771(2)	0.41934(14)
O(2)	0.52370(14)	0.26026(12)	0.58154(9)	C(12)	0.7425(2)	0.3229(2)	0.40877(14)
O(3)	0.51937(13)	0.36492(11)	0.46570(10)	C(13)	0.6458(2)	0.3944(2)	0.53062(14)
O(4)	0.66035(13)	0.20936(13)	0.34979(9)	C(14)	0.6193(2)	0.4869(2)	0.5312(2)
O(5)	0.6514(2)	-0.02427(14)	0.36083(10)	C(15)	0.6423(4)	0.5293(2)	0.5833(2)
C(1)	0.4335(2)	0.1536(2)	0.48702(13)	C(16a)	0.7059(7)	0.5060(6)	0.6154(5)
C(2)	0.4686(2)	0.1172(2)	0.53776(13)	C(16)	0.6014(5)	0.5053(4)	0.6276(3)
C(3)	0.4653(2)	0.2239(2)	0.38669(13)	C(17)	0.7982(2)	0.1541(2)	0.39778(14)
C(4)	0.3857(2)	0.1873(2)	0.36417(13)	C(18)	0.8506(2)	0.1741(2)	0.34878(15)
C(5)	0.3452(2)	0.2459(2)	0.32350(15)	C(19)	0.9172(2)	0.1085(2)	0.3410(2)
C(6)	0.2636(3)	0.2104(3)	0.3027(2)	C(20)	0.9698(3)	0.1236(2)	0.2919(2)
				C(21)	0.6377(3)	0.0040(2)	0.3084(2)
				C(22)	0.6884(4)	-0.0444(5)	0.2733(2)

Table A.1 9. Hydrogen bond parameters for A-H...B interactions.

A	H	B	A...B	A-H	H...B	A-H...B
O(5)	H(45)	O(1)	2.963(3)	0.90	2.12	155.7
O(5)	H(45)	Cl(2)	3.301(3)	0.90	2.71	124.1
C(12)	H(26)	O(5)	3.189(4)	0.98	2.50	127.5
C(21)	H(47)	O(4)	3.421(4)	0.98	2.55	148.5

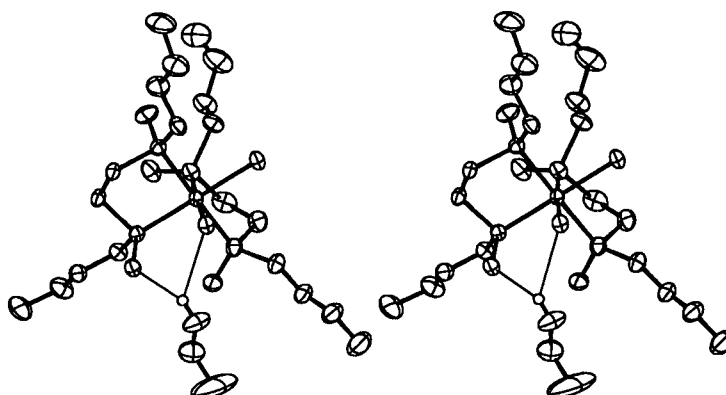


Figure A.1.1. Stereoview of *cis*-RuCl₂(BBSE)₂·EtOH.

Appendix 1.3 Crystallographic Data for *cis*-RuCl₂(BCySE)₂·EtOH·1/3MeOH**Table A.1 10.** Experimental Details for X-ray Crystal Structure of *cis*-RuCl₂(BCySE)₂·EtOH·1/3MeOH*A. Crystal Data*

Empirical Formula	C _{30.333} H _{59.333} Cl ₂ O _{5.333} RuS ₄
Formula Weight	809.68
Crystal Colour, Habit	yellow, hexagonal prism
Crystal Dimensions	0.15 x 0.50 x 0.50 mm
Crystal System	trigonal
Lattice Type	Primitive
Lattice Parameters	a = 23.2038(7) Å c = 12.1481(2) Å V = 5664.4(2) Å ³
Space Group	P $\bar{3}$ (# 147)
Z Value	6
D _{calc}	1.424 g/cm ³
F ₀₀₀	2556.00
μ (MoK α)	8.14 cm ⁻¹

B. Intensity Measurements

Diffractionmeter	Rigaku/ADSC CCD
Radiation	MoK α (λ = 0.71069 Å) graphite monochromated
Detector Aperature	94 mm x 94 mm
Data Images	768 exposures of 12.0 seconds
ϕ oscillation Range (χ = -90)	0.0 - 189.9 °
ω oscillation Range (χ = -90)	-23.0 - 17.8 °
Detector Position	39.23(3) mm
Detector Swing Angle	-10.0 °
2 θ_{max}	60.1 °
No. of Reflections Measured	Total: 51678 Unique: 10114 (R_{int} = 0.050)
Corrections	Lorentz-polarization Absorption/scaling (trans. factors: 0.7224 - 1.0000)

C. Structure Solution and Refinement

Structure Solution	Patterson Methods (DIRDIF92 PATTY)
Refinement	Full-matrix least-squares
Function Minimized	$\Sigma \omega (Fo^2 - Fc^2)^2$
Least Squares Weights	$\omega = 1/\sigma^2(Fo^2)$
p-factor	0.0000
Anomalous Dispersion	All non-hydrogen atoms
No. Observations	10114
No. Variables	370
Reflection/Parameter Ratio	27.34
Residuals (on F ² , all data): R; Rw	0.096; 0.090
Goodness of Fit Indicator	1.11
No. Observations ($I > 3\sigma(I)$)	3492
Residuals (on F, $I > 3\sigma(I)$): R; Rw	0.045; 0.041
Max Shift/Error in Final Cycle	0.0007
Maximum peak in Final Diff. Map	2.08 e ⁻ /Å ³ (at origin)

Minimum peak in Final Diff. Map

 $-1.64 \text{ e}^-/\text{\AA}^3$ **Table A.1 11.** Bond Angles ($^\circ$) for *cis*-RuCl₂(BCySE)₂·EtOH·1/3MeOH

atom	atom	atom	angle	atom	atom	atom	angle
Cl(1)	Ru(1)	Cl(2)	88.25(4)	S(2)	C(2)	C(1)	106.7(4)
Cl(1)	Ru(1)	S(1)	178.01(5)	S(1)	C(3)	C(4)	113.4(4)
Cl(1)	Ru(1)	S(2)	92.03(5)	S(1)	C(3)	C(8)	109.0(3)
Cl(1)	Ru(1)	S(3)	92.96(5)	C(4)	C(3)	C(8)	109.9(4)
Cl(1)	Ru(1)	S(4)	87.61(5)	C(3)	C(4)	C(5)	108.5(5)
Cl(2)	Ru(1)	S(1)	90.08(5)	C(4)	C(5)	C(6)	110.1(5)
Cl(2)	Ru(1)	S(2)	86.27(5)	C(5)	C(6)	C(7)	109.4(5)
Cl(2)	Ru(1)	S(3)	176.38(5)	C(6)	C(7)	C(8)	111.7(5)
Cl(2)	Ru(1)	S(4)	96.50(5)	C(3)	C(8)	C(7)	112.0(5)
S(1)	Ru(1)	S(2)	86.78(5)	S(2)	C(9)	C(10)	106.3(3)
S(1)	Ru(1)	S(3)	88.65(5)	S(2)	C(9)	C(14)	112.3(4)
S(1)	Ru(1)	S(4)	93.65(5)	C(10)	C(9)	C(14)	111.7(4)
S(2)	Ru(1)	S(3)	90.28(5)	C(9)	C(10)	C(11)	109.9(4)
S(2)	Ru(1)	S(4)	177.19(5)	C(10)	C(11)	C(12)	112.7(6)
S(3)	Ru(1)	S(4)	86.96(5)	C(11)	C(12)	C(13)	110.4(5)
Ru(1)	S(1)	O(1)	119.2(1)	C(12)	C(13)	C(14)	113.3(5)
Ru(1)	S(1)	C(1)	102.8(2)	C(9)	C(14)	C(13)	110.5(5)
Ru(1)	S(1)	C(3)	118.2(2)	S(3)	C(15)	C(16)	109.6(3)
O(1)	S(1)	C(1)	107.8(2)	S(4)	C(16)	C(15)	108.8(4)
O(1)	S(1)	C(3)	106.5(2)	S(3)	C(17)	C(18)	112.0(4)
C(1)	S(1)	C(3)	100.0(2)	S(3)	C(17)	C(22)	108.4(4)
Ru(1)	S(2)	O(2)	118.2(2)	C(18)	C(17)	C(22)	108.5(5)
Ru(1)	S(2)	C(2)	101.5(2)	C(17)	C(18)	C(19)	110.1(6)
Ru(1)	S(2)	C(9)	116.0(2)	C(18)	C(19)	C(20)	107.3(7)
O(2)	S(2)	C(2)	107.6(3)	C(19)	C(20)	C(21)	107.7(7)
O(2)	S(2)	C(9)	107.6(2)	C(20)	C(21)	C(22)	106.2(7)
C(2)	S(2)	C(9)	104.5(2)	C(17)	C(22)	C(21)	107.1(5)
Ru(1)	S(3)	O(3)	117.5(2)	S(4)	C(23)	C(24)	108.7(4)
Ru(1)	S(3)	C(15)	104.3(2)	S(4)	C(23)	C(28)	112.1(4)
Ru(1)	S(3)	C(17)	117.8(2)	C(24)	C(23)	C(28)	111.5(5)
O(3)	S(3)	C(15)	106.8(2)	C(23)	C(24)	C(25)	109.6(6)
O(3)	S(3)	C(17)	106.7(2)	C(24)	C(25)	C(26)	109.5(6)
C(15)	S(3)	C(17)	102.1(2)	C(25)	C(26)	C(27)	110.5(6)
Ru(1)	S(4)	O(4)	119.8(2)	C(26)	C(27)	C(28)	110.6(7)
Ru(1)	S(4)	C(16)	102.6(2)	C(23)	C(28)	C(27)	110.5(5)
Ru(1)	S(4)	C(23)	116.4(2)	O(5)	C(29)	C(30)	124(2)
O(4)	S(4)	C(16)	106.5(2)				
O(4)	S(4)	C(23)	107.9(2)				
C(16)	S(4)	C(23)	101.3(3)				
S(1)	C(1)	C(2)	109.5(3)				

Angles are in degrees. Estimated standard deviations in the least significant figure are given in parentheses.

Table A.1 12. Bond Lengths (\AA) for *cis*-RuCl₂(BCySE)₂·EtOH·1/3MeOH

atom	atom	distance		atom	atom	distance
Ru(1)	Cl(1)	2.420(1)		C(5)	C(6)	1.555(8)
Ru(1)	Cl(2)	2.434(1)		C(6)	C(7)	1.506(8)
Ru(1)	S(1)	2.299(1)		C(7)	C(8)	1.532(7)
Ru(1)	S(2)	2.336(1)		C(9)	C(10)	1.547(6)
Ru(1)	S(3)	2.272(1)		C(9)	C(14)	1.530(7)

Ru(1)	S(4)	2.348(1)		C(10)	C(11)	1.528(7)
S(1)	O(1)	1.470(3)		C(11)	C(12)	1.503(8)
S(1)	C(1)	1.815(5)		C(12)	C(13)	1.486(8)
S(1)	C(3)	1.835(5)		C(13)	C(14)	1.526(7)
S(2)	O(2)	1.444(4)		C(15)	C(16)	1.494(7)
S(2)	C(2)	1.782(5)		C(17)	C(18)	1.497(7)
S(2)	C(9)	1.842(5)		C(17)	C(22)	1.530(7)
S(3)	O(3)	1.470(3)		C(18)	C(19)	1.585(8)
S(3)	C(15)	1.814(5)		C(19)	C(20)	1.55(1)
S(3)	C(17)	1.837(5)		C(20)	C(21)	1.454(9)
S(4)	O(4)	1.464(4)		C(21)	C(22)	1.662(9)
S(4)	C(16)	1.821(5)		C(23)	C(24)	1.523(7)
S(4)	C(23)	1.812(5)		C(23)	C(28)	1.496(7)
O(5)	C(29)	1.39(2)		C(24)	C(25)	1.569(9)
O(6)	C(31)	1.57(2)		C(25)	C(26)	1.527(9)
C(1)	C(2)	1.508(7)		C(26)	C(27)	1.496(9)
C(3)	C(4)	1.497(7)		C(27)	C(28)	1.560(9)
C(3)	C(8)	1.531(6)		C(29)	C(30)	1.24(2)
C(4)	C(5)	1.549(7)				

Distances are in angstroms. Estimated standard deviations in the least significant figure are given in parentheses.

Table A.1 13. Atomic Coordinates for *cis*-RuCl₂(BCySE)₂·EtOH·1/3MeOH

atom	x	y	z	atom	x	y	z
Ru(1)	0.23894(2)	0.40975(2)	0.49281(3)	C(10)	0.3571(3)	0.4190(3)	0.7646(4)
Cl(1)	0.21241(7)	0.31625(6)	0.61228(10)	C(11)	0.4029(3)	0.3959(4)	0.8134(5)
Cl(2)	0.31782(6)	0.38685(6)	0.39821(9)	C(12)	0.4741(4)	0.4511(4)	0.8205(5)
S(1)	0.26788(6)	0.49927(6)	0.37892(10)	C(13)	0.4987(3)	0.4810(3)	0.7102(6)
S(2)	0.32838(6)	0.48219(6)	0.60370(10)	C(14)	0.4564(3)	0.5066(3)	0.6565(5)
S(3)	0.17089(6)	0.43702(7)	0.58553(11)	C(15)	0.0964(2)	0.4035(3)	0.5014(4)
S(4)	0.14555(7)	0.33764(7)	0.38722(11)	C(16)	0.0771(2)	0.3346(3)	0.4654(4)
O(1)	0.2173(2)	0.5169(2)	0.3487(3)	C(17)	0.1375(3)	0.3963(3)	0.7186(4)
O(2)	0.3151(2)	0.5122(2)	0.6972(4)	C(18)	0.1914(3)	0.4139(3)	0.8019(6)
O(3)	0.1940(2)	0.5081(2)	0.6011(3)	C(19)	0.1603(4)	0.3771(5)	0.9147(5)
O(4)	0.1390(2)	0.3560(2)	0.2745(3)	C(20)	0.1134(5)	0.4019(5)	0.9561(6)
O(5)	-0.0396(9)	0.1081(9)	0.0229(12)	C(21)	0.0582(4)	0.3786(5)	0.8790(6)
O(6)	0.3333	0.6667	-0.3194(14)	C(22)	0.0903(4)	0.4192(4)	0.7620(5)
C(1)	0.3323(3)	0.5682(2)	0.4568(4)	C(23)	0.1229(3)	0.2507(3)	0.3868(4)
C(2)	0.3778(3)	0.5470(2)	0.5090(4)	C(24)	0.1713(3)	0.2424(3)	0.3130(6)
C(3)	0.3140(2)	0.5057(2)	0.2525(4)	C(25)	0.1537(4)	0.1677(4)	0.3138(7)
C(4)	0.2770(3)	0.4482(3)	0.1758(4)	C(26)	0.0818(4)	0.1235(3)	0.2762(6)
C(5)	0.3223(4)	0.4576(3)	0.0757(5)	C(27)	0.0352(4)	0.1322(4)	0.3504(7)
C(6)	0.3385(4)	0.5223(3)	0.0125(5)	C(28)	0.0523(3)	0.2063(3)	0.3517(6)
C(7)	0.3724(3)	0.5810(3)	0.0893(5)	C(29)	-	0.1469(12)	0.0605(15)
					0.0655(10)		
C(8)	0.3313(3)	0.5708(3)	0.1938(4)	C(30)	-0.0334(7)	0.2087(8)	0.0633(10)
C(9)	0.3836(2)	0.4513(3)	0.6507(4)	C(31)	0.3333	0.6667	-0.190(2)

Table A.1 14. Hydrogen bond structural parameters for A-H...B interactions.

A	H	B	A...B	A-H	H...B	A-H...B
O(5)	H(58)	O(5)	3.12(2)	0.95	2.23	156.6

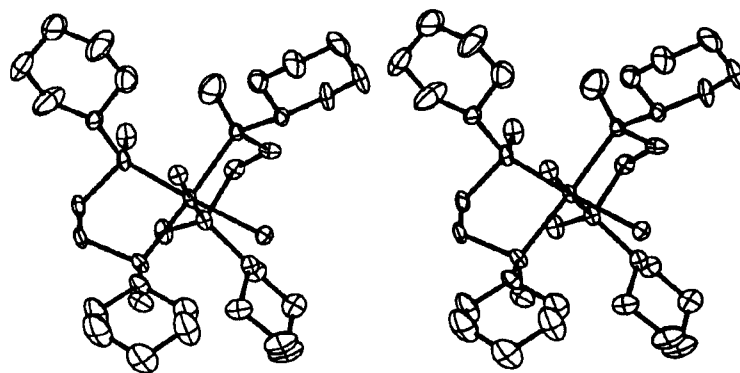


Figure A.1.2. Stereoview of *cis*-RuCl₂(BCySE)₂·EtOH·1/3MeOH.

Appendix 1.4 Crystallographic Data for *cis*-RuCl₂(BESP)₂·EtOH·H₂O**Table A.1 15.** Experimental Details for X-ray Crystal Structure of *cis*-RuCl₂(BESP)₂·EtOH·H₂O*A. Crystal Data*

Empirical Formula	C ₁₆ H ₄₀ Cl ₂ RuS ₄
Formula Weight	628.70
Crystal Colour, Habit	yellow, plate
Crystal Dimensions	0.05 x 0.20 x 0.35 mm
Crystal System	monoclinic
Lattice Type	Primitive
Lattice Parameters	a = 10.1443(7) Å b = 21.287(3) Å c = 11.9548(4) Å β = 98.8216(9) ° V = 2551.0(3) Å ³
Space Group	P2 ₁ /a (# 14)
Z Value	4
D _{calc}	1.637 g/cm ³
F ₀₀₀	1304.00
μ(MoKα)	11.80 cm ⁻¹

B. Intensity Measurements

Diffractometer	Rigaku/ADSC CCD
Radiation	MoKα (λ = 0.71069 Å) graphite monochromated
Detector Aperature	94 mm x 94 mm
Data Images	462 exposures of 70.0 seconds
φ oscillation Range (χ = -90)	0.0 - 190.0 °
ω oscillation Range (χ = -90)	-23.0 - 18.0 °
Detector Position	39.21(3) mm
Detector Swing Angle	-10 °
2θ _{max}	60.1 °
No. of Reflections Measured	Total: 21407 Unique: 6125 (R _{int} = 0.037)
Corrections	Lorentz-polarization Absorption/scaling (trans. factors: 0.7749 - 1.0000)

C. Structure Solution and Refinement

Structure Solution	Patterson Methods (DIRDIF92 PATTY)
Refinement	Full-matrix least-squares
Function Minimized	Σω(F _o ² - F _c ²) ²
Least Squares Weights	ω = 1/σ ² (F _o ²)
p-factor	0.0000
Anomalous Dispersion	All non-hydrogen atoms
No. Observations	6125
No. Variables	262
Reflection/Parameter Ratio	23.38
Residuals (on F ² , all data): R; Rw	0.072; 0.065
Goodness of Fit Indicator	1.77
No. Observations (I > 3σ(I))	4104
Residuals (on F, I > 3σ(I)): R; Rw	0.038; 0.031

Max Shift/Error in Final Cycle	0.002
Maximum peak in Final Diff. Map	1.56 e ⁻ /Å ³
Minimum peak in Final Diff. Map	-1.46 e ⁻ /Å ³

Table A.1 16. Bond Angles (°) for *cis*-RuCl₂(BESP)₂·EtOH·H₂O

atom	atom	atom	angle	atom	atom	atom	angle
Cl(1)	Ru(1)	Cl(2)	89.53(3)	O(2)	S(2)	C(6)	107.7(2)
Cl(1)	Ru(1)	S(1)	176.35(4)	C(3)	S(2)	C(6)	100.9(2)
Cl(1)	Ru(1)	S(2)	91.89(3)	Ru(1)	S(3)	O(3)	116.3(1)
Cl(1)	Ru(1)	S(3)	86.89(3)	Ru(1)	S(3)	C(8)	112.7(1)
Cl(1)	Ru(1)	S(4)	88.90(3)	Ru(1)	S(3)	C(11)	113.8(1)
Cl(2)	Ru(1)	S(1)	92.94(3)	O(3)	S(3)	C(8)	107.3(2)
Cl(2)	Ru(1)	S(2)	86.72(4)	O(3)	S(3)	C(11)	106.7(2)
Cl(2)	Ru(1)	S(3)	175.56(3)	C(8)	S(3)	C(11)	98.4(2)
Cl(2)	Ru(1)	S(4)	84.96(3)	Ru(1)	S(4)	O(4)	113.4(1)
S(1)	Ru(1)	S(2)	90.94(3)	Ru(1)	S(4)	C(10)	115.8(1)
S(1)	Ru(1)	S(3)	90.76(3)	Ru(1)	S(4)	C(13)	112.2(1)
S(1)	Ru(1)	S(4)	88.63(3)	O(4)	S(4)	C(10)	107.2(2)
S(2)	Ru(1)	S(3)	90.78(4)	O(4)	S(4)	C(13)	107.8(2)
S(2)	Ru(1)	S(4)	171.64(4)	C(10)	S(4)	C(13)	99.4(2)
S(3)	Ru(1)	S(4)	97.57(4)	S(1)	C(1)	C(2)	116.5(3)
Ru(1)	S(1)	O(1)	115.8(1)	C(1)	C(2)	C(3)	117.1(3)
Ru(1)	S(1)	C(1)	109.5(1)	S(2)	C(3)	C(2)	112.9(3)
Ru(1)	S(1)	C(4)	115.1(1)	S(1)	C(4)	C(5)	111.9(3)
O(1)	S(1)	C(1)	106.3(2)	S(2)	C(6)	C(7)	112.8(3)
O(1)	S(1)	C(4)	106.4(2)	S(3)	C(8)	C(9)	112.4(2)
C(1)	S(1)	C(4)	102.5(2)	C(8)	C(9)	C(10)	111.7(3)
Ru(1)	S(2)	O(2)	117.9(1)	S(4)	C(10)	C(9)	113.3(3)
Ru(1)	S(2)	C(3)	109.0(1)	S(3)	C(11)	C(12)	112.2(3)
Ru(1)	S(2)	C(6)	112.5(1)	S(4)	C(13)	C(14)	112.7(3)
O(2)	S(2)	C(3)	107.4(2)	O(5)	C(15)	C(16)	111.8(5)

Angles are in degrees. Estimated standard deviations in the least significant figure are given in parentheses.

Table A.1 17. Bond Lengths (Å) for *cis*-RuCl₂(BESP)₂·EtOH·H₂O

atom	atom	distance	atom	atom	distance
Ru(1)	Cl(1)	2.4167(8)	S(3)	C(11)	1.820(3)
Ru(1)	Cl(2)	2.431(1)	S(4)	O(4)	1.489(2)
Ru(1)	S(1)	2.2766(8)	S(4)	C(10)	1.806(4)
Ru(1)	S(2)	2.331(1)	S(4)	C(13)	1.792(4)
Ru(1)	S(3)	2.291(1)	O(5)	C(15)	1.376(7)
Ru(1)	S(4)	2.353(1)	C(1)	C(2)	1.547(5)
S(1)	O(1)	1.481(3)	C(2)	C(3)	1.536(5)
S(1)	C(1)	1.799(4)	C(4)	C(5)	1.529(5)
S(1)	C(4)	1.791(4)	C(6)	C(7)	1.500(5)
S(2)	O(2)	1.490(3)	C(8)	C(9)	1.524(5)
S(2)	C(3)	1.789(4)	C(9)	C(10)	1.513(5)
S(2)	C(6)	1.808(4)	C(11)	C(12)	1.484(6)
S(3)	O(3)	1.479(2)	C(13)	C(14)	1.527(5)
S(3)	C(8)	1.802(4)	C(15)	C(16)	1.533(9)

Distances are in angstroms. Estimated standard deviations in the least significant figure are given in parentheses.

Table A.1 18. Atomic Coordinates for *cis*-RuCl₂(BESP)₂·EtOH·H₂O

atom	x	y	z
Ru(1)	0.71815(2)	0.402560(14)	0.29850(3)
Cl(1)	0.95155(7)	0.38026(4)	0.36032(8)
Cl(2)	0.69663(8)	0.43432(5)	0.49019(8)
S(1)	0.49722(8)	0.41752(4)	0.23460(8)
S(2)	0.76308(8)	0.50771(4)	0.26506(8)
S(3)	0.75461(8)	0.37600(5)	0.12011(8)
S(4)	0.66649(8)	0.30141(4)	0.35820(8)
O(1)	0.4294(2)	0.36644(12)	0.1637(2)
O(2)	0.7842(2)	0.52583(12)	0.1487(2)
O(3)	0.6513(2)	0.39595(12)	0.0257(2)
O(4)	0.5257(2)	0.29492(12)	0.3781(2)
O(5)	0.6262(4)	0.7273(3)	0.1793(4)
C(1)	0.4757(3)	0.4876(2)	0.1497(4)
C(2)	0.5028(3)	0.5507(2)	0.2133(4)
C(3)	0.6301(3)	0.5551(2)	0.3009(3)
C(4)	0.3968(3)	0.4333(2)	0.3422(3)
C(5)	0.2504(3)	0.4437(2)	0.2923(4)
C(6)	0.9023(3)	0.5377(2)	0.3631(4)
C(7)	0.9526(3)	0.5995(2)	0.3264(3)
C(8)	0.7799(3)	0.2929(2)	0.1044(4)
C(9)	0.6688(3)	0.2538(2)	0.1422(4)
C(10)	0.6991(3)	0.2376(2)	0.2667(3)
C(11)	0.9138(3)	0.4035(2)	0.0863(3)
C(12)	0.9155(4)	0.4056(3)	-0.0375(4)
C(13)	0.7726(3)	0.2781(2)	0.4853(3)
C(14)	0.7393(4)	0.2127(2)	0.5254(4)
C(15)	0.4890(7)	0.7293(3)	0.1638(6)
C(16)	0.4339(5)	0.7166(3)	0.2741(6)

Table A.1 19. Hydrogen bond structural parameters for A-H...B interactions.

A	H	B	A...B	A-H	H...B	A-H...B
C(16)	H(36)	O(5)	3.374(7)	0.98	2.47	152.9
O(5)	H(38)	O(6)	2.755(6)	0.95	1.83	165.2
O(6)	H(39)	O(2)	2.814(4)	0.95	1.95	150.3
O(6)	H(40)	O(1)	2.752(4)	0.95	1.83	165.2

S(1)

Appendix 1.5 Crystallographic Data for [RuCl(BESE)(H₂O)]₂(μ-Cl)₂·H₂O**Table A.1 20.** Experimental Details for X-ray Crystal Structure of [RuCl(BESE)(H₂O)]₂(μ-Cl)₂·H₂O*A: Crystal Data*

Empirical Formula	C ₁₂ H ₃₄ Cl ₄ O ₇ Ru ₂ S ₄
Formula Weight	762.59
Crystal Colour, Habit	orange, prism
Crystal Dimensions	0.25 x 0.20 x 0.10 mm
Crystal System	triclinic
Lattice Type	Primitive
Lattice Parameters	a = 10.2101(6) Å

	$b = 10.8016(10) \text{ \AA}$
	$c = 13.391(2) \text{ \AA}$
	$\alpha = 93.968(3)^\circ$
	$\beta = 97.099(2)^\circ$
	$\gamma = 117.5490(9)^\circ$
	$V = 1285.9(2) \text{ \AA}^3$
Space Group	$P\bar{1} \text{ (# 2)}$
Z Value	2
D_{calc}	1.969 g/cm^3
F_{000}	764.00
$\mu(\text{MoK}\alpha)$	19.45 cm^{-1}

B. Intensity Measurements

Diffractometer	Rigaku/ADSC CCD
Radiation	MoK α ($\lambda = 0.71069 \text{ \AA}$) graphite monochromated
Detector Aperature	94 mm x 94 mm
Data Images	462 exposures of 16.0 seconds
ϕ oscillation Range ($\chi = -90$)	$0.0 - 190.0^\circ$
ω oscillation Range ($\chi = -90$)	$-23.0 - 18.0^\circ$
Detector Position	38.845(7) mm
Detector Swing Angle	-10.0°
$2\theta_{max}$	61.1°
No. of Reflections Measured	Total: 11840 Unique: 5905 ($R_{int} = 0.035$)
Corrections	Lorentz-polarization Absorption/scaling (trans. factors: 0.8181 - 1.0000)

C. Structure Solution and Refinement

Structure Solution	Direct Methods (SIR97)
Refinement	Full-matrix least-squares
Function Minimized	$\Sigma \omega(F_o^2 - F_c^2)^2$
Least Squares Weights	$\omega = 1/\sigma^2(F_o)$
p-factor	0.0000
Anomalous Dispersion	All non-hydrogen atoms
No. Observations	5905
No. Variables	262
Reflection/Parameter Ratio	22.54
Residuals (on F^2 , all data): R; Rw	0.056; 0.064
Goodness of Fit Indicator	1.10
No. Observations ($I > 3\sigma(I)$)	4055
Residuals (on F, $I > 3\sigma(I)$): R; Rw	0.029; 0.031
Max Shift/Error in Final Cycle	0.0016
Maximum peak in Final Diff. Map	1.33 e/\AA^3 (1.8 \AA from O(7))
Minimum peak in Final Diff. Map	-1.33 e/\AA^3

Table A.1 21. Bond Angles ($^\circ$) for $[\text{RuCl}(\text{BESE})(\text{H}_2\text{O})]_2(\mu\text{-Cl})_2 \cdot \text{H}_2\text{O}$

atom	atom	atom	angle		atom	atom	atom	angle
Cl(1)	Ru(1)	Cl(1)	82.11(3)		Ru(1)	S(1)	O(1)	118.5(1)
Cl(1)	Ru(1)	Cl(2)	171.77(4)		Ru(1)	S(1)	C(1)	105.6(1)
Cl(1)	Ru(1)	S(1)	92.56(4)		Ru(1)	S(1)	C(3)	114.3(1)
Cl(1)	Ru(1)	S(2)	93.31(4)		O(1)	S(1)	C(1)	106.8(2)

Cl(1)	Ru(1)	O(3)	86.53(8)	O(1)	S(1)	C(3)	107.4(2)
Cl(1)	Ru(1)	Cl(2)	91.93(3)	C(1)	S(1)	C(3)	102.9(2)
Cl(1)	Ru(1)	S(1)	174.31(4)	Ru(1)	S(2)	O(2)	119.2(1)
Cl(1)	Ru(1)	S(2)	95.11(3)	Ru(1)	S(2)	C(2)	107.4(1)
Cl(1)	Ru(1)	O(3)	86.83(8)	Ru(1)	S(2)	C(5)	116.7(1)
Cl(2)	Ru(1)	S(1)	93.17(4)	O(2)	S(2)	C(2)	107.2(2)
Cl(2)	Ru(1)	S(2)	92.87(4)	O(2)	S(2)	C(5)	104.9(2)
Cl(2)	Ru(1)	O(3)	87.48(8)	C(2)	S(2)	C(5)	99.3(2)
S(1)	Ru(1)	S(2)	87.15(4)	Ru(2)	S(3)	O(4)	117.3(1)
S(1)	Ru(1)	O(3)	90.88(8)	Ru(2)	S(3)	C(7)	105.3(2)
S(2)	Ru(1)	O(3)	178.01(8)	Ru(2)	S(3)	C(9)	115.5(2)
Cl(3)	Ru(2)	Cl(3)	83.17(3)	O(4)	S(3)	C(7)	106.6(2)
Cl(3)	Ru(2)	Cl(4)	171.20(4)	O(4)	S(3)	C(9)	107.2(2)
Cl(3)	Ru(2)	S(3)	92.98(4)	C(7)	S(3)	C(9)	103.7(2)
Cl(3)	Ru(2)	S(4)	94.74(4)	Ru(2)	S(4)	O(5)	120.8(1)
Cl(3)	Ru(2)	O(6)	87.33(7)	Ru(2)	S(4)	C(8)	106.7(2)
Cl(3)	Ru(2)	Cl(4)	92.49(3)	Ru(2)	S(4)	C(11)	116.4(2)
Cl(3)	Ru(2)	S(3)	176.04(3)	O(5)	S(4)	C(8)	106.8(2)
Cl(3)	Ru(2)	S(4)	94.09(4)	O(5)	S(4)	C(11)	104.7(2)
Cl(3)	Ru(2)	O(6)	86.26(8)	C(8)	S(4)	C(11)	98.8(2)
Cl(4)	Ru(2)	S(3)	91.21(4)	S(1)	C(1)	C(2)	106.3(3)
Cl(4)	Ru(2)	S(4)	93.19(4)	S(2)	C(2)	C(1)	108.6(3)
Cl(4)	Ru(2)	O(6)	84.74(7)	S(1)	C(3)	C(4)	111.6(3)
S(3)	Ru(2)	S(4)	87.10(4)	S(2)	C(5)	C(6)	110.9(3)
S(3)	Ru(2)	O(6)	92.68(8)	S(3)	C(7)	C(8)	106.1(3)
S(4)	Ru(2)	O(6)	177.92(8)	S(4)	C(8)	C(7)	109.3(3)
Ru(1)	Cl(1)	Ru(1)	97.89(3)	S(3)	C(9)	C(10)	114.1(4)
Ru(2)	Cl(3)	Ru(2)	96.83(3)	S(4)	C(11)	C(12)	111.6(3)

Angles are in degrees. Estimated standard deviations in the least significant figure are given in parentheses.

Table A.1 22. Bond Lengths (Å) for $[\text{RuCl}(\text{BESE})(\text{H}_2\text{O})]_2(\mu\text{-Cl})_2\cdot\text{H}_2\text{O}$

atom	atom	distance		atom	atom	distance
Ru(1)	Cl(1)	2.410(1)		S(2)	O(2)	1.496(2)
Ru(1)	Cl(1)	2.464(1)		S(2)	C(2)	1.805(4)
Ru(1)	Cl(2)	2.401(1)		S(2)	C(5)	1.805(4)
Ru(1)	S(1)	2.199(1)		S(3)	O(4)	1.482(3)
Ru(1)	S(2)	2.196(1)		S(3)	C(7)	1.800(5)
Ru(1)	O(3)	2.140(3)		S(3)	C(9)	1.776(5)
Ru(2)	Cl(3)	2.426(1)		S(4)	O(5)	1.483(3)
Ru(2)	Cl(3)	2.468(1)		S(4)	C(8)	1.813(4)
Ru(2)	Cl(4)	2.3748(9)		S(4)	C(11)	1.807(4)
Ru(2)	S(3)	2.198(1)		C(1)	C(2)	1.531(5)
Ru(2)	S(4)	2.193(1)		C(3)	C(4)	1.518(6)
Ru(2)	O(6)	2.155(3)		C(5)	C(6)	1.514(6)
S(1)	O(1)	1.475(3)		C(7)	C(8)	1.505(7)
S(1)	C(1)	1.803(5)		C(9)	C(10)	1.512(6)
S(1)	C(3)	1.803(4)		C(11)	C(12)	1.519(7)

Distances are in angstroms. Estimated standard deviations in the least significant figure are given in parentheses.

Table A.1 23. Atomic Coordinates for $[\text{RuCl}(\text{BESE})(\text{H}_2\text{O})]_2(\mu\text{-Cl})_2\cdot\text{H}_2\text{O}$

atom	x	y	z
Ru(1)	0.05846(3)	0.86283(4)	0.49128(2)
Ru(2)	0.36391(3)	0.32199(4)	0.01720(2)
Cl(1)	0.11786(10)	1.08352(11)	0.42905(7)
Cl(2)	0.00001(10)	0.65984(11)	0.57629(8)
Cl(3)	0.63194(10)	0.47823(11)	0.06388(7)
Cl(4)	0.10770(10)	0.17152(12)	-0.05468(8)
S(1)	0.22818(10)	0.83737(11)	0.41901(8)
S(2)	-0.10391(10)	0.73688(11)	0.35331(7)
S(3)	0.37718(10)	0.15122(12)	0.09048(8)
S(4)	0.31050(11)	0.38575(12)	0.15921(8)
O(1)	0.3270(3)	0.9524(3)	0.3673(2)
O(2)	-0.1954(3)	0.7945(3)	0.2980(2)
O(3)	0.2228(3)	0.9857(3)	0.6232(2)
O(4)	0.5277(3)	0.1770(4)	0.1391(3)
O(5)	0.4005(3)	0.5318(3)	0.2135(2)
O(6)	0.4079(3)	0.2538(3)	-0.1240(2)
O(7)	0.7793(4)	0.1666(4)	0.2242(3)
C(1)	0.1245(4)	0.6835(5)	0.3239(3)
C(2)	-0.0018(4)	0.7019(5)	0.2643(3)
C(3)	0.3461(4)	0.7893(5)	0.5009(3)
C(4)	0.4531(5)	0.7634(5)	0.4443(4)
C(5)	-0.2370(4)	0.5578(5)	0.3635(3)
C(6)	-0.3482(4)	0.5549(5)	0.4295(3)
C(7)	0.2677(4)	0.1252(5)	0.1901(3)
C(8)	0.3206(5)	0.2694(5)	0.2476(3)
C(9)	0.2894(5)	-0.0166(5)	0.0138(4)
C(10)	0.2983(6)	-0.1321(6)	0.0672(4)
C(11)	0.1177(5)	0.3463(6)	0.1570(4)
C(12)	0.0762(6)	0.4368(6)	0.0919(4)

Table A.1 24. Hydrogen bond parameters for A-H...B interactions.

A	H	B	A...B	A-H	H...B	A-H...B
O(7)	H(33)	O(4)	2.733(4)	0.92	1.81	179.6
O(7)	H(34)	Cl(2)	3.105(4)	0.89	2.28	152.8

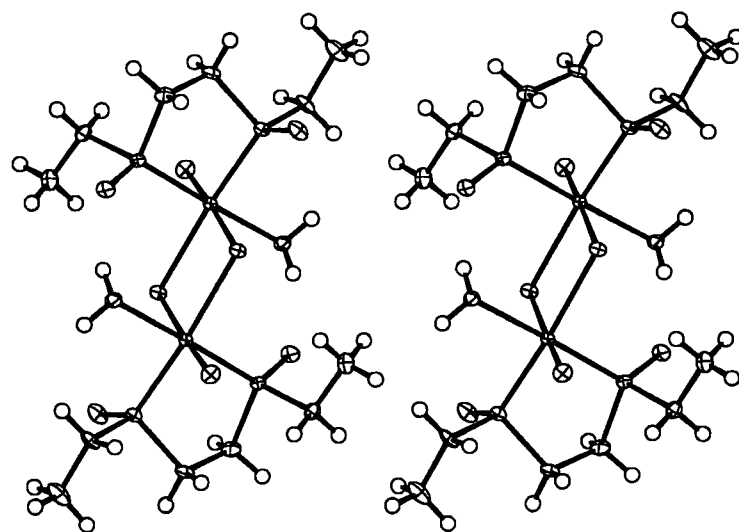


Figure A.1.3. Stereoview of $[\text{RuCl}(\text{BESE})(\text{H}_2\text{O})]_2(\mu\text{-Cl})_2 \cdot \text{H}_2\text{O}$.

Appendix 1.6 Crystallographic Data for $[\text{RuCl}(\text{BPSP})]_2(\mu\text{-Cl})_3 \cdot 2\text{H}_2\text{O} \cdot 2.5\text{CH}_2\text{Cl}_2$ **Table A.1 25.** Experimental Details for X-ray Crystal Structure of $[\text{RuCl}(\text{BPSP})]_2(\mu\text{-Cl})_3 \cdot 2\text{H}_2\text{O} \cdot 2.5\text{CH}_2\text{Cl}_2$ *A. Crystal Data*

Empirical Formula	$\text{C}_{20.50}\text{H}_{49}\text{Cl}_{10}\text{O}_6\text{Ru}_2\text{S}_4$
Formula Weight	1076.52
Crystal Colour, Habit	orange, plate
Crystal Dimensions	0.10 x 0.20 x 0.40 mm
Crystal System	monoclinic
Lattice Type	Primitive
Lattice Parameters	$a = 10.5354(4) \text{ \AA}$ $b = 15.8739(11) \text{ \AA}$ $c = 24.6983(4) \text{ \AA}$ $\beta = 96.6438(6)^\circ$ $V = 4102.8(3) \text{ \AA}^3$
Space Group	Pn (# 7)
Z Value	4
D_{calc}	1.743 g/cm^3
F_{000}	2168.00
$\mu(\text{MoK}\alpha)$	16.22 cm^{-1}

B. Intensity Measurements

Diffractometer	Rigaku/ADSC CCD
Radiation	MoK α ($\lambda = 0.71069 \text{ \AA}$) graphite monochromated
Detector Aperature	94 mm x 94 mm
Data Images	766 exposures of 70.0 seconds
ϕ oscillation Range ($\chi = -90$)	$-22.0 - 17.9^\circ$
ω oscillation Range ($\chi = -90$)	$0.0 - 190.2^\circ$
Detector Position	39.18(1) mm
Detector Swing Angle	-10°
$2\theta_{\text{max}}$	60.1°
No. of Reflections Measured	Total: 37619 Unique: 10572 ($R_{\text{int}} = 0.045$)
Corrections	Lorentz-polarization Absorption/scaling (trans. factors: 0.7434 - 1.0016)

C. Structure Solution and Refinement

Structure Solution	Patterson Methods (DIRDIF92 PATTY)
Refinement	Full-matrix least-squares
Function Minimized	$\sum \omega (F_o ^2 - F_c ^2)^2$
Least Squares Weights	$\omega = 1/\sigma^2(F_o^2) = [\sigma^2(F_o^2) + p^2(F_o^2)]^{-1}$
p-factor	0.0000
Anomalous Dispersion	All non-hydrogen atoms
No. Observations (Including Friedel pairs)	16879
No. Variables	785
Reflection/Parameter Ratio	21.50
Residuals (on F^2 , all data): R; Rw	0.077; 0.088
Goodness of Fit Indicator	1.75
No. Observations ($I > 3\sigma(I)$)	13319
Residuals (on F, $I > 3\sigma(I)$): R1; R1w	0.040; 0.042
Max Shift/Error in Final Cycle	0.02

Maximum peak in Final Diff. Map	1.65 e/Å ³ (near Ru)
Minimum peak in Final Diff. Map	-2.96 e/Å ³ (near Ru)

Table A.1 26. Bond Angles (°) for [RuCl(BPSP)]₂(μ-Cl)₃·2H₂O·2.5CH₂Cl₂

atom	atom	atom	angle	atom	atom	atom	angle
Cl(1)	Ru(1)	Cl(2)	81.46(5)	Cl(5)	Ru(2)	S(4)	91.93(6)
Cl(1)	Ru(1)	Cl(3)	82.63(5)	S(3)	Ru(2)	S(4)	88.48(6)
Cl(1)	Ru(1)	Cl(4)	170.87(5)	Cl(6)	Ru(3)	Cl(7)	82.65(5)
Cl(1)	Ru(1)	S(1)	92.33(5)	Cl(6)	Ru(3)	Cl(8)	80.76(5)
Cl(1)	Ru(1)	S(2)	94.19(6)	Cl(6)	Ru(3)	Cl(9)	168.66(6)
Cl(2)	Ru(1)	Cl(3)	79.33(5)	Cl(6)	Ru(3)	S(5)	97.29(5)
Cl(2)	Ru(1)	Cl(4)	91.09(5)	Cl(6)	Ru(3)	S(6)	92.47(5)
Cl(2)	Ru(1)	S(1)	172.11(6)	Cl(7)	Ru(3)	Cl(8)	79.74(5)
Cl(2)	Ru(1)	S(2)	95.78(6)	Cl(7)	Ru(3)	Cl(9)	87.63(6)
Cl(3)	Ru(1)	Cl(4)	90.83(5)	Cl(7)	Ru(3)	S(5)	174.70(6)
Cl(3)	Ru(1)	S(1)	95.11(6)	Cl(7)	Ru(3)	S(6)	96.05(6)
Cl(3)	Ru(1)	S(2)	174.50(6)	Cl(8)	Ru(3)	Cl(9)	91.80(5)
Cl(4)	Ru(1)	S(1)	94.61(5)	Cl(8)	Ru(3)	S(5)	95.00(6)
Cl(4)	Ru(1)	S(2)	91.80(6)	Cl(8)	Ru(3)	S(6)	172.40(6)
S(1)	Ru(1)	S(2)	89.49(6)	Cl(9)	Ru(3)	S(5)	91.86(6)
Cl(1)	Ru(2)	Cl(2)	81.70(5)	Cl(9)	Ru(3)	S(6)	94.36(6)
Cl(1)	Ru(2)	Cl(3)	82.46(5)	S(5)	Ru(3)	S(6)	89.25(6)
Cl(1)	Ru(2)	Cl(5)	169.83(6)	Cl(6)	Ru(4)	Cl(7)	82.08(5)
Cl(1)	Ru(2)	S(3)	94.70(5)	Cl(6)	Ru(4)	Cl(8)	80.66(5)
Cl(1)	Ru(2)	S(4)	92.71(6)	Cl(6)	Ru(4)	Cl(10)	170.20(5)
Cl(2)	Ru(2)	Cl(3)	79.21(5)	Cl(6)	Ru(4)	S(7)	92.63(5)
Cl(2)	Ru(2)	Cl(5)	88.73(6)	Cl(6)	Ru(4)	S(8)	96.27(6)
Cl(2)	Ru(2)	S(3)	173.16(5)	Cl(7)	Ru(4)	Cl(8)	79.79(5)
Cl(2)	Ru(2)	S(4)	97.46(6)	Cl(7)	Ru(4)	Cl(10)	90.10(5)
Cl(3)	Ru(2)	Cl(5)	92.42(5)	Cl(7)	Ru(4)	S(7)	173.01(6)
Cl(3)	Ru(2)	S(3)	94.59(6)	Cl(7)	Ru(4)	S(8)	93.86(6)
Cl(3)	Ru(2)	S(4)	174.46(6)	Cl(8)	Ru(4)	Cl(10)	92.19(6)
Cl(5)	Ru(2)	S(3)	94.47(6)	Cl(8)	Ru(4)	S(7)	94.89(6)
Cl(8)	Ru(4)	S(8)	173.25(6)	Ru(3)	S(6)	C(25)	113.9(2)
Cl(10)	Ru(4)	S(7)	94.66(6)	O(6)	S(6)	C(21)	104.3(3)
Cl(10)	Ru(4)	S(8)	90.12(6)	O(6)	S(6)	C(25)	106.2(3)
S(7)	Ru(4)	S(8)	91.24(6)	C(21)	S(6)	C(25)	102.0(3)
Ru(1)	Cl(1)	Ru(2)	85.01(5)	Ru(4)	S(7)	O(7)	117.4(2)
Ru(1)	Cl(2)	Ru(2)	81.26(5)	Ru(4)	S(7)	C(28)	112.4(2)
Ru(1)	Cl(3)	Ru(2)	81.45(5)	Ru(4)	S(7)	C(31)	115.8(2)
Ru(3)	Cl(6)	Ru(4)	84.69(5)	O(7)	S(7)	C(28)	104.5(3)
Ru(3)	Cl(7)	Ru(4)	82.61(5)	O(7)	S(7)	C(31)	104.3(3)
Ru(3)	Cl(8)	Ru(4)	81.25(5)	C(28)	S(7)	C(31)	100.5(3)
Cl(17a)	Cl(17)	C(40)	73.1(8)	Ru(4)	S(8)	O(8)	118.4(2)
Cl(17)	Cl(17a)	C(40)	70.8(8)	Ru(4)	S(8)	C(30)	112.7(2)
Cl(18)	Cl(18a)	C(40)	86(1)	Ru(4)	S(8)	C(34)	111.4(2)
Cl(18a)	Cl(18)	C(40)	47.5(7)	O(8)	S(8)	C(30)	105.7(3)
Cl(19)	Cl(19a)	Cl(20)	129.5(7)	O(8)	S(8)	C(34)	107.0(3)
Cl(19)	Cl(19a)	C(41)	81.4(7)	C(30)	S(8)	C(34)	99.9(3)
Cl(20)	Cl(19a)	C(41)	53.1(4)	S(1)	C(1)	C(2)	109.5(4)
Cl(19a)	Cl(19)	C(41)	64.6(6)	C(1)	C(2)	C(3)	115.0(5)
Cl(20)	Cl(20a)	C(41)	50.0(4)	S(2)	C(3)	C(2)	111.3(4)

Cl(19a	Cl(20)	Cl(20a	85.7(4)	S(1)	C(4)	C(5)	117.6(5)
Cl(19a	Cl(20)	C(41)	50.7(4)	C(4)	C(5)	C(6)	110.2(7)
Cl(20a	Cl(20)	C(41)	58.8(4)	S(2)	C(7)	C(8)	113.9(5)
Ru(1)	S(1)	O(1)	117.1(2)	C(7)	C(8)	C(9)	112.9(6)
Ru(1)	S(1)	C(1)	112.3(2)	S(3)	C(10)	C(11)	109.8(4)
Ru(1)	S(1)	C(4)	115.3(2)	C(10)	C(11)	C(12)	116.2(5)
O(1)	S(1)	C(1)	105.1(3)	S(4)	C(12)	C(11)	109.8(4)
O(1)	S(1)	C(4)	104.5(3)	S(3)	C(13)	C(14)	117.0(5)
C(1)	S(1)	C(4)	100.9(3)	C(13)	C(14)	C(15)	109.0(6)
Ru(1)	S(2)	O(2)	118.6(2)	S(4)	C(16)	C(17)	111.6(4)
Ru(1)	S(2)	C(3)	111.9(2)	C(16)	C(17)	C(18)	112.0(5)
Ru(1)	S(2)	C(7)	112.7(2)	S(5)	C(19)	C(20)	112.8(5)
O(2)	S(2)	C(3)	104.2(3)	C(19)	C(20)	C(21)	115.1(6)
O(2)	S(2)	C(7)	106.7(3)	S(6)	C(21)	C(20)	110.2(4)
C(3)	S(2)	C(7)	101.0(3)	S(5)	C(22)	C(23)	115.8(5)
Ru(2)	S(3)	O(3)	118.1(2)	C(22)	C(23)	C(24)	111.8(6)
Ru(2)	S(3)	C(10)	110.6(2)	S(6)	C(25)	C(26)	110.7(4)
Ru(2)	S(3)	C(13)	114.3(2)	C(25)	C(26)	C(27)	109.7(5)
O(3)	S(3)	C(10)	106.1(3)	S(7)	C(28)	C(29)	110.5(4)
O(3)	S(3)	C(13)	104.7(3)	C(28)	C(29)	C(30)	115.1(5)
C(10)	S(3)	C(13)	101.4(3)	S(8)	C(30)	C(29)	111.7(4)
Ru(2)	S(4)	O(4)	117.9(2)	S(7)	C(31)	C(32)	116.3(5)
Ru(2)	S(4)	C(12)	111.5(2)	C(31)	C(32)	C(33)	110.5(7)
Ru(2)	S(4)	C(16)	113.0(2)	S(8)	C(34)	C(35)	114.3(5)
O(4)	S(4)	C(12)	104.4(3)	C(34)	C(35)	C(36)	110.3(6)
O(4)	S(4)	C(16)	106.3(3)	Cl(11)	C(37)	Cl(12)	111.9(4)
C(12)	S(4)	C(16)	102.3(3)	Cl(13)	C(38)	Cl(14)	114.0(5)
Ru(3)	S(5)	O(5)	119.7(2)	Cl(15)	C(39)	Cl(16)	112.9(6)
Ru(3)	S(5)	C(19)	112.0(2)	Cl(17)	C(40)	Cl(17a	36.1(4)
Ru(3)	S(5)	C(22)	111.3(2)	Cl(17)	C(40)	Cl(18a	141(1)
O(5)	S(5)	C(19)	105.6(3)	Cl(17)	C(40)	Cl(18)	110.3(8)
O(5)	S(5)	C(22)	105.8(3)	Cl(17a	C(40)	Cl(18a	149(1)
C(19)	S(5)	C(22)	100.3(3)	Cl(17a	C(40)	Cl(18)	101.7(9)
Ru(3)	S(6)	O(6)	117.1(2)	Cl(18a	C(40)	Cl(18)	46.9(8)
Ru(3)	S(6)	C(21)	111.8(2)	Cl(19a	C(41)	Cl(19)	34.0(4)
Cl(19a	C(41)	Cl(20a	105.9(5)				
Cl(19a	C(41)	Cl(20)	76.2(6)				
Cl(19)	C(41)	Cl(20a	103.9(6)				
Cl(19)	C(41)	Cl(20)	107.6(6)				
Cl(20a	C(41)	Cl(20)	71.2(5)				

Angles are in degrees. Estimated standard deviations in the least significant figure are given in parentheses.

Table A.1 27. Bond Lengths (Å) for $[\text{RuCl}(\text{BPSP})]_2(\mu\text{-Cl})_3 \cdot 2\text{H}_2\text{O} \cdot 2.5\text{CH}_2\text{Cl}_2$

atom	atom	distance	atom	atom	distance	atom	atom	distance
Ru(1)	Cl(1)	2.393(2)	Cl(13)	C(38)	1.74(1)	C(2)	C(3)	1.528(9)
Ru(1)	Cl(2)	2.483(1)	Cl(14)	C(38)	1.733(9)	C(4)	C(5)	1.50(1)
Ru(1)	Cl(3)	2.469(2)	Cl(15)	C(39)	1.74(1)	C(5)	C(6)	1.51(1)
Ru(1)	Cl(4)	2.383(2)	Cl(16)	C(39)	1.67(1)	C(7)	C(8)	1.51(1)
Ru(1)	S(1)	2.209(2)	Cl(17)	Cl(17a	1.10(1)	C(8)	C(9)	1.50(1)
Ru(1)	S(2)	2.206(2)	Cl(17)	C(40)	1.76(1)	C(10)	C(11)	1.54(1)
Ru(2)	Cl(1)	2.388(1)	Cl(17a	C(40)	1.78(2)	C(11)	C(12)	1.515(9)
Ru(2)	Cl(2)	2.477(2)	Cl(18a	Cl(18)	1.27(1)	C(13)	C(14)	1.523(9)

Ru(2)	Cl(3)	2.482(2)	Cl(18a)	C(40)	1.28(2)	C(14)	C(15)	1.52(1)
Ru(2)	Cl(5)	2.390(2)	Cl(18)	C(40)	1.73(1)	C(16)	C(17)	1.513(9)
Ru(2)	S(3)	2.209(2)	Cl(19a)	Cl(19)	1.027(9)			
Ru(2)	S(4)	2.208(2)	Cl(19a)	Cl(20)	2.08(1)			
Ru(3)	Cl(6)	2.390(1)	Cl(19a)	C(41)	1.66(1)			
Ru(3)	Cl(7)	2.444(2)	Cl(19)	C(41)	1.81(1)			
Ru(3)	Cl(8)	2.488(2)	Cl(20a)	Cl(20)	2.12(1)			
Ru(3)	Cl(9)	2.388(2)	Cl(20a)	C(41)	1.92(1)			
Ru(3)	S(5)	2.205(2)	Cl(20)	C(41)	1.71(1)			
Ru(3)	S(6)	2.207(2)	S(1)	O(1)	1.490(4)			
Ru(4)	Cl(6)	2.408(2)	S(1)	C(1)	1.800(6)			
Ru(4)	Cl(7)	2.453(1)	S(1)	C(4)	1.789(7)			
Ru(4)	Cl(8)	2.476(2)	S(2)	O(2)	1.491(4)			
Ru(4)	Cl(10)	2.377(2)	S(2)	C(3)	1.805(6)			
Ru(4)	S(7)	2.200(2)	S(2)	C(7)	1.801(6)			
Ru(4)	S(8)	2.224(2)	S(3)	O(3)	1.487(4)			
Cl(11)	C(37)	1.750(8)	S(3)	C(10)	1.805(6)			
Cl(12)	C(37)	1.750(8)	S(3)	C(13)	1.796(7)			
S(4)	O(4)	1.490(4)	C(17)	C(18)	1.50(1)			
S(4)	C(12)	1.800(6)	C(19)	C(20)	1.523(9)			
S(4)	C(16)	1.788(7)	C(20)	C(21)	1.52(1)			
S(5)	O(5)	1.501(4)	C(22)	C(23)	1.512(9)			
S(5)	C(19)	1.809(6)	C(23)	C(24)	1.50(1)			
S(5)	C(22)	1.804(7)	C(25)	C(26)	1.538(9)			
S(6)	O(6)	1.497(4)	C(26)	C(27)	1.52(1)			
S(6)	C(21)	1.796(6)	C(28)	C(29)	1.51(1)			
S(6)	C(25)	1.800(7)	C(29)	C(30)	1.536(9)			
S(7)	O(7)	1.489(4)	C(31)	C(32)	1.52(1)			
S(7)	C(28)	1.802(6)	C(32)	C(33)	1.50(1)			
S(7)	C(31)	1.804(7)	C(34)	C(35)	1.52(1)			
S(8)	O(8)	1.474(5)	C(35)	C(36)	1.52(1)			
S(8)	C(30)	1.776(6)	S(8)	C(34)	1.799(6)			
C(1)	C(2)	1.514(9)	C(1)	C(2)	1.514(9)			

Distances are in angstroms. Estimated standard deviations in the least significant figure are given in parentheses.

Table A.1 28. Atomic Coordinates for $[\text{RuCl}(\text{BPSP})]_2(\mu\text{-Cl})_3 \cdot 2\text{H}_2\text{O} \cdot 2.5\text{CH}_2\text{Cl}_2$

atom	x	y	z	B(eq)
Ru(1)	0.4973	0.93066(2)	0.5020	1.076(8)
Ru(2)	0.74647(4)	0.82149(2)	0.54648(2)	1.153(8)
Ru(3)	0.17353(4)	0.47576(2)	0.33053(2)	1.145(8)
Ru(4)	0.41381(4)	0.36548(2)	0.38406(2)	1.181(8)
Cl(1)	0.55025(10)	0.78507(7)	0.49337(5)	1.25(2)
Cl(2)	0.72494(10)	0.94752(7)	0.48699(5)	1.45(2)
Cl(3)	0.60312(10)	0.91018(7)	0.59562(5)	1.47(2)
Cl(4)	0.47834(11)	1.07804(7)	0.51770(5)	1.85(3)
Cl(5)	0.93411(11)	0.88287(8)	0.59434(6)	2.04(3)
Cl(6)	0.36512(10)	0.51354(7)	0.38674(5)	1.23(2)
Cl(7)	0.18397(10)	0.35297(7)	0.39055(5)	1.49(3)
Cl(8)	0.32840(10)	0.38690(7)	0.28737(5)	1.44(2)
Cl(9)	-0.00404(11)	0.41011(8)	0.27806(6)	2.15(3)
Cl(10)	0.42739(11)	0.21724(7)	0.37227(5)	1.96(3)
Cl(11)	-0.0818(2)	0.11076(14)	0.32572(10)	7.15(6)

Cl(12)	-0.0025(2)	0.17855(11)	0.43332(8)	4.65(4)
Cl(13)	0.3373(2)	0.67487(13)	0.60869(9)	5.17(5)
Cl(14)	0.2849(2)	0.50223(13)	0.63999(10)	6.01(5)
Cl(15)	0.0901(2)	0.3810(2)	0.72513(13)	9.16(8)
Cl(16)	0.1325(3)	0.2071(2)	0.74737(15)	10.87(10)
Cl(17)	0.4759(4)	0.1605(2)	0.6984(2)	8.25(10)
Cl(17a)	0.5662(8)	0.1685(6)	0.6809(4)	6.7(2)
Cl(18a)	0.6236(9)	0.0469(7)	0.7704(4)	8.6(2)
Cl(18)	0.6810(2)	0.1163(2)	0.77944(11)	5.46(7)
Cl(19a)	0.8820(6)	1.1805(3)	0.5723(2)	7.71(15)
Cl(19)	0.9512(6)	1.1387(4)	0.5636(3)	8.5(2)
Cl(20a)	0.8782(6)	1.0826(3)	0.6691(2)	8.92(15)
Cl(20)	0.7500(5)	1.1710(3)	0.6285(2)	9.4(2)
S(1)	0.30356(10)	0.90033(7)	0.52220(5)	1.39(3)
S(2)	0.41971(11)	0.94440(7)	0.41561(5)	1.32(2)
S(3)	0.74339(10)	0.71334(7)	0.60260(5)	1.37(2)
S(4)	0.86066(10)	0.74423(7)	0.49566(5)	1.48(3)
S(5)	0.17477(10)	0.57985(8)	0.27151(5)	1.46(3)
S(6)	0.05391(10)	0.55325(8)	0.37881(5)	1.47(3)
S(7)	0.61382(11)	0.38943(8)	0.37129(6)	1.65(3)
S(8)	0.46771(11)	0.35031(7)	0.47326(6)	1.61(3)
O(1)	0.2485(3)	0.8177(2)	0.50290(15)	1.94(8)
O(2)	0.3782(3)	0.8672(2)	0.38402(15)	2.11(8)
O(3)	0.6705(3)	0.6370(2)	0.58276(13)	1.69(7)
O(4)	0.7986(3)	0.6691(2)	0.46781(14)	1.92(8)
O(5)	0.2549(3)	0.6565(2)	0.28605(14)	1.99(8)
O(6)	0.1141(3)	0.6303(2)	0.40575(14)	2.02(8)
O(7)	0.6689(3)	0.4728(2)	0.3889(2)	2.13(8)
O(8)	0.4938(3)	0.4266(2)	0.50666(15)	2.33(8)
O(9)	0.3088(3)	0.6592(3)	0.4794(2)	5.30(12)
O(10)	0.4163(4)	0.7102(3)	0.3682(2)	7.8(2)
O(11)	0.5130(3)	0.5906(2)	0.49572(14)	2.25(8)
O(12)	0.6173(3)	0.6387(2)	0.38562(14)	2.01(8)
C(1)	0.1872(4)	0.9775(3)	0.4960(2)	1.90(10)
C(2)	0.1708(4)	0.9745(3)	0.4343(2)	2.12(10)

Table A.1 29. Hydrogen bonds and C-H...Cl/O interactions.

A	H	B	A...B	A-H	H...B	A-H...B
O(9)	H(1)	O(1)	2.676(7)	0.95	1.73	170.8
O(9)	H(2)	O(6)	2.620(6)	0.95	1.68	170.4
O(10)	H(3)	O(2)	2.563(7)	0.95	1.61	179.0
O(10)	H(4)	O(5)	2.633(7)	0.95	1.68	179.4
O(11)	H(5)	O(3)	2.663(6)	0.95	1.72	175.7
O(11)	H(6)	O(8)	2.628(6)	0.95	1.68	175.5
O(12)	H(7)	O(4)	2.665(6)	0.95	1.73	166.1
O(12)	H(8)	O(7)	2.688(6)	0.95	1.76	166.5
O(9)	H(1)	Cl(1)	3.222(5)	0.95	2.90	101.5
O(11)	H(5)	Cl(1)	3.113(4)	0.95	2.90	94.1
O(12)	H(8)	Cl(6)	3.320(4)	0.95	2.95	104.7
C(6)	H(19)	Cl(17)	3.578(12)	0.98	2.86	132.1
C(7)	H(22)	Cl(10)	3.592(6)	0.98	2.81	137.2
C(18)	H(47)	Cl(16)	3.750(9)	0.98	2.92	143.1
C(19)	H(49)	Cl(17)	3.733(8)	0.98	2.90	144.0

C(19)	H(49)	Cl(17a)	3.847(14)	0.98	2.93	156.8
C(23)	H(58)	Cl(20)	3.647(9)	0.98	2.91	132.4
C(29)	H(71)	Cl(19a)	3.682(9)	0.98	2.85	143.1
C(36)	H(88)	Cl(17)	3.543(9)	0.98	2.77	135.7
C(37)	H(90)	Cl(7)	3.254(8)	0.98	2.75	112.8
C(38)	H(92)	Cl(9)	3.650(10)	0.98	2.74	154.8
C(40)	H(96)	Cl(20a)	3.59(2)	0.98	2.82	136.8
C(40)	H(96)	Cl(20)	3.47(2)	0.98	2.85	122.7
C(41)	H(97)	Cl(2)	3.546(9)	0.98	2.73	140.9
C(41)	H(98)	Cl(5)	3.555(10)	0.98	2.85	129.7
C(41)	H(98a)	Cl(5)	3.555(10)	0.98	2.76	138.3
C(41)	H(98a)	Cl(2)	3.546(9)	0.98	2.80	133.7

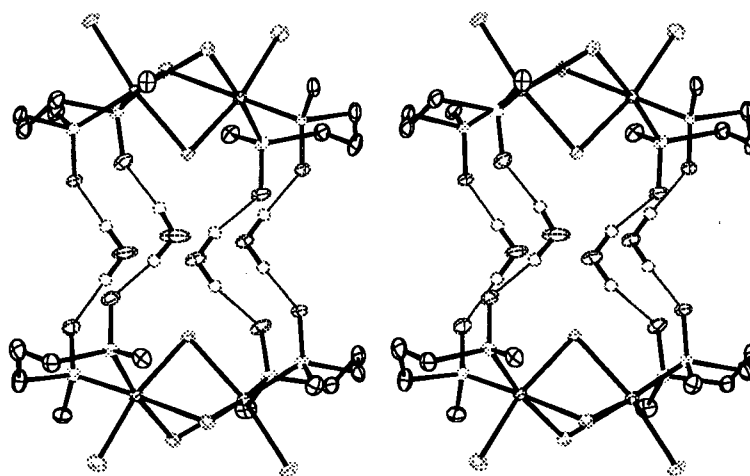


Figure A.1.4. Stereoview of $[\text{RuCl}(\text{BPSP})]_2(\mu\text{-Cl})_3 \cdot 2\text{H}_2\text{O} \cdot 2.5\text{CH}_2\text{Cl}_2$.

Appendix 1.7 Crystallographic Data for *trans*-RuCl₂(BCyTE)₂·2CH₂Cl₂**Table A.1 30.** Experimental Details for X-ray Crystal Structure of *trans*-RuCl₂(BCyTE)₂·2CH₂Cl₂*A. Crystal Data*

Empirical Formula	C ₃₀ H ₅₆ Cl ₆ RuS ₄
Formula Weight	858.80
Crystal Colour, Habit	orange, irregular
Crystal Dimensions	0.45 x 0.35 x 0.25 mm
Crystal System	triclinic
Lattice Type	Primitive
Lattice Parameters	a = 7.5953(10) Å b = 10.638(2) Å c = 12.5100(13) Å α = 103.349 ° β = 96.6436(13) ° γ = 96.3757(14) ° V = 966.9(2) Å ³
Space Group	P $\bar{1}$ (# 2)
Z Value	1
D _{calc}	1.475 g/cm ³
F ₀₀₀	446.00
μ(MoKα)	10.56 cm ⁻¹

B. Intensity Measurements

Diffractometer	CCD
Radiation	MoKα (λ = 0.71069 Å) graphite monochromated
Detector Aperature	94 mm x 94 mm
Data Images	462 exposures @ 16.0 seconds
φ oscillation Range (χ = 0)	0.0 -190.0 °
ω oscillation Range (χ = -90)	-23.0 - 18.0 °
Detector Position	39.24 mm
Detector Swing Angle	-10.00 °
2θ _{max}	60.0 °
No. of Reflections Measured	Total: 8775 Unique: 4348 (R _{int} = 0.033)
Corrections	Lorentz-polarization Absorption/scaling (trans. factors: 0.8770 - 1.0000)

C. Structure Solution and Refinement

Structure Solution	Patterson Methods (DIRDIF92 PATTY)
Refinement	Full-matrix least-squares
Function Minimized	Σω(F _o ² - F _c ²) ²
Least Squares Weights	ω = 1/σ ² (F _o) = [σ ² _e (F _o) + p ² /4(F _o) ²] ⁻¹
p-factor	0.0000
Anomalous Dispersion	All non-hydrogen atoms
No. Observations	4348
No. Variables	187
Reflection/Parameter Ratio	23.25
Residuals (on F ² , all data): R; R _w	0.055; 0.061
Goodness of Fit Indicator	1.52
Max Shift/Error in Final Cycle	0.00

Maximum peak in Final Diff. Map	0.84 e ⁻ /Å ³
Minimum peak in Final Diff. Map	-0.95 e ⁻ /Å ³

Table A.1 31. Bond Angles (°) for *trans*-RuCl₂(BCyTE)₂·2CH₂Cl₂

atom	atom	atom	angle		atom	atom	atom	angle
Cl(1)	Ru(1)	Cl(1)	180.00		C(2)	S(2)	C(9)	97.9(1)
Cl(1)	Ru(1)	S(1)	95.86(2)		S(1)	C(1)	C(2)	112.3(2)
Cl(1)	Ru(1)	S(1)	84.14(2)		S(2)	C(2)	C(1)	110.4(2)
Cl(1)	Ru(1)	S(2)	92.42(2)		S(1)	C(3)	C(4)	112.6(2)
Cl(1)	Ru(1)	S(2)	87.58(2)		S(1)	C(3)	C(8)	105.5(2)
Cl(1)	Ru(1)	S(1)	84.14(2)		C(4)	C(3)	C(8)	111.4(2)
Cl(1)	Ru(1)	S(1)	95.86(2)		C(3)	C(4)	C(5)	109.1(2)
Cl(1)	Ru(1)	S(2)	87.58(2)		C(4)	C(5)	C(6)	111.6(2)
Cl(1)	Ru(1)	S(2)	92.42(2)		C(5)	C(6)	C(7)	111.6(3)
S(1)	Ru(1)	S(1)	180.00		C(6)	C(7)	C(8)	110.6(3)
S(1)	Ru(1)	S(2)	87.22(2)		C(3)	C(8)	C(7)	110.7(2)
S(1)	Ru(1)	S(2)	92.78(2)		S(2)	C(9)	C(10)	111.3(2)
S(1)	Ru(1)	S(2)	92.78(2)		S(2)	C(9)	C(14)	109.3(2)
S(1)	Ru(1)	S(2)	87.22(2)		C(10)	C(9)	C(14)	111.2(2)
S(2)	Ru(1)	S(2)	180.00		C(9)	C(10)	C(11)	110.6(2)
Ru(1)	S(1)	C(1)	101.76(9)		C(10)	C(11)	C(12)	111.1(3)
Ru(1)	S(1)	C(3)	110.98(9)		C(11)	C(12)	C(13)	110.7(3)
C(1)	S(1)	C(3)	104.3(1)		C(12)	C(13)	C(14)	112.0(2)
Ru(1)	S(2)	C(2)	104.13(9)		C(9)	C(14)	C(13)	109.6(2)
Ru(1)	S(2)	C(9)	117.26(9)		Cl(2)	C(15)	Cl(3)	112.8(2)

Angles are in degrees. Estimated standard deviations in the least significant figure are given in parentheses.

Table A.1 32. Bond Lengths (Å) for *trans*-RuCl₂(BCyTE)₂·2CH₂Cl₂

atom	atom	distance		atom	atom	distance
Ru(1)	Cl(1)	2.4262(6)		C(3)	C(4)	1.526(4)
Ru(1)	Cl(1)	2.4262(6)		C(3)	C(8)	1.525(4)
Ru(1)	S(1)	2.3629(6)		C(4)	C(5)	1.536(4)
Ru(1)	S(1)	2.3629(6)		C(5)	C(6)	1.513(4)
Ru(1)	S(2)	2.3646(7)		C(6)	C(7)	1.531(4)
Ru(1)	S(2)	2.3646(7)		C(7)	C(8)	1.527(4)
Cl(2)	C(15)	1.740(4)		C(9)	C(10)	1.507(4)
Cl(3)	C(15)	1.718(4)		C(9)	C(14)	1.529(4)
S(1)	C(1)	1.813(3)		C(10)	C(11)	1.536(4)
S(1)	C(3)	1.840(3)		C(11)	C(12)	1.522(4)
S(2)	C(2)	1.830(3)		C(12)	C(13)	1.500(4)
S(2)	C(9)	1.837(3)		C(13)	C(14)	1.547(4)
C(1)	C(2)	1.515(4)				

Distances are in angstroms. Estimated standard deviations in the least significant figure are given in parentheses.

Table A.1 33. Atomic Coordinates for *trans*-RuCl₂(BCyTE)₂·2CH₂Cl₂

atom	x	y	z	atom	x	y	z
Ru(1)	0.5000	0.5000	0.5000	C(6)	0.2008(5)	0.1089(3)	0.0454(2)
Cl(1)	0.30784(9)	0.56458(7)	0.35930(5)	C(7)	0.1198(4)	0.1981(3)	0.1355(2)
Cl(2)	0.2417(2)	0.48924(12)	-0.04824(8)	C(8)	0.2364(4)	0.2226(3)	0.2482(2)
Cl(3)	0.2281(2)	0.74202(12)	0.09370(10)	C(9)	0.7353(4)	0.7213(3)	0.3690(2)
S(1)	0.55040(9)	0.30267(6)	0.38305(5)	C(10)	0.6625(4)	0.8376(3)	0.4327(2)

S(2)	0.76224(9)	0.60009(7)	0.45092(5)	C(11)	0.6425(5)	0.9383(3)	0.3633(3)
C(1)	0.7835(4)	0.3399(3)	0.3675(2)	C(12)	0.8200(5)	0.9807(3)	0.3276(3)
C(2)	0.8248(4)	0.4721(3)	0.3429(2)	C(13)	0.8939(5)	0.8647(3)	0.2656(3)
C(3)	0.4282(4)	0.2775(3)	0.2422(2)	C(14)	0.9151(4)	0.7621(3)	0.3341(2)
C(4)	0.5096(4)	0.1859(3)	0.1547(2)	C(15)	0.2760(7)	0.5865(4)	0.0869(3)
C(5)	0.3921(4)	0.1628(3)	0.0415(2)				

Table A.1 34. Hydrogen bond parameters for A-H...B interactions.

A	H	B	A...B	A-H	H...B	A-H...B
C(2)	H(3)	Cl(2)	3.785(3)	0.98	2.91	148.7

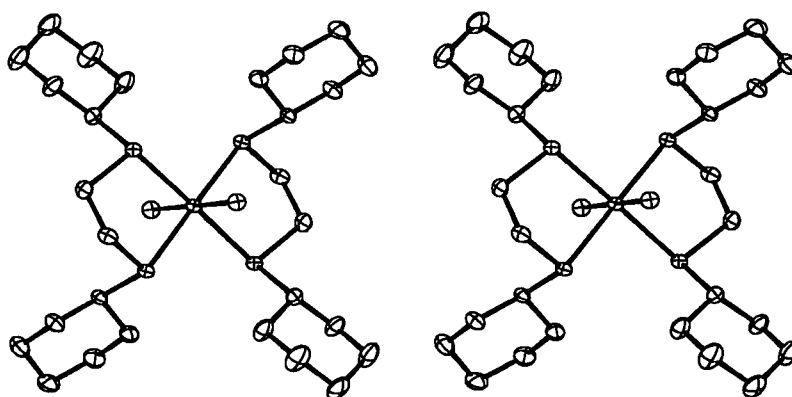


Figure A.1.5. Stereoview of *trans*-RuCl₂(BCyTE)₂·2CH₂Cl₂.

Appendix 1.8 Crystallographic Data for *trans*-RuCl₂(BPhTE)₂**Table A.1 35.** Experimental Details for X-ray Crystal Structure of *trans*-RuCl₂(BPhTE)₂*A. Crystal Data*

Empirical Formula	C ₂₈ H ₂₈ Cl ₂ RuS ₄
Formula Weight	664.75
Crystal Colour, Habit	orange-red, plate
Crystal Dimensions	0.05 x 0.25 x 0.25 mm
Crystal System	triclinic
Lattice Type	Primitive
Lattice Parameters	a = 10.264(2) Å b = 10.866(2) Å c = 12.9980(14) Å α = 93.802(5)° β = 108.4136(13) γ = 92.490(2)° V = 1875.9(3) Å ³
Space Group	P $\bar{1}$ (# 2)
Z Value	2
D _{calc}	1.612 g/cm ³
F ₀₀₀	676.00
μ(MoKα)	10.90 cm ⁻¹

B. Intensity Measurements

Diffractometer	Rigaku/ADSC CCD
Radiation	MoKα (λ = 0.71069 Å) graphite monochromated
Detector Aperature	94 mm x 94 mm
Data Images	462 exposures of 30.0 seconds
φ oscillation Range (χ = -90)	0.0 - 190.0°
ω oscillation Range (χ = -90)	-23.0 - 18.0°
Detector Position	39.23(1) mm
Detector Swing Angle	-10.0°
2θ _{max}	60.1°
No. of Reflections Measured	Total: 12689 Unique: 6147 (R _{int} = 0.036)
Corrections	Lorentz-polarization Absorption/scaling (trans. factors: 0.7088 - 1.0000)

C. Structure Solution and Refinement

Structure Solution	Patterson Methods (DIRDIF92 PATTY)
Refinement	Full-matrix least-squares
Function Minimized	Σω(F _o ² - F _c ²) ²
Least Squares Weights	ω = 1/σ ² (F _o ²)
p-factor	0.0000
Anomalous Dispersion	All non-hydrogen atoms
No. Observations	6147
No. Variables	316
Reflection/Parameter Ratio	19.45
Residuals (on F ² , all data): R; Rw	0.055; 0.052
Goodness of Fit Indicator	1.35
No. Observations (I > 3σ(I))	4088
Residuals (on F, I > 3σ(I)): R; Rw	0.031; 0.025

Max Shift/Error in Final Cycle	0.0007
Maximum peak in Final Diff. Map	1.05 e ⁻ /Å ³ (near Ru)
Minimum peak in Final Diff. Map	-1.45 e ⁻ /Å ³

Table A.1 36. Bond Angles (°) for *trans*-RuCl₂(BPhTE)₂

atom	atom	atom	angle	atom	atom	atom	angle
Cl(1)	Ru(1)	Cl(2)	178.13(4)	C(3)	C(4)	C(5)	119.7(3)
Cl(1)	Ru(1)	S(1)	84.14(3)	C(4)	C(5)	C(6)	120.4(3)
Cl(1)	Ru(1)	S(2)	95.08(3)	C(5)	C(6)	C(7)	119.9(4)
Cl(1)	Ru(1)	S(3)	83.65(3)	C(6)	C(7)	C(8)	119.5(4)
Cl(1)	Ru(1)	S(4)	96.90(3)	C(3)	C(8)	C(7)	121.3(3)
Cl(2)	Ru(1)	S(1)	94.09(3)	S(2)	C(9)	C(10)	116.6(2)
Cl(2)	Ru(1)	S(2)	84.18(3)	S(2)	C(9)	C(14)	124.3(3)
Cl(2)	Ru(1)	S(3)	98.09(3)	C(10)	C(9)	C(14)	119.1(3)
Cl(2)	Ru(1)	S(4)	83.92(3)	C(9)	C(10)	C(11)	120.1(3)
S(1)	Ru(1)	S(2)	86.03(3)	C(10)	C(11)	C(12)	119.9(4)
S(1)	Ru(1)	S(3)	167.66(3)	C(11)	C(12)	C(13)	120.6(4)
S(1)	Ru(1)	S(4)	97.97(3)	C(12)	C(13)	C(14)	120.2(3)
S(2)	Ru(1)	S(3)	93.26(3)	C(9)	C(14)	C(13)	120.0(3)
S(2)	Ru(1)	S(4)	167.69(3)	S(3)	C(15)	C(16)	107.2(2)
S(3)	Ru(1)	S(4)	85.29(3)	S(4)	C(16)	C(15)	108.4(2)
Ru(1)	S(1)	C(1)	102.6(1)	S(3)	C(17)	C(18)	123.3(3)
Ru(1)	S(1)	C(3)	121.9(1)	S(3)	C(17)	C(22)	115.6(2)
C(1)	S(1)	C(3)	98.5(1)	C(18)	C(17)	C(22)	121.1(3)
Ru(1)	S(2)	C(2)	103.59(9)	C(17)	C(18)	C(19)	118.8(3)
Ru(1)	S(2)	C(9)	117.0(1)	C(18)	C(19)	C(20)	120.7(3)
C(2)	S(2)	C(9)	102.2(2)	C(19)	C(20)	C(21)	119.8(3)
Ru(1)	S(3)	C(15)	103.6(1)	C(20)	C(21)	C(22)	120.5(3)
Ru(1)	S(3)	C(17)	119.2(1)	C(17)	C(22)	C(21)	119.1(3)
C(15)	S(3)	C(17)	100.3(1)	S(4)	C(23)	C(24)	122.1(2)
Ru(1)	S(4)	C(16)	104.1(1)	S(4)	C(23)	C(28)	116.5(3)
Ru(1)	S(4)	C(23)	121.0(1)	C(24)	C(23)	C(28)	121.2(3)
C(16)	S(4)	C(23)	99.7(1)	C(23)	C(24)	C(25)	119.9(3)
S(1)	C(1)	C(2)	108.9(2)	C(24)	C(25)	C(26)	119.2(3)
S(2)	C(2)	C(1)	106.8(2)	C(25)	C(26)	C(27)	120.0(3)
S(1)	C(3)	C(4)	122.6(3)	C(26)	C(27)	C(28)	121.4(3)
S(1)	C(3)	C(8)	118.2(3)	C(23)	C(28)	C(27)	118.3(3)
C(4)	C(3)	C(8)	119.1(3)				

Angles are in degrees. Estimated standard deviations in the least significant figure are given in parentheses.

Table A.1 37. Bond Lengths (Å) for *trans*-RuCl₂(BPhTE)₂

atom	atom	distance	atom	atom	distance
Ru(1)	Cl(1)	2.4266(8)	C(7)	C(8)	1.372(5)
Ru(1)	Cl(2)	2.4244(8)	C(9)	C(10)	1.393(4)
Ru(1)	S(1)	2.3557(9)	C(9)	C(14)	1.387(4)
Ru(1)	S(2)	2.3424(7)	C(10)	C(11)	1.378(5)
Ru(1)	S(3)	2.3440(9)	C(11)	C(12)	1.368(5)
Ru(1)	S(4)	2.3594(8)	C(12)	C(13)	1.370(5)
S(1)	C(1)	1.844(3)	C(13)	C(14)	1.377(5)
S(1)	C(3)	1.788(3)	C(15)	C(16)	1.508(4)
S(2)	C(2)	1.815(4)	C(17)	C(18)	1.378(4)
S(2)	C(9)	1.777(3)	C(17)	C(22)	1.388(5)
S(3)	C(15)	1.835(3)	C(18)	C(19)	1.397(4)

S(3)	C(17)	1.799(3)	C(19)	C(20)	1.383(5)
S(4)	C(16)	1.836(4)	C(20)	C(21)	1.373(5)
S(4)	C(23)	1.793(3)	C(21)	C(22)	1.394(5)
C(1)	C(2)	1.514(5)	C(23)	C(24)	1.373(4)
C(3)	C(4)	1.389(4)	C(23)	C(28)	1.403(4)
C(3)	C(8)	1.384(5)	C(24)	C(25)	1.401(4)
C(4)	C(5)	1.390(5)	C(25)	C(26)	1.397(4)
C(5)	C(6)	1.377(6)	C(26)	C(27)	1.378(5)
C(6)	C(7)	1.389(5)	C(27)	C(28)	1.383(4)

Distances are in angstroms. Estimated standard deviations in the least significant figure are given in parentheses.

Table A.1 38. Atomic Coordinates for *trans*-RuCl₂(BPhTE)₂

atom	x	y	z
Ru(1)	0.17633(3)	0.42116(3)	0.28037(2)
Cl(1)	0.38363(8)	0.30901(7)	0.32390(6)
Cl(2)	-0.03416(8)	0.52838(7)	0.23181(6)
S(1)	0.07126(8)	0.23633(7)	0.17658(6)
S(2)	0.19651(8)	0.48748(8)	0.11791(6)
S(3)	0.32480(8)	0.58400(7)	0.38769(6)
S(4)	0.12045(8)	0.38616(8)	0.43917(6)
C(1)	0.0429(4)	0.2765(3)	0.0359(2)
C(2)	0.1717(4)	0.3453(3)	0.0304(2)
C(3)	-0.1013(3)	0.1836(3)	0.1629(3)
C(4)	-0.1778(3)	0.2414(3)	0.2209(3)
C(5)	-0.3100(4)	0.1933(4)	0.2090(3)
C(6)	-0.3647(4)	0.0880(4)	0.1413(3)
C(7)	-0.2873(4)	0.0289(4)	0.0850(3)
C(8)	-0.1579(4)	0.0778(3)	0.0954(3)
C(9)	0.3620(3)	0.5466(3)	0.1210(2)
C(10)	0.3748(4)	0.6709(3)	0.1030(3)
C(11)	0.5022(4)	0.7266(4)	0.1141(3)
C(12)	0.6159(4)	0.6591(4)	0.1405(3)
C(13)	0.6040(4)	0.5356(4)	0.1538(3)
C(14)	0.4780(4)	0.4791(3)	0.1454(3)
C(15)	0.2620(4)	0.6101(3)	0.5042(3)
C(16)	0.2481(4)	0.4861(3)	0.5468(2)
C(17)	0.3147(3)	0.7359(3)	0.3397(3)
C(18)	0.1957(3)	0.7774(3)	0.2714(3)
C(19)	0.2001(4)	0.8954(3)	0.2356(3)
C(20)	0.3217(4)	0.9691(3)	0.2673(3)
C(21)	0.4387(4)	0.9272(4)	0.3369(3)
C(22)	0.4371(4)	0.8095(3)	0.3732(3)
C(23)	0.1473(3)	0.2409(3)	0.4979(2)
C(24)	0.1873(3)	0.1413(3)	0.4474(2)
C(25)	0.1977(4)	0.0274(3)	0.4929(3)
C(26)	0.1665(4)	0.0170(4)	0.5892(3)
C(27)	0.1252(4)	0.1177(4)	0.6380(3)
C(28)	0.1138(4)	0.2306(3)	0.5937(3)

S(1)
S(2)
C(1)
C(2)
C(3)
C(4)
C(5)
C(6)
C(7)
C(8)

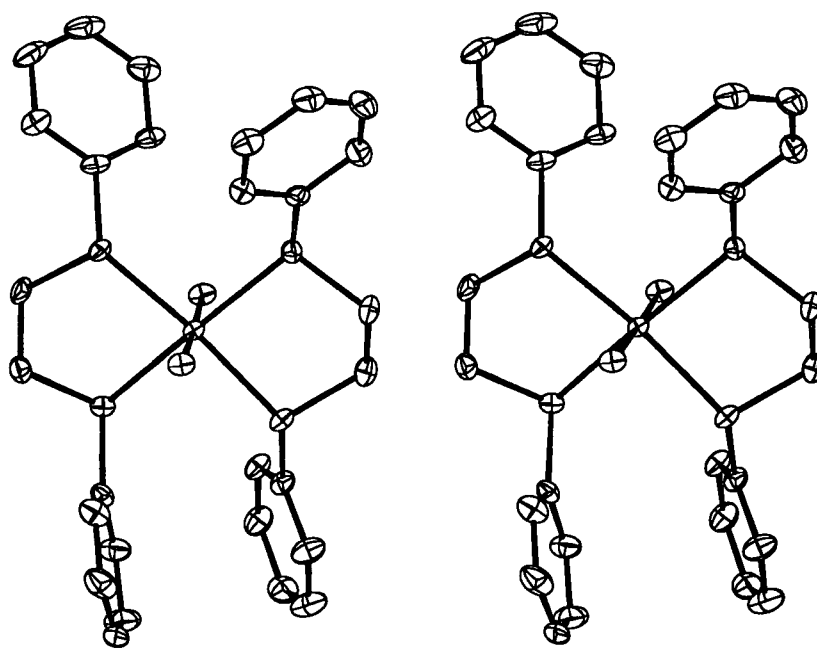


Figure A.1.6. Stereoview of *trans*-RuCl₂(BPhTE)₂.

Appendix 1.9 Crystallographic Data for $[\text{RuCl}_2(\text{BETP})]_2(\mu\text{-Cl})_2$ **Table A.1 39.** Experimental Details for X-ray Crystal Structure of $[\text{RuCl}_2(\text{BETP})]_2(\mu\text{-Cl})_2$ *A. Crystal Data*

Empirical Formula	$\text{C}_{14}\text{H}_{32}\text{Cl}_6\text{Ru}_2\text{S}_4$
Formula Weight	743.50
Crystal Colour, Habit	orange, block
Crystal Dimensions	0.30 x 0.40 x 0.45 mm
Crystal System	monoclinic
Lattice Type	Primitive
Lattice Parameters	$a = 9.4203(13) \text{ \AA}$ $b = 7.8644(13) \text{ \AA}$ $c = 17.2910(5) \text{ \AA}$ $\beta = 98.8128(7)^\circ$ $V = 1265.3(2) \text{ \AA}^3$
Space Group	$P2_1/n$ (# 14)
Z Value	2
D_{calc}	1.951 g/cm^3
F_{000}	740.00
$\mu(\text{MoK}\alpha)$	21.58 cm^{-1}

B. Intensity Measurements

Diffractionmeter	Rigaku/ADSC CCD
Radiation	$\text{MoK}\alpha$ ($\lambda = 0.71069 \text{ \AA}$) graphite monochromated
Detector Aperature	94 mm x 94 mm
Data Images	462 exposures of 40.0 seconds
ϕ oscillation Range ($\chi = -90$)	$0.0 - 190.0^\circ$
ω oscillation Range ($\chi = -90$)	$-23.0 - 18.0^\circ$
Detector Position	$39.22(1) \text{ mm}$
Detector Swing Angle	-10°
$2\theta_{\text{max}}$	63.6°
$2\theta_{\text{full}}$	60.1°
No. of Reflections Measured	Total: 10528 Unique: 3419 ($R_{\text{int}} = 0.024$)
Corrections	Lorentz-polarization Absorption/scaling (trans. factors: 0.7434 - 1.0018)

C. Structure Solution and Refinement

Structure Solution	Patterson Methods (DIRDIF92 PATTY)
Refinement	Full-matrix least-squares
Function Minimized	$\Sigma \omega (Fo^2 - Fc^2)^2$
Least Squares Weights	$\omega = 1/\sigma^2(Fo^2) = [\sigma^2(Fo^2) + p^2Fo^2]^{-1}$
p-factor	0.0200
Anomalous Dispersion	All non-hydrogen atoms
No. Observations	3419
No. Variables	118
Reflection/Parameter Ratio	28.97
Residuals (on F^2 , all data): R; Rw	0.060; 0.076
Goodness of Fit Indicator	1.90
No. Observations ($I > 3\sigma(I)$)	2650
Residuals (on F, $I > 3\sigma(I)$): R1; R1w	0.034; 0.036
Max Shift/Error in Final Cycle	0.001

Maximum peak in Final Diff. Map	1.15 e/ \AA^3 (near Ru)
Minimum peak in Final Diff. Map	-1.50 e/ \AA^3 (near Ru)

Table A.1 40. Bond Angles ($^\circ$) for $[\text{RuCl}_2(\text{BETP})]_2(\mu\text{-Cl})_2$

atom	atom	atom	angle	atom	atom	atom	angle
Cl(1)	Ru(1)	Cl(1)*	84.14(3)	Cl(1)	Ru(1)	Cl(2)	173.59(3)
Cl(1)	Ru(1)	Cl(3)	90.35(3)	Cl(1)	Ru(1)	S(1)	85.46(3)
Cl(1)	Ru(1)	S(2)	96.74(3)	Cl(1)*	Ru(1)	Cl(2)	91.62(3)
Cl(1)*	Ru(1)	Cl(3)	86.95(3)	Cl(1)*	Ru(1)	S(1)	92.49(3)
Cl(1)*	Ru(1)	S(2)	172.05(3)	Cl(2)	Ru(1)	Cl(3)	94.22(3)
Cl(2)	Ru(1)	S(1)	89.94(3)	Cl(2)	Ru(1)	S(2)	88.13(3)
Cl(3)	Ru(1)	S(1)	175.81(3)	Cl(3)	Ru(1)	S(2)	85.14(3)
S(1)	Ru(1)	S(2)	95.45(3)	Ru(1)	Cl(1)	Ru(1)*	95.86(3)
Ru(1)	S(1)	C(1)	110.16(11)	Ru(1)	S(1)	C(4)	107.85(11)
C(1)	S(1)	C(4)	99.78(15)	Ru(1)	S(2)	C(3)	111.62(11)
Ru(1)	S(2)	C(6)	110.65(10)	C(3)	S(2)	C(6)	100.54(15)
S(1)	C(1)	C(2)	112.9(2)	C(1)	C(2)	C(3)	113.6(3)
S(2)	C(3)	C(2)	117.3(2)	S(1)	C(4)	C(5)	112.5(3)
S(2)	C(6)	C(7)	110.7(2)				

Angles are in degrees. Estimated standard deviations in the least significant figure are given in parentheses.

Table A.1 41. Bond Lengths (\AA) for $[\text{RuCl}_2(\text{BETP})]_2(\mu\text{-Cl})_2$

atom	atom	distance	atom	atom	distance
Ru(1)	Cl(1)	2.3915(7)	S(1)	C(4)	1.823(3)
Ru(1)	Cl(1)	2.4617(7)	S(2)	C(3)	1.808(3)
Ru(1)	Cl(2)	2.3258(7)	S(2)	C(6)	1.813(3)
Ru(1)	Cl(3)	2.3501(8)	C(1)	C(2)	1.523(5)
Ru(1)	S(1)	2.3677(8)	C(2)	C(3)	1.521(5)
Ru(1)	S(2)	2.3201(8)	C(4)	C(5)	1.511(5)
S(1)	C(1)	1.815(3)	C(6)	C(7)	1.521(5)

Distances are in angstroms. Estimated standard deviations in the least significant figure are given in parentheses.

Table A.1 42. Atomic Coordinates for $[\text{RuCl}_2(\text{BETP})]_2(\mu\text{-Cl})_2$

atom	x	y	z
Ru(1)	0.01544(2)	0.07158(3)	0.402663(12)
Cl(1)	-0.11601(7)	0.15130(10)	0.50486(4)
Cl(2)	0.16600(8)	-0.00636(10)	0.31390(4)
Cl(3)	-0.16463(8)	-0.12495(10)	0.35461(4)
S(1)	0.18705(8)	0.27429(10)	0.45849(4)
S(2)	-0.10155(8)	0.25303(10)	0.30786(4)
C(1)	0.2389(4)	0.4103(4)	0.3827(2)
C(2)	0.1131(4)	0.5094(4)	0.3385(2)
C(3)	0.0208(3)	0.4055(4)	0.2757(2)
C(4)	0.3563(3)	0.1630(5)	0.4888(2)
C(5)	0.4615(4)	0.2672(5)	0.5443(2)
C(6)	-0.2217(3)	0.3943(4)	0.3497(2)
C(7)	-0.3655(3)	0.3083(5)	0.3524(2)

Appendix 1.10 Crystallographic Data for $[\text{RuCl}_2(\text{BTP})]_2(\mu\text{-Cl})_2$ **Table A.1 43.** Experimental Details for X-ray Crystal Structure of $[\text{RuCl}_2(\text{BTP})]_2(\mu\text{-Cl})_2$ *A. Crystal Data*

Empirical Formula	$\text{C}_{20}\text{H}_{44}\text{Cl}_{10}\text{Ru}_2\text{S}_4$
Formula Weight	969.48
Crystal Colour, Habit	red, platelet
Crystal Dimensions	0.40 x 0.20 x 0.03 mm
Crystal System	monoclinic
Lattice Type	Primitive
Lattice Parameters	$a = 11.803(2) \text{ \AA}$ $b = 7.4111(6) \text{ \AA}$ $c = 21.7417(8) \text{ \AA}$ $\beta = 99.4766(10)^\circ$ $V = 1875.9(3) \text{ \AA}^3$
Space Group	$P2_1/n$ (# 14)
Z Value	2
D_{calc}	1.716 g/cm ³
F_{000}	972.00
$\mu(\text{MoK}\alpha)$	17.52 cm ⁻¹

B. Intensity Measurements

Diffractionmeter	Rigaku/ADSC CCD
Radiation	MoK α ($\lambda = 0.71069 \text{ \AA}$) graphite monochromated
Detector Aperature	94 mm x 94 mm
Data Images	462 exposures of 50.0 seconds
ϕ oscillation Range ($\chi = -90$)	$0.0 - 190.0^\circ$
ω oscillation Range ($\chi = -90$)	$-23.0 - 18.0^\circ$
Detector Position	39.180(7) mm
Detector Swing Angle	-10°
$2\theta_{\text{max}}$	60.1°
No. of Reflections Measured	Total: 17721 Unique: 4854 ($R_{\text{int}} = 0.037$)
Corrections	Lorentz-polarization Absorption/scaling (trans. factors: 0.6735 - 1.0000)

C. Structure Solution and Refinement

Structure Solution	Direct Methods (SIR92)
Refinement	Full-matrix least-squares
Function Minimized	$\sum \omega (F_o ^2 - F_c ^2)^2$
Least Squares Weights	$\omega = 1/\sigma^2(F_o^2)$
p-factor	0.0000
Anomalous Dispersion	All non-hydrogen atoms
No. Observations	4854
No. Variables	163
Reflection/Parameter Ratio	29.78
Residuals (on F^2 , all data): R; Rw	0.077; 0.070
Goodness of Fit Indicator	1.52
No. Observations ($I > 3\sigma(I)$)	2896

Residuals (on F, $I > 3\sigma(I)$): R; Rw	0.037; 0.029
Max Shift/Error in Final Cycle	0.0007
Maximum peak in Final Diff. Map	$2.35 \text{ e}^-/\text{\AA}^3$ (near Ru)
Minimum peak in Final Diff. Map	$-3.98 \text{ e}^-/\text{\AA}^3$ (near Ru)

Table A.1 44. Bond Angles ($^\circ$) for $[\text{RuCl}_2(\text{BPTP})]_2(\mu\text{-Cl})_2$

atom	atom	atom	angle		atom	atom	atom	angle
Cl(1)	Ru(1)	Cl(1)*	82.98(3)		Cl(1)	Ru(1)	Cl(2)	174.10(4)
Cl(1)	Ru(1)	C(3)	90.06(3)		Cl(1)	Ru(1)	S(1)	85.89(3)
Cl(1)	Ru(1)	S(2)	97.50(3)		Cl(1)*	Ru(1)	Cl(2)	92.56(3)
Cl(1)*	Ru(1)	Cl(3)	88.83(3)		Cl(1)*	Ru(1)	S(1)	91.07(3)
Cl(1)*	Ru(1)	S(2)	173.32(4)		Cl(2)	Ru(1)	Cl(3)	93.72(4)
Cl(2)	Ru(1)	S(1)	90.36(4)		Cl(2)	Ru(1)	S(2)	87.39(3)
Cl(3)	Ru(1)	S(1)	175.93(4)		Cl(3)	Ru(1)	S(2)	84.51(4)
S(1)	Ru(1)	S(2)	95.62(4)		Ru(1)	Cl(1)	Ru(1)*	97.02(3)
Ru(1)	S(1)	C(1)	110.27(14)		Ru(1)	S(1)	Cl(4)	110.74(13)
C(1)	S(1)	C(4)	99.0(2)		Ru(1)	S(2)	C(3)	112.80(14)
Ru(1)	S(2)	C(7)	109.73(13)		C(3)	S(2)	C(7)	100.6(2)
S(1)	C(1)	C(2)	112.0(3)		C(1)	C(2)	C(3)	114.1(3)
S(2)	C(3)	C(2)	117.5(3)		S(1)	C(4)	C(5)	112.8(3)
C(4)	C(5)	C(6)	112.3(4)		S(2)	C(7)	C(8)	111.3(3)
C(7)	C(8)	C(9)	114.0(4)		Cl(4)	C(10)	Cl(5)	112.0(3)

Angles are in degrees. Estimated standard deviations in the least significant figure are given in parentheses.

Table A.1 45. Bond Lengths (\AA) for $[\text{RuCl}_2(\text{BPTP})]_2(\mu\text{-Cl})_2$

atom	atom	distance		atom	atom	distance
Ru(1)	Cl(1)	2.3833(9)		S(1)	C(4)	1.814(4)
Ru(1)	Cl(1)	2.4605(9)		S(2)	C(3)	1.806(4)
Ru(1)	Cl(2)	2.3213(9)		S(2)	C(7)	1.821(4)
Ru(1)	Cl(3)	2.358(1)		C(1)	C(2)	1.515(5)
Ru(1)	S(1)	2.356(1)		C(2)	C(3)	1.531(6)
Ru(1)	S(2)	2.331(1)		C(4)	C(5)	1.511(6)
Cl(4)	C(10)	1.746(6)		C(5)	C(6)	1.509(6)
Cl(5)	C(10)	1.782(6)		C(7)	C(8)	1.527(6)
S(1)	C(1)	1.813(4)		C(8)	C(9)	1.500(6)

Distances are in angstroms. Estimated standard deviations in the least significant figure are given in parentheses.

Table A.1 46. Atomic Coordinates for $[\text{RuCl}_2(\text{BPTP})]_2(\mu\text{-Cl})_2$

atom	x	y	z
Ru(1)	0.44366(3)	0.43216(4)	0.420673(14)
Cl(1)	0.46196(8)	0.30652(11)	0.52274(4)
Cl(2)	0.44475(9)	0.56642(12)	0.32431(4)
Cl(3)	0.26444(8)	0.55676(12)	0.43201(4)
Cl(4)	0.15729(15)	0.3947(2)	0.21330(7)
Cl(5)	0.14123(14)	0.7728(2)	0.24937(7)
S(1)	0.62293(9)	0.29734(12)	0.41622(4)
S(2)	0.33402(9)	0.20132(12)	0.36777(4)
C(1)	0.6184(4)	0.1775(5)	0.3432(2)
C(2)	0.5319(4)	0.0247(5)	0.3364(2)
C(3)	0.4080(4)	0.0842(5)	0.3133(2)
C(4)	0.7292(4)	0.4670(5)	0.4063(2)

C(5)	0.8507(4)	0.3956(6)	0.4195(2)
C(6)	0.9385(5)	0.5396(7)	0.4135(3)
C(7)	0.3168(4)	0.0193(4)	0.4217(2)
C(8)	0.2161(4)	0.0554(5)	0.4560(2)
C(9)	0.1007(4)	0.0433(7)	0.4153(2)
C(10)	0.1353(5)	0.5429(9)	0.2726(2)

Appendix 1.11 Crystallographic Data for *Mer-Cis*-RuCl₃(DPSO)₂(DPSO)

Table A.1 47. Experimental Details for X-ray Crystal Structure of *Mer-Cis*-RuCl₃(DPSO)₂(DPSO)

A. Crystal Data

Empirical Formula	C ₃₆ H ₃₀ Cl ₃ O ₃ RuS ₃
Formula Weight	814.24
Crystal Colour, Habit	orange, plate
Crystal Dimensions	0.15 x 0.35 x 0.40 mm
Crystal System	triclinic
Lattice Type	Primitive
No. of Reflections Used for Unit Cell	25 (22.6-28.4 °)
Determinations (2 θ range)	0.37 °
Omega Scan Peak Width at Half-height	
Lattice Parameters	a = 13.097(2) Å b = 15.701(2) Å c = 10.312(1) Å α = 106.765(9) ° β = 102.02(1) ° γ = 103.14(1) ° V = 1890.2(5) Å ³
Space Group	P $\bar{1}$ (# 2)
Z Value	2
D _{calc}	1.431 g/cm ³
F ₀₀₀	826
μ (MoK α)	8.25 cm ⁻¹

B. Intensity Measurements

Diffractometer	Rigaku AFC6S
Radiation	MoK α (λ = 0.71069 Å) graphite monochromated
Take-off Angle	6.0 °
Detector Aperature	6.0 mm horizontal 6.0 mm vertical
Crystal to Detector Distance	285 mm
Temperature	21.0 °C
Scan Type	ω -2 θ
Scan Rate	16° /min (in ω) (up to 9 scans)
Scan Width	(1.21 + 0.35 tan θ) °
2 θ_{max}	60 °
No. of Reflections Measured	Total: 11483 Unique: 11033 (R_{int} = 0.044)
Corrections	Lorentz-polarization Absorption (trans. factors: 0.906 - 1.000)

C. Structure Solution and Refinement

Structure Solution	Patterson Methods (DIRDIF92 PATTY)
Refinement	Full-matrix least-squares
Function Minimized	$\Sigma w(F_o - F_c)^2$
Least Squares Weights	$w = 1/\sigma^2(F_o) = [\sigma_c^2(F_o) + p^2/4F_o^2]^{-1}$
p-factor	0.0000
Anomalous Dispersion	All non-hydrogen atoms
No. Observations ($I > 3\sigma(I)$)	5914
No. Variables	451
Reflection/Parameter Ratio	13.11
Residuals: R; Rw	0.040; 0.045
Goodness of Fit Indicator	2.01
Max Shift/Error in Final Cycle	0.01
Maximum peak in Final Diff. Map	$0.73 \text{ e}/\text{\AA}^3$
Minimum peak in Final Diff. Map	$-0.50 \text{ e}/\text{\AA}^3$

Table A.1 48. Bond Angles ($^\circ$) for *Mer-Cis-RuCl₃(DPSO)₂(DPSO)*

atom	atom	atom	angle		atom	atom	atom	angle
Cl(1)	Ru(1)	Cl(2)	172.63(5)		S(1)	C(7)	C(12)	120.1(4)
Cl(1)	Ru(1)	S(3)	91.18(5)		C(7)	C(8)	C(9)	118.1(5)
Cl(1)	Ru(1)	O(2)	86.82(9)		C(9)	C(10)	C(11)	121.1(6)
Cl(2)	Ru(1)	S(3)	91.73(5)		C(7)	C(12)	C(11)	118.4(5)
Cl(2)	Ru(1)	O(2)	89.57(9)		S(2)	C(13)	C(18)	120.4(4)
Cl(3)	Ru(1)	O(1)	173.70(9)		C(13)	C(14)	C(15)	118.9(5)
S(3)	Ru(1)	O(1)	87.42(9)		C(15)	C(16)	C(17)	120.5(5)
O(1)	Ru(1)	O(2)	86.5(1)		C(13)	C(18)	C(17)	119.8(5)
O(1)	S(1)	C(1a)	112.0(5)		S(2)	C(19)	C(24)	120.9(4)
C(1)	S(1)	C(7)	97.9(4)		C(19)	C(20)	C(21)	119.4(5)
O(2)	S(2)	C(13)	103.0(2)		C(21)	C(22)	C(23)	121.0(5)
C(13)	S(2)	C(19)	101.4(2)		C(19)	C(24)	C(23)	118.8(5)
Ru(1)	S(3)	C(25)	117.1(2)		S(3)	C(25)	C(30)	123.4(4)
O(3)	S(3)	C(25)	106.0(2)		C(25)	C(26)	C(27)	118.8(5)
C(25)	S(3)	C(31)	99.0(2)		C(27)	C(28)	C(29)	119.7(5)
Ru(1)	O(2)	S(2)	120.0(2)		C(25)	C(30)	C(29)	119.2(5)
S(1)	C(1)	C(6)	123.9(9)		S(3)	C(31)	C(36)	122.0(4)
S(1)	C(1a)	C(2)	123.6(10)		C(31)	C(32)	C(33)	118.6(5)
C(2)	C(1a)	C(6a)	112(1)		C(33)	C(34)	C(35)	119.5(5)
C(1a)	C(2)	C(3)	132.3(9)		C(31)	C(36)	C(35)	118.1(5)
C(2)	C(3)	C(4a)	108.9(9)		C(8)	C(7)	C(12)	120.9(5)
C(3)	C(4a)	C(5a)	124(1)		C(8)	C(9)	C(10)	121.2(6)
C(4a)	C(5a)	C(6a)	120(1)		C(10)	C(11)	C(12)	120.4(6)
C(1a)	C(6a)	C(5a)	118(1)		S(2)	C(13)	C(14)	118.2(4)
Cl(1)	Ru(1)	Cl(3)	93.22(5)		C(14)	C(13)	C(18)	121.0(5)
Cl(1)	Ru(1)	O(1)	87.14(9)		C(14)	C(15)	C(16)	120.1(5)
Cl(2)	Ru(1)	Cl(3)	93.02(4)		C(16)	C(17)	C(18)	119.7(5)
Cl(2)	Ru(1)	O(1)	86.23(9)		S(2)	C(19)	C(20)	117.3(4)
Cl(3)	Ru(1)	S(3)	98.86(4)		C(20)	C(19)	C(24)	121.6(5)
Cl(3)	Ru(1)	O(2)	87.28(9)		C(20)	C(21)	C(22)	119.9(5)
S(3)	Ru(1)	O(2)	173.65(9)		C(22)	C(23)	C(24)	119.3(6)
O(1)	S(1)	C(1)	94.9(4)		S(3)	C(30)	C(29)	119.2(5)
O(1)	S(1)	C(7)	105.2(2)		C(26)	C(25)	C(30)	121.1(4)
C(1a)	S(1)	C(7)	107.1(5)		C(26)	C(27)	C(28)	121.3(5)
O(2)	S(2)	C(19)	103.5(2)		C(28)	C(29)	C(30)	119.8(5)

Ru(1)	S(3)	O(3)	113.0(1)		S(3)	C(31)	C(32)	116.5(4)
Ru(1)	S(3)	C(31)	114.5(2)		C(32)	C(31)	C(36)	121.5(5)
O(3)	S(3)	C(31)	105.8(2)		C(32)	C(33)	C(34)	120.9(6)
Ru(1)	O(1)	S(1)	119.8(2)		C(34)	C(35)	C(36)	121.4(5)
S(1)	C(1)	C(2)	115.9(8)					
C(2)	C(1)	C(6)	119(1)					
S(1)	C(1a)	C(6a)	123(1)					
C(1)	C(2)	C(3)	123.1(3)					
C(2)	C(3)	C(4)	123.0(9)					
C(3)	C(4)	C(5)	115(1)					
C(4)	C(5)	C(6)	119(1)					
C(1)	C(6)	C(5)	116(1)					
S(1)	C(7)	C(8)	118.9(4)					

Angles are in degrees. Estimated standard deviations in the least significant figure are given in parentheses.

Table A.1 49. Bond Lengths (Å) for *Mer-Cis*-RuCl₃(DPSO)₂(DPSO)

atom	atom	distance		atom	atom	distance
Ru(1)	Cl(1)	2.338(1)		C(8)	C(9)	1.359(8)
Ru(1)	Cl(2)	2.324(1)		C(9)	C(10)	1.335(8)
Ru(1)	Cl(3)	2.305(3)		C(10)	C(11)	1.335(9)
Ru(1)	S(3)	2.251(1)		C(11)	C(12)	1.375(8)
Ru(1)	O(1)	2.090(3)		C(13)	C(14)	1.379(6)
Ru(1)	O(2)	2.111(3)		C(13)	C(18)	1.385(6)
S(1)	O(1)	1.524(3)		C(14)	C(15)	1.365(7)
S(1)	C(1)	1.93(1)		C(15)	C(16)	1.397(8)
S(1)	C(1a)	1.65(1)		C(16)	C(17)	1.365(8)
S(1)	C(7)	1.790(5)		C(17)	C(18)	1.368(7)
S(2)	C(13)	1.788(5)		C(19)	C(20)	1.377(6)
S(2)	C(19)	1.780(5)		C(19)	C(24)	1.373(7)
S(3)	O(3)	1.472(3)		C(20)	C(21)	1.370(7)
S(3)	C(25)	1.798(4)		C(21)	C(22)	1.359(8)
S(3)	C(31)	1.806(5)		C(22)	C(23)	1.394(8)
C(1)	C(2)	1.18(1)		C(23)	C(24)	1.379(7)
C(1)	C(6a)	1.85(2)		C(25)	C(26)	1.385(6)
C(1)	C(6)	1.38(1)		C(25)	C(30)	1.371(6)
S(4)	C(10)	1.806(4)		C(26)	C(27)	1.362(7)
C(1a)	C(2)	1.38(2)		C(27)	C(28)	1.371(7)
C(1a)	C(6a)	1.35(2)		C(28)	C(29)	1.382(7)
C(2)	C(3)	1.347(5)		C(29)	C(30)	1.385(6)
C(3)	C(4)	1.30(1)		C(31)	C(32)	1.381(6)
C(3)	C(4a)	1.34(2)		C(31)	C(36)	1.384(6)
C(4)	C(5)	1.38(2)		C(32)	C(33)	1.371(7)
C(4a)	C(5a)	1.36(2)		C(33)	C(34)	1.370(8)
C(5)	C(6)	1.41(1)		C(34)	C(35)	1.374(8)
C(5a)	C(6a)	1.40(2)		C(35)	C(36)	1.369(7)
C(7)	C(8)	1.379(7)				
C(7)	C(12)	1.366(7)				

Distances are in angstroms. Estimated standard deviations in the least significant figure are given in parentheses.

Table A.1 50. Atomic Coordinates for *Mer-Cis-RuCl₃(DPSO)₂(DPSO)*

atom	x	y	z	atom	x	y	z
Ru(1)	0.11952(3)	0.35548(3)	0.21549(4)	C(17)	-0.4144(4)	0.2955(4)	0.1702(7)
Cl(1)	0.0664(1)	0.23915(9)	-0.0082(1)	C(18)	-0.3131(4)	0.3151(4)	0.2618(6)
Cl(2)	0.17137(10)	0.45567(8)	0.4495(1)	C(19)	-0.1110(4)	0.2882(3)	0.4516(5)
Cl(3)	0.02953(9)	0.44822(9)	0.1329(1)	C(20)	-0.0696(4)	0.3426(4)	0.5932(5)
S(1)	0.1149(1)	0.16519(10)	0.2600(2)	C(21)	-0.0755(5)	0.3011(5)	0.6927(6)
S(2)	-0.08971(10)	0.34429(8)	0.3277(1)	C(22)	-0.1225(5)	0.2073(5)	0.6510(7)
S(3)	0.28516(9)	0.41504(8)	0.1919(1)	C(23)	-0.1653(5)	0.1520(4)	0.5078(7)
O(1)	0.1854(2)	0.2652(2)	0.2955(3)	C(24)	-0.1588(5)	0.1933(4)	0.4073(6)
O(2)	0.0299(2)	0.2870(2)	0.2400(3)	C(25)	0.2887(4)	0.4226(3)	0.0221(5)
O(3)	0.3627(2)	0.3644(2)	0.2261(3)	C(26)	0.3753(4)	0.4013(4)	-0.0232(6)
C(1)	0.1724(9)	0.1609(8)	0.446(1)	C(27)	0.3867(5)	0.4101(5)	-0.1474(6)
C(1a)	0.110(1)	0.13989(10)	0.403(2)	C(28)	0.3156(5)	0.4408(4)	-0.2264(5)
C(2)	0.1455(7)	0.2059(5)	0.5378(8)	C(29)	0.2288(4)	-0.4612(4)	-0.1815(5)
C(3)	0.1635(7)	0.1989(6)	0.6673(8)	C(30)	0.2153(4)	0.4520(4)	-0.0559(5)
C(4)	0.234(1)	0.1611(10)	0.715(1)	C(31)	0.3535(4)	0.5363(3)	0.3011(5)
C(4a)	0.114(1)	0.111(1)	0.654(2)	C(32)	0.4592(4)	0.5573(4)	0.3854(5)
C(5)	0.284(1)	0.1181(10)	0.617(2)	C(33)	0.5149(4)	0.6486(5)	0.4692(6)
C(5a)	0.061(1)	0.039(1)	0.585(2)	C(34)	0.4674(5)	0.7178(4)	0.4686(6)
C(6)	0.2501(10)	0.1178(9)	0.477(1)	C(35)	0.3620(5)	0.6952(4)	0.3841(6)
C(6a)	0.057(1)	0.0544(9)	0.400(1)	C(36)	0.3031(4)	0.6047(4)	0.3006(6)
C(7)	0.1833(4)	0.0929(3)	0.1670(5)				
C(8)	0.1306(5)	-0.0017(4)	0.1015(7)				
C(9)	0.1826(6)	-0.0550(4)	0.0279(7)				
C(10)	0.2815(6)	-0.0171(5)	0.0181(8)				
C(11)	0.3322(6)	0.0748(5)	0.0790(9)				
C(12)	0.2839(5)	0.1322(4)	0.1554(7)				
C(13)	-0.2235(4)	0.3068(3)	0.2094(5)				
C(14)	-0.2380(4)	0.2797(4)	0.0659(6)				
C(15)	-0.3398(6)	0.2580(4)	-0.0250(6)				
C(16)	-0.4284(5)	0.2667(5)	0.0278(7)				

Appendix 1.12 Crystallographic Data for *RuCl₂(DMSO)(L)***Table A.1 51.** Experimental Details for X-ray Crystal Structure of *RuCl₂(DMSO)(L)**A. Crystal Data*

Empirical Formula	C ₁₂ H ₂₀ Cl ₂ ORuS ₅
Formula Weight	512.57
Crystal Colour, Habit	red, prism
Crystal Dimensions	0.12 x 0.15 x 0.35 mm
Crystal System	tetragonal
Lattice Type	Primitive
No. of Reflections Used for Unit Cell	25 (56.1-64.1 °)
Determinations (2θ range)	
Omega Scan Peak Width at Half-height	0.42 °
Lattice Parameters	a = 20.784(2) Å c = 9.284(2) Å V = 4010(1) Å ³
Space Group	P4 ₂ c (# 114)
Z Value	8

D_{calc}	1.698 g/cm ³
F_{000}	2064.00
$\mu(\text{CuK}\alpha)$	136.13 cm ⁻¹

B. Intensity Measurements

Diffractionmeter	Rigaku AFC6S
Radiation	CuK α ($\lambda = 1.54178 \text{ \AA}$) graphite monochromated
Take-off Angle	6.0 °
Detector Aperature	6.0 mm horizontal 6.0 mm vertical
Crystal to Detector Distance	285 mm
Voltage, Current	0 kV, 0 mA
Temperature	21.0 °C
Scan Type	ω -2 θ
Scan Rate	8.0 °/min (in ω) (up to 9 scans)
Scan Width	(0.89 + 0.20 tan θ) °
2 θ_{max}	154.7 °
No. of Reflections Measured	Total: 4647 Unique: 2428 ($R_{int} = 0.063$)
Corrections	Lorentz-polarization Absorption (trans. factors: 0.5012 - 1.0000)

C. Structure Solution and Refinement

Structure Solution	Direct Methods (SIR92)
Refinement	Full-matrix least-squares
Function Minimized	$\Sigma \omega (F_o - F_c)^2$
Least Squares Weights	$\omega = 1/\sigma^2(F_o) = [\sigma_c^2(F_o) + p^2/4F_o^2]^{-1}$
p-factor	0.0000
Anomalous Dispersion	All non-hydrogen atoms
No. Observations ($I > 3.00\sigma(I)$)	1951
No. Variables	190
Reflection/Parameter Ratio	10.27
Residuals: R; R _w	0.033; 0.037
Goodness of Fit Indicator	0.81
Max Shift/Error in Final Cycle	0.00
Maximum peak in Final Diff. Map	0.58 e ⁻ /Å ³
Minimum peak in Final Diff. Map	-0.48 e ⁻ /Å ³

Table A.1 52. Bond Angles (°) for RuCl₂(DMSO)(L)

atom	atom	atom	angle	atom	atom	atom	angle
Cl(1)	Ru(1)	Cl(2)	90.39(9)	Cl(2)	Ru(1)	S(1)	97.64(8)
Cl(1)	Ru(1)	S(2)	86.46(9)	Cl(2)	Ru(1)	S(3)	88.41(8)
Cl(1)	Ru(1)	S(5)	91.43(9)	S(1)	Ru(1)	S(2)	85.64(9)
Cl(2)	Ru(1)	S(2)	175.80(9)	S(1)	Ru(1)	S(5)	86.14(8)
Cl(2)	Ru(1)	S(5)	90.53(9)	S(2)	Ru(1)	S(5)	92.31(9)
S(1)	Ru(1)	S(3)	100.25(8)	Ru(1)	S(1)	C(1)	106.5(3)
S(2)	Ru(1)	S(3)	88.42(7)	C(1)	S(1)	C(8)	92.3(5)
S(3)	Ru(1)	S(5)	173.61(9)	Ru(1)	S(2)	C(3)	102.7(3)
Ru(1)	S(1)	C(8)	132.9(3)	Ru(1)	S(3)	C(4)	100.9(3)
Ru(1)	S(2)	C(2)	106.4(3)	C(4)	S(3)	C(5)	101.9(4)
C(2)	S(2)	C(3)	97.3(5)	Ru(1)	S(5)	O(1)	116.3(3)

Ru(1)	S(3)	C(5)	112.0(3)	Ru(1)	S(5)	C(12)	114.5(4)
C(6)	S(4)	C(7)	100.7(4)	O(1)	S(5)	C(12)	105.8(5)
Ru(1)	S(5)	C(11)	113.0(4)	S(1)	C(1)	C(2)	115.4(7)
O(1)	S(5)	C(11)	104.5(7)	C(2)	C(1)	C(10)	133.0(9)
C(11)	S(5)	C(12)	101.2(8)	S(2)	C(3)	C(4)	109.6(6)
S(1)	C(1)	C(10)	111.0(7)	S(3)	C(5)	C(6)	106.6(6)
S(2)	C(2)	C(1)	110.3(7)	S(4)	C(7)	C(8)	114.2(7)
S(3)	C(4)	C(3)	111.7(6)	S(1)	C(8)	C(9)	108.1(8)
S(4)	C(6)	C(5)	113.9(6)	C(8)	C(9)	C(10)	115.2(10)
S(1)	C(8)	C(7)	122.4(7)				
C(7)	C(8)	C(9)	129.4(9)				
C(1)	C(10)	C(9)	112.8(9)				
Cl(1)	Ru(1)	S(1)	171.63(8)				
Cl(1)	Ru(1)	S(3)	82.27(8)				

Angles are in degrees. Estimated standard deviations in the least significant figure are given in parentheses.

Table A.1 53. Bond Lengths (Å) for RuCl₂(DMSO)(L)

atom	atom	distance	atom	atom	distance
Ru(1)	Cl(1)	2.400(2)	Ru(1)	S(5)	2.290(2)
Ru(1)	S(1)	2.320(2)	S(1)	C(8)	1.749(9)
Ru(1)	S(3)	2.375(2)	S(2)	C(3)	1.846(10)
S(1)	C(1)	1.764(9)	S(3)	C(5)	1.808(9)
S(2)	C(2)	1.82(1)	S(4)	C(7)	1.81(1)
S(3)	C(4)	1.822(9)	S(5)	C(11)	1.75(1)
S(4)	C(6)	1.784(10)	C(1)	C(2)	1.48(1)
S(5)	O(1)	1.479(8)	C(3)	C(4)	1.49(1)
S(5)	C(12)	1.79(1)	C(7)	C(8)	1.50(1)
C(1)	C(10)	1.32(1)	C(9)	C(10)	1.44(2)
C(5)	C(6)	1.57(1)			
C(8)	C(9)	1.36(1)			
Ru(1)	Cl(2)	2.430(2)			
Ru(1)	S(2)	2.300(2)			

Distances are in angstroms. Estimated standard deviations in the least significant figure are given in parentheses.

Table A.1 54. Atomic Coordinates for RuCl₂(DMSO)(L)

atom	x	y	z	atom	x	y	z
Ru(1)	0.49905(3)	0.21941(2)	0.32258(6)	C(5)	0.3540(4)	0.1718(4)	0.168(1)
Cl(1)	0.5282(1)	0.1497(1)	0.5180(3)	C(6)	0.3148(4)	0.2298(5)	0.232(1)
Cl(2)	0.4351(1)	0.2850(1)	0.4853(3)	C(7)	0.3589(5)	0.3345(5)	0.077(1)
S(1)	0.48339(9)	0.2801(1)	0.1157(2)	C(8)	0.4150(5)	0.2991(4)	0.0147(10)
S(2)	0.55666(10)	0.1508(1)	0.1771(3)	C(9)	0.4247(6)	0.2784(6)	-0.123(1)
S(3)	0.41066(10)	0.14742(9)	0.3052(2)	C(10)	0.4820(5)	0.2407(5)	-0.1447(10)
S(4)	0.2876(1)	0.2858(1)	0.0999(3)	C(11)	0.5677(6)	0.3652(5)	0.375(2)
S(5)	0.5870(1)	0.2833(1)	0.3631(3)	C(12)	0.6255(6)	0.2703(7)	0.533(1)
O(1)	0.6387(4)	0.2803(4)	0.2538(8)				
C(1)	0.5175(4)	0.2359(5)	-0.027(1)				
C(2)	0.5732(5)	0.1950(5)	0.012(1)				
C(3)	0.4936(5)	0.0975(4)	0.104(1)				
C(4)	0.4490(4)	0.0780(4)	0.222(1)				

Appendix 1.13 Crystallographic Data for $[\text{Ru}(12\text{-S-4})(\text{DMSO})(\text{H}_2\text{O})][\text{OTf}]_2$ **Table A.1 55.** Experimental Details for X-ray Crystal Structure of $[\text{Ru}(12\text{-S-4})(\text{DMSO})(\text{H}_2\text{O})][\text{OTf}]_2$ *A. Crystal Data*

Empirical Formula	$\text{C}_{12}\text{H}_{24}\text{F}_6\text{O}_8\text{RuS}_7$
Formula Weight	735.80
Crystal Colour, Habit	yellow, plate
Crystal Dimensions	0.04 x 0.18 x 0.35 mm
Crystal System	monoclinic
Lattice Type	Primitive
No. of Reflections Used for Unit Cell	5461 (3.0-76.6 °)
Determinations (2θ range)	
Lattice Parameters	$a = 11.6308(2) \text{ \AA}$ $b = 12.2220(2) \text{ \AA}$ $c = 18.0054(1) \text{ \AA}$ $\beta = 91.736(1)^\circ$ $V = 2558.32(5) \text{ \AA}^3$
Space Group	$P2_1/n$ (# 14)
Z Value	4
D_{calc}	1.910 g/cm^3
F_{000}	1480.00
$\mu(\text{MoK}\alpha)$	12.64 cm^{-1}

B. Intensity Measurements

Diffractometer	Siemens SMART CCD
Radiation	$\text{MoK}\alpha$ ($\lambda = 0.71073 \text{ \AA}$) graphite monochromated
Take-off Angle	2.8°
Detector Aperature	35 mm circle
Crystal to Detector Distance	2.964 mm
Voltage, Current	50 kV, 40 mA
Temperature	-80.0°C
Scan Type	ω
Sec/frame	10
Scan Width	-0.30°
$2\theta_{\text{max}}$	67.0°
No. of Reflections Measured	Total: 27813 Unique: 9942 ($R_{\text{int}} = 0.055$)
Corrections	Lorentz-polarization Absorption (trans. factors: 0.661 - 0.814)

C. Structure Solution and Refinement

Structure Solution	Direct Methods
Refinement	Full-matrix least-squares
Function Minimized	$\Sigma \omega (F_o - F_c)^2$
Least Squares Weights	$\omega = 1/\sigma^2(F_o^2) = [\sigma_c^2(F_o^2)]^{-1}$
p-factor	0.0000
Anomalous Dispersion	All non-hydrogen atoms
No. Observations	9942
No. Variables	403
Reflection/Parameter Ratio	24.67
Residuals (based on F^2): R; Rw	0.064; 0.073

No. Observations ($I > 3\sigma(I)$)	6560
Residuals (on F, $I > 3\sigma(I)$): R1; R1w	0.042; 0.034
Goodness of Fit Indicator	1.44
Max Shift/Error in Final Cycle	0.005
Maximum peak in Final Diff. Map	$2.04 e^-/\text{\AA}^3$
Minimum peak in Final Diff. Map	$-1.93 e^-/\text{\AA}^3$

Table A.1 56. Bond Angles ($^\circ$) for $[\text{Ru}(12\text{-S-4})(\text{DMSO})(\text{H}_2\text{O})][\text{OTf}]_2$

atom	atom	atom	angle	atom	atom	atom	angle
S(1)	Ru(1)	S(2)	84.29(2)	Ru(1)	S(2)	C(3)	99.36(9)
S(1)	Ru(1)	S(4)	87.46(2)	Ru(1)	S(3)	C(4)	103.87(8)
S(1)	Ru(1)	O(1)	94.28(5)	C(4)	S(3)	C(5)	100.6(1)
S(2)	Ru(1)	S(4)	91.98(2)	Ru(1)	S(4)	C(7)	102.56(9)
S(2)	Ru(1)	O(1)	87.62(5)	Ru(1)	S(5)	O(2)	113.97(7)
S(3)	Ru(1)	S(5)	100.72(2)	Ru(1)	S(5)	C(10)	114.18(9)
S(4)	Ru(1)	S(5)	87.18(2)	O(2)	S(5)	C(10)	106.7(1)
S(5)	Ru(1)	O(1)	93.36(5)	O(3)	S(6)	O(4)	114.4(1)
Ru(1)	S(1)	C(8)	101.23(8)	O(3)	S(6)	C(11)	103.3(1)
Ru(1)	S(2)	C(2)	98.96(9)	O(4)	S(6)	C(11)	102.7(1)
C(2)	S(2)	C(3)	106.2(1)	O(6)	S(7)	O(7)	114.5(1)
Ru(1)	S(3)	C(5)	101.31(8)	O(6)	S(7)	C(12)	102.9(1)
Ru(1)	S(4)	C(6)	102.59(9)	O(7)	S(7)	C(12)	103.3(1)
C(6)	S(4)	C(7)	106.4(1)	S(1)	C(1)	C(2)	113.5(2)
Ru(1)	S(5)	C(9)	113.77(10)	S(2)	C(3)	C(4)	106.6(2)
O(2)	S(5)	C(9)	107.8(1)	S(3)	C(4)	C(3)	112.4(2)
C(9)	S(5)	C(10)	99.3(1)	S(4)	C(6)	C(5)	105.7(2)
O(3)	S(6)	O(5)	113.3(1)	S(1)	C(8)	C(7)	113.9(2)
O(4)	S(6)	O(5)	116.8(1)	S(6)	C(11)	F(2)	111.8(2)
O(5)	S(6)	C(11)	102.2(1)	F(1)	C(11)	F(2)	107.7(3)
O(6)	S(7)	O(8)	115.5(1)	F(2)	C(11)	F(3)	107.4(3)
O(7)	S(7)	O(8)	114.4(1)	S(7)	C(12)	F(5)	110.4(2)
O(8)	S(7)	C(12)	103.9(1)	F(4)	C(12)	F(5)	107.9(3)
S(2)	C(2)	C(1)	107.7(2)	F(5)	C(12)	F(6)	107.0(3)
S(1)	Ru(1)	S(3)	116.83(2)	S(3)	C(5)	C(6)	113.6(2)
S(1)	Ru(1)	S(5)	91.10(2)	S(4)	C(7)	C(8)	105.7(2)
S(2)	Ru(1)	S(3)	83.80(2)	S(6)	C(11)	F(1)	110.8(2)
S(2)	Ru(1)	S(5)	175.35(2)	S(6)	C(11)	F(3)	111.1(2)
S(3)	Ru(1)	S(4)	87.35(2)	F(1)	C(11)	F(3)	107.9(2)
S(3)	Ru(1)	O(1)	90.83(5)	S(7)	C(12)	F(4)	112.4(2)
S(4)	Ru(1)	O(1)	178.17(5)	S(7)	C(12)	F(6)	111.2(2)
Ru(1)	S(1)	C(1)	103.60(8)	F(4)	C(12)	F(6)	107.8(3)
C(1)	S(1)	C(8)	101.5(1)				

Angles are in degrees. Estimated standard deviations in the least significant figure are given in parentheses.

Table A.1 57. Bond Lengths (\AA) for $[\text{Ru}(12\text{-S-4})(\text{DMSO})(\text{H}_2\text{O})][\text{OTf}]_2$

atom	atom	distance	atom	atom	distance
Ru(1)	S(1)	2.3852(6)	Ru(1)	S(2)	2.3708(6)
Ru(1)	S(3)	2.3907(6)	Ru(1)	S(4)	2.2903(6)
Ru(1)	S(5)	2.3011(6)	Ru(1)	O(1)	2.193(2)
S(1)	C(1)	1.864(3)	S(1)	C(8)	1.860(3)
S(2)	C(2)	1.822(3)	S(2)	C(3)	1.823(3)
S(3)	C(4)	1.872(3)	S(3)	C(5)	1.851(3)

S(4)	C(6)	1.836(3)	S(4)	C(7)	1.837(3)
S(5)	O(2)	1.494(2)	S(5)	C(9)	1.794(3)
S(5)	C(10)	1.798(3)	S(6)	O(3)	1.461(2)
S(6)	O(4)	1.445(2)	S(6)	O(5)	1.444(2)
S(6)	C(11)	1.837(3)	S(7)	O(6)	1.442(2)
S(7)	O(7)	1.463(2)	S(7)	O(8)	1.442(2)
S(7)	C(12)	1.829(3)	F(1)	C(11)	1.341(4)
F(2)	C(11)	1.339(3)	F(3)	C(11)	1.335(4)
F(4)	C(12)	1.331(4)	F(5)	C(12)	1.347(3)
F(6)	C(12)	1.344(4)	C(1)	C(2)	1.525(4)
C(3)	C(4)	1.526(4)	C(5)	C(6)	1.533(4)
C(7)	C(8)	1.528(4)			

Distances are in angstroms. Estimated standard deviations in the least significant figure are given in parentheses.

Table A.1 58. Atomic Coordinates for [Ru(12-S-4)(DMSO)(H₂O)][OTf]₂

atom	x	y	Z
Ru(1)	0.55767(2)	0.14052(2)	0.27009(1)
S(1)	0.74761(5)	0.20227(5)	0.30121(3)
S(2)	0.61800(5)	-0.02319(5)	0.33019(4)
S(3)	0.38734(5)	0.03806(5)	0.24033(3)
S(4)	0.62666(5)	0.08322(5)	0.15882(3)
S(5)	0.51429(5)	0.30424(5)	0.21269(3)
S(6)	0.16915(6)	0.16505(6)	0.37392(4)
S(7)	0.69027(5)	0.33126(6)	0.50386(3)
F(1)	0.0652(2)	0.1233(2)	0.4986(1)
F(2)	0.0796(2)	0.2961(2)	0.4738(1)
F(3)	0.2286(2)	0.2062(2)	0.5133(1)
F(4)	0.6086(2)	0.5146(2)	0.5591(1)
F(5)	0.6536(2)	0.3909(2)	0.64105(9)
F(6)	0.4987(2)	0.3739(2)	0.5724(1)
O(1)	0.4868(2)	0.1919(2)	0.37607(10)
O(2)	0.6159(1)	0.3609(1)	0.18159(10)
O(3)	0.2570(1)	0.2455(2)	0.3561(1)
O(4)	0.2113(2)	0.0542(2)	0.3809(1)
O(5)	0.0623(2)	0.1804(2)	0.3323(1)
O(6)	0.6857(2)	0.2205(2)	0.5312(1)
O(7)	0.6251(2)	0.3498(2)	0.43423(9)
O(8)	0.8023(2)	0.3819(2)	0.5072(1)
C(1)	0.7993(2)	0.1031(2)	0.3734(1)
C(2)	0.7030(2)	0.0361(2)	0.4067(2)
C(3)	0.4819(2)	-0.0648(2)	0.3691(2)
C(4)	0.3982(2)	-0.0835(2)	0.3034(2)
C(5)	0.4252(2)	-0.0251(1)	0.1509(1)
C(6)	0.5540(2)	-0.0488(2)	0.1447(2)
C(7)	0.7778(2)	0.0519(2)	0.1827(2)
C(8)	0.8271(2)	0.1555(2)	0.2189(2)
C(9)	0.4062(2)	0.2933(2)	0.1398(2)
C(10)	0.4449(2)	0.4018(2)	0.2712(2)
C(11)	0.1338(3)	0.1997(2)	0.4699(2)
C(12)	0.6087(3)	0.4074(2)	0.5721(2)

Table A.1 59. Hydrogen bonds and C-H...O/F interactions.

A	H	B	A...B	A-H	H...B	A-H...B
O(1)	H(1)	O(3)	2.765(3)	0.84(4)	1.96(4)	178(4)
O(1)	H(2)	O(7)	2.703(3)	0.85(3)	1.85(4)	173(3)
C(1)	H(3)	O(2)	3.283(3)	0.91(2)	2.53(3)	140(2)
C(2)	H(5)	O(6)	3.189(4)	0.93(3)	2.46(3)	135(2)
C(2)	H(6)	F(3)	3.378(3)	0.92(3)	2.50(3)	161(2)
C(3)	H(7)	O(1)	3.141(4)	0.91(2)	2.55(3)	124(2)
C(4)	H(10)	O(4)	3.112(4)	0.95(3)	2.49(3)	122(2)
C(5)	H(11)	O(8)	3.401(3)	0.95(3)	2.46(3)	169(2)
C(6)	H(14)	O(8)	3.357(3)	0.93(3)	2.46(3)	161(2)
C(8)	H(17)	O(5)	3.378(3)	0.94(3)	2.51(3)	154(2)
C(10)	H(23)	O(3)	3.311(3)	0.96(3)	2.40(3)	158(2)

Appendix 1.14 Crystallographic Data for Ru(OEP)(CO)(THF)

Table A.1 60. Experimental Details for X-ray Crystal Structure of Ru(OEP)(CO)(THF)*A. Crystal Data*

Empirical Formula	C ₄₁ H ₅₂ N ₄ O ₂ Ru
Formula Weight	733.96
Crystal Colour, Habit	red, irregular
Crystal Dimensions	0.30 x 0.15 x 0.08 mm
Crystal System	monoclinic
Lattice Type	Primitive
Lattice Parameters	a = 10.4420(8) Å b = 32.418(2) Å c = 10.7811(2) Å β = 99.5847(7) ° V = 3598.6(3) Å ³
Space Group	P2 ₁ /c (# 14)
Z Value	4
D _{calc}	1.355 g/cm ³
F ₀₀₀	1544.00
μ(MoKα)	4.77 cm ⁻¹

B. Intensity Measurements

Diffractometer	Rigaku/ADSC CCD
Radiation	MoKα (λ = 0.71069 Å) graphite monochromated
Detector Aperature	94 mm x 94 mm
Data Images	768 exposures of 30.0 seconds
φ oscillation Range (χ = -90)	0.0 - 189.9 °
ω oscillation Range (χ = -90)	-23.0 - 17.8 °
Detector Position	39.218(8) mm
Detector Swing Angle	-10.0 °
2θ _{max}	60.1 °
No. of Reflections Measured	Total: 33364 Unique: 9166 (R _{int} = 0.057)
Corrections	Lorentz-polarization Absorption/scaling (trans. factors: 0.8404 - 1.0000)

C. Structure Solution and Refinement

Structure Solution	Patterson Methods (DIRDIF92 PATTY)
Refinement	Full-matrix least-squares
Function Minimized	$\Sigma w(F_o ^2 - F_c ^2)^2$
Least Squares Weights	$w = 1/\sigma^2(F_o^2)$
p-factor	0.0000
Anomalous Dispersion	All non-hydrogen atoms
No. Observations	9166
No. Variables	505
Reflection/Parameter Ratio	18.15
Residuals (on F^2 , all data): R; Rw	0.096; 0.077
Goodness of Fit Indicator	1.21
No. Observations ($I > 3\sigma(I)$)	4171
Residuals (on F, $I > 3\sigma(I)$): R; Rw	0.044; 0.034
Max Shift/Error in Final Cycle	0.01
Maximum peak in Final Diff. Map	$3.07 e/\text{\AA}^3$ (1.37 Å from Ru)
Minimum peak in Final Diff. Map	$-2.21 e/\text{\AA}^3$

Table A.1 61. Bond Angles (°) for Ru(OEP)(CO)(THF)

atom	atom	atom	angle	atom	atom	atom	angle
O(2)	Ru(1)	N(1)	87.0(1)	C(16)	N(4)	C(19)	106.6(3)
O(2)	Ru(1)	N(2)	85.3(1)	N(1)	C(1)	C(2)	110.2(3)
O(2)	Ru(1)	N(3)	87.0(1)	N(1)	C(1)	C(20)	124.1(3)
O(2)	Ru(1)	N(4)	87.4(1)	C(2)	C(1)	C(20)	125.6(3)
O(2)	Ru(1)	C(37)	177.2(1)	C(1)	C(2)	C(3)	106.6(3)
N(1)	Ru(1)	N(2)	89.89(9)	C(1)	C(2)	C(21)	125.2(3)
N(1)	Ru(1)	N(3)	174.0(1)	C(3)	C(2)	C(21)	128.2(3)
N(1)	Ru(1)	N(4)	90.0(1)	C(2)	C(3)	C(4)	107.6(3)
N(1)	Ru(1)	C(37)	92.5(1)	C(2)	C(3)	C(23)	128.4(3)
N(2)	Ru(1)	N(3)	89.5(1)	C(4)	C(3)	C(23)	124.0(3)
N(2)	Ru(1)	N(4)	172.7(1)	N(1)	C(4)	C(3)	108.7(3)
N(2)	Ru(1)	C(37)	97.4(1)	N(1)	C(4)	C(5)	124.6(3)
N(3)	Ru(1)	N(4)	89.8(1)	C(3)	C(4)	C(5)	126.7(3)
N(3)	Ru(1)	C(37)	93.5(1)	C(4)	C(5)	C(6)	127.8(3)
N(4)	Ru(1)	C(37)	89.9(1)	N(2)	C(6)	C(5)	124.8(3)
Ru(1)	O(2)	C(38)	123.1(3)	N(2)	C(6)	C(7)	109.9(3)
Ru(1)	O(2)	C(41)	127.1(3)	C(5)	C(6)	C(7)	125.3(3)
C(38)	O(2)	C(41)	109.0(4)	C(6)	C(7)	C(8)	106.6(3)
Ru(1)	N(1)	C(1)	126.7(2)	C(6)	C(7)	C(25)	125.3(3)
Ru(1)	N(1)	C(4)	126.3(2)	C(8)	C(7)	C(25)	128.1(3)
C(1)	N(1)	C(4)	106.9(3)	C(7)	C(8)	C(9)	106.8(3)
Ru(1)	N(2)	C(6)	126.5(2)	C(7)	C(8)	C(27)	127.7(3)
Ru(1)	N(2)	C(9)	126.3(2)	C(9)	C(8)	C(27)	125.4(3)
C(6)	N(2)	C(9)	107.2(3)	N(2)	C(9)	C(8)	109.5(3)
Ru(1)	N(3)	C(11)	126.6(2)	N(2)	C(9)	C(10)	124.8(3)
Ru(1)	N(3)	C(14)	125.6(2)	C(8)	C(9)	C(10)	125.7(3)
C(11)	N(3)	C(14)	107.7(3)	C(9)	C(10)	C(11)	127.7(3)
Ru(1)	N(4)	C(16)	126.6(2)	N(3)	C(11)	C(10)	124.6(3)
Ru(1)	N(4)	C(19)	126.7(2)	N(3)	C(11)	C(12a)	106.3(5)
N(3)	C(11)	C(12)	110.4(4)	C(13)	C(13a)	C(14)	81(1)
C(10)	C(11)	C(12a)	124.3(5)	C(13)	C(13a)	C(31)	60(1)
C(10)	C(11)	C(12)	124.5(4)	C(13)	C(13a)	C(31a)	97(1)
C(12a)	C(11)	C(12)	30.4(4)	C(14)	C(13a)	C(31)	113.6(8)

C(11)	C(12a)	C(12)	76(1)	C(14)	C(13a)	C(31a)	127.1(9)
C(11)	C(12a)	C(13)	99.2(7)	C(31)	C(13a)	C(31a)	37.1(6)
C(11)	C(12a)	C(13a)	106.6(9)	N(3)	C(14)	C(13)	108.2(4)
C(11)	C(12a)	C(29a)	124.6(9)	N(3)	C(14)	C(13a)	107.7(5)
C(11)	C(12a)	C(29)	109.2(8)	N(3)	C(14)	C(15)	125.0(3)
C(12)	C(12a)	C(13)	63(1)	C(13)	C(14)	C(13a)	30.5(4)
C(12)	C(12a)	C(13a)	95(2)	C(13)	C(14)	C(15)	126.1(4)
C(12)	C(12a)	C(29a)	90(1)	C(13a)	C(14)	C(15)	123.1(6)
C(12)	C(12a)	C(29)	56(1)	C(14)	C(15)	C(16)	127.5(3)
C(13)	C(12a)	C(13a)	31.1(5)	N(4)	C(16)	C(15)	125.2(3)
C(13)	C(12a)	C(29a)	122.1(9)	N(4)	C(16)	C(17)	110.4(3)
C(13)	C(12a)	C(29)	101.2(8)	C(15)	C(16)	C(17)	124.4(3)
C(13a)	C(12a)	C(29a)	128(1)	C(16)	C(17)	C(18)	106.6(3)
C(13a)	C(12a)	C(29)	124(1)	C(16)	C(17)	C(33)	125.1(3)
C(29a)	C(12a)	C(29)	34.1(6)	C(18)	C(17)	C(33)	128.2(3)
C(11)	C(12)	C(12a)	73(1)	C(17)	C(18)	C(19)	106.9(3)
C(11)	C(12)	C(13)	105.7(6)	C(17)	C(18)	C(35a)	127.4(5)
C(11)	C(12)	C(13a)	93.6(6)	C(17)	C(18)	C(35)	125.2(5)
C(11)	C(12)	C(29a)	111.8(6)	C(19)	C(18)	C(35a)	120.2(5)
C(11)	C(12)	C(29)	125.8(7)	C(19)	C(18)	C(35)	126.9(5)
C(12a)	C(12)	C(13)	86(1)	C(35a)	C(18)	C(35)	30.1(5)
C(12a)	C(12)	C(13a)	57(1)	N(4)	C(19)	C(18)	109.4(3)
C(12a)	C(12)	C(29a)	63(1)	N(4)	C(19)	C(20)	124.1(3)
C(12a)	C(12)	C(29)	98(1)	C(18)	C(19)	C(20)	126.4(3)
C(13)	C(12)	C(13a)	29.0(4)	C(1)	C(20)	C(19)	128.0(3)
C(13)	C(12)	C(29a)	119.7(7)	C(2)	C(21)	C(22)	112.3(4)
C(13)	C(12)	C(29)	127.3(8)	C(3)	C(23)	C(24)	115.1(4)
C(13a)	C(12)	C(29a)	102.5(7)	C(7)	C(25)	C(26)	112.5(3)
C(13a)	C(12)	C(29)	126.5(8)	C(8)	C(27)	C(28)	113.4(3)
C(29a)	C(12)	C(29)	34.5(5)	C(12a)	C(29a)	C(12)	26.7(5)
C(12a)	C(13)	C(12)	30.9(5)	C(12a)	C(29a)	C(29)	84(1)
C(12a)	C(13)	C(13a)	63(1)	C(12a)	C(29a)	C(30)	158(2)
C(12a)	C(13)	C(14)	95.3(6)	C(12a)	C(29a)	C(30a)	104(1)
C(12a)	C(13)	C(31)	124.4(7)	C(12)	C(29a)	C(29)	57.0(9)
C(12)	C(13)	C(13a)	94(1)	C(12)	C(29a)	C(30)	169(2)
C(12)	C(13)	C(14)	106.8(6)	C(12)	C(29a)	C(30a)	77.8(9)
C(12)	C(13)	C(31)	129.2(8)	C(29)	C(29a)	C(30)	116(2)
C(13a)	C(13)	C(14)	68(1)	C(29)	C(29a)	C(30a)	22.3(9)
C(13a)	C(13)	C(31)	92(1)	C(30)	C(29a)	C(30a)	97(1)
C(14)	C(13)	C(31)	122.2(7)	C(12a)	C(29)	C(12)	26.3(4)
C(12a)	C(13a)	C(12)	28.8(5)	C(12a)	C(29)	C(29a)	62(1)
C(12a)	C(13a)	C(13)	86(1)	C(12a)	C(29)	C(30)	90.3(7)
C(12a)	C(13a)	C(14)	107.3(9)	C(12a)	C(29)	C(30a)	160(2)
C(12a)	C(13a)	C(31)	119.6(9)	C(12)	C(29)	C(29a)	88(1)
C(12a)	C(13a)	C(31a)	125(1)	C(12)	C(29)	C(30)	116.6(7)
C(12)	C(13a)	C(13)	57(1)	C(12)	C(29)	C(30a)	142(2)
C(12)	C(13a)	C(14)	98.8(7)	C(29a)	C(29)	C(30)	28.6(9)
C(12)	C(13a)	C(31)	101.1(8)	C(29a)	C(29)	C(30a)	123(3)
C(12)	C(13a)	C(31a)	124.5(9)	C(30)	C(29)	C(30a)	98(2)
C(29a)	C(30)	C(29)	35(1)	C(31)	C(32a)	C(32)	69(2)
C(29a)	C(30)	C(30a)	55(1)	C(31a)	C(32a)	C(32)	26.6(6)
C(29)	C(30)	C(30a)	21.9(4)	C(17)	C(33)	C(34)	112.3(3)
C(29a)	C(30a)	C(29)	34(2)	C(18)	C(35a)	C(35)	61(1)

C(29a)	C(30a)	C(30)	27.5(5)	C(18)	C(35a)	C(36)	160(2)
C(29)	C(30a)	C(30)	60(2)	C(18)	C(35a)	C(36a)	93(1)
C(13)	C(31)	C(13a)	27.6(4)	C(35)	C(35a)	C(36)	137(3)
C(13)	C(31)	C(31a)	93(1)	C(35)	C(35a)	C(36a)	35(1)
C(13)	C(31)	C(32)	117.2(9)	C(36)	C(35a)	C(36a)	107(2)
C(13)	C(31)	C(32a)	153(2)	C(18)	C(35)	C(35a)	89(1)
C(13a)	C(31)	C(31a)	66(1)	C(18)	C(35)	C(36)	109.6(7)
C(13a)	C(31)	C(32)	89.7(8)	C(18)	C(35)	C(36a)	147(1)
C(13a)	C(31)	C(32a)	168(2)	C(35a)	C(35)	C(36)	21(1)
C(31a)	C(31)	C(32)	25(1)	C(35a)	C(35)	C(36a)	113(2)
C(31a)	C(31)	C(32a)	111(3)	C(36)	C(35)	C(36a)	96(1)
C(32)	C(31)	C(32a)	86(2)	C(35a)	C(36)	C(35)	22(1)
C(13a)	C(31a)	C(31)	77(1)	C(35a)	C(36a)	C(35)	32(1)
C(13a)	C(31a)	C(32)	157(2)	Ru(1)	C(37)	O(1)	176.6(3)
C(13a)	C(31a)	C(32a)	103(1)	O(2)	C(38)	C(39)	108.7(4)
C(31)	C(31a)	C(32)	119(3)	C(38)	C(39)	C(40)	104.6(4)
C(31)	C(31a)	C(32a)	26.9(9)	C(39)	C(40)	C(41)	103.7(4)
C(32)	C(31a)	C(32a)	92(2)	O(2)	C(41)	C(40)	112.0(5)
C(31)	C(32)	C(31a)	37(2)				
C(31)	C(32)	C(32a)	25.3(4)				
C(31a)	C(32)	C(32a)	62(2)				
C(31)	C(32a)	C(31a)	42(2)				

Angles are in degrees. Estimated standard deviations in the least significant figure are given in parentheses.

Table A.1 62. Bond Lengths (Å) for Ru(OEP)(CO)(THF)

atom	atom	distance	atom	atom	distance
Ru(1)	O(2)	2.241(3)	C(3)	C(23)	1.524(5)
Ru(1)	N(1)	2.052(2)	C(4)	C(5)	1.387(4)
Ru(1)	N(2)	2.059(2)	C(5)	C(6)	1.392(4)
Ru(1)	N(3)	2.056(2)	C(6)	C(7)	1.454(4)
Ru(1)	N(4)	2.054(3)	C(7)	C(8)	1.362(4)
Ru(1)	C(37)	1.805(4)	C(7)	C(25)	1.512(4)
O(1)	C(37)	1.144(4)	C(8)	C(9)	1.452(4)
O(2)	C(38)	1.413(5)	C(8)	C(27)	1.510(4)
O(2)	C(41)	1.306(6)	C(9)	C(10)	1.388(4)
N(1)	C(1)	1.364(4)	C(10)	C(11)	1.382(5)
N(1)	C(4)	1.374(4)	C(11)	C(12a)	1.49(1)
N(2)	C(6)	1.360(3)	C(11)	C(12)	1.507(9)
N(2)	C(9)	1.371(3)	C(12a)	C(12)	0.78(1)
N(3)	C(11)	1.370(4)	C(12a)	C(13)	1.52(1)
N(3)	C(14)	1.376(4)	C(12a)	C(13a)	1.36(2)
N(4)	C(16)	1.354(4)	C(12a)	C(29a)	1.56(2)
N(4)	C(19)	1.361(4)	C(12a)	C(29)	1.75(1)
C(1)	C(2)	1.443(4)	C(12)	C(13)	1.37(1)
C(1)	C(20)	1.393(5)	C(12)	C(13a)	1.62(1)
C(2)	C(3)	1.348(5)	C(12)	C(29a)	1.75(2)
C(2)	C(21)	1.493(5)	C(12)	C(29)	1.46(1)
C(3)	C(4)	1.455(4)	C(13)	C(13a)	0.79(1)
C(13)	C(14)	1.535(8)	C(29a)	C(30a)	1.47(2)
C(13)	C(31)	1.48(1)	C(29)	C(30)	1.54(1)
C(13a)	C(14)	1.44(1)	C(29)	C(30a)	0.67(1)
C(13a)	C(31)	1.70(1)	C(30)	C(30a)	1.76(2)
C(13a)	C(31a)	1.59(2)	C(31)	C(31a)	1.05(2)

C(14)	C(15)	1.391(5)	C(31)	C(32)	1.56(2)
C(15)	C(16)	1.376(4)	C(31)	C(32a)	0.71(1)
C(16)	C(17)	1.441(4)	C(31a)	C(32)	0.75(1)
C(17)	C(18)	1.342(4)	C(31a)	C(32a)	1.47(2)
C(17)	C(33)	1.510(4)	C(32)	C(32a)	1.67(2)
C(18)	C(19)	1.451(5)	C(33)	C(34)	1.526(5)
C(18)	C(35a)	1.70(2)	C(35a)	C(35)	0.85(1)
C(18)	C(35)	1.483(9)	C(35a)	C(36)	0.79(1)
C(19)	C(20)	1.405(5)	C(35a)	C(36a)	1.49(2)
C(21)	C(22)	1.504(7)	C(35)	C(36)	1.53(1)
C(23)	C(24)	1.494(6)	C(35)	C(36a)	0.93(1)
C(25)	C(26)	1.519(5)	C(38)	C(39)	1.504(6)
C(27)	C(28)	1.510(5)	C(39)	C(40)	1.466(7)
C(29a)	C(29)	0.99(1)	C(40)	C(41)	1.498(7)
C(29a)	C(30)	0.82(1)			

Distances are in angstroms. Estimated standard deviations in the least significant figure are given in parentheses.

Table A.1 63. Atomic Coordinates for Ru(OEP)(CO)(THF)

atom	x	y	z	atom	x	y	z
Ru(1)	0.56609(3)	0.373289(8)	0.26066(3)	C(33)	0.1207(3)	0.38011(12)	0.4961(4)
O(1)	0.3995(2)	0.37021(8)	0.0117(2)	C(34)	0.1720(4)	0.3655(2)	0.6297(4)
O(2)	0.6812(2)	0.37786(9)	0.4552(2)	C(35a)	0.1566(13)	0.4763(5)	0.3869(13)
N(1)	0.6195(3)	0.43320(7)	0.2352(3)	C(35)	0.2017(9)	0.4719(3)	0.4592(8)
N(2)	0.7369(2)	0.35312(7)	0.2095(3)	C(36)	0.0976(8)	0.4906(3)	0.3582(10)
N(3)	0.5239(3)	0.31366(8)	0.3047(3)	C(36a)	0.2160(11)	0.4953(4)	0.5085(11)
N(4)	0.4086(2)	0.39373(8)	0.3348(3)	C(37)	0.4671(3)	0.37092(10)	0.1067(4)
C(1)	0.5511(4)	0.46782(9)	0.2544(4)	C(38)	0.7628(5)	0.3459(2)	0.5117(5)
C(2)	0.6162(4)	0.50401(10)	0.2180(4)	C(39)	0.8182(4)	0.3585(2)	0.6441(5)
C(3)	0.7260(4)	0.49074(10)	0.1805(4)	C(40)	0.7680(8)	0.4003(2)	0.6567(5)
C(4)	0.7287(4)	0.44597(10)	0.1906(4)	C(41)	0.6694(8)	0.40574(15)	0.5400(6)
C(5)	0.8258(3)	0.41992(9)	0.1636(3)	C(25)	1.0600(3)	0.36703(10)	0.1057(3)
C(6)	0.8309(3)	0.37710(10)	0.1731(3)	C(26)	1.0404(3)	0.37301(12)	-0.0360(4)
C(7)	0.9389(3)	0.35150(9)	0.1502(3)	C(27)	0.9858(3)	0.27338(10)	0.1633(4)
C(8)	0.9058(3)	0.31178(9)	0.1714(3)	C(28)	0.9548(4)	0.25166(10)	0.0381(4)
C(9)	0.7782(3)	0.31302(9)	0.2081(3)	C(29a)	0.6058(12)	0.2013(4)	0.3739(13)
C(10)	0.7092(3)	0.27911(10)	0.2399(4)	C(29)	0.5561(10)	0.1982(2)	0.2878(11)
C(11)	0.5918(4)	0.27897(10)	0.2831(4)	C(30)	0.6565(7)	0.1826(2)	0.3987(8)
C(12a)	0.5495(12)	0.2460(3)	0.3630(11)	C(30a)	0.5370(13)	0.1801(3)	0.2624(15)
C(12)	0.5121(8)	0.2409(3)	0.2954(7)	C(31)	0.3079(7)	0.2304(3)	0.3958(12)
C(13)	0.4039(7)	0.2543(2)	0.3395(7)	C(31a)	0.3569(14)	0.2351(4)	0.4884(15)
C(13a)	0.4427(11)	0.2606(3)	0.4060(10)	C(32)	0.3215(10)	0.2309(3)	0.5418(10)
C(14)	0.4167(4)	0.30131(11)	0.3540(4)	C(32a)	0.2451(12)	0.2216(4)	0.3958(15)
C(15)	0.3253(3)	0.32777(11)	0.3911(4)				
C(16)	0.3225(3)	0.37014(11)	0.3838(3)				
C(17)	0.2277(3)	0.39571(11)	0.4298(3)				
C(18)	0.2585(4)	0.43493(11)	0.4078(4)				
C(19)	0.3723(4)	0.43364(11)	0.3469(4)				
C(20)	0.4375(4)	0.46771(11)	0.3063(5)				
C(21)	0.5673(5)	0.54719(11)	0.2215(6)				
C(22)	0.4545(5)	0.55555(12)	0.1184(6)				
C(23)	0.8313(4)	0.51621(11)	0.1342(5)				
C(24)	0.8188(4)	0.51964(13)	-0.0054(5)				

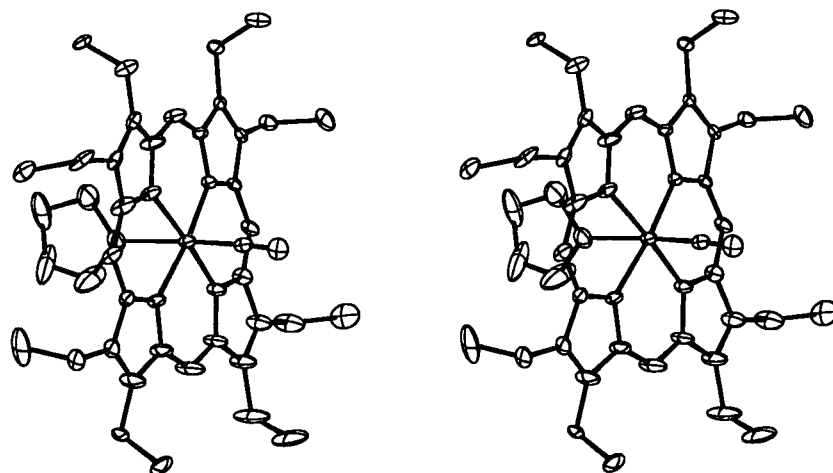


Figure A.1.7. Stereoview of Ru(OEP)(CO)(THF).

Appendix 1.15 Crystallographic Data for Ru(TPhP)(CO)(py).

Table A.1 64. Experimental Details for X-ray Crystal Structure of Ru(TPhP)(CO)(py)*A. Crystal Data*

Empirical Formula	C _{60.50} H ₄₅ N ₅ ORu
Formula Weight	959.09
Crystal Colour, Habit	red, plate
Crystal Dimensions	0.50 x 0.45 x 0.12 mm
Crystal System	triclinic
Lattice Parameters	a = 10.6294(3) Å b = 11.6314(3) Å c = 19.6878(5) Å α = 96.460(1) ° β = 99.5847(7) ° γ = 93.815(1) ° V = 2409.81(11) Å ³
Space Group	P $\bar{1}$
Z Value	2
D _{calc}	1.322 Mg/m ³
F ₀₀₀	990
absorption coefficient	0.373 mm ⁻¹

B. Data Collection

Diffractometer	Siemens SMART Platform CCD
Wavelength	0.71073 Å
Temperature	173(2) K
θ range for data collection	1.77 to 25.01 °
Index ranges	-10 ≤ h ≤ 12, -11 ≤ k ≤ 13, -21 ≤ l ≤ 23
Reflections Collected	11799
Independent Reflections	7993 (R _{int} = 0.0223)

C. Solution and Refinement

System used	SHELXTL-V5.0
Solution	Direct Methods
Refinement method	Full-matrix least-squares on F ²
Weighting Scheme	ω = 1/σ ² (F _o ²) + (AP) ² (BP), where P = (Fo ² + 2Fc ²)/3, A = 0.0291, and B = 1.9388
Absorption correction	SADABS (Sheldrick, 1996)
Max. and min. transmission	0.96 and 0.83
Data/restraints/parameters	7993/13/646
Final R indices [I > 2σ(I)]	R1 = 0.0369, wR2 = 0.0814
R indices (all data)	R1 = 0.0478, wR2 = 0.0868
Goodness of Fit on F ²	1.017
Largest diff. peak and hole	0.345 and -0.391 eÅ ³

Table A.1 65. Bond Angles (°) for Ru(TPhP)(CO)(py)

atoms	angle		atoms	angle
C(45)-Ru(1)-N(4)	91.53(10)		C(11)-C(10)-C(27)	118.0(2)
C(45)-Ru(1)-N(1)	92.91(10)		N(3)-C(11)-C(10)	125.9(2)
N(4)-Ru(1)-N(1)	89.81(8)		N(3)-C(11)-C(12)	108.8(2)
C(45)-Ru(1)-N(3)	90.06(10)		C(10)-C(11)-C(12)	125.3(2)
N(4)-Ru(1)-N(3)	90.14(8)		C(13)-C(12)-C(11)	107.2(2)

N(1)-Ru(1)-N(3)	177.03(8)
C(45)-Ru(1)-N(2)	93.37(10)
N(4)-Ru(1)-N(2)	175.09(8)
N(1)-Ru(1)-N(2)	89.80(8)
N(3)-Ru(1)-N(2)	90.00(8)
C(45)-Ru(1)-N(5)	178.27(10)
N(4)-Ru(1)-N(5)	87.91(8)
N(1)-Ru(1)-N(5)	88.73(8)
N(3)-Ru(1)-N(5)	88.30(8)
N(2)-Ru(1)-N(5)	87.19(8)
C(1)-N(1)-C(4)	107.3(2)
C(1)-N(1)-Ru(1)	126.4(2)
C(4)-N(1)-Ru(1)	126.3(2)
N(1)-C(1)-C(20)	126.0(2)
N(1)-C(1)-C(2)	108.9(2)
C(20)-C(1)-C(2)	125.2(2)
C(9)-N(2)-C(6)	107.3(2)
C(9)-N(2)-Ru(1)	126.1(2)
C(6)-N(2)-Ru(1)	126.6(2)
C(3)-C(2)-C(1)	107.7(2)
C(14)-N(3)-C(11)	107.5(2)
C(14)-N(3)-Ru(1)	126.2(2)
C(11)-N(3)-Ru(1)	126.2(2)
C(2)-C(3)-C(4)	107.3(3)
C(16)-N(4)-C(19)	107.2(2)
C(16)-N(4)-Ru(1)	126.2(2)
C(19)-N(4)-Ru(1)	126.6(2)
N(1)-C(4)-C(5)	125.7(2)
N(1)-C(4)-C(3)	108.9(2)
C(5)-C(4)-C(3)	125.3(3)
C(46)-N(5)-C(50)	117.0(3)
C(46)-N(5)-Ru(1)	121.9(2)
C(50)-N(5)-Ru(1)	121.1(2)
C(6)-C(5)-C(4)	125.9(3)
C(6)-C(5)-C(21)	117.2(2)
C(4)-C(5)-C(21)	116.9(2)
N(2)-C(6)-C(5)	125.5(2)
N(2)-C(6)-C(7)	108.9(2)
C(5)-C(6)-C(7)	125.6(3)
C(8)-C(7)-C(6)	107.4(2)
C(7)-C(8)-C(9)	107.3(2)
N(2)-C(9)-C(10)	126.4(2)
N(2)-C(9)-C(8)	109.0(2)
C(10)-C(9)-C(8)	124.6(2)
C(9)-C(10)-C(11)	125.3(2)
C(42)-C(41)-C(40)	120.7(4)
C(43)-C(42)-C(41)	118.7(3)
C(42)-C(43)-C(44)	120.8(3)
C(39)-C(44)-C(43)	121.7(3)
O(1)-C(45)-Ru(1)	177.8(2)
N(5)-C(46)-C(47)	122.9(3)
C(48)-C(47)-C(46)	118.5(3)
C(49)-C(48)-C(47)	120.1(3)
C(48)-C(49)-C(50)	118.7(3)

C(12)-C(13)-C(14)	107.9(2)
N(3)-C(14)-C(15)	125.5(2)
N(3)-C(14)-C(13)	108.6(2)
C(15)-C(14)-C(13)	125.9(3)
C(16)-C(15)-C(14)	126.0(2)
C(16)-C(15)-C(33)	116.4(2)
C(14)-C(15)-C(33)	117.6(2)
N(4)-C(16)-C(15)	125.8(2)
N(4)-C(16)-C(17)	108.9(2)
C(15)-C(16)-C(17)	125.3(2)
C(18)-C(17)-C(16)	107.5(2)
C(17)-C(18)-C(19)	107.6(2)
N(4)-C(19)-C(20)	125.7(2)
N(4)-C(19)-C(18)	108.8(2)
C(20)-C(19)-C(18)	125.4(2)
C(19)-C(20)-C(1)	125.5(2)
C(19)-C(20)-C(39)	117.6(2)
C(1)-C(20)-C(39)	116.9(2)
C(22)-C(21)-C(26)	118.7(3)
C(22)-C(21)-C(5)	120.4(3)
C(26)-C(21)-C(5)	120.9(3)
C(21)-C(22)-C(23)	120.2(4)
C(24)-C(23)-C(22)	120.0(4)
C(25)-C(24)-C(23)	119.9(4)
C(24)-C(25)-C(26)	120.8(4)
C(21)-C(26)-C(25)	120.4(4)
C(28)-C(27)-C(32)	117.7(3)
C(28)-C(27)-C(10)	121.6(2)
C(32)-C(27)-C(10)	120.7(2)
C(27)-C(28)-C(29)	121.6(3)
C(30)-C(29)-C(28)	119.7(3)
C(31)-C(30)-C(29)	119.3(3)
C(30)-C(31)-C(32)	120.9(3)
C(31)-C(32)-C(27)	120.8(3)
C(38)-C(33)-C(34)	117.7(3)
C(38)-C(33)-C(15)	121.5(3)
C(34)-C(33)-C(15)	120.8(3)
C(33)-C(34)-C(35)	121.5(3)
C(36)-C(35)-C(34)	120.1(3)
C(37)-C(36)-C(35)	119.1(3)
C(36)-C(37)-C(38)	120.9(4)
C(33)-C(38)-C(37)	120.8(3)
C(40)-C(39)-C(44)	117.1(3)
C(40)-C(39)-C(20)	120.7(3)
C(44)-C(39)-C(20)	122.2(3)
C(57)-C(52)-C(51)	119.8(4)
C(53)-C(52)-C(51)	121.8(3)
C(52)-C(53)-C(54)	120.8(3)
C(55)-C(54)-C(53)	120.1(3)
C(54)-C(55)-C(56)	119.3(3)
C(57)-C(56)-C(55)	120.5(3)
C(52)-C(57)-C(56)	121.0(4)
C(60)-C(59)-C(58)	122.3(4)
C(59)-C(60)-C(61)	121.8(4)

N(5)-C(50)-C(49)	122.8(3)	C(39)-C(40)-C(41)	121.0(3)
C(57)-C(52)-C(53)	118.3(3)		

Table A.1 66. Bond Lengths (Å) for Ru(TPhP)(CO)(py)

atom	distance	atom	distance
Ru(1)-C(45)	1.837(3)	C(11)-C(12)	1.449(4)
Ru(1)-N(4)	2.057(2)	C(12)-C(13)	1.351(4)
Ru(1)-N(1)	2.057(2)	C(13)-C(14)	1.447(4)
Ru(1)-N(3)	2.062(2)	C(14)-C(15)	1.404(4)
Ru(1)-N(2)	2.062(2)	C(15)-C(16)	1.401(4)
Ru(1)-N(5)	2.207(2)	C(15)-C(33)	1.504(4)
N(1)-C(1)	1.377(3)	C(16)-C(17)	1.448(4)
N(1)-C(4)	1.379(3)	C(17)-C(18)	1.346(4)
C(1)-C(20)	1.403(4)	C(18)-C(19)	1.446(4)
C(1)-C(2)	1.444(4)	C(19)-C(20)	1.401(4)
O(1)-C(45)	1.151(3)	C(20)-C(39)	1.497(4)
N(2)-C(9)	1.374(3)	C(21)-C(22)	1.382(4)
N(2)-C(6)	1.377(3)	C(21)-C(26)	1.386(4)
C(2)-C(3)	1.350(4)	C(22)-C(23)	1.403(5)
N(3)-C(14)	1.377(3)	C(23)-C(24)	1.371(6)
N(3)-C(11)	1.381(3)	C(24)-C(25)	1.362(7)
C(3)-C(4)	1.447(4)	C(25)-C(26)	1.387(5)
N(4)-C(16)	1.378(3)	C(27)-C(28)	1.380(4)
N(4)-C(19)	1.378(3)	C(27)-C(32)	1.388(4)
C(4)-C(5)	1.402(4)	C(28)-C(29)	1.390(4)
N(5)-C(46)	1.343(4)	C(29)-C(30)	1.377(4)
N(5)-C(50)	1.349(4)	C(30)-C(31)	1.369(4)
C(5)-C(6)	1.403(4)	C(31)-C(32)	1.381(4)
C(5)-C(21)	1.505(4)	C(33)-C(38)	1.360(4)
C(6)-C(7)	1.445(4)	C(33)-C(34)	1.367(4)
C(7)-C(8)	1.352(4)	C(34)-C(35)	1.389(5)
C(8)-C(9)	1.447(4)	C(35)-C(36)	1.358(5)
C(9)-C(10)	1.404(4)	C(36)-C(37)	1.347(5)
C(10)-C(11)	1.406(4)	C(37)-C(38)	1.397(5)
C(10)-C(27)	1.505(4)	C(39)-C(40)	1.370(4)
C(39)-C(44)	1.374(4)	C(56)-C(57)	1.379(5)
C(40)-C(41)	1.395(5)	C(58)-C(59)	1.576(8)
C(41)-C(42)	1.367(5)	C(59)-C(60)	1.366(6)
C(42)-C(43)	1.350(5)	C(60)-C(61)	1.396(6)
C(43)-C(44)	1.386(5)		
C(46)-C(47)	1.379(4)		
C(47)-C(48)	1.365(5)		
C(48)-C(49)	1.360(5)		
C(49)-C(50)	1.377(4)		
C(51)-C(52)	1.515(5)		
C(52)-C(57)	1.382(5)		
C(52)-C(53)	1.379(5)		
C(53)-C(54)	1.395(5)		
C(54)-C(55)	1.374(5)		
C(55)-C(56)	1.378(5)		

Table A.1 67. Atomic Coordinates for Ru(TPhP)(CO)(py)

atom	x	y	z	atom	x	y	z
Ru(1)	1156(1)	1742(1)	7607(1)	C(25)	-4819(4)	3675(5)	6583(2)
N(1)	340(2)	2210(2)	6721(1)	C(26)	-3763(3)	3110(4)	6758(2)
C(1)	779(3)	2010(2)	6074(1)	C(27)	223(2)	2353(2)	10067(1)
O(1)	-244(2)	-595(2)	7448(1)	C(28)	570(3)	3383(3)	10472(2)
N(2)	-219(2)	2529(2)	8159(1)	C(29)	272(4)	3555(3)	11154(2)
C(2)	-88(3)	2440(2)	5593(1)	C(30)	-384(3)	2683(3)	11438(2)
N(3)	2025(2)	1355(2)	8503(1)	C(31)	-752(3)	1665(3)	11039(2)
C(3)	-1032(3)	2891(2)	5948(1)	C(32)	-460(3)	1496(3)	10360(1)
N(4)	2611(2)	1093(2)	7064(1)	C(33)	5066(3)	-115(2)	8188(1)
C(4)	-772(3)	2746(2)	6661(1)	C(34)	6193(3)	532(3)	8301(2)
N(5)	2256(2)	3437(2)	7755(1)	C(35)	7309(3)	26(4)	8442(2)
C(5)	-1503(2)	3139(2)	7203(1)	C(36)	7300(3)	-1138(3)	8463(2)
C(6)	-1238(2)	3040(2)	7898(1)	C(37)	6196(4)	-1787(3)	8352(2)
C(7)	-1993(3)	3452(2)	8454(1)	C(38)	5073(3)	-1279(3)	8214(2)
C(8)	-1426(3)	3188(2)	9040(1)	C(39)	2193(3)	1362(2)	5166(1)
C(9)	-308(3)	2605(2)	8857(1)	C(40)	2831(4)	2252(3)	4896(2)
C(10)	524(2)	2174(2)	9324(1)	C(41)	3073(4)	2166(4)	4203(2)
C(11)	1602(2)	1589(2)	9154(1)	C(42)	2665(3)	1194(3)	3773(2)
C(12)	2466(3)	1150(2)	9636(1)	C(43)	2047(4)	308(3)	4035(2)
C(13)	3384(3)	667(2)	9274(1)	C(44)	1810(4)	388(3)	4725(2)
C(14)	3118(2)	792(2)	8560(1)	C(45)	275(3)	314(2)	7503(1)
C(15)	3872(2)	441(2)	8018(1)	C(46)	1847(3)	4370(2)	7492(2)
C(16)	3630(2)	582(2)	7327(1)	C(47)	2486(3)	5451(3)	7607(2)
C(17)	4418(3)	217(2)	6774(1)	C(48)	3582(4)	5577(3)	8006(2)
C(18)	3872(3)	505(2)	6193(1)	C(49)	4039(3)	4643(3)	8265(2)
C(19)	2730(3)	1053(2)	6368(1)	C(50)	3362(3)	3585(3)	8129(2)
C(20)	1889(3)	1479(2)	5905(1)	C(51)	3477(4)	5765(4)	5147(2)
C(21)	-2663(3)	3741(3)	7023(1)	C(52)	2449(3)	6210(3)	5593(2)
C(22)	-2643(4)	4938(3)	7111(2)	C(53)	1357(3)	5539(3)	5669(2)
C(23)	-3717(5)	5496(4)	6928(2)	C(54)	404(4)	5981(3)	6063(2)
C(24)	-4793(4)	4854(5)	6664(2)	C(55)	543(4)	7100(3)	6380(2)
C(56)	1638(4)	7771(3)	6311(2)	C(59)	5456(4)	3896(3)	10059(2)
C(57)	2580(4)	7329(3)	5923(2)	C(60)	4192(4)	4049(3)	10029(2)
C(59')	5456(4)	3896(3)	10059(2)	C(61)	3735(4)	5134(4)	9975(3)
C(58)	5990(7)	2703(7)	10189(5)				

Appendix 2. Experimental for the Kinetic Studies of $[\text{RuCl}(\text{BPSP})]_2(\mu\text{-Cl})_3$.

The chemical behaviour of $[\text{RuCl}(\text{BPSP})]_2(\mu\text{-Cl})_3$ in aqueous solution was monitored spectrophotometrically in a thermostated Hewlett-Packard HP 8452A Diode Array instrument using quartz cells of path length 1.0 cm fitted with a plastic cap. The cell was thermostated at temperatures in the range of 15-35 °C and $[\text{RuCl}(\text{BPSP})]_2(\mu\text{-Cl})_3$ was added to H_2O (10 mL) or $\text{H}_2\text{O}/\text{CH}_3\text{CN}$ (10 mL). The sample was shaken to ensure complete mixing prior to monitoring absorbance changes at a fixed wavelength. The concentration of $[\text{RuCl}(\text{BPSP})]_2(\mu\text{-Cl})_3$ ranged from $(0.15\text{-}1.5) \times 10^{-3}$ M and that of H_2O from (0-55.6) M; thus pseudo-first-order conditions were maintained. Log (absorbance difference) vs. time plots gave linear plots for at least 2.5 to 3 half-lives, from which the pseudo-first-order rate constants, k_{obs} , were determined.

Appendix 3. Thermal Gravimetric Analyses Plots

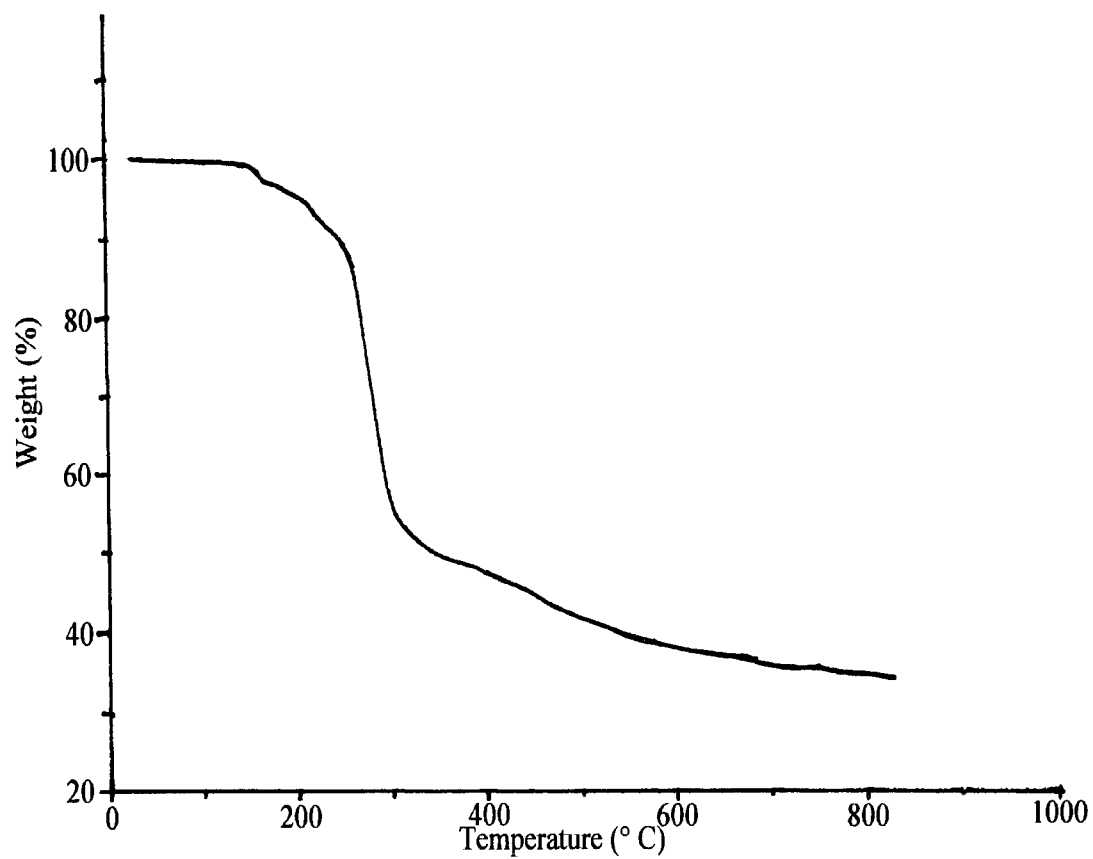


Figure A.3.1. TGA of $[\text{RuCl}(\text{BESE})(\text{H}_2\text{O})]_2(\mu\text{-Cl})_2 \cdot \text{H}_2\text{O}$.

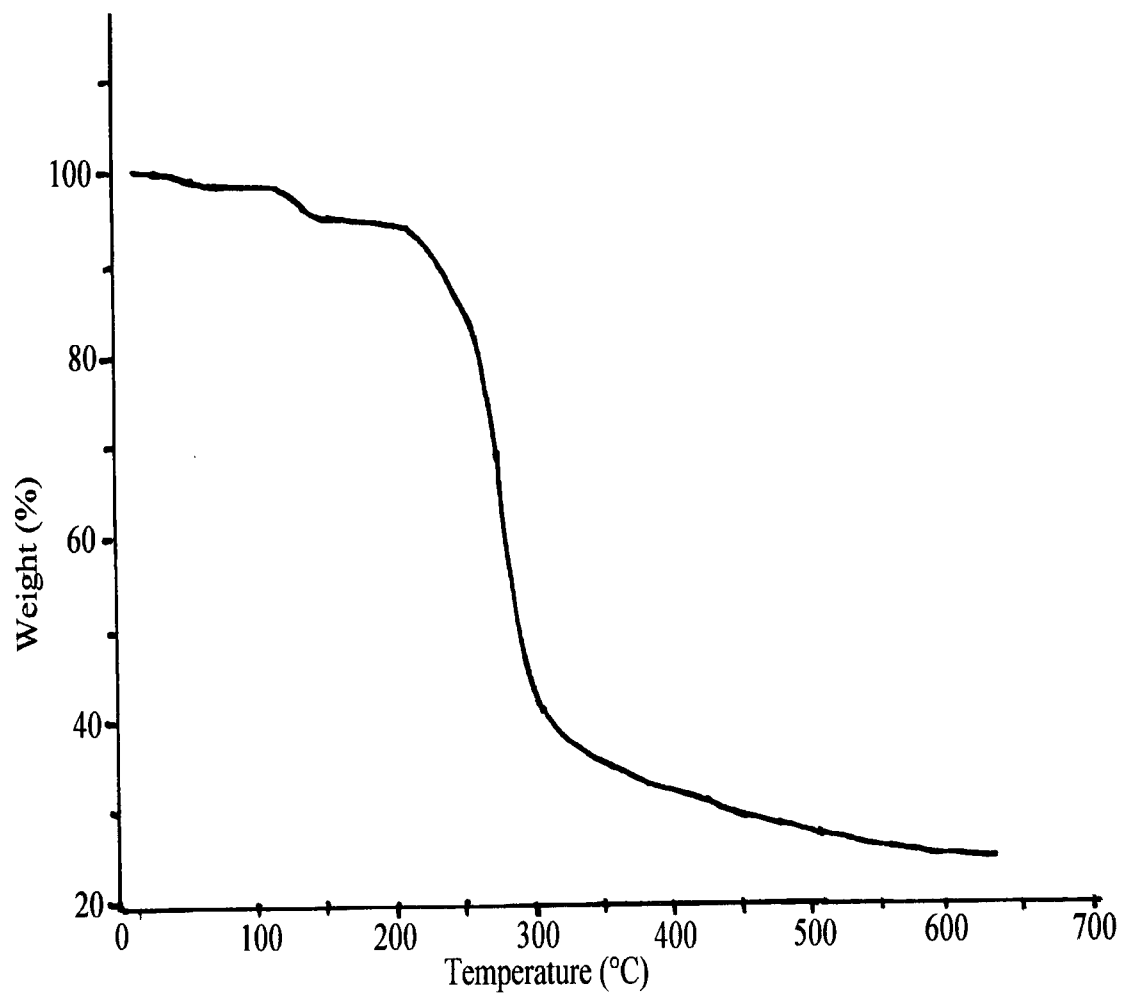


Figure A.3.2. TGA of $[\text{RuCl}(\text{BPSP})]_2(\mu\text{-Cl})_3 \cdot 2\text{H}_2\text{O} \cdot 2.5\text{CH}_2\text{Cl}_2$.

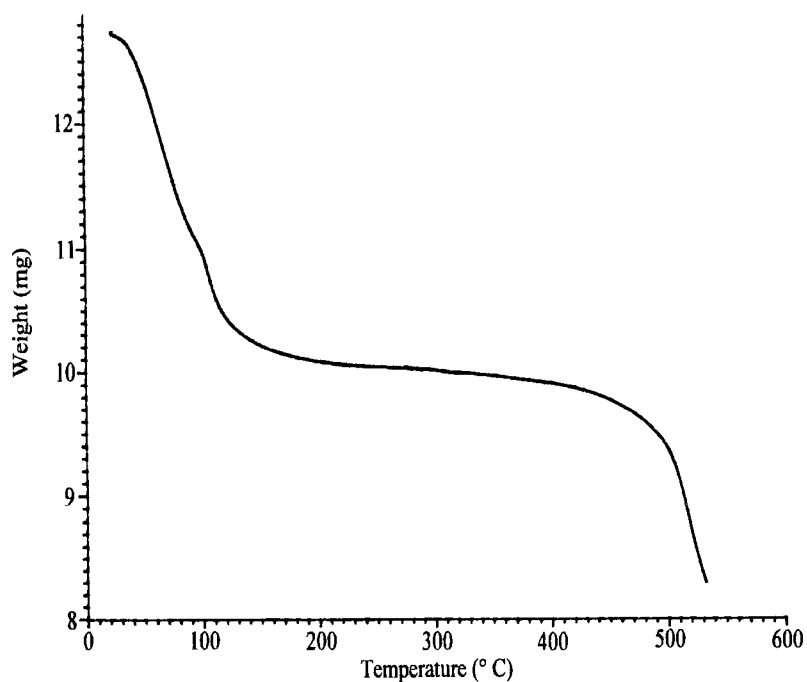


Figure A.3.3. TGA of $\text{Na}_4(\text{H}_2\text{TSPbP}) \cdot 15\text{H}_2\text{O}$ (12.7460 mg).

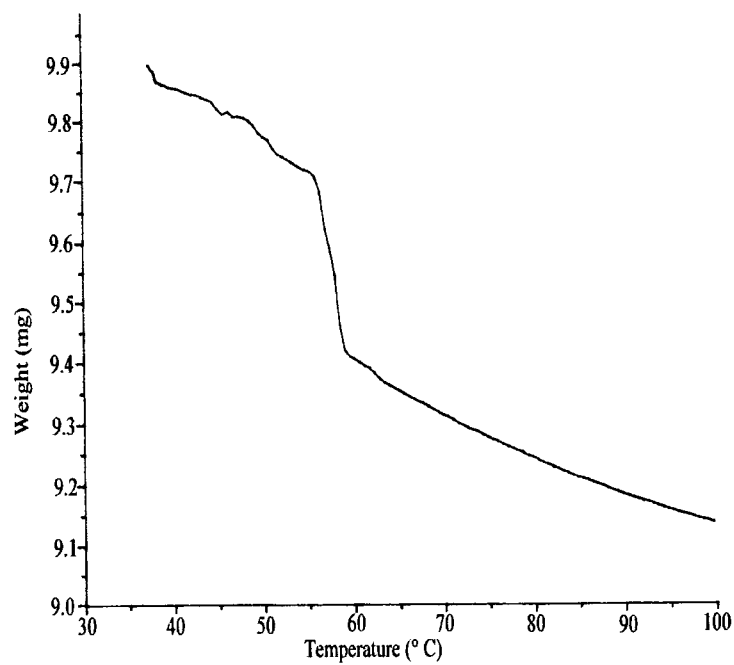


Figure A.3.4. TGA of $\text{Na}_4[\text{Ru}(\text{TSPbP})(\text{CO})] \cdot 4\text{H}_2\text{O}$ (9.9060 mg).

Appendix 4. Accumulation Data of Ru in CHO Cells

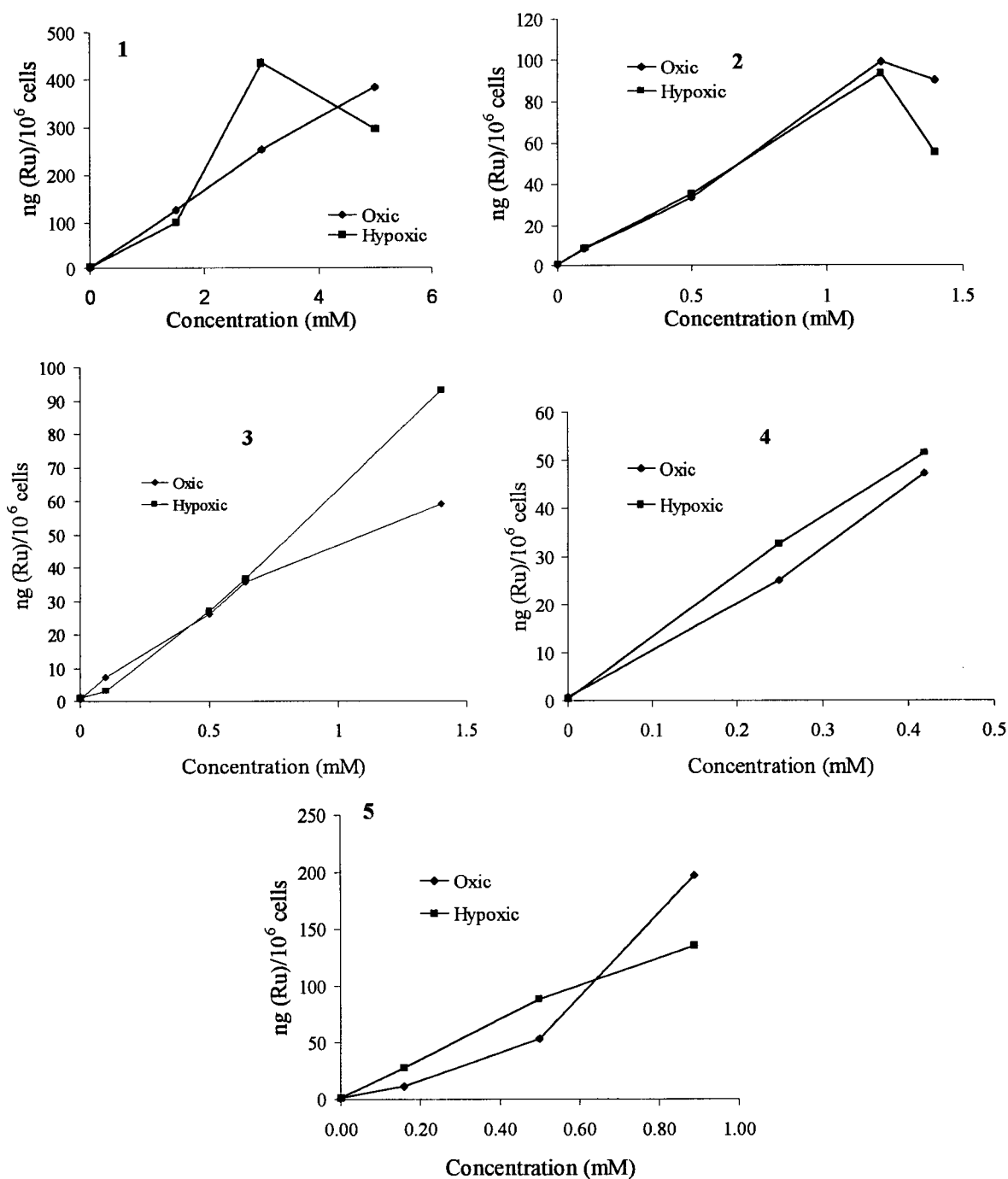


Figure A.4.1. Accumulation of Ru in CHO cells after a 2 h incubation with [Ru(12-S-4)(DMSO)(H₂O)][OTf]₂ (1), [RuCl(BPSP)]₂(μ-Cl)₃ (2), [RuCl(BESE)(H₂O)]₂(μ-Cl)₂ (3), [RuCl(BPSE)(H₂O)]₂(μ-Cl)₂ (4), [RuCl(BBSE)(H₂O)]₂(μ-Cl)₂ (5).

Appendix 5. DNA-binding Data of Ru in CHO Cells

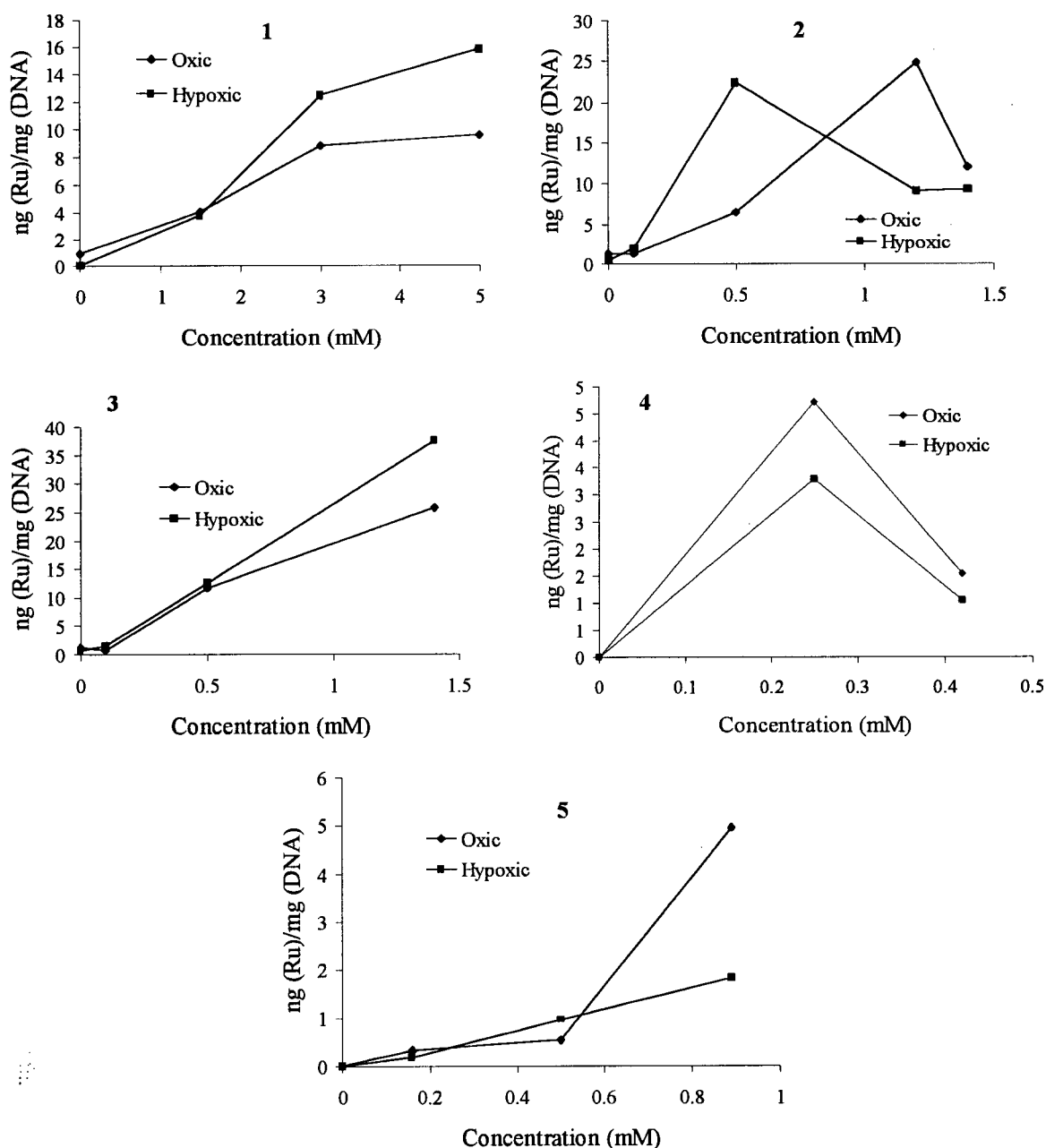


Figure A.5.1. Ru-DNA-binding after incubation with [Ru(12-S-4)(DMSO)(H₂O)][OTf]₂ (1), [RuCl(BPSP)]₂(μ-Cl)₃ (2), [RuCl(BESE)(H₂O)]₂(μ-Cl)₂ (3), [RuCl(BPSE)(H₂O)]₂(μ-Cl)₂ (4), [RuCl(BBSE)(H₂O)]₂(μ-Cl)₂ (5) (CHO cells, 2 h).